TRANSPORT OF VAPOURS IN SILICONE AND GRAFTED SILICONE RUBBER

by

ALAN CHRISTOPHER SHEER

A thesis presented for the degree of

DOCTOR OF PHILISOPHY

in the University of London

Department of Chemistry
Imperial College of Science and Technology
London SW7 2AY.

September 1976.

ABSTRACT

The sorption, permeation and diffusion (both steady-state and transient) of water vapour in the temperature range 35.0 - 55.0°C have been measured in a series of graft copolymers (poly([c.ℓ.] - dimethylsiloxane-g-vinyl acetate) P(DMS-g-VAc)) containing 3.4%, 9.3%, 15.7%, 21.4% and 44.2% PVAc by volume and in [c.ℓ.] - poly(dimethylsiloxane) and poly(vinyl acetate), and of methanol, ethanol and 2-propanol vapours in [c.ℓ.] - PDMS and of 2-propanol in [c.ℓ.] - poly (3,3,3 - trifluoropropylmethylsiloxane). The copolymers were prepared by mutual irradiation of [c.ℓ.] - PDMS swollen with vinyl acetate monomer using ^{60}Co γ-radiation. Glass transition, density, and solubility measurements, and also electron microscopy, indicated complete phase separation in these two-phase systems with PDMS the continuum and PVAc dispersed as discrete spherical domains of radii less than 100 nm.

Various approximations, derived to predict permeabilities of two-phase systems, have been examined and the best representations of the experimental data were the Higuchi, Bruggeman and Böttcher models, all of which were derived for a random lattice of domains. For copolymers and PDMS, D decreases and E_D increases with increasing concentration due to an increase of relative immobilisation of penetrant with increasing concentration. Transient (sorption-kinetics) and steady-state diffusion measurements were in reasonable agreement and indicated that pseudo-Fickian mechanisms may be present.

For the transport of alcohol vapours through silicone rubber the dominant feature is the relative immobilisation of the penetrant molecules with increasing concentration due to clustering of the penetrant through hydrogen bond formation which leads to a diffusion coefficient which decreases with concentration. Swelling and plasticization of the network increase with penetrant size so that the decrease of the diffusion coefficient with concentration is less pronounced the larger is the penetrant. The results are in reasonable agreement with models based on polycondensation theory.

ACKNOWLEDGEMENTS

I am greatly indebted to Dr. J. A. Barrie for his encouragement and guidance throughout this research.

I am grateful to the Science Research Council for a bursary for this work, to Dow-Corning Corp. (U.S.A.) for gifts of material samples, and to the technical staff of the Departmental Workshops for their help throughout the research.

I would like to thank Mr. K. Munday and Mr. R. N. Sheppard for their assistance, and Mrs. M. M. Barrie for typing this manuscript.

I would like to acknowledge the help of Dr. P. G. Clay of the Chemical Technology Department with the ^{60}Co γ-Radiation Source, and of Prof. E. H. Andrews and Dr. B. Edwards of the Department of Materials Science, Queen Mary College, for the production of the Scanning Electron Micrographs.

Finally, I would like to thank my wife, Julia, for her constant help and encouragement during the last three years.

CONTENTS

	PAGE
LIST OF TABLES	8
LIST OF ILLUSTRATIONS	9
CHAPTER 1 : INTRODUCTION	11
1.1 Factors affecting D, σ and P	12
1.1.1 Temperature Dependence	12
1.1.2 Nature of the Polymer and Penetrant	13
1.1.3 Macroheterogeneity of the Polymer	14
1.2 Graft Copolymerisation	15
1.2.1 Chemical Syntheses	15
1.2.2 Radiation Syntheses	15
1.2.3 Mechanical Syntheses	16
1.3 The Present Investigation	16
CHAPTER 2 : THEORY	18
2.1 Basic Diffusion Equations	18
2.2 Solution of the Diffusion Equations	18
2.2.1 Steady-State Permeation	19
2.2.2 Transient-State Permeation	19
2.2.3 Sorption- and Desorption-Kinetics	21
2.3 Determination of Concentration-Dependent Diffusion Coefficients	22
2.3.1 Steady-State Measurements	22
2.3.2 Transient Permeation Measurements	22
2.3.3 Sorption- and Desorption-Kinetics	23
2.4 Thermodynamics of Vapour Sorption by Polymers	25
2.4.1 Free Energy, Heat and Entropy of Dilution	25
2.4.2 Clustering Theory	25
2.5 Molecular Theories of Diffusion	26
CHAPTER 3 : EXPERIMENT	28
3.1 Materials	28
3.1.1 Poly ([c.ℓ.] - dimethylsiloxane)	28
3.1.2 Poly (vinyl acetate)	28

PAGE

3.1.3 Poly ([c.ℓ.] - dimethylsiloxane-g-vinyl acetate) 28
3.1.4 [c.ℓ.] - Poly(3,3,3-trifluoropropylmethylsiloxane) 29
3.1.5 Penetrant Vapours 29

3.2 Apparatus 30
3.2.1 The Pumping Systems 30
3.2.2 The Permeability System 30
3.2.3 Spring-Sorption Apparatus 35
3.2.4 Microbalance-Sorption Apparatus 35
3.2.5 Grafting System 40

3.3 Procedure 40
3.3.1 Steady-State Permeability 40
3.3.2 Spring-Sorption 42
3.3.3 Microbalance-Sorption 43
3.3.4 Preparation of Graft Copolymers 44

CHAPTER 4 : DIFFUSION IN HETEROGENEOUS MEDIA 45

4.1 Literature Survey 45
4.1.1 Copolymers of Poly(ethylene) 45
4.1.2 Poly (dimethylsiloxane) 49
4.1.3 Cellulose and Cellulose Acetate 49
4.1.4 Wool 51
4.1.5 Poly (oxides) 53
4.1.6 Poly (tetrafluoroethylene) 54
4.1.7 Miscellaneous Polymers 55

4.2 Models of Heterogeneous Diffusion 55
4.2.1 Classical Solutions 56
4.2.2 Ordered Arrangements 57
4.2.3 Approximations 58

4.3 Conclusions 59

CHAPTER 5 : RESULTS AND DISCUSSION : GRAFT COPOLYMERS 60

5.1 Preparation and Physical Properties of the Graft Copolymers 60
5.1.1 Radiation Units 60
5.1.2 Radiation Grafting 60
5.1.3 Structure and Physical Properties 65

5.2 Equilibrium Sorption Results 70
5.2.1 Sorptive Capacities of the Polymers 70
5.2.2 Heats of Sorption 80

PAGE

5.2.3 Clustering Analysis 83
5.2.4 Heats and Entropies of Dilution 87

5.3 Steady-State Permeability Results 87
5.3.1 Difficulties Associated with Water Vapour Permeation 87
5.3.2 Absolute Magnitudes of Permeabilities 100
5.3.3 Permeability Temperature Dependence 120

5.4 Diffusion Results 124
5.4.1 Steady-State Diffusion 124
5.4.2 Transient-State Diffusion 142
5.4.3 Temperature Dependence of D 160

CHAPTER 6 : RESULTS AND DISCUSSION : ALCOHOLS 178

6.1 Equilibrium Sorption Results 178
6.1.1 Sorptive Capacities of the Polymers 178
6.1.2 Isotherm Shapes 186
6.1.3 Comparison with Theoretical Isotherms 189
6.1.4 Heats of Sorption and Dilution 194

6.2 Steady-State Permeability Results 196
6.2.1 Absolute Magnitudes of P 202
6.2.2 Temperature Dependence of P 203

6.3 Transient-State Permeation 203
6.3.1 Magnitudes of Time Lags 205

6.4 Steady-State Diffusion Results 212
6.4.1 Values of $D_{c=o}$ 213
6.4.2 Concentration-Dependence of D 216
6.4.3 Temperature Dependence of D 225

CHAPTER 7 : CONCLUSIONS 235

7.1 Summary and Reappraisal of Results 235
7.1.1 Heterogeneous Media 235
7.1.2 Alcohol Vapour Transport 237
7.1.3 Water Vapour Permeation 237

CHAPTER 8 : APPENDIX 238

8.1 Scanning Electron Microscopy 238

		PAGE
8.2	Basic Experimental Data	238
	8.2.1 Equilibrium Sorption Results	243
	8.2.2 Sorption- and Desorption-Kinetic Results	254
	8.2.3 Steady-State Permeation Results	264
	8.2.4 Time Lag Results	271
	8.2.5 Steady-State Spring-Permeation Results	272
8.3	Sample Calculations	274
	8.3.1 Equilibrium Sorption	274
	8.3.2 Sorption- and Desorption-Kinetics	276
	8.3.3 Steady-State Permeability	276
	8.3.4 Models of Permeation in Heterogeneous Media	278
8.4	Accuracy of Measurements	278
	8.4.1 Baratron-Permeability Measurements	278
	8.4.2 Spring-Permeability Measurements	279
	8.4.3 Microbalance-Sorption Measurements	279
	8.4.4 Spring-Sorption Measurements	280
	8.4.5 Rates of Sorption Measurements	280
REFERENCES		282

LIST OF TABLES

PAGE

CHAPTER 3 : EXPERIMENT

3.1 T_g, T_m and ρ for PDMS, PVAc and P(DMS-g-VAc) 29

CHAPTER 5 : RESULTS AND DISCUSSION : GRAFT COPOLYMERS

5.1 Scanning Electron Microscopy of P(DMS-g-VAc) 67

5.2 Limiting Henry's Law Solubility Coefficients 70

5.3 Heats of Sorption in the limit ($c \rightarrow o$) 80

5.4 Clustering Functions for P(DMS-g-VAc) 86

5.5 Mean Heats and Entropies of Dilution 97

5.6 Baratron and Spring Flux-Rates 102

5.7 Permeability Coefficients 102

5.8 Smoothed and Extrapolated "Experimental" Permeabilities 112

5.9 Effects of Occlusions on ϕ and Domain Radii 118

5.10 Permeabilities of Occluded Systems 119

5.11 Temperature Coefficients of P 120

5.12 Values of $D_{c=o}$ Coefficients 124

5.13 Values of $D_{c=o}$ for Experiment and Models at $35^{o}C$ 128

5.14 Steady-State and Transient Diffusion Coefficients 146

5.15 Values of E_D at Various Penetrant Concentrations 176

CHAPTER 6 : RESULTS AND DISCUSSION : ALCOHOLS

6.1 Limiting Henry's Law Solubility Coefficients 183

6.2 Clustering Functions 188

6.3 Heats of Sorption in the limit ($c \rightarrow o$) 194

6.4 Mean Heats and Entropies of Dilution 196

6.5 Permeability Coefficients 202

6.6 Temperature Coefficients of P 203

6.7 Values of $D_{c=o}$ Coefficients 213

6.8 Values of E_D at Various Penetrant Concentrations 234

CHAPTER 8 : APPENDIX

8.1 Magnification of the Electron Micrographs 238

8.2 - 8.12 Equilibrium Sorption Isotherms 244-254

8.13 - 8.22 Sorption- and Desorption-Kinetics 255-264

8.23-8.33 Steady-State Permeation 264-271

8.34-8.36 Time Lag Data 271-272

8.37 Steady-State Spring-Permeation 273

8.38 Baratron- and Spring - Permeation 273

LIST OF ILLUSTRATIONS

		PAGE
CHAPTER 3 : EXPERIMENT		
3.1	The Pumping System	31
3.2	The Permeability System	32
3.3	Diffusion Cell and Membrane Holder	34
3.4	Spring-Sorption Apparatus	36
3.5	Microbalance-Sorption Apparatus	37
3.6	Blank Isotherm for the Microbalance	39
3.7	The Grafting System	41
CHAPTER 5 : RESULTS AND DISCUSSION : GRAFT COPOLYMERS		
5.1	Sorption of Monomer by PDMS	62
5.2	Graft Dependence on Dose	63
5.3	Densities of P(DMS-g-VAc) Copolymers	69
5.4-5.10	Equilibrium Sorption Isotherms	71 - 77
5.11	Limiting Henry's Law Solubility Coefficients	79
5.12	Temperature Variation of Solubility Coefficients	81
5.13	Heats of Sorption of P(DMS-g-VAc)	82
5.14-5.15	Clustering Analyses for PDMS and PVAc	84 - 85
5.16-5.17	Heats and Entropies of Dilution of PDMS	88 - 89
5.18-5.24	Permeation Flux Isotherms	90 - 96
5.25	Time Lags for P(DMS-g-0.157 VAc)	98
5.26	Calibration for Baratron- and Spring-Permeation	101
5.27-5.28	Permeability Analyses	106 & 108
5.29	Extrapolation of Experimental $D_{c=o}$ Values	110
5.30	Smoothed & Extrapolated Permeabilities	111
5.31	Permeability Analysis for $\phi_D = 0 \rightarrow 1$	114
5.32	Phase Inversion Analysis at 35°C	117
5.33	Temperature Variations of P	121
5.34-5.36	E_p Analyses over Composition Range	122 - 125
5.37	$D_{c=o}$ Values for Böttcher Model	127
5.38-5.44	Reduced D-C Curves	130 - 136
5.45-5.49	Intrinsic and Experiment D Values	137 - 141
5.50-5.52	Conjugate Rate Curves at 42°C	143 - 145
5.53-5.62	Average Sorption- and Desorption-Kinetics	147 - 156
5.63	Conjugate Rate Curves at 55°C	159
5.64-5.70	Transient and Steady-State Diffusion	161 - 167
5.71-5.77	Temperature Dependence of D	168 - 174
5.78	Variation of E_D with composition	175

		PAGE
CHAPTER 6 : RESULTS AND DISCUSSION : ALCOHOLS		
6.1-6.4	Equilibrium Sorption Isotherms	179 - 182
6.5-6.6	Sorptive Capacities of the Polymers	184 - 185
6.7	Clustering Analysis for FMS	187
6.8-6.11	Theoretical Sorption Isotherms	190 - 193
6.12	Temperature Dependence of Solubility	195
6.13-6.16	Permeation Flux Isotherms	197 - 200
6.17	Spring and Baratron Flux Isotherms	201
6.18	Temperature Dependence of Permeability	204
6.19-6.24	Time Lag Data	206 - 211
6.25-6.26	Variation of $D_{c=o}$ with Penetrant	214 - 215
6.27-6.30	Concentration-Dependence of D	217 - 220
6.31-6.34	Theoretical D^{l} - C Curves	221 - 224
6.35-6.38	Intrinsic and Mutual D Values	226 - 229
6.39-6.42	Temperature Dependence of D	230 - 233
CHAPTER 8 : APPENDIX		
8.1-8.8	Electron Micrographs of P(DMS-g-VAc)	239 - 242

CHAPTER 1

INTRODUCTION

Transport of a gas or vapour through a polymer membrane can be regarded as comprised of three stages:

(a) Sorption of penetrant molecules onto the surface of the polymer from the gas phase.

(b) Diffusion of the sorbed molecules through the membrane by a series of random displacements leading to a net flux or transport across the membrane in the presence of a concentration gradient.

(c) Desorption of the penetrant molecules from the membrane into the gas phase.

Step (b) (the diffusion process) is considered to be rate-determining.

Since diffusion requires some degree of co-operative movement of the polymer segments, a study of the mechanism of the transport process can be of value in elucidating the microstructure of the polymer itself. Consequently the chemical structure of both polymer and penetrant, the physical state and morphology of the polymer have been studied in detail and is the subject of several review articles (41, 55, 88, 106, 128).

The interpretation and analysis of diffusion data is usually carried out in terms of Fick's equations, which will be expressed mathematically in Chapter 2. The three quantities measured are a diffusion coefficient (D), a solubility (σ) and a permeability coefficient (P). The diffusion coefficient may be defined as the amount of penetrant passing across a plane of unit area under a unit concentration gradient in unit time. It usually has units of $cm^2.s^{-1}$. Similarly a solubility coefficient can be defined as the concentration (c) of penetrant sorbed per unit volume of dry polymer at unit gas phase pressure, and is expressed in $cm^3(S.T.P.).cm^{-3}.(cm\ Hg)^{-1}$. The permeability coefficient is defined as the amount of penetrant passing through a membrane of unit area and of unit thickness in unit time under a unit pressure difference. It is usually expressed as $cm^3(S.T.P.).cm^{-1}.s^{-1}.(cm\ Hg)^{-1}$. When P, D and σ are independent of concentration or in the limit of $c \to o$, then

$$P = D.\sigma \qquad \ldots.(1.1)$$

provided that each is expressed in the units given.

D and σ are usually constant at a given temperature for moderate pressures of permanent gas penetrants in polymers (117). This has been interpreted as due to the low solubilities of these gases in polymers and negligible gas-gas and gas-polymer interactions.

On the other hand, for organic vapours in polymers, D generally increases with increasing concentration, as does σ in many instances (54). In this case polymer-penetrant interactions are more important leading to higher solubilities and plasticisation of the polymer matrix with a subsequent increase in segmental mobilities.

The concentration dependence of D and σ for water in polymers is more varied, depending upon the type of polymer (17). For hydrophilic polymers, the water sorbed swells the polymer as for organic vapours and D usually increases with increasing c. However hydrophobic polymers tend to show D decreasing with increasing c. This has been interpreted in terms of clustering or association of the water molecules within the polymer such that the water molecules within these clusters become relatively immobile. As might be expected for this type of behaviour, water-water interactions are much more favourable than polymer-water interactions and hence predominate throughout.

1.1 Factors affecting D, σ and P

This work has been reviewed previously (41, 55, 88, 106, 128) and is mentioned but briefly here. Sample preparation is very important (42) and reproducible results are not always obtained from different samples.

1.1.1 Temperature Dependence

The temperature dependence of penetrant diffusion in polymers can be represented by an Arrhenius-type relationship since it is an activated process:

$$D = D_o . \exp(-E_D/RT) \qquad \ldots.(1.2)$$

where E_D is the activation energy for diffusion and D_o a pre-exponential factor.

For a comparatively small temperature range E_D is constant for many polymer-penetrant systems.

There is a similar relationship for the solubility coefficient:

$$\sigma = \sigma_o . \exp(-\Delta\overline{H}_S/RT) \qquad \ldots.(1.3)$$

where $\Delta\overline{H}_S$ is the heat of sorption. This may be regarded as comprising of two contributions, namely the heat of condensation of penetrant ($\Delta\overline{H}_{cond}$) and the heat of dilution of sorbed penetrant ($\Delta\overline{H}_A$). For permanent gases the hypothetical $\Delta\overline{H}_{cond}$ is expected to be very small so that $\Delta\overline{H}_S$ is essentially determined by $\Delta\overline{H}_A$ (106), and hence $\Delta\overline{H}_S$ is small and positive. However $\Delta\overline{H}_{cond}$ is the dominating factor where vapours are concerned so that $\Delta\overline{H}_S$ is negative and often quite large.

Combination of equations (1.1), (1.2) and (1.3) yields

$$P = P_0 . \exp(-E_P/RT) \qquad \ldots.(1.4)$$

where E_P is the temperature coefficient of the permeability coefficient. It is a composite quantity as

$$E_P = E_D + \Delta\overline{H}_S, \qquad P_0 = D_0 \cdot \sigma_0 \qquad \text{and}$$

may be positive or negative depending on the relative magnitudes of E_D and $\Delta\overline{H}_S$. Generally P increases with increasing temperature but the opposite trend has been observed for polymers that are quite permeable, such as the silicone rubbers.

1.1.2 Nature of the Polymer and Penetrant

In general, the higher the boiling point of the penetrant the greater is the solubility of the penetrant in the polymer. The sorptive capacity of the polymer is generally governed by an extension of the "like dissolves like" principle. Thus organic vapours tend to sorb better in hydrophobic polymers, whilst water vapour uptakes are largest in polymers containing a high proportion of hydrophilic groups.

Penetrant size is a very important factor. At a constant temperature D decreases almost exponentially with increasing penetrant molar volume (88), whilst the corresponding E_D increases. In addition, the more branched the penetrant the lower is the corresponding D. This factor, in many instances, is more critical than the actual size in determining the magnitude of D (1). For many polymers, there appears to be a critical size of penetrant above which there is little effect on E_D as penetrant size increases (88). This is the situation when diffusion is controlled by the polymer having to undertake large co-operative segmental motion in order to accommodate the penetrant molecule.

Values of D generally decrease the more symmetrical the polymer chain becomes and the more bulky the side-chains from it.

Crosslinking of the polymer causes very little change in solubility of the penetrant, but D decreases and E_D increases since the crosslinks reduce the mobility of the polymer segments. However, in the situations normally encountered, i.e. very light crosslinking, this difference in D is usually very small. Diffusion in crystalline polymers generally takes place in the amorphous regions. As the crystalline content of the polymer increases D decreases since the amorphous content decreases and the penetrant undertakes a more tortuous diffusion path round the crystallites.

On lowering the temperature towards the glass transition temperature (T_g) of the polymer there is a catastrophic slowing of segmental motions and below T_g such large scale motions are virtually frozen out. For a number of systems a change in E_D is observed on going through T_g, being constant in the regions above and below T_g (89): whilst for other systems no change in E_D is observed although clearly there must be different mechanisms operative above and below T_g. Vapour transport in the glassy state has been extensively studied and is complicated by the presence of slow relaxation processes in the matrix (41, 106).

1.1.3 Macroheterogeneity of the Polymer

Heterogeneous membranes generally consist of a discontinuous phase dispersed in a continuous phase, or laminates of two or more polymers. Laminate properties have been studied in some detail (12, 106) and for constant D, σ systems relationships can be obtained for P, D and σ of the laminate in terms of the P, D and σ for the individual components.

Dispersions of A in a continum of B are more complex than laminates since domain sizes, their spatial distributions and the volume fraction of each phase will affect the transport behaviour of these heterogeneous systems (12). The transport problem is more complex and exact solutions of the diffusion equations are not available but numerous steady-state models have been developed in an attempt to describe the electrical and transport properties of these systems.

If the disperse phase consists of impermeable filler particles, diffusion occurs largely in the polymer phase although contributions to flow arise in channels formed by aggregation of filler particles. This system can be considered as similar, in some ways, to that of a partially crystalline polymer since transport does not occur within

the highly regular crystalline regions. Polyblends and block and graft copolymers are all examples of two polymer systems. Polyblends are physical mixtures of two polymers whereas the copolymers consist of chains of the two polymers combined together such that one or both of the polymers can be considered as backbone polymer. In such systems the two polymers tend to be in separate phases since most polymers are incompatible, except for a few special cases in which there are some kind of interactions between the polymers.

1.2 Graft Copolymerisation

Graft copolymerisation can be considered to be classified according to the method as: (a) chemical, (b) radiation or (c) mechanical (26, 29, 30, 31, 32, 64, 98, 115, 122). Both chemical and radiation syntheses have been used extensively and dominate the literature.

1.2.1 Chemical Syntheses

Chemical synthesis is a general term which encompasses many different mechanisms and which can be further divided into ionic and radical attack. Both cationic and anionic mechanisms have been used, but anionic, especially "living-polymer" polymerisation using sodium and naphthalene as initiator, is much more common. Chain transfer from growing monomer to polymer by the removal of a labile atom, initiator attack on the α-H atom of a double bond, peroxide and redox initiation have all been employed for radical polymerisation. The polymer structure is an important feature since each method is applicable to a particular class of structure.

1.2.2 Radiation Syntheses

Radiation polymerisation is usually accomplished by (a) mutual irradiation, (b)pre-irradiation in air or (c)pre-irradiation in vacuum. Radical attack predominates even though ionic attack is known. Mutual irradiation is achieved by direct irradiation of the polymer swollen with monomer at room temperature and in the absence of oxygen. Any free radicals formed on the polymer matrix initiate polymerisation of the monomer. During irradiation of the polymer at low temperatures in air, stable peroxide groups are formed on the polymer which, on heating in the absence of air, decompose liberating free radicals and initiating polymerisation. Free radicals are trapped on the polymer if it is irradiated under vacuum at low temperatures, especially if the

polymer is partially crystalline. Diffusion of monomer to these reactive radicals produces the desired graft copolymer.

1.2.3 Mechanical Syntheses

Although mechanical degradation often forms block copolymers, graft copolymers are obtained if the polymers present undergo disproportionation reactions. The desired product can be achieved by subjecting a mixture of two or more polymers to mechanical degradation in either the solid, elastic-melt or solution states. The usual processes are vibromilling, mastication, extrusion, stirring and discharge of high voltage sparks.

1.3 The Present Investigation

The principal aim of the work presented here is the investigation of water vapour transport in a series of graft copolymer membranes by diffusion, permeation and sorption studies. Poly ([c.ℓ.] - dimethyl-siloxane - g - vinyl acetate)P(DMS - g - VAc) copolymers were prepared from [c.ℓ.] - PDMS by mutual irradiation from a ^{60}Co γ-radiation source. The copolymers contained 0-50% PVAc by volume and this was the discontinuous phase in each membrane. The structure of each copolymer has been established by scanning electron microscopy which gave a good indication of the size, shape and distribution of the PVAc domains. PDMS is hydrophobic in nature since its water uptake close to saturation amounts only to 0.1% by weight of dry polymer. The dispersed polymer (PVAc), on the other hand, is relatively hydrophilic having a water uptake of about 4% by weight of dry polymer.

The measurement of P, σ and D for each of the series, of different composition, has been undertaken in order to present data which may be used to test the proposed models for heterogeneous diffusion. By preparing the membranes using similar means it should be possible to eliminate many of the uncertainties of using different samples and hence render more reliable any comparison of the results. Diffusion data for each copolymer and the two homopolymers were obtained mainly for steady-state conditions, although some sorption-rate measurements were taken for comparison. All measurements were taken at temperatures above the T_g of each polymer.

The second part of the investigation consists of the transport of methanol, ethanol and 2-propanol vapours through two related silicone polymers, PDMS and FMS ([c.ℓ.] - poly (3,3,3-trifluoropropylmethyl-siloxane)). This is an extension of earlier studies (20, 84) in which

water vapour transport through these two hydrophobic polymers was investigated with particular reference to clustering of the penetrant molecules within the polymers. This extension has been undertaken with a view to investigating the relative importance of penetrant-polymer and penetrant-penetrant interactions as the hydrophobic nature of the penetrant increases since the hydrocarbon part of the penetrant will plasticise the polymer and oppose the clustering of penetrant molecules brought about by the hydroxyl group interactions.

CHAPTER 2

THEORY

2.1 Basic Diffusion Equations

For an isotropic medium the rate of transfer of diffusing matter under a concentration gradient through an area of unit cross-section normal to the direction of flow is expressed in terms of Fick's first equation of diffusion (50),

$$J = -D.\frac{\partial c}{\partial x} \qquad \ldots.(2.1)$$

where J is the rate of transfer, c is the concentration of diffusing material at a point x along the direction of flow and D is the diffusion coefficient. Provided that J and c are expressed in terms of the same units then D is independent of these units and has dimensions $(\text{length})^2\ (\text{time})^{-1}$. The negative sign in equation (2.1) arises from the fact that flow is in the reverse direction to that of the concentration gradient, i.e. from high to low penetrant concentration.

Fick's second equation can be derived from equation (2.1) by applying the law of conservation of material:

$$\frac{\partial c}{\partial t} = D\,.\,\frac{\partial^2 c}{\partial x^2} \qquad \ldots.(2.2)$$

This is applicable for constant D, and for D a function of c becomes

$$\frac{\partial c}{\partial t} = \frac{\partial}{\partial c}\left[D(c)\,.\,\frac{\partial c}{\partial x}\right] \qquad \ldots.(2.3)$$

Equation (2.1) refers to diffusion across an arbitrarily chosen plane, or frame of reference. The definition of D requires, for a two component system, a frame of reference with respect to which the flux J is measured. There are a variety of frames of reference (38) which can be applied; total mass fixed, total volume fixed or mass of one component fixed. In this work the frame of reference is that in which the mass of polymer remains constant at the faces of the membrane. As there is no significant swelling of polymer by penetrant both volume and mass fixed approaches give the same D, referred to as the mutual diffusion coefficient, and this will be used throughout this work.

2.2 Solution of the Diffusion Equations

The appropriate solution of equations (2.1) and (2.2) depends upon the sample geometry and the initial and boundary conditions imposed

(11, 36, 41, 71, 106). The two most common situations for a plane sheet are:

(1) Permeation through a sheet containing no penetrant initially and with fixed, but different penetrant concentrations maintained at each face.

(2) Sorption into and desorption from a sheet, with each face maintained at the same fixed concentration which is different to that initially in the sheet.

The solutions illustrated here are applicable to transport through a plane sheet only (37, 42, 106).

2.2.1 Steady-State Permeation

Consider a membrane of thickness ℓ whose ingoing and outgoing faces ($x=o$, $x=\ell$) are maintained at concentrations c_o and c_ℓ respectively ($c_o > c_\ell$). Equation (2.2) yields for steady-state conditions with D constant

$$\frac{\partial^2 c}{\partial x^2} = 0 \qquad \ldots.(2.4)$$

Integration and application of the boundary conditions yields

$$\frac{x}{\ell} = \frac{C_o - C}{C_o - C_\ell} \qquad \ldots.(2.5)$$

which indicates a constant concentration gradient across the membrane. From equations (2.1) and (2.5) one obtains

$$J = D\,\frac{(C_o - C_\ell)}{\ell} \qquad \ldots.(2.6)$$

When D varies with c equation (2.1) is still valid. The form of equation (2.6) can be retained by defining an average diffusion coefficient $\overline{D}$. Then integration of equation (2.1) yields

$$J = \frac{\overline{D}\,(C_o - C_\ell)}{\ell} = \frac{1}{\ell}\int_{C_\ell}^{C_o} D(c).dc \qquad \ldots.(2.7)$$

where

$$\overline{D} = \frac{1}{C_o - C_\ell} \cdot \int_{C_\ell}^{C_o} D(c)\,.\,dc \qquad \ldots.(2.8)$$

2.2.2 Transient-State Permeation

(i) Time Lag

In the permeation experiment, the concentration of penetrant at

the outgoing face is maintained such that it is negligible compared to that at the ingoing face. If the membrane is initially free of penetrant the following boundary conditions are applicable:-

$$c = c_o \qquad x = 0 \qquad t \geqslant 0$$
$$c = 0 \qquad 0 < x < \ell \qquad t = 0$$
$$c = 0 \qquad x = \ell \qquad t \geqslant 0$$

The solution of equation (2.2) then becomes

$$\frac{Q_t}{\ell\, C_o} = \frac{Dt}{\ell^2} - \frac{1}{6} - \frac{2}{\pi^2} \sum_{n=1}^{\infty} \left[\frac{(-1)^n}{n^2} \cdot \exp\left(- \frac{D.n^2.\pi^2.t}{\ell^2} \right) \right] \qquad \ldots.(2.9)$$

where Q_t is the amount of penetrant which has passed through unit area of sheet in time t. As the steady-state is approached ($t \to \infty$) equation (2.9) tends to the steady-state line

$$Q_t = \frac{D.C_o}{\ell} \left(t - \frac{\ell^2}{6D} \right) \qquad \ldots.(2.10)$$

Hence a graph of Q_t vs. t yields an intercept, the time lag (L), on the time axis given by (11, 45)

$$L = \frac{\ell^2}{6D} \qquad \ldots.(2.11)$$

Equations (2.10) and (2.11) are valid if D is constant, but when D varies with c the time lag can be obtained from (53)

$$L = \frac{\int_o^{\ell} x \cdot c_s(x) \cdot dx}{\int_o^{c_o} D(c) \cdot dc} \qquad \ldots.(2.12)$$

where $c_s(x)$ is the concentration distribution of penetrant in the sheet in the steady-state.

(ii) Early-Time Analysis

An alternative to equation (2.9) which has been proposed (109) is

$$\frac{dQ_t}{dt} = C_o \left(\frac{4D}{\pi}\right)^{\frac{1}{2}} \sum_{m=o}^{\infty} \exp\left(- \frac{\ell^2.\,(2m+1)^2}{4\,Dt} \right) \qquad \ldots.(2.13)$$

which at small time reduces to

$$\ln\left(t^{\frac{1}{2}} \cdot \frac{dQ_t}{dt} \right) = \ln\left[\frac{4\,C_o^2\,D}{\pi} \right] - \frac{\ell^2}{4Dt} \qquad \ldots.(2.14)$$

Hence a graph of $\ln (t^{\frac{1}{2}} \cdot dQ_t/dt)$ vs. $1/t$ yields D from the slope.

2.2.3 Sorption- and Desorption-Kinetics

For the boundary conditions

$$c = c_o \qquad x = 0 \qquad x = \ell \qquad t \geq 0$$

$$c = 0 \qquad 0 < x < \ell \qquad t = 0$$

and for a constant D, the solution of equation (2.2) may be written as

$$\frac{M_t}{M_\infty} = 4\left(\frac{Dt}{\ell^2}\right)^{\frac{1}{2}}\left(\frac{1}{\pi^{\frac{1}{2}}} + 2\sum_{n=o}^{\infty}\left\{(-1)^n \cdot \text{ierfc}\left[\frac{n\ell}{(4Dt)^{\frac{1}{2}}}\right]\right\}\right) \quad \ldots.(2.15)$$

or

$$\frac{M_t}{M_\infty} = 1 - \frac{8}{\pi^2}\sum_{m=o}^{\infty}\left(\frac{1}{(2m+1)^2} \cdot \exp\left[\frac{-D(2m+1)^2\pi^2 t}{\ell^2}\right]\right) \quad \ldots.(2.16)$$

where M_t is the amount of penetrant taken up at time t and M_∞ is the equilibrium uptake. Equation (2.15) is best suited for application at small times when the summation term tends to zero.

i.e.
$$\frac{M_t}{M_\infty} = 4\left(\frac{Dt}{\pi\ell^2}\right)^{\frac{1}{2}} \quad \ldots.(2.17)$$

Hence a graph of M_t/M_∞ vs. $t^{\frac{1}{2}}$ readily yields D from the slope of the straight line. This equation usually applies up to $M_t/M_\infty = 0.5$ if D is constant.

Equation (2.16) is more useful at longer times whereupon only the (m=o) terms of the summation need be considered, so that

$$\ln (1 - M_t/M_\infty) = \ln (8/\pi^2) - D\pi^2 t/\ell^2 \quad \ldots.(2.18)$$

Hence D can be obtained from the slope of a graph of $\ln(1-M_t/M_\infty)$ vs. t. This relationship usually holds for $M_t/M_\infty > 0.5$ provided that D is constant.

The desorption experiment from a plane sheet entails the following boundary conditions :

$$c = 0 \qquad x = 0 \qquad x = \ell \qquad t \geq 0$$

$$c = c_o \qquad o < x < \ell \qquad t = 0$$

However equations (2.15) to (2.18) are still applicable provided that M_t is taken as the amount of penetrant lost from the sheet at time t.

For a concentration-dependent D this analysis yields some average value $\overline{D}$ over the concentration range 0 - C_o. The extraction of the true D from $\overline{D}$ will be dealt with in Section (2.3).

2.3 Determination of Concentration-Dependent Diffusion Coefficients (38)

2.3.1 Steady-State Measurements

For steady-state permeation of penetrant through a sheet the concentration at the outgoing face is effectively zero so that equation (2.8) becomes

$$J = 1/\ell \int_0^{C_o} D(c)\, dc \qquad \ldots.(2.19)$$

In practice values of flux J are measured for a series of ingoing pressures p so that the J-p relationship can be obtained. In addition equilibrium isotherms are obtained so that the C_o- p relationship can also be found. Hence a combination of permeation and sorption experiments yields J as a function of C_o. The required D-c relationship can be obtained by graphical or analytical differentiation of the J - C_o curve using equation (2.20):

$$D_{c=c_o} = \ell\, (dJ/dc)_{c=c_o} \qquad \ldots.(2.20)$$

2.3.2 Transient Permeation Measurements

(i) Time Lag

Since, under steady-state conditions, the flux of penetrant at any point in the sheet remains constant throughout, equation (2.12) can be modified to

$$\int_{C_s}^{C_o} D(c)dc = x/\ell \int_0^{C_o} D(c)\, dc \qquad \ldots.(2.21)$$

where C_s is the steady-state concentration at a distance x inside the sheet. By eliminating x from equations (2.12) and (2.21) (53)

$$L = \frac{\ell^2 \int_0^{C_o} c_s \cdot D(c_s) \int_{C_s}^{C_o} D(u)\, du\, dc_s}{\left(\int_0^{C_o} D(u)\, du\right)^3} \qquad \ldots.(2.22)$$

where u is a dummy variable. Equation (2.21) can be written in terms of fluxes at differing ingoing concentrations as

$$\ell\ (J_{C_o} - J_{C_s}) = x \cdot J_{C_o} \qquad \ldots.(2.23)$$

Hence from equations (2.12) and (2.23), elimination of x yields (6)

$$L = \frac{\ell \int_0^{J_{C_o}} C_s\ (J_{C_o} - J_{C_s})\ dJ_{C_s}}{J_{C_o}^3} \qquad \ldots.(2.24)$$

In general, it is not possible to obtain the D-c relationship very accurately from a known L-c dependence as the variation of L with concentration is much less than that of D (21).

(ii) Early-time Permeation

When equation (2.14) is applied at small t, $D_{c=o}$ is obtained to a good approximation (90). A knowledge of $D_{c=o}$ together with the mathematical form of D-c can be utilised to fit the L-c results using equations (2.12) or (2.22), so that the best values of the unknown parameters of the D-c relationship can be determined.

2.3.3 Sorption- and Desorption- Kinetics

When D varies with c equations (2.17) and (2.18) become

$$\frac{M_t}{M_\infty} = 4\ \left(\frac{\overline{D}t}{\pi\ell^2}\right)^{\frac{1}{2}} \qquad \ldots.(2.25)$$

$$\ln\ (1 - M_t/M_\infty) = \ln\ (8/\pi^2) - \overline{D}\pi^2 t/\ell^2 \qquad \ldots.(2.26)$$

where $\overline{D}$ is some average value of D, but not necessarily the same one as is obtained from permeation methods. If measurements can be made close to equilibrium, the $\overline{D}$ obtained from equation (2.26) is a good approximation to the actual D at concentration C_o in the sorption experiment and to $D_{c=o}$ in the case of desorption. However this often presents difficulties so that equation (2.25) has been favoured by most workers since the D-c relationship can be calculated from the $\overline{D}$-C_o relationship at a series of different equilibrium concentrations. The various procedures adopted to obtain the D-c relationship will be illustrated in the following subsections.

(i) Successive Approximations

To a first approximation $\overline{D}$ can be taken as

$$\overline{D} = 1/C_o \int_0^{C_o} D(c)\ dc \qquad \ldots.(2.27)$$

so that

$$D(c) = \bar{D}(c) + C_o \cdot d\bar{D}/dC_o \quad \ldots.(2.28)$$

The D(c) values obtained can be used to construct sorption-time curves for various values of C_o by numerical methods. $\bar{D}$ values can be obtained from these curves using equation (2.25) and compared with the original values of $1/C_o \int_0^{C_o} D(c)\, dc$. From a graph of calculated $\bar{D}$ vs. $1/C_o \int_0^{C_o} D(c)\, dc$ improved values of the latter are obtained corresponding to the observed values of $\bar{D}$. These improved values are then differentiated to give a second approximation to D(c) and the whole process is repeated until the observed and calculated values of $\bar{D}$ are in agreement (43).

This method tends to be laborious although the advent of high-speed computers facilitates its use. However, it is also of value for "interval" sorption studies for which the sheet has a non-zero penetrant concentration initially (36).

(ii) Mean Diffusion Coefficients for Sorption and Desorption

From integral sorption and desorption curves one may obtain $\bar{D}_s$ and $\bar{D}_d$ respectively using equation (2.25). It has been established that $1/2\ (\bar{D}_s + \bar{D}_d)$ is an accurate approximation to $1/C_o \int_0^{C_o} D(c)\, dc$ for several D-c relationships:

$$D(c) = \frac{1}{2} \frac{d\left(C_o\ (\bar{D}_s + \bar{D}_d)\right)}{dC_o} \quad \ldots.(2.29)$$

A similar procedure can be initiated as for the successive approximations technique (43) if it is necessary.

(iii) Weighted Mean Diffusion Coefficients

Crank (40) has shown that, using equation (2.24), D(c) is much more accurately obtained if a weighted mean expression is employed:

$$\bar{D}_s = p \cdot C_o^{-p} \int_0^{C_o} c^{p-1} D(c)\, dc \quad \ldots.(2.30)$$

$$\bar{D}_d = q \cdot C_o^{-q} \int_0^{C_o} (C_o - c)^{q-1} D(c)\, dc \quad \ldots.(2.31)$$

where p and q represent the weighting values for sorption and desorption respectively. It has been found that p = 1.67 and q = 1.85 for systems

in which D increases with increasing c (40), and p = 1.85 and q = 1.67 for those in which D decreases with increasing c (23).

(iv) Other Procedures

The above methods are the ones usually employed for sorption-kinetics analysis, though several others have occasionally been used. Lin Hwang (79) employs a procedure when D can be expressed in the form $D(c) = D_{c=o}\ (1 + \alpha c + \beta c^2 + \ldots)$ which is readily amenable to computational analysis. However, this method breaks down if the concentration dependence of D is too great. Prager (102), Fujita and Kishimoto (56), and Barrer and Brook (16) have all used alternative procedures which are described in more detail by Crank (38).

2.4 Thermodynamics of Vapour Sorption by Polymers

2.4.1 Free Energy, Heat and Entropy of Dilution

The dependence of the heat and entropy of dilution on concentration and temperature yields information regarding the sorption process. The free energy of dilution ($\Delta\bar{G}_A$) is defined as the change in free energy on transferring, isothermally and reversibly, one mole of penetrant from pure liquid to an infinite amount of polymer-penetrant mixture at a given composition. Thus

$$\Delta\bar{G}_A = RT \ln (p/p_o) \qquad \ldots.(2.32)$$

where p is the vapour pressure in equilibrium with the mixture and p_o is the saturated vapour pressure at the same temperature. The corresponding heat ($\Delta\bar{H}_A$) and entropy ($\Delta\bar{S}_A$) of dilution are then given by

$$\Delta\bar{H}_A = \left[\frac{\partial\ (\Delta\bar{G}_A/T)}{\partial\ (1/T)}\right]_{P,C} = R\left[\frac{\partial\ (\ln p/p_o)}{\partial\ (1/T)}\right]_{P,C} \qquad \ldots.(2.33)$$

$$\Delta\bar{S}_A = -\left[\frac{\partial\Delta\bar{G}_A}{\partial\ T}\right]_{P,C} = -R\left[\ln (p/p_o) + T.\ \frac{\partial\ \ln\ (p/p_o)}{\partial\ T}\right]_{P,C} \qquad \ldots.(2.34)$$

where P is the hydrostatic pressure on the mixture phase. In the experiments used in the present investigation P = p, the pressure of vapour in equilibrium with the mixture.

2.4.2 Clustering Theory

Penetrant clustering within the polymer matrix is a common

phenomenon for the sorption of non-solvents and poor solvents in the polymer. This implies that penetrant-penetrant interactions are much stronger than those of penetrant-polymer (106).

Zimm (137, 138) proposed a model for this type of system which is based on the statistical mechanics of fluctuations, such that

$$\frac{G_{AA}}{V_A} = -(1 - \phi_A) \cdot \left[\frac{\partial\,(a_A/\phi_A)}{\partial\, a_A}\right]_{P,T} - 1 \qquad \ldots.(2.35)$$

where G_{AA} is the penetrant cluster integral, and V_A, ϕ_A and a_A are respectively the partial molar volume, volume fraction and vapour activity of the penetrant.

G_{AA}/V_A can be taken as a measure of the tendency of the penetrant to cluster within a given mixture and is -1 for random mixing, < -1 for sorption at specific sites and > -1 for clustering of penetrant. $\phi_A\, G_{AA}/V_A$ is the mean number of penetrant molecules in excess of the mean concentration of penetrant molecules in the neighbourhood of a particular penetrant molecule.

Starkweather (119) obtained similar expressions for the mean number of penetrant molecules around a particular penetrant molecule, such that

$$\frac{\phi_A\, G_{AA}}{V_A} = (1 - \phi_A) \cdot \left[\frac{\partial \ln \phi_A}{\partial \ln a_A}\right]_{P,T} - 1 \qquad \ldots.(2.36)$$

$$\frac{\phi_A\, G_{AB}}{V_A} = -\phi_A \left[\frac{\partial \ln \phi_A}{\partial \ln a_A}\right]_{P,T} - 1 \qquad \ldots.(2.37)$$

where $\phi_A G_{AB}/V_A$ is the excess mean number of penetrant molecules around a given polymer molecule.

2.5 Molecular Theories of Diffusion

The most widely used theories have been reviewed previously (75) and hence only a brief mention will be given here. Barrer's zone theory (13, 15) postulates that penetrant diffusion in polymers takes place due to the prior formation of activated zones which arise from the normal fluctuations of the thermal energy of the system. The

activation energy is shared by both the penetrant and surrounding polymer segments so that a "hot" zone is created which has a large number of degrees of freedom available for storage of the activation energy.

The free volume theory (75, 85) postulates that the principal energy barrier to diffusion is that of hole formation. The probability of a penetrant molecule undergoing a unit diffusion step is related to the probability that an element of free volume greater than some critical size is located in the near neighbourhood of the penetrant molecule. This means, in practice, the co-operative motion of several polymer segments is needed to create a hole large enough for diffusion and this is a common feature of both theories.

CHAPTER 3

EXPERIMENT

3.1 Materials

3.1.1 Poly ([c.ℓ.] - dimethylsiloxane) (PDMS)

Sheets of [c.ℓ.] - PDMS were supplied by Dow Corning Ltd. and were prepared by press-curing PDMS gum, containing 0.143 methylvinyl-siloxane units per 100 dimethylsiloxane units, with 1% by weight 2,4-dichlorobenzoyl peroxide. The samples were cured at 115°C for 5 hours and post-cured at 200°C for 4 hours. Traces of low molecular weight material were removed by refluxing the sample with ethyl acetate in a sohxlet apparatus followed by outgassing under high vacuum for 24 hours.

3.1.2 Poly (vinyl acetate) (PVAc)

PVAc of molecular weight 1.5 million was supplied by Shawinigan Resins Corp. (grade Gelva V800), and cast into films on a clean mercury surface from a 5% acetone solution. The films were leeched in distilled water at 50°C for 7 days to remove low molecular weight material and outgassed under high vacuum at room temperature for 48 hours. It was necessary also to outgas the films under high vacuum for 48 hours at temperatures of about 60°C.

3.1.3 Poly ([c.ℓ.] - dimethylsiloxane-g-vinyl acetate) P(DMS-g- VAc)

The graft copolymers were prepared by mutual irradiation of [c.ℓ.] - PDMS which was swollen with vinyl acetate monomer. The irradiation was carried out at the ^{60}Co γ-radiation unit of the Nuclear Technology Department, which produced radiation of intensity 0.8 Mrad $hr.^{-1}$. Irradiation was performed at room temperature and under high vacuum since air acted as an inhibitor to grafting. After irradiation the sample was refluxed with ethyl acetate in a sohxlet apparatus until constant weight was attained, about 6-7 days. It was assumed that the reflux process removed any loosely-bound homopolymer from the system and hence any remaining PVAc in the sample was grafted to the PDMS matrix. Finally the sample was outgassed under high vacuum for 48 hours at room temperature.

Vinyl acetate monomer was supplied by Hopkin & Williams Ltd. and contained an inhibitor, quinol, which was removed by shaking the monomer with a 1% sodium hydroxide solution, washing three times with

distilled water and finally drying over anhydrous calcium sulphate. The monomer was then used immediately or stored at 5°C in an attempt to reduce any possible polymerisation of the monomer.

3.1.4 [c.ℓ.] - Poly (3,3,3-trifluoropropylmethylsiloxane) (FMS)

Sheets of [c.ℓ.] - FMS, as supplied by Dow Corning Corp., were crosslinked with 2,5-bis (t-butylperoxy) 2,5 - dimethylhexane and post-cured at 150°C for 1 hour. They were refluxed in a sohxlet apparatus for 24 hours with ethyl acetate and outgassed for 24 hours under high vacuum.

Some physical properties of the polymers are given in Table 3.1.

Table 3.1

Density (ρ, $g.cm^{-3}$), Glass Transition Temperature (T_g, °C) and Melting Point (T_m, °C) for the Poly(siloxanes), PVAc and the Graft Copolymers.

Polymer	ρ	PDMS T_g	PDMS T_m	PVAc T_g
PDMS	0.976	- 123	- 44	-
PDMS-g-3% PVAc	0.985	- 123	- 44	-
PDMS-g-9% PVAc	0.997	- 123	- 45	31
PDMS-g-16% PVAc	1.016	- 123	- 46	33
PDMS-g-21% PVAc	1.033	- 122	- 46	32
PDMS-g-44% PVAc	1.081	- 122	- 48	32
PVAc	1.193	-	-	33
FMS	1.019	- 67	-	-

Densities were determined by the water displacement method. T_g and T_m data were measured on a Du Pont 990 Thermal Analyser.

3.1.5 Penetrant Vapours

(i) Water Vapour

Distilled water was introduced into a pear-shaped flask and connected to vacuum for a short while to remove the surrounding atmosphere. The water was then frozen with liquid nitrogen and the

frozen ice pumped for about an hour until most of the trapped air had been removed. The ice was finally allowed to thaw, being occasionally connected to vacuum to remove any air released. This procedure was then repeated four or five times and this was considered sufficient to remove all the air present.

(ii) Methanol, Ethanol and 2-Propanol Vapours

These liquids were also introduced in pear-shaped flasks and outgassed by the "freeze-thaw" method described above for water vapour.

3.2 Apparatus

3.2.1 The Pumping Systems

Two separate but similar pumping systems were used. One was used for the microbalance-sorption system and the other for the permeability, grafting and spring-sorption apparatus.

The essential features of each system are shown in Figure 3.1, the design being standard in outline.

A three-stage mercury diffusion pump (A), Edwards two-stage rotary oil pump (B) and liquid nitrogen trap (C) produced an ultimate vacuum of about 10^{-6} mm Hg. The water supply to the mercury pump (A) was controlled such that the power to the pump was automatically switched off if the water flow was stopped. This prevented mercury from distilling into the apparatus.

An Edwards Pirani gauge head (D) was attached to the "hivac" line as a check on leak and outgassing rates. A mercury manometer (E) was connected to the "hivac" line of the permeability system for calibration of pressure transducers. As mercury vapour is corrosive to the vacuum microbalance, a piece of gold foil (F) was placed in the "hivac" line and the mercury present in the system was restricted to the mercury diffusion pump.

3.2.2 The Permeability System

The system is illustrated in Figure 3.2.

(i) The High Pressure Side

Vapour was supplied from a liquid reservoir (R) to which a 500 cm^3 buffer volume (A) was attached. Both were accurately thermostatted in a water bath to within $\pm$ 0.05°C. The bath was heated by three 300 W

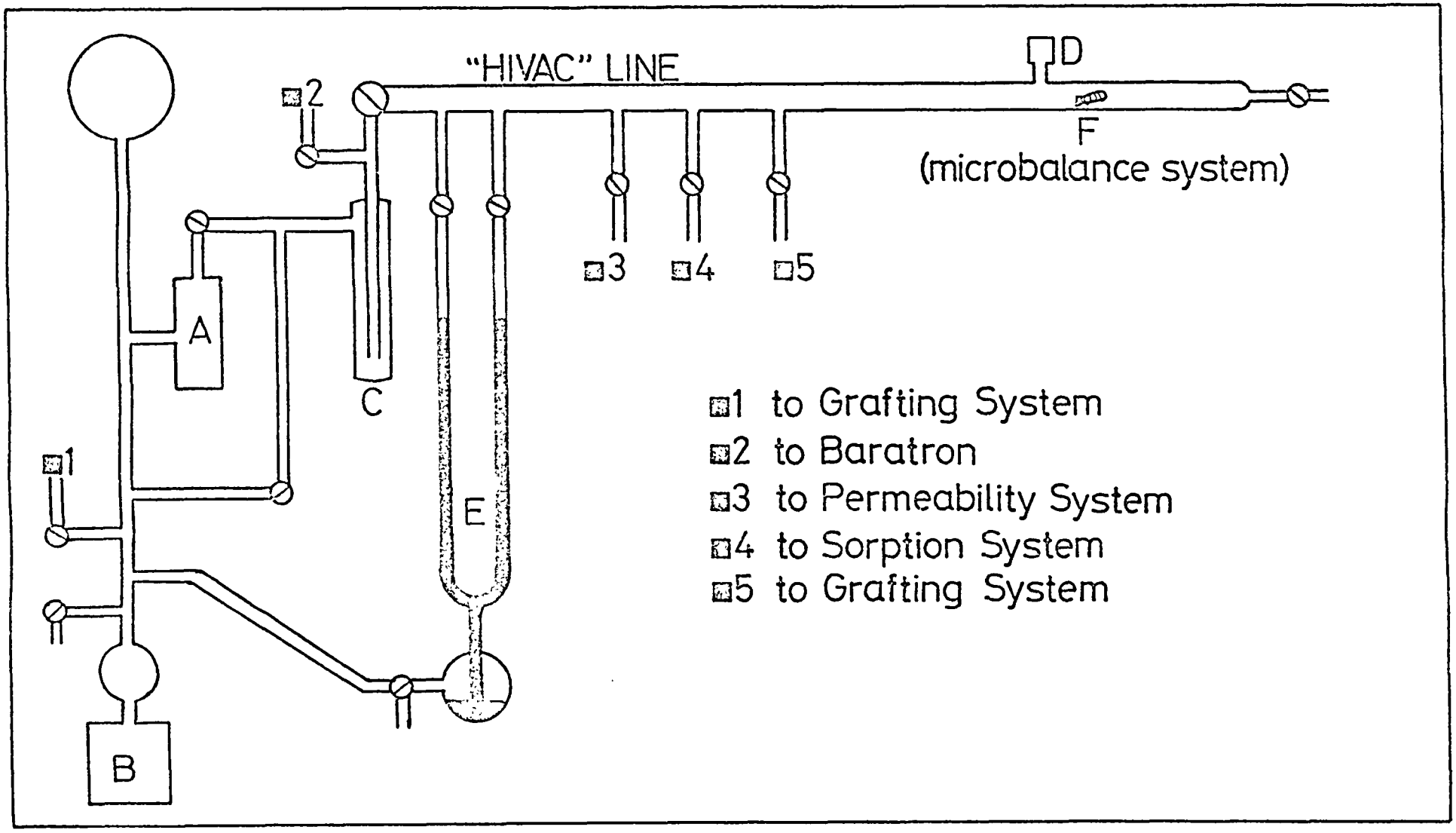


FIGURE 3.1 PUMPING SYSTEMS

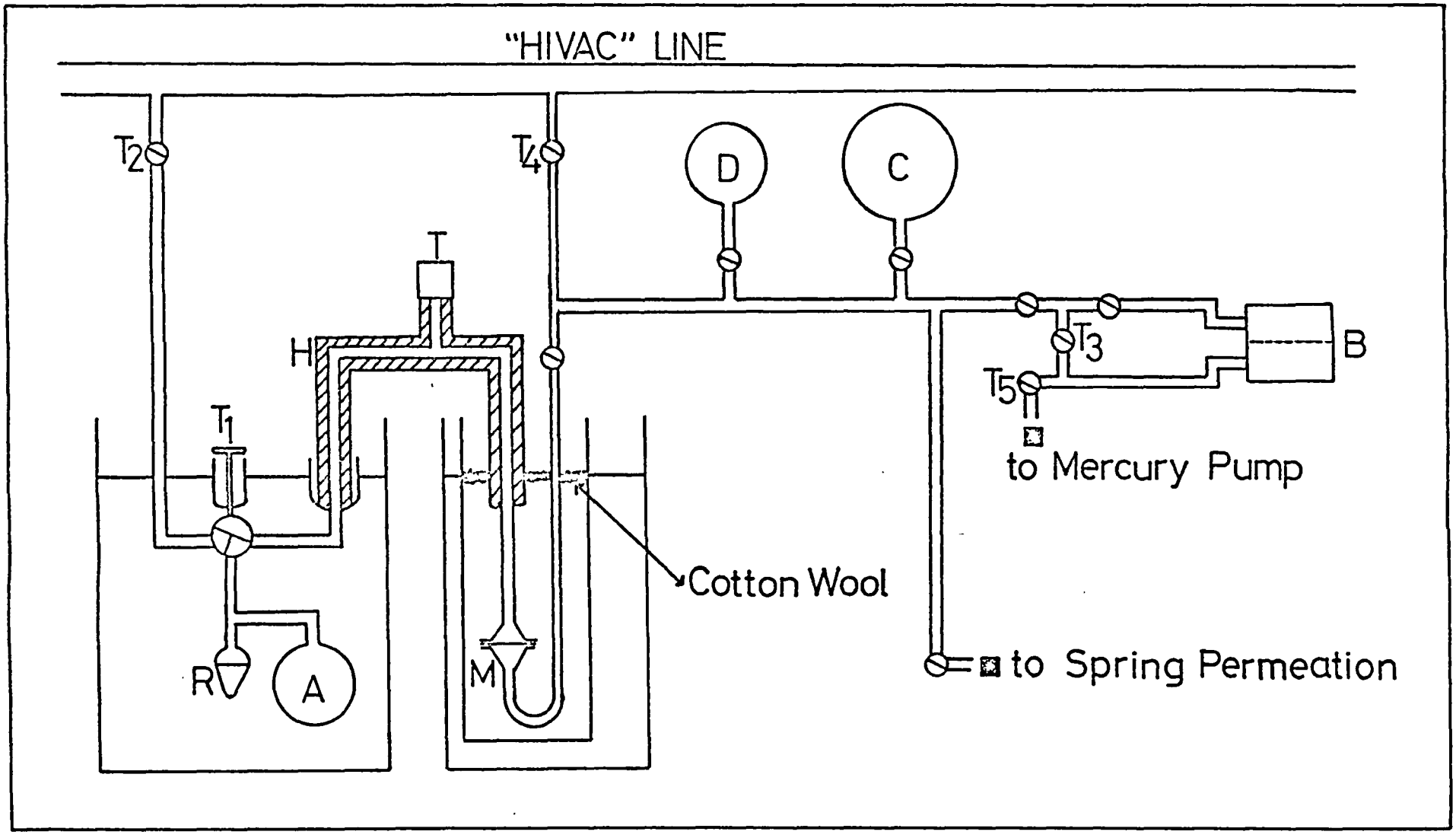


FIGURE 3.2 PERMEABILITY SYSTEM

"red-hot" heaters and cooled, when necessary, by circulating tap water through a metal tubular coil immersed in it. The three-way underwater tap (T_1) was specially made by Springhams Ltd. and designed such that the membrane (M) could be connected to the reservoir (R) or to the "hivac" line. The "ingoing" vapour pressure was measured by a stain-gauge pressure transducer (T) (0-15p.s.i. Absolute, Bell & Howell Ltd.) operated from a stable 10V D.C. supply. The voltage signal (in millivolts) from the transducer was measured by a sensitive potentiometer and was directly proportional to the pressure.

When the reservoir (R) and membrane (M) were above room temperature heating tape (H) was used to prevent condensation of vapour in the connecting glassware.

(ii) Low Pressure Side

The "downstream" pressure of the vapour permeating through the membrane (M) was measured directly by a capacitance manometer (Baratron) (B) (MKS Baratron Pressure Meter, Series 90; M.K.S. Instruments Inc.) which had a pressure range of 10^{-5} to 1 mm Hg. The pressure is sensed by a thin metal diaphragm clamped under pressure between two ceramic insulating discs which support the capacitance electrodes. The signal is derived from a bridge circuit of which the capacitances of the reference and measuring sides form two parts. The diaphragm is displaced by the difference in pressure on each side and this is the measured signal. In practice, one side was always connected directly to the mercury pump so that the measured pressure was effectively that of the absolute pressure. The measured pressure is independent of the nature of the vapour (or gas) and of the temperature of the Baratron. The sensing head of the Baratron was maintained at $50^{\circ}C$ so as to prevent the introduction of mercury vapour by thermal convection. Tap (T_3) cross-connected both sides of the head for zeroing purposes.

Two buffer volumes (C,D; 4ℓ and 2ℓ) were connected to the measuring side of the Baratron and were used with high flux rates to maintain the pressure within the range of the Baratron.

(iii) Membrane Holder and Diffusion Cell

The membrane holder is illustrated in Figure 3.3(a). The membrane (M) was gripped between two circular steel plates (P), each

FIGURE 3.3(a)

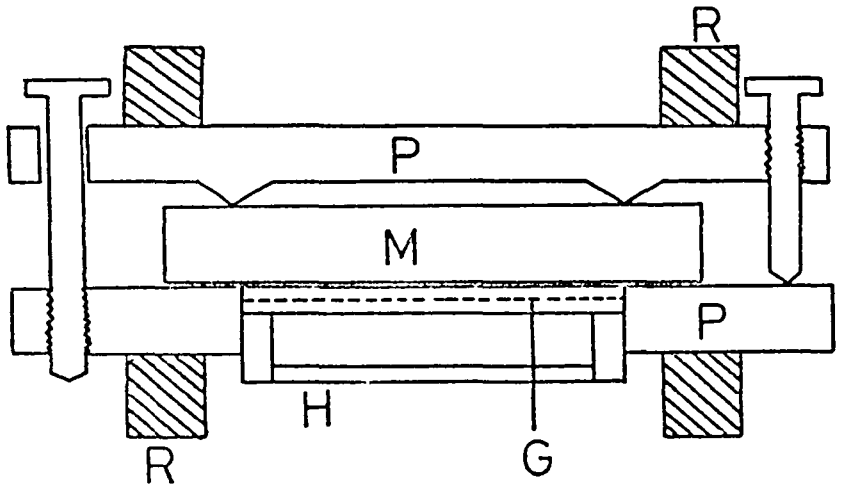


FIGURE 3.3(b)

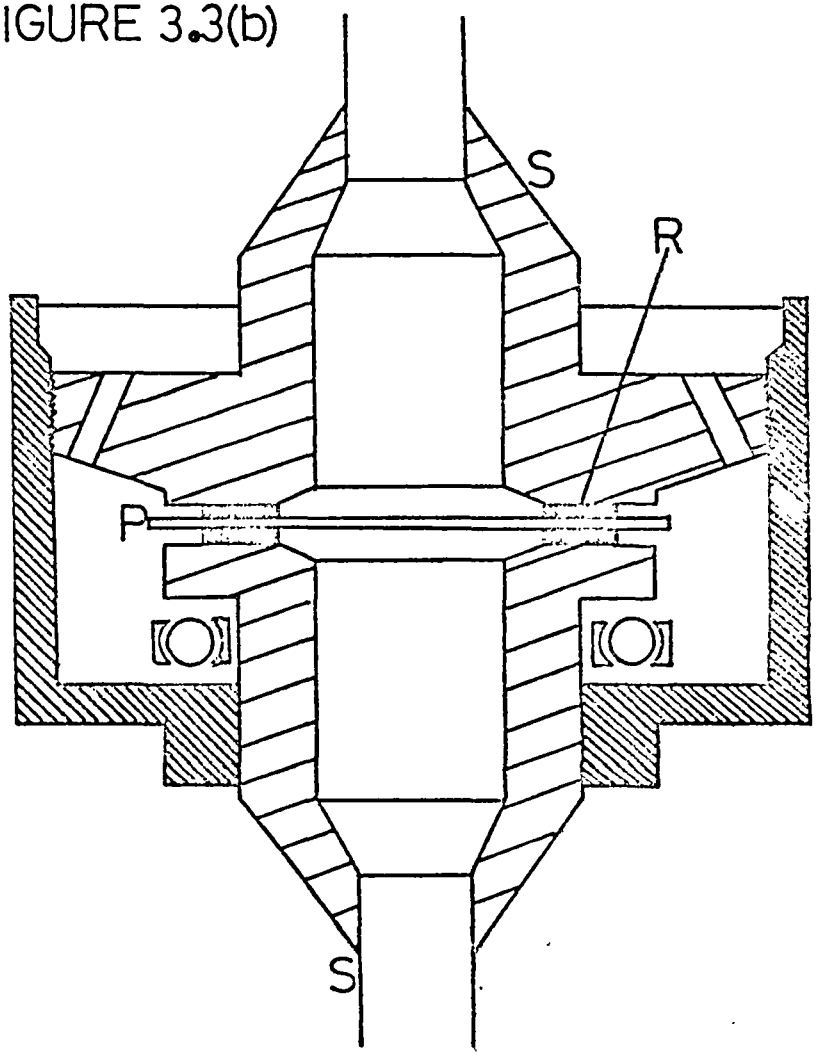


FIGURE 3.3 MEMBRANE HOLDER(a) & DIFFUSION CELL(b)

having a central, circular hole of the same well-defined diameter. The membrane was supported on the "downstream" side by a thin wire gauze (G) resting on a metal ring (H) screwed into the hole of one of the plates (P). A piece of hardened filter paper prevented the membrane from being cut by the gauze. The plates were screwed together by six screws so that bulging and distortion of the membrane could be eliminated as much as possible.

The membrane holder was held in a standard diffusion cell (14) as shown in Figure 3.3(b). The holder was separated from the steel tubes (S) by natural rubber gaskets (R) which had holes cut to the diameter of the holes of the plates (P). The gaskets had been refluxed with ethyl acetate to remove any impurities. Mercury was poured into the cell to ensure a gas-tight seal.

The diffusion cell was contained in a copper tube which was placed in a water bath controlled to within $\pm$ 0.05°C.

3.2.3 Spring-Sorption Apparatus.

The apparatus is shown in Figure 3.4. It consists of a calibrated quartz spring-balance (82) which was used for penetrant uptakes greater than 0.2% of the dry weight of polymer. The vapour source (R) was connected to the balance by a three-way tap (T_1) and heating tape (H) wound round the connecting glass tubing. The vapour pressure of penetrant was measured by a pressure transducer (T) similar to that described in Section 3.2.2(i).

The polymer sample (P) was suspended from the quartz spring (S), obtained from Thermal Syndicate Ltd., by a piece of platinum wire.

The spring was enclosed within a vertical, cylindrical glass envelope (C) immersed in a water bath which was thermostatted to within $\pm$ 0.05°C. The thermostat had two plate glass-sides so that the length of the spring could be measured by a cathetometer. The spring was calibrated at several temperatures by hanging on known weights.

3.2.4 Microbalance-Sorption Apparatus

An electronic vacuum microbalance (Model 4102, Sartorius-Werke GMBH) was used for penetrant uptakes of less than 0.2% of the dry polymer. The balance, illustrated in Figure 3.5(a), was of the beam type and was capable of measuring to within 1 μg. The polymer sample (M)

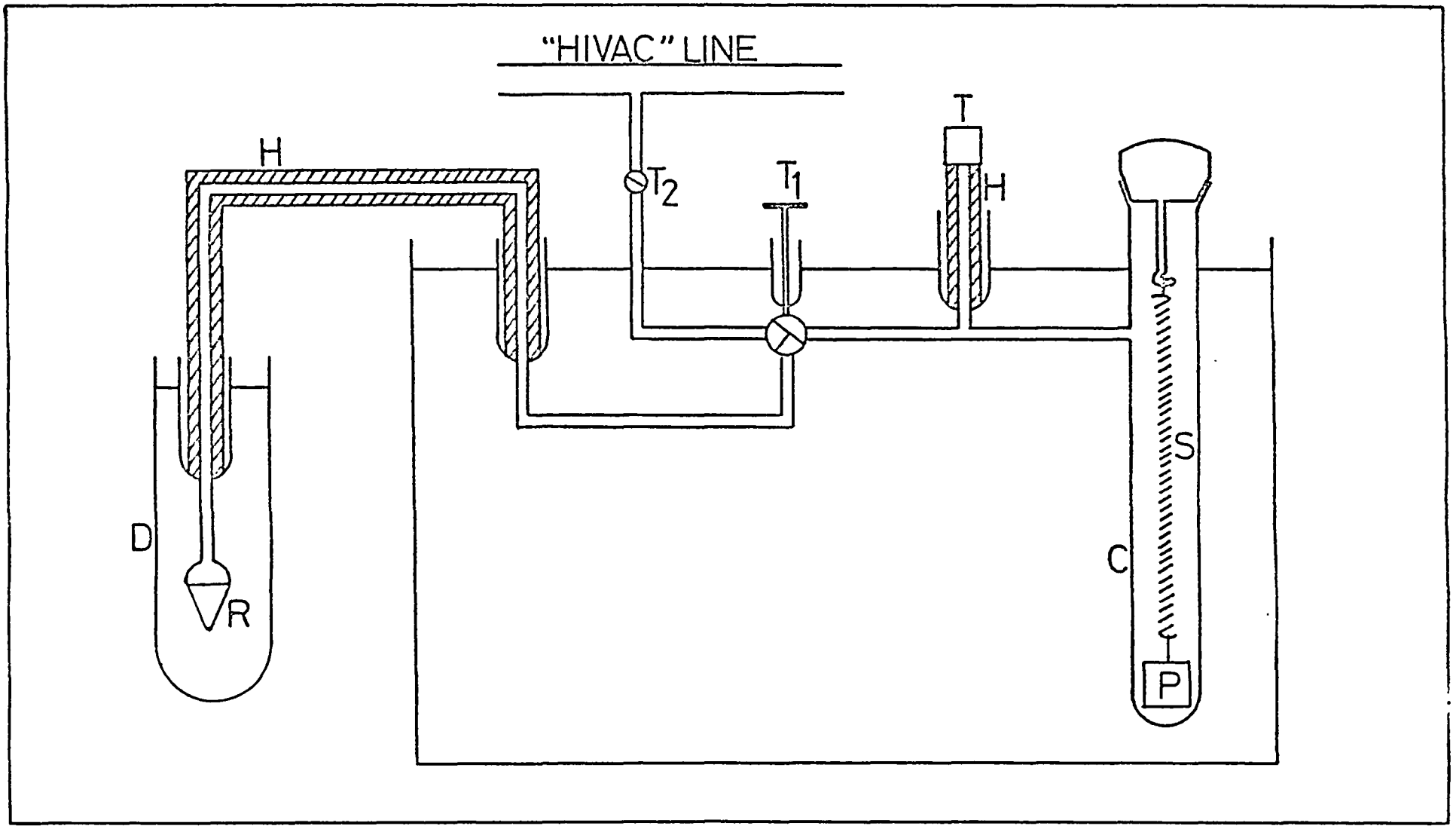


FIGURE 3.4 SPRING-SORPTION APPARATUS

FIGURE 3.5(a)

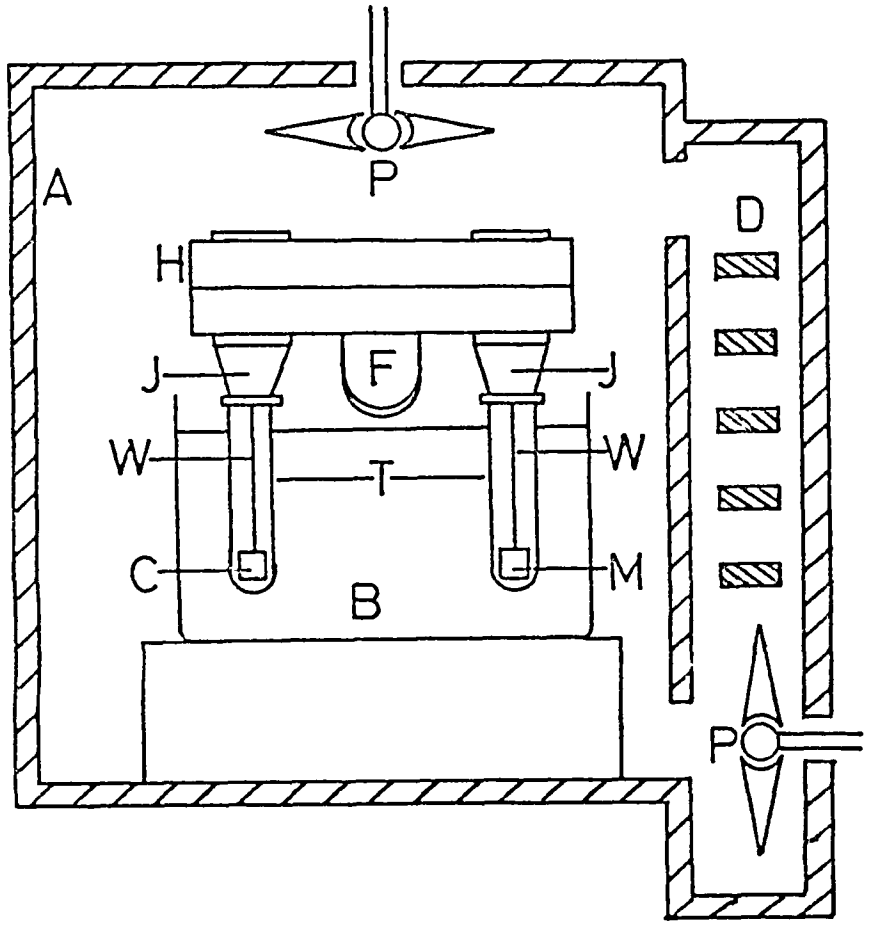


FIGURE 3.5(b)

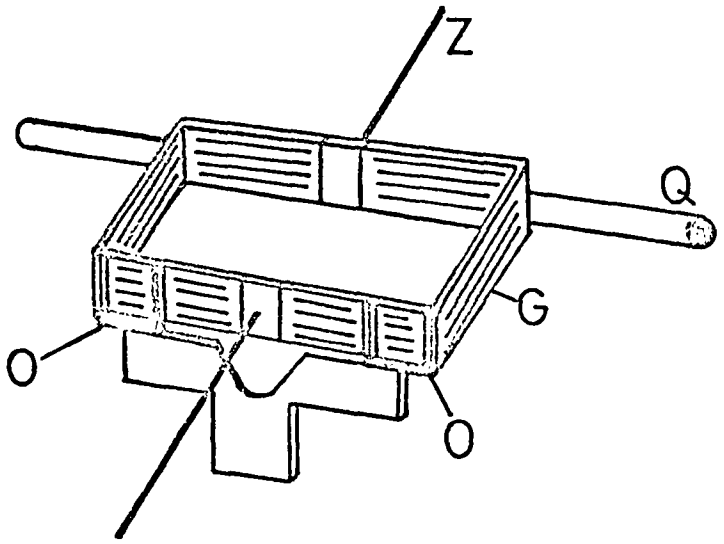


FIGURE 3.5 SARTORIUS MICROBALANCE: OVERALL & BEAM ASSEMBLY

and metal counterweight (C) were hung from the beam via platinum wires (W) and aluminium stirrups. The downhangers were contained inside glass tubes (T) which were connected to the stainless steel case (H) by cone-socket joints (J). The glass tubes (T) were sprayed with metal salts and earthed to facilitate the removal of static electrical charges from the system. A metal flange (F) connected the balance to the remainder of the apparatus via a flexible, bellows-type metal coupling.

The weighing principle depended upon automatic electrical compensation of a torque moment induced by the load. Figure 3.5(b) shows the beam (Q), a quartz tube, attached to a moving coil (G) supported by a torsion wire suspension (Z). A permanent magnet (not shown) inside (G) supported an oscillated coil (O) through which high frequency A.C. was passed. When the beam deviated from the horizontal position the high frequency field from the coil (O) induced an H.F. signal in the coil (G) which was rectified, phase-adjusted, amplified and returned to (G) as a compensating current. Consequently the balance was a continuous, null-point instrument with a D.C. output which was measured on a Honeywell strip chart recorder.

It was found that there was a shift of the base-line of the balance with the relative pressure of water vapour, and that this was independent of temperature. Since the base-line shifts were found to take about 15 minutes, it was concluded that sorption of the water vapour occurred somewhere on the weighing mechanism. A single "blank" isotherm was found to be sufficient for all sorption experiments (Figure 3.6) and water uptakes could be obtained from the measured weight changes by applying "blank" and buoyancy corrections.

The balance was supported by wall-brackets and enclosed within a large air thermostat (A), as shown in Figure 3.5(a), which was constructed of "Syndanio" board with a plate-glass window. A circulating air channel (D) contained five 500W heaters, some of which were controlled by a Pye Ether electronic relay and a mercury contact thermometer which was contained in the main body of (A). Air circulation was provided by two fans (P). It was found that, above room temperature, there existed a temperature gradient within (A) in the vertical direction only, which amounted to 8-10^{o}C when the average temperature was about 60^{o}C. This ensured that the balance head was always at a slightly higher temperature than the rest of the system and

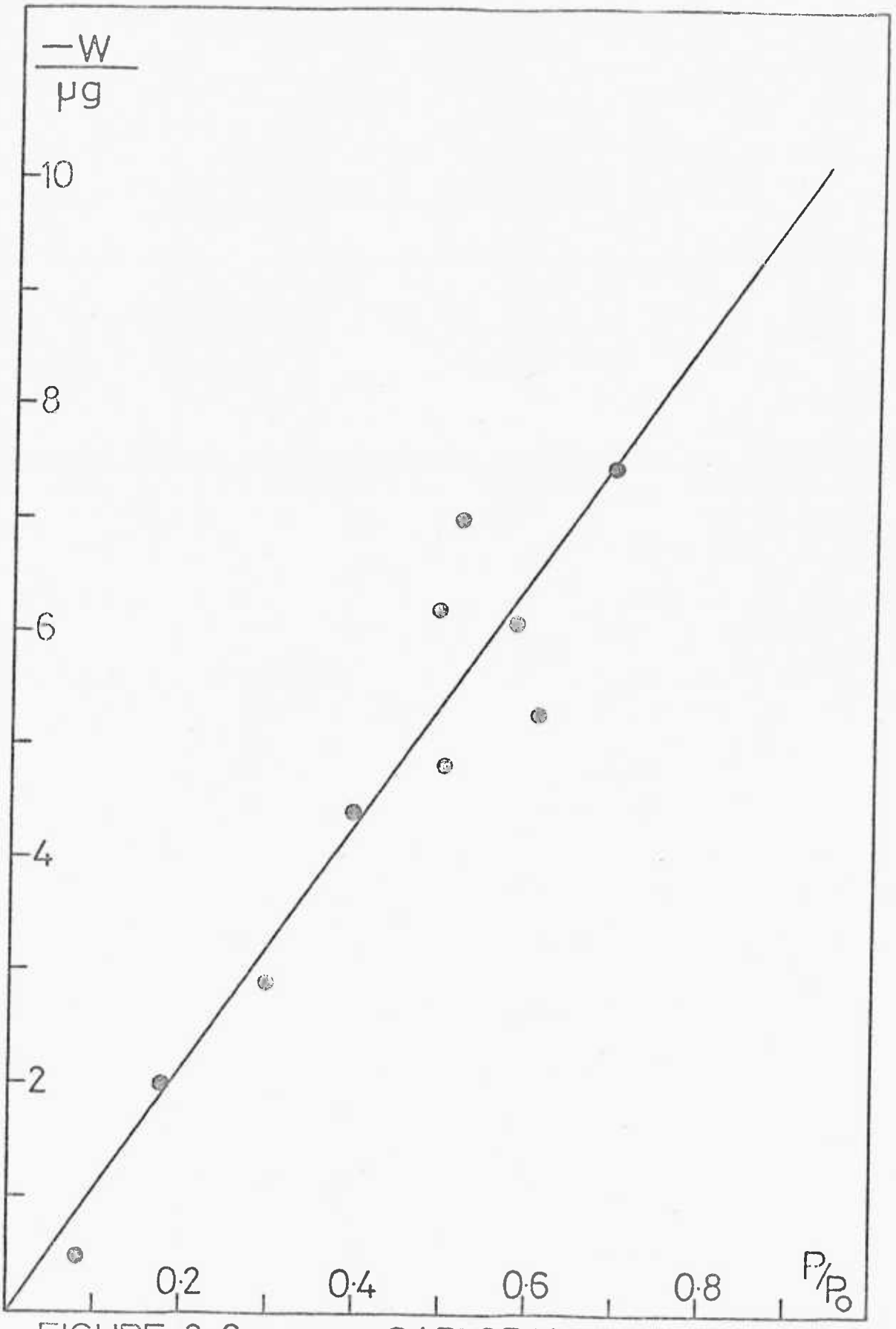


FIGURE 3.6 SARTORIUS MICROBALANCE
BLANK ISOTHERM FOR WATER VAPOUR

prevented any possible condensation of water vapour on the beam.

The lower portions of the tubes (T) in Figure 3.5(a) were immersed in a water bath (B) which was connected to an external thermocirculator (Churchill Instrument Co.) which enabled the polymer to be thermostatted to within $\pm$ 0.1°C in the range 20-60°C.

Water vapour pressures were measured by a pressure transducer as described in section 3.2.2(i) with the output recorded directly on a Honeywell strip chart recorder.

The rest of the apparatus was similar to that of the spring-sorption apparatus (Section 3.2.3) except that tap (T_1) and reservoir (R) were immersed in an external water bath thermostatted to within $\pm$ 0.05°C. A one litre buffer volume was connected to the reservoir (R) and heating tape wound round the glassware connecting the balance to the water bath.

3.2.5 Grafting System

The system is illustrated in Figure 3.7. The polymer sample (P) was contained in the vessel (A) and the monomer in (B). Each vessel was attached to the vacuum line by cone-socket joints (J_1, J_2) for easy removal. A long tube (C) of 3 mm bore was used as a measure for the monomer to be used in the particular experiment. The apparatus could be evacuated either by the mercury diffusion pump (T_6) or the rotary oil pump (T_5) and the cold trap (D) ensured that all vapours were condensed and did not interfere with the remainder of the apparatus.

Taps (T_2, T_3, T_4) and joints (J_1, J_2) were lubricated with silicone high vacuum grease since monomer had a tendency to attack hydrocarbon grease when left in contact for long periods. The joint and tap (T_1) of the polymer vessel were lubricated with apeizon 'T' vacuum grease as silicone grease tends to crosslink when irradiated.

3.3 Procedure

3.3.1 Steady-State Permeability (Figure 3.2)

After assembly, the diffusion cell containing the membrane (M) was tested for vacuum tightness and then connected to the apparatus. The membrane was outgassed at temperatures rising to 60°C until the pressure was less than 10^{-5} mm Hg and then left at the required temperature for 24 hours to ensure thermal equilibrium.

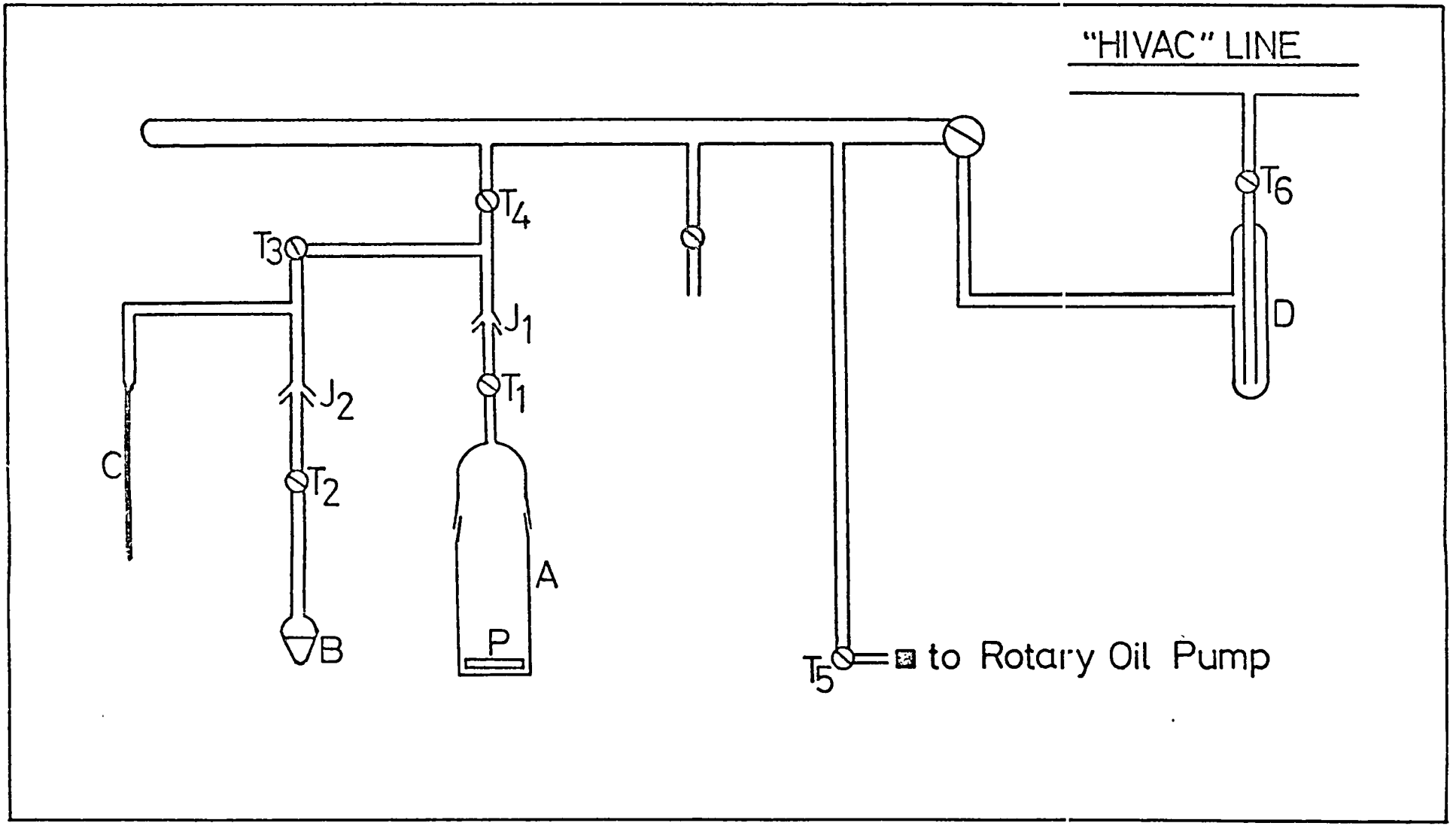


FIGURE 3.7 GRAFTING SYSTEM

The Baratron head was pumped to a pressure of 10^{-5} mm Hg and then baked at about 140°C for 24 hours under high vacuum and finally left to come to the working temperature of 50°C. Throughout the baking, both sides of the Baratron were connected via tap (T_3) and were left so during the quadrature minimisation and meter zeroing. Tap (T_3) was then closed for the remainder of the experiments whilst the reference side of the Baratron was connected to the mercury pump via tap (T_5).

Taps (T_2, T_4) were closed and water vapour admitted to the membrane via tap (T_1). The "ingoing" pressure of water vapour was measured by the pressure transducer at the beginning of the experiment and periodically, to ensure that it remained constant throughout.

The "downstream" side of the membrane was initially evacuated. The pressure build-up was followed as a function of time from when the vapour was admitted to the membrane. Once the steady-state of flow was established, the pressure as indicated by the Baratron was recorded as a function of time. The "downstream" pressure should never exceed 0.5% ingoing pressure since this affects the permeation characteristics of the experiment. When this limit was reached, tap (T_4) was opened and the water vapour pumped away. After about ten minutes tap (T_4) was closed and the pressure measured as before.

The membrane area was calculated by measuring the diameter of the hole of the membrane holder with vernier calipers. The membrane thickness was measured by a micrometer-screw gauge after the membrane had been clamped in the holder.

Sample calculations and estimations of errors for all experimental techniques are given in Appendix 8.3.

3.3.2 Spring-Sorption (Figure 3.4)

The sample (P) was outgassed at about 60°C until the pressure was less than 10^{-5} mm Hg and the length of the spring (S) was constant. After thermal equilibrium had been established at the required temperature the initial length of the spring (S) and the transducer output (T) were determined. Tap(T_2)was closed and tap (T_1) adjusted to isolate the liquid reservoir, which was brought to its required temperature by surrounding it with water in a Dewar flask (D). Vapour was admitted to the polymer and the sample section isolated at tap (T_1)

after a few minutes. A constant spring length and transducer output indicated that equilibrium had been attained. The reservoir (R) was then brought to an appropriate temperature so as to admit a further charge of vapour to the polymer. After equilibration the procedure was repeated until the complete sorption isotherm was established.

3.3.3 Microbalance-Sorption (Figure 3.5(a))

The sample (M) and counterweight (C) were outgassed at about 60°C until the pressure was less than 10^{-5} mm Hg. The balance head (H) was maintained at a temperature 10°C higher than that of the sample in order to reduce the magnitude of the blank correction as described in Section 3.2.4. Some water vapour ($\sim$ 3 cm Hg) was admitted to the balance to facilitate the removal of static charges and eventually pumped away. The sample and balance were then ready for operation at the required temperature.

The zero output of the pressure transducer and balance were recorded on the Honeywell chart recorders. The reservoir (R) was then connected to the balance via tap (T_1) and the system left to come to equilibrium as indicated by there being no weight change on the recorder. The balance was connected to vacuum via tap (T_1) to outgas the polymer sample. This served as a check on the initial and final outputs of the balance which had a slight tendency for baseline drift during an experiment. During the desorption process, the temperature of the bath containing the reservoir (R) was adjusted to a new value in readiness for the admission of the next charge of vapour. The process was repeated several times to complete the sorption isotherm.

The counterweight was a piece of copper wire (density 8.93 g. cm^{-3}) which did not sorb water. Thus buoyancy corrections could not be eliminated by symmetry and had to be applied to the observed weight changes of the balance.

The above experimental procedure was also applied when sorption-kinetic data were required. For both sorption- and desorption-kinetics, the recorder trace of weight increase or decrease against time yielded a plot of (M_t/M_∞) against $t^{\frac{1}{2}}$, where M_t, M_∞ (μg) were the weight increase (decrease) at time t and at equilibrium respectively. In all cases, buoyancy and blank corrections were applied where necessary.

3.3.4 Preparation of Graft Copolymers (Figure 3.7)

The sample (P) was refluxed with ethyl acetate for 24 hours in a sohxlet apparatus and outgassed at room temperature until the pressure was less than 10^{-5} mm Hg. The sample (P) was then placed in the vessel (A) and connected to vacuum overnight. The vessel (A) was isolated at tap (T_1) and the monomer, which was contained in vessel (B), outgassed by the "freeze-thaw" method as described in Section 3.1.5(i). The required amount of monomer was condensed in (C) whilst tap (T_3) was closed and finally tap (T_2) was closed so as to isolate the dose of monomer. With tap (T_4) closed the monomer was admitted to the polymer sample (P) via taps (T_3) and (T_1). The vessel (A) meanwhile was cooled with liquid nitrogen so that all monomer was transferred to the irradiation vessel. The sample vessel (A) was then isolated at tap (T_1), removed from the apparatus (J_1), left overnight to allow equilibration of monomer with the polymer and irradiated in the ^{60}Co γ-radiation source at room temperature for the appropriate length of time (usually 2-3 hours).

After irradiation, the grafted polymer was outgassed for 24 hours and the weight increase noted. It was refluxed in ethyl acetate in a sohxlet apparatus to constant weight (6-7 days) and finally weighed to obtain the amount of Poly(vinyl acetate) that was grafted to the polymer sample.

CHAPTER 4

DIFFUSION IN HETEROGENEOUS MEDIA

4.1 Literature Survey

Crystalline and filled polymers, block and graft copolymers, blends and laminae constitute types of heterogeneous polymer systems. Of these the laminates are the most amenable to exact treatment and the transport parameters of the laminate can be related to those of the individual homopolymer components. With filled and crystalline polymers the filler and crystalline phases are generally regarded as impermeable. The immediate effect of these disperse phases is to decrease the area of cross-section available for diffusion and to increase the diffusion path length. Much of this work has been reviewed elsewhere (12) and the main objective of this Chapter is a review of studies involving block and graft copolymers and polymer blends. The study of diffusion in these systems is not extensive but has been increasing more recently as commercial exploitation of these materials has been sought. In most instances, however, only basic results have been reported and little attempt has been made to interpret them in terms of models which have been proposed to predict diffusion behaviour in heterogeneous systems.

4.1.1 Copolymers of Poly(ethylene) (48, 60, 67, 72, 97, 107, 118, 121)

The diffusion of gases and vapours in poly(ethylene) has been the subject of a large number of investigations and is well characterised. As a result of this and also because of its widespread commercial use the diffusion properties of poly(ethylene) graft copolymers have also been extensively studied.

It is reported (48, 67, 72, 97) that the permeability of both gases and vapours in low-density poly(ethylene) grafted with poly(styrene) decreased as the amount of grafting increased to a region of 20-30% graft. To account for this the authors postulate that grafting, since it occurs in the amorphous regions, reduces the "free volume" available for diffusion and reduces the segmental mobility of the poly(ethylene) chains. However no-one (48, 67, 72, 97) defines the term "free volume" and it seems that they interpret this as the volume fraction of amorphous poly(ethylene) phase and not free volume in the accepted sense. Although the microstructure of the graft copolymers is not given it must be

assumed that two phases exist within the amorphous regions. It has been found that the activation energy of permeation changes with poly(styrene) content (67, 72, 97). As poly(styrene) is soluble in styrene monomer the grafted chains in the domains ought to be set in an expanded configuration and hence play a part in the diffusion process.

When the amount of poly(styrene) in the graft copolymers is increased above 30%, the permeability of the graft copolymers goes through a minimum and starts to rise as the poly(styrene) content is increased still further. This has been interpreted as due to a change in the crystallinity of the poly(ethylene) phase (62, 72, 97) caused by the swollen grafted poly(styrene) chains penetrating and disrupting some of the crystalline regions. This opens up new regions which are available for permeation (67, 72) and hence there is a net increase in permeability of the system. It has been reported (48) that this decrease in crystallinity occurs even up to 30% poly(styrene) content although to a lesser extent.

High-density linear poly(ethylene) shows similar behaviour to the low-density polymer except for a small increase of permeability with initial grafting. This has been interpreted (97) as due to a relaxation process accompanying the treatment of a highly crystalline polymer with a good swelling agent, i.e. styrene monomer. This has been reported previously for high-density poly(ethylene) and increases the amorphous content to some extent.

Further evidence of these structural changes on grafting poly(styrene) to poly(ethylene) (67) is given by density and thickness measurements. Up to 20% graft, film thickness remains constant and polymer density increases rapidly as the poly(styrene) fills the "free volume" of the amorphous regions. However above this graft content, the change in film thickness becomes pronounced and density only increases slowly, indicative of the disruption of the closely-packed crystalline regions.

When poly(ethylene) is grafted with poly(acrylonitrile) (72, 97), a slightly different situation arises since poly(acrylonitrile) is insoluble in its monomer. This means that when formed, the polymer has a tightly coiled, highly compact structure which can be considered impermeable as compared to poly(ethylene). As in the case of poly(styrene) graft copolymers there is initially a decrease in permeability as the poly(acrylonitrile) fills the "free volume" of the amorphous phase. However there is no upsurge in permeability above 30% graft content as

the tightly packed poly(acrylonitrile) chains can remain within the amorphous region without affecting the crystalline region. Hence the grafted polymer behaves as an impermeable filler, decreasing the overall permeability and the temperature dependence of permeation constant as the graft content increases.

Water vapour permeation has been carried out, to a limited extent, on various poly(ethylene) graft copolymers (60). Permeabilities, in general, of the graft copolymers were greater than for poly(ethylene) since the grafted polymers were more permeable to water vapour. A striking example is the poly(N-vinylpyrrolidone) graft copolymer which, being a hydrophilic material, shows an increase in permeability of three orders of magnitude.

The graft copolymers considered previously have all possessed a uniform distribution of graft polymer throughout the parent polymer (as far as this is possible in a semi-crystalline polymer such as poly(ethylene)). However graft copolymers have been prepared with a gradient of grafted polymer from one face of the membrane to the other (107, 118, 121).

A graded poly(2-vinylpyridine) graft copolymer was prepared from a uniform graft copolymer (118) by treatment with ethanol, keeping one face of the membrane continuously pumped. Water vapour permeabilities were greater for those membranes having a higher graft content at the ingoing face. In fact, due to the hydrophilic nature of the grafted polymer, both "along" and "against the gradient" permeabilities were greater than for pure poly(ethylene).

A large directional effect can be observed for the permeation of water vapour through poly(ethylene) films grafted with poly (vinyl alcohol) (107). Permeabilities against and along the gradient are always lower than for pure poly(ethylene) at low vapour pressures since the diffusion coefficient of water vapour in poly(ethylene) is about 18 times greater than in poly(vinyl alcohol). However, as the pressure increases, poly(vinyl alcohol) sorbs much more water vapour than poly(ethylene) (8700 times greater). This dominates the permeation process so that permeation along the gradient is enhanced and permeation along the gradient is 6 times greater than against the gradient.

Permeation of nitrogen and carbon dioxide through graded copolymers of poly(ethylene) grafted with poly(acrylonitrile),

poly(styrene), poly(vinyl acetate) and poly(vinyl alcohol) shows no directional tendencies at all (107, 121). Vapour transport through these copolymers does however show directional permeabilities. For example, the permeation of n-hexane is greater against the gradient of grafted polymer whilst the reverse is true of benzene transport (107). This has been explained by the authors (107, 121) by the difference of solubilities of the various polymers for the respective penetrants. Since gas solubilities in polymers tend to be very low, the dispersed polymers tend to act merely as impermeable fillers and hence no directional properties are to be found. n-Hexane, on the other hand, is a swelling agent for poly(ethylene) and a non-solvent for the grafted polymers (107) and benzene is preferentially a solvent for the grafted polymers. Hence the authors postulate that permeation rates are greater when along the gradient of the component for which the penetrant solubility is the greatest.

These qualitative observations have been given a more mathematical treatment by Rogers (121). He applied a distance dependence to solubilities whilst keeping D constant. This approach was tested using permeation data of methanol vapour in a graded poly(ethylene-g-5% vinyl acetate) copolymer and gave satisfactory agreement. The approach can be considered as one example of a more comprehensive treatment on directional diffusion in membranes (36). It has been indicated that, in general, different rates of permeation for each direction are expected if the diffusion coefficient depends upon both concentration and distance through the membrane. This is general for any membrane and graded membranes are special cases for which x-dependent diffusion coefficients are a natural consequence. If the concentration and distance dependences of diffusion coefficients can be separated, then there will be no directional effects. These dependences are usually not separable so that directional properties can be expected.

This explains all the previous results obtained for graded membranes. Permeation of gases in these membranes shows no directional characteristics as D is constant and hence there is only the x-dependence imposed by the grading process. This is the situation for which Rogers (121) postulated his analysis so that it can be seen that this treatment is very restricted. The diffusion coefficients of vapours are invariably concentration-dependent so that a combination

with the x-dependence imposed by the membrane forces directional properties upon the system.

4.1.2 Poly(dimethylsiloxane) (86, 105)

Block copolymers of poly(dimethylsiloxane) (PDMS) with poly(carbonate), poly(sulphone) or poly(aryl ether) segments have been studied (86, 105). In each instance the block copolymers were of the $(AB)_n$ type but the authors do not indicate a value for n, even though they specify the molecular weights of the respective segments. The advantage of these block copolymers is that they combine a very permeable rubbery polymer (PDMS) with one which has greater mechanical strength over a wide temperature range and greatly reduced permeability (a factor of 560).

The permeability results,which show P decreasing with increasing poly(sulphone) content, have been interpreted in terms of a two phase model since the block lengths are sufficient to allow phase separation. The model employed in this treatment (105) is that proposed by Maxwell which is applicable to a single spherical domain embedded in a matrix. This is thus most applicable to systems with low dispersion compositions and it was there that good agreement was obtained between the predicted and experimental permeabilities up to 20% poly(sulphone) by volume. The authors argue that, in the intermediate compositions, a linear combination of the limiting expressions would apply (an expression for each component as the continuous phase). They suggest that this method, by observing where the experimental and proposed permeabilities coincide, can yield the phase inversion point of the system and in this respect it was found to be very reasonable (53% poly(sulphone) by volume).

4.1.3 Cellulose and Cellulose Acetate (7,66,77,123,127,131)

Various vinyl polymers have been grafted onto cellulose, though poly(styrene) is the most widely reported. Water sorption in cellulose is reduced when grafted with poly(acrylonitrile) or poly(styrene) (7, 77, 127) and increased when grafted with poly(acrylic acid) or poly(methacrylamide) (77, 127). This is entirely in keeping with the hydrophobic and hydrophilic natures of the grafted polymers.

A detailed study of the effect of the grafting of poly(styrene) onto cellulose has been made to correlate structure and properties of the copolymers with grafting conditions.

The sorption of water vapour by cellulose is characterised by a two-stage isotherm, namely site-sorption at low humidities and random sorption at high humidities. Water sorption of cellulose-g-poly(styrene) copolymers (8 to 68% poly(styrene)) decreased with increasing poly(styrene) content. If the total sorption is related to the amount of the hydrophilic cellulose backbone present it ought to be possible to interpret what effect the poly(styrene) phase is having on the sorption process. It was found that the total sorption is less than that expected from the cellulose content and this effect was greatest at low water activities. This suggests that the discrete domain model is not applicable and the poly(styrene) chains are admixed molecularly, to some extent, throughout the cellulose matrix. Confirmation of this is available from density measurements since experimental values are significantly higher than expected from the discrete two phase model.

Water sorption isotherms have been determined for (cellulose-g- 70% poly(styrene)) copolymer prepared in the presence of three solvents; water, p-dioxane and methanol. Water is a solvent for cellulose and a non-solvent for poly(styrene) so that long, tightly-coiled poly(styrene) chains are produced which remain in domains. p-Dioxane, on the other hand, is a solvent for poly(styrene) and a non-solvent for cellulose. This produces more short poly(styrene) chains which are likely to admix with the cellulose. Methanol is a swelling agent for both cellulose and poly(styrene) and thus tends to give an intermediate structure. Consequently the sorption isotherms of cellulose and the graft copolymers decrease with solvent for polymerisation in the order :
cellulose > water solvent > methanol > p-dioxane.

Diffusion properties of the poly(styrene) graft copolymer (dioxane solvent) have been investigated. It was found that grafting actually increased the magnitude of the diffusion coefficient of water vapour, even though cellulose has a higher diffusion coefficient than poly(styrene). Presumably this is due to some destructuring of the cellulose matrix by breaking some of the hydrogen bonds present.

Sorption of acetone vapour by poly(vinyl acetate)-grafted-cellulose acetate is reduced as the extent of grafting is increased (123). Though acetone is a solvent for both polymers, the relative reduction of the cellulose acetate phase and the possibility of

crosslinking of the poly(vinyl acetate) chains would both give a reduction in solvent power.

Diffusion and solubility properties of poly(styrene) graft copolymers of cellulose acetate have also been studied (66, 131). As with cellulose copolymers, water vapour sorption decreases with increasing graft content and uptake is lower than expected when based on the cellulose acetate content since the poly(styrene) has an extended configuration. Sorption-kinetic data (66) indicates that the rate curve ($\sqrt{t}$) is initially non-linear due to a small scale relaxation process after which it becomes linear and Fickian. However time lag and sorption-kinetic measurements yielded similar diffusion coefficients (D), but different concentration-dependences. The time lag D was constant whilst that obtained by sorption-kinetics decreased linearly with increasing concentration. This behaviour has been reported elsewhere and is probably due to difficulty in measuring time lags when water vapour sorbs on metal and glass. D decreasing with water concentration is a puzzling feature of the system. This is normally interpreted in terms of clustering of the water molecules in the polymer matrix but analysis of sorption data shows little indication of clustering. Consequently this must be associated with the non-Fickian aspects of the sorption process. The actual values of the diffusion coefficients of the copolymer lie close to those calculated on the cellulose acetate content. The copolymer is postulated to contain domains of poly(styrene) with a diffusion coefficient 16 times greater than cellulose acetate. Hence the continuous cellulose acetate phase is rate-determining. The method of preparation of the copolymers, especially the monomer-solvent ratio, is critical when determining the absolute magnitude of the diffusion coefficient (66, 131).

4.1.4 Wool (76, 130, 134)

Water sorption isotherms and sorption-kinetics have been measured for some wool-g-poly(styrene) copolymers prepared by γ-radiation (143). Since poly(styrene) is hydrophobic the total water uptake of the copolymers is reduced by grafting, though this is dependent on the method of preparation. If the wool is swollen during grafting the poly(styrene) phase is expected to be distributed throughout the fibre, whereas low swelling grafting is expected to produce graft copolymer close to the fibre surface only. Hence these low swelling copolymers are expected to

have a lower reducing power of sorption since the hydrophobic poly(styrene) is clear of the bulk of the fibre. The main difficulty found in the measurement of sorption-kinetics was the initial heat change, 10°C for both sorption and desorption. Corrections can be incorporated to allow for this but the resulting accuracy is very much reduced. The wool-water system has a diffusion coefficient which increases rapidly with concentration as plasticisation takes place, and this was also found with the 25% graft sample after an initial constant D region. However a 59% poly(styrene) sample has a D decreasing with concentration, indicative of the onset of clustering within the grafted wool caused by the presence of the hydrophobic poly(styrene) (134). Water sorption for wool grafted with poly(acrylonitrile), another hydrophobic polymer, (76, 130) was slightly greater than for wool at low and intermediate humidities but lower at higher humidities. However this system appears to obey addivity of volumes to a certain degree, there being a small reduction in sorption due to the presence of polymer filling the free volume of the wool and blocking some of the sorption sites.

Quite different results are obtained when a hydrophilic polymer, poly(acrylic acid) or poly(acrylamide), is incorporated into wool (76, 130). In each case the observed sorption was considerably reduced when compared with additive volume sorption, especially for poly(acrylic acid), although it has greater affinity for water than pure wool. An ionic interaction between the $-COO^-$ and $-{}^+NH_3$ groups has been suggested which would mean that the paired hydrophilic centres sorb less water than the two free centres, especially at high humidities. The strongest interaction between wool and poly(acrylamide) is expected to be hydrogen bonds, which can be readily broken by water molecules. Consequently sorption obeys the additive rule up to about 40% humidity at which point sorption is reduced relative to the additive volumes estimate as the presence of the other polymer blocks some of the water being sorbed.

Quite different mechanisms have been reported for the sorption-kinetics of water vapour in wool and wool graft copolymers. Unmodified wool sorption consists of an initial diffusion-controlled process at low water contents followed by some coupled diffusion-relaxation mechanism. On adding graft polymer to wool, the relative rates of the diffusion and relaxation mechanisms are changed so that different

apparent diffusion coefficients are obtained. For wool-g- poly (acrylonitrile) it was found that desorption rates were comparable with wool whilst sorption rates were much reduced.

4.1.5 Poly(oxides) (69, 116, 133)

Grafting poly(oxymethylene) with poly(butadiene) or poly(acrylonitrile) yields polymers with quite different diffusion properties (133). Poly(acrylonitrile) is insoluble in its monomer so that, when grafting takes place, it is argued that a relatively compact graft structure is formed and then polymerisation stops. Consequently diffusion and permeability coefficients are lower than those of poly(oxymethylene) as the "net free volume" has been reduced, thus increasing the diffusion path. Poly(butadiene), on the other hand, is very soluble in butadiene so that the grafted polymer swells in the monomer as grafting proceeds. This means that much more monomer is concentrated in the regions of graft growth and a relatively expanded graft structure is formed. However poly(butadiene) is well above its T_g so that the existence of such a structure would not appear to be reasonable. This structure is reflected in increased diffusion and permeability coefficients and corresponding decreased activation energies. The density of the poly(butadiene) graft copolymer is less than that of poly(oxymethylene) as the structure becomes more expanded whilst that of the poly(acrylonitrile) copolymer is greater.

Transport of permanent gases (116) and vapours (69) in blends of poly(styrene) and poly(phenylene oxide) has been reported. The presence of a single T_g lying between those of the homopolymer components confirms that the two polymers are compatible, probably a result of a very weak dipolar interaction between the components. With argon and krypton as penetrants, diffusion coefficients decreased and solubilities increased with increasing penetrant size; as the poly (phenylene oxide) content of the blends was increased diffusion coefficients were constant and solubilities increased steadily. Neon, however, exhibited some distinct differences; thus as the poly(phenylene oxide) content increased a minimum in diffusion coefficient and a maximum in solubility was observed. In addition, for a 75% poly(phenylene oxide) blend, the heat of sorption is positive whereas all the other blends have negative ones. Some kind of Knudsen flow has been suggested but the reason probably lies in the use of diffusion

with immobilising adsorption in the holes of the polymer. Hence it has been assumed that blending alters the number and size distribution of holes within the polymers.

Sorption of n-hexane vapour by the blends (69) indicates that a Case II relaxation-controlled process is the primary mode of sorption, whilst desorption is nearly Fickian. This is a feature observed with poly(styrene) itself. There is a near linear relationship between equilibrium sorption and blend composition but the same relationship for diffusion coefficients obtained from sorption-kinetics is more complex.

4.1.6 Poly(tetrafluoroethylene) (2, 3, 4, 5, 72)

Copolymers of poly(tetrafluoroethylene) (PTFE) with poly (styrene) and poly(acrylonitrile) (72) have been prepared in which the grafted polymer was distributed either homogeneously throughout the PTFE or at its surface. It is assumed that grafting occurs initially in the surface region. This graft polymer swells with more monomer so that the monomer may diffuse into the ungrafted regions of PTFE and be polymerised. Poly(styrene), since it is soluble in its monomer, tends to be distributed throughout the PTFE whereas poly(acrylonitrile) is grafted entirely at the surface. Grafting of poly(styrene) slightly decreases the crystallinity of PTFE whilst causing a change in the size distribution of the crystallites.

Permeability of nitrogen and methane through the films showed an initial decrease with increasing graft content. However at an increased amount of grafting, the rate of decrease is reduced as the change of crystallinity amount and distribution begins to take effect, causing a levelling off in permeability. Poly(acrylonitrile) grafted PTFE has a constant activation energy for diffusion, indicative of an inert filler. That for the poly(styrene) graft, however, decreases slightly with graft content so that the poly(styrene) must play some part in the diffusion process.

PTFE-g-PVP (poly(N-vinylpyrrolidone)) membranes have been prepared for the separation of liquid mixtures by pervaporation (liquid on the ingoing side of the membrane and vapour on the downstream side) (2, 3, 4, 5). The results indicate that non-polar mixtures are easier to separate than polar ones as there is less interaction between the components of the mixture. However, in each case, the proton donor

of the mixture pervaporates selectively through the membrane.

4.1.7 Miscellaneous Polymers (35, 58, 60, 112, 113, 136)

Some preliminary work on nylon grafted with various polymers (58, 60) indicates that the permeability of water vapour through the membrane is increased when a hydrophilic polymer is grafted. Thus poly(ethylene oxide) graft copolymers show an increased permeability of as much as 20 times and poly(N-vinylpyrrolidone) showed a similar increase, whilst water sorption was found to be proportional to the square of the extent of grafting (58, 60). Poly(methyl methacrylate) and poly(vinyl acetate), being very much less hydrophilic, cause only slight increases in permeability.

Permeation in semi-compatible polymer blends (112, 113), poly(vinyl chloride) with either ethylene - vinyl acetate copolymer (EVA) or acrylonitrile - butadiene copolymer (NBR), is similar in each system. The greater the vinyl acetate or acrylonitrile content of the copolymer the more compatible the two phases become. This results in a reduction in polymer segmental motion as polymer-polymer interactions increase and hence an increase in activation energy for diffusion of permanent gases. Dynamic mechanical data and density measurements confirm that more poly(vinyl chloride) becomes associated with the rubber phase as interactions increase. Permeation and diffusion coefficients for the blends increase with increasing rubber content.

When measured by time lag experiments, inconsistent gas solubility data was found for the blends (113). Helium appears to have the same solubility for various blend compositions, probably due to the fact that its size is less than that of any holes present in the blends. However the larger gas solubilities (CO_2) fluctuated with blend composition. In fact solubility, and permeability, was a minimum and activation energies for transport a maximum at a 50/50 blend composition. This has been reported as due to the increased polymer-polymer interactions as blend compatibility increases. This reduces segmental mobility and changes the sorption character of the blends.

4.2 Models of Heterogeneous Diffusion

Many models have been proposed in an attempt to interpret experimental data for diffusion and permeation in heterogeneous media.

A detailed review is not attempted here as there exist already several reviews (12, 39, 92) on this subject although none is comprehensive. Attention is restricted here to those analyses which have been used to interpret the results of this investigation.

The following symbols will be used throughout this section:

P_M - Permeability of the heterogeneous medium.
P_C - Permeability of the continuous phase.
P_D - Permeability of the discontinuous phase.
V_C - Volume fraction of the continuous phase.
V_D - Volume fraction of the discontinuous phase.

Any other symbols that are required will be defined in the appropriate part of the text. The following models are applicable to dispersions of spheres in a continuous medium. Dispersions of spheroids and cylinders have been ignored since, as will be shown later, the system studied approximates more closely to a disperse phase of spherical domains.

4.2.1 Classical Solutions

The simplest model is that proposed by Maxwell (87) who considered a single sphere in a continuous medium.

$$P_M = P_C\left[\frac{P_D + 2P_C - 2V_D\,(P_C - P_D)}{P_D + 2P_C + V_D\,(P_C - P_D)}\right] \qquad \ldots.(4.1)$$

This expression may be applied to media in which either the continuous or discontinuous phase has the higher permeability. Because of the implicit assumptions of the model it is applicable only to dilute suspensions of identical spheres when there is no distortion of the concentration gradient around each sphere due to the neighbouring spheres. Consequently meaningful results may be obtained up to a limit of about 20% discontinuous phase.

The Maxwell expression may be modified for media in which the dispersed phase consists of an inner occluded sphere of radius R_1 and permeability P_D surrounded by an outer spherical shell of radius R_2 and permeability P_R (91) :

$$\frac{P_M - P_C}{P_M + 2P_C} = V_D\left[\frac{(P_R-P_C)(2P_R+P_D)(R_2/R_1) + (2P_R+P_C)(P_D-P_R)}{(P_R+2P_C)(2P_R+P_D)(R_2/R_1) + 2(P_R-P_C)(P_D-P_R)}\right] \qquad \ldots.(4.2)$$

It is assumed that the disperse phase consists of spheres of uniform size since dispersions of spheres of different sizes present formidable difficulties and no analytic solution to this problem has been proposed (92).

Wagner (129) has attempted to simplify Maxwell's expression, but this departs significantly from Maxwell as the disperse phase fraction increases :

$$P_M = P_C\left[\frac{2P_C + P_D + 3V_D\,(P_D - P_C)}{2P_C + P_D}\right] \qquad \ldots.(4.3)$$

4.2.2 Ordered Arrangements

When concentrated dispersions are to be considered the arrangement of the dispersed phase becomes important. The position of each sphere needs to be fixed within some simple symmetrical geometry, the nature of which can greatly alter the final results.

Rayleigh (103) treated the situation of uniform spheres in a cubic lattice :

$$P_M=P_C\left[\frac{(2P_C+P_D)(4P_C+3P_D)-2V_D(P_C-P_D)(4P_C+3P_D)-1.575(V_D^{10/3})(P_C-P_D)^2}{(2P_C+P_D)(4P_C+3P_D)+ V_D(P_C-P_D)(4P_C+3P_D)-1.575(V_D^{(10/3)})(P_C-P_D)^2}\right] \qquad \ldots.(4.4)$$

This includes a correction by Runge (110), and at low concentrations of the dispersed phase reduces to Maxwell's expression. This expression loses physical significance above concentrations corresponding to the close packing of spheres (V_D = 0.524).

Rayleigh's derivation has been reappraised by Meredith and Tobias (93) and appears to yield more realistic results at higher concentrations (20-45%) of the disperse phase :

$$P_M = P_C\left[\frac{\begin{array}{l}(2P_C+ P_D)(4P_C+ 3P_D) - 2V_D(4P_C+ 3P_D)(P_C- P_D)\\ + 1.227(V_D^{7/3})(2P_C+ P_D)(P_C- P_D) - 6.399(V_D^{10/3})(P_C- P_D)^2\end{array}}{\begin{array}{l}(2P_C+ P_D)(4P_C+ 3P_D) + V_D(4P_C+ 3P_D)(P_C- P_D)\\ + 1.227(V_D^{7/3})(2P_C+ P_D)(P_C- P_D) - 2.748\,(V_D^{10/3})(P_C- P_D)^2\end{array}}\right] \qquad \ldots.(4.5)$$

Other approaches have been made (59, 99, 104, 114) but do not offer any real advantages for systems of the type studied here and are therefore not considered further.

4.2.3 Approximations

Bruggeman (28), in a comprehensive text on the conductivities of heterogeneous systems suggests that in mixtures with high concentrations of the disperse phase, one should use the effective conductance as a whole rather than that of the continuous phase only.

$$V_C\left[\frac{P_D - P_C}{P_D - P_M}\right] = 3\sqrt{\frac{P_C}{P_M}} \qquad \ldots.(4.6)$$

This treatment tends to overcorrect and is appropriate when the disperse phase has a large range of particle sizes. Meredith and Tobias (94) have attempted to adapt the Bruggeman approach to that for identical spheres :

$$P_M = P_C\left[\frac{2(P_D+2P_C)+2(P_D-P_C)V_D}{2(P_D+2P_C)-(P_D-P_C)V_D}\right] \times \left[\frac{(2-V_D)(P_D+2P_C)+2(P_D-P_C)V_D}{(2-V_D)(P_D+2P_C)-(P_D-P_C)V_D}\right] \qquad \ldots.(4.7)$$

Böttcher (27) has tried a slightly different approach to Bruggeman :

$$\left[\frac{(P_M - P_C)}{3P_M}\right] = \left[\frac{P_D - P_C}{P_D + 2P_M}\right] V_D \qquad \ldots.(4.8)$$

This is strictly applicable only to spheres in the disperse phase and is most meaningful for dilute dispersions.

Several empirical expressions have been suggested (47, 78, 101) but the most commonly used is the series / parallel model (95, 105, 125, 132).

Series : $$P_M = P_C P_D \,/\, (V_C P_D + V_D P_C) \qquad \ldots.(4.9)$$

Parallel : $$P_M = V_C P_C + V_D P_D \qquad \ldots.(4.10)$$

These are the extremes of discontinuous type structures which can be represented as laminae normal and parallel, respectively, to the direction of flow. Thus the series model is applicable to systems in which the discontinuous phase has a higher permeability than the continuous phase and vice versa for the parallel model.

More recently Higuchi (62, 63) considered the effect of neighbouring particles with respect to field interactions as the suspension of spheres becomes concentrated. As a random dispersion of spheres was considered, Higuchi found it necessary to introduce an

empirical constant (K = 0.78) which is a "neglected" function of the volume fraction of the disperse phase. Thus K ought to be a function of volume fraction of the dispersed spheres but, in practice, it is found to be constant :

$$P_M = P_C \left[\frac{(2P_C + P_D - X) - V_D (2P_C - 2P_D - X)}{(2P_C + P_D - X) + V_D (P_C - P_D + X)} \right] \quad \ldots.(4.11)$$

where $X = K (P_D - P_C)^2 / (2P_C + P_D)$.

The value of K chosen is that which makes the theory fit most closely the data obtained by Pearce (99) for thermal conductivity measurements. In principle this approach is correct but equation (4.11) only reduces to that of Maxwell when K=0 and not as it stands, even at low dispersed phase concentrations.

In the case where the dispersed phase consists of an inner occluded sphere of radius R_1 and permeability P_D surrounded by an outer spherical shell of permeability P_R, the Higuchi relationship still holds provided that P_D in equation (4.11) is replaced by P_D^* (63), such that :-

$$P_D^* = P_R \left[\frac{(2P_R + P_D)R^3 - 2(P_R - P_D)R_1^3}{(2P_R + P_D)R^3 + (P_R - P_D) R_1^3} \right] \quad \ldots.(4.12)$$

where R is the radius of the total domain.

4.3 Conclusions

There are many models proposed to predict permeabilities (thermal conductivities) of heterogeneous systems. The model of Higuchi is theoretically the most realistic and it may be expected that this ought to be the test of the experimental data.

The literature of permeation in heterogeneous systems, especially block and graft copolymers, is quite extensive and yet little attempt has been made to correlate experimental data with these models. One feels that the authors have been remiss as these models are probably sufficient to explain most of data without having to postulate many of the theories used. Perhaps the prime example is the poly (ethylene-g-styrene) copolymer system for which gas and vapour permeation data is governed by the changes in "free volume" on grafting. Even a preliminary examination of any of the models will show the same results as was found, and this purely is a natural consequence of grafting a polymer, which has a different permeability, onto the substrate.

CHAPTER 5

RESULTS AND DISCUSSION : GRAFT COPOLYMERS

The aim of this section of work is to prepare a series of copolymers of known composition and physical properties in order to test some of the models proposed to predict the permeability behaviour of heterogeneous systems.

5.1 Preparation and Physical Properties of the Graft Copolymers

Preparation of the graft copolymers was achieved by mutual irradiation of [c.l.] - poly (dimethylsiloxane) (PDMS) swollen with vinyl acetate monomer by γ-radiation from a ^{60}Co source (see Section 3.3.4). Radiation synthesis was preferred to chemical means since the latter tends to leave impurities within the sample, e.g. initiators (34). In addition, there is no problem of solvent affecting the polymerisation unless it is deliberately added to the monomer, and initiation is essentially dependent only on the intensity of the radiation and not temperature.

5.1.1 Radiation Units

It is appropriate to define several terms that are commonly encountered in radiation work. The unit of radiation dose is the rad which is defined as the absorption of 10^{-5} Joules of energy per gram of the particular medium being studied. In practice, the Mrad ($10J.\ g^{-1}$) is the most common unit used. Reactions which are caused by radiation are expressed in terms of a G value; this is the number of chemical changes of a given kind produced per 100 e.V. ($9.6 . 10^{6}J$) of energy absorbed. Several G terms are encountered such as G_R for the production of free radicals by a polymer, G(c.l.) for crosslinking of polymers, and G_{in} for the production of free radicals by a monomer (33, 34, 49).

5.1.2 Radiation Grafting

γ-Radiation was used in this study since it is more penetrating than, say, accelerated electrons so that a uniform exposure can be obtained in the relatively thick 2 mm samples. The dose-rate used throughout was 0.8 Mrad. $hr.^{-1}$. It has been found that the dose-rate determines the rate of initiation and length of the grafted chains whilst the dose itself determines the number of chains.

Irradiation was carried out at room temperature and no attempt was made to maintain any particular temperature. Irradiation of a polymer produces a heating rate of 10 $J.g^{-1}$. $Mrad^{-1}$ throughout the sample. However temperature changes are most likely caused by the heat evolved in the polymerisation process. In most instances this has little effect on the outcome of the irradiation and only affects a kinetic study which was not attempted here.

Mutual irradiation was found to be a very efficient means of preparing the particular graft copolymers required; from Figures 5.1 and 5.2, about 70% of the monomer present finished as graft polymer. Percentage grafting (G%) is defined as the weight of grafted polymer to the original weight of backbone polymer and grafting efficiency as the weight of grafted polymer to the total weight of polymer polymerised (graft polymer and homopolymer). After extraction of polymer to constant weight, about 10% of the total monomer polymerised was removed so that a very acceptable grafting efficiency of 90% could be achieved. The polymer sample in the grafting tube rested on poly(ethylene) supports (stoppers of "Polytop" bottles). Sorption by the supports probably accounts for most of the unreacted monomer although small amounts of homopolymerisation on the glass walls of the apparatus is not excluded. Extraction is the usual procedure for removing homopolymer from crosslinked samples and any remaining poly(vinyl acetate) (PVAc) is termed "graft polymer". However there has always been some doubt here as some PVAc homopolymer of high molecular weight which is heavily entangled may not be too easily extracted. In an attempt to overcome this problem it has been suggested (111) that, for uncrosslinked samples, solvents for both polymers should be used to eliminate both unreacted backbone polymer and homopolymerised polymer. This, however, is unnecessary with crosslinked samples so that one would anticipate that most of the polymerised PVAc is present as graft polymer. Attempts have been made to determine whether the irradiated material obtained by mutual irradiation is a homogeneous product (9, 10) in the context of graft and homopolymer formation. From the thermal behaviour of the products (10) it was concluded that both grafted polymer and homopolymer are formed, a conclusion that has universal acceptance. Photomicrographs of these systems indicate the homopolymer is present in domains that are much larger than those of the grafted polymer. Subsequent treatment of these systems with a good solvent produces bubbles within the samples which have a tendency to rupture with excess swelling of the domains

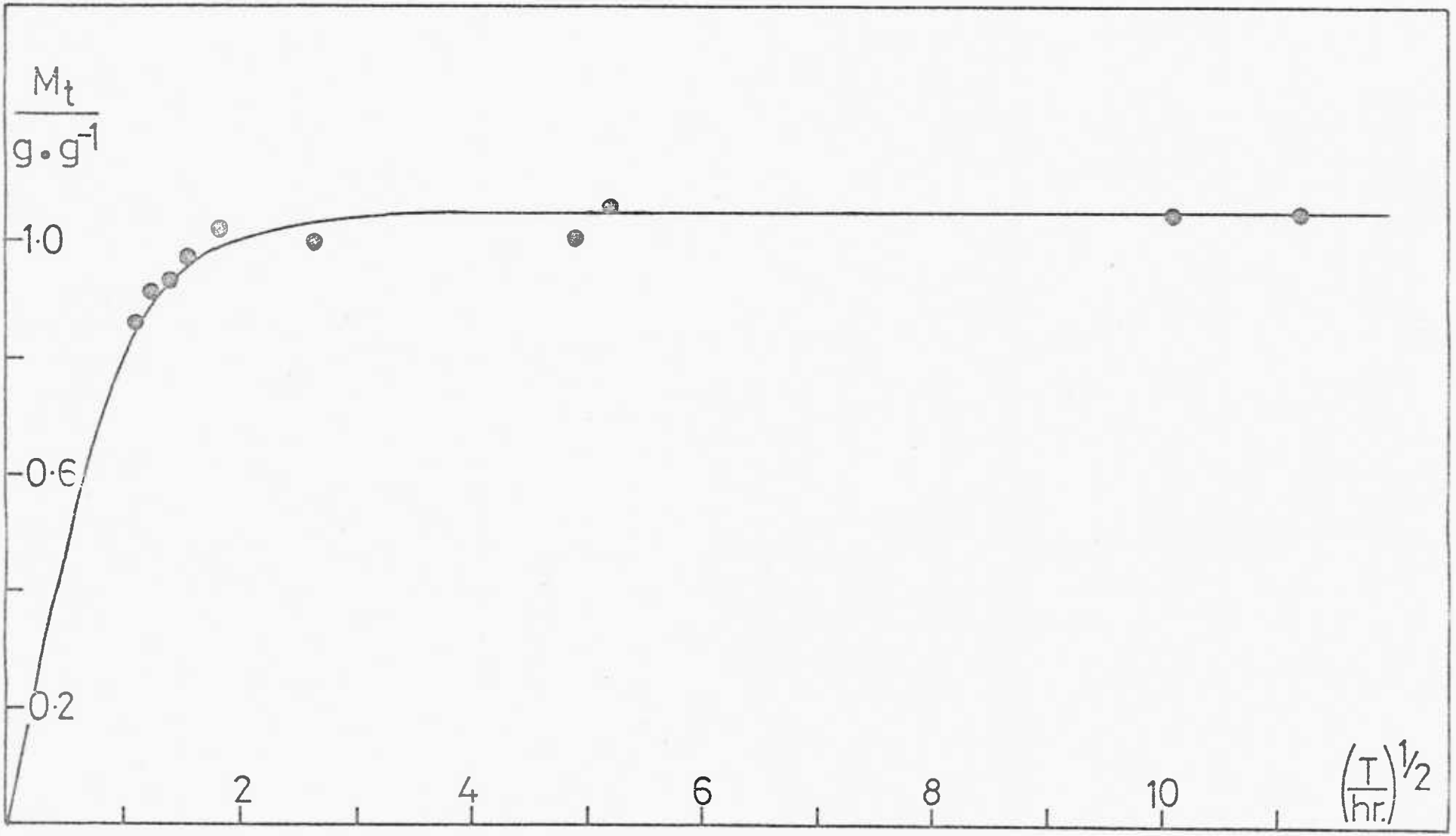


FIGURE 5.1 SORPTION OF VAc MONOMER BY PDMS

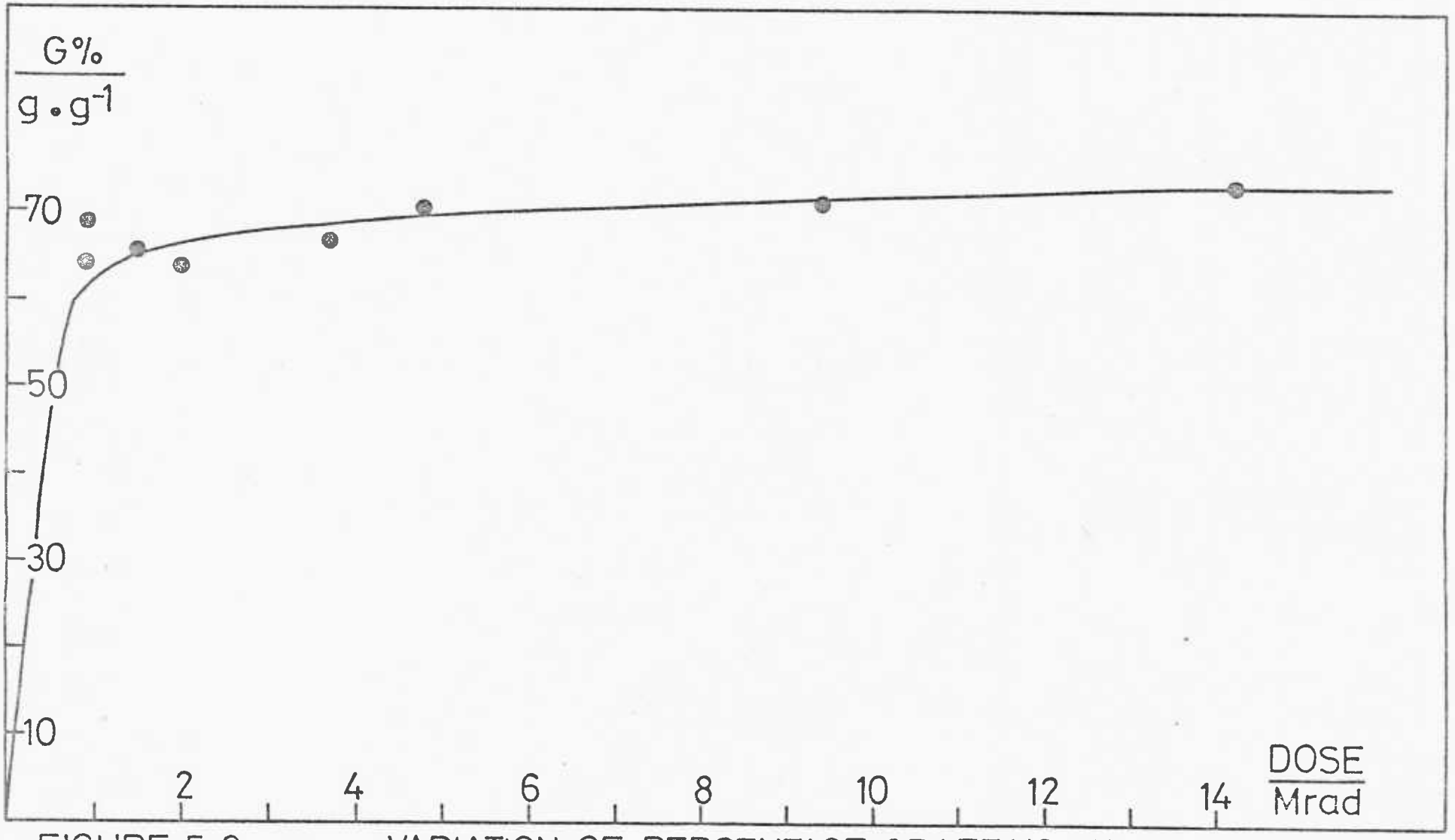


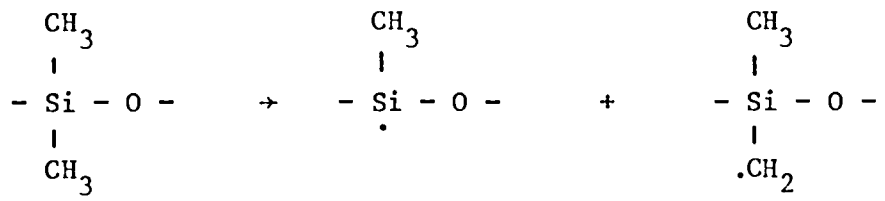
FIGURE 5.2 VARIATION OF PERCENTAGE GRAFTING WITH DOSE

(83). No attempt was made to extract the irradiated material prior to these investigations and hence homopolymer is expected to be present. Testing of the irradiated product after homopolymer removal would be of more value in assessing the physical properties of graft copolymers. Use of homopolymer extraction by a mutual solvent relieves this pressure to produce regular samples.

The graft polymer - homopolymer ratio is something that must be considered when mutual irradiation has been chosen as the means of polymerisation. Ideally the radiation should produce free radicals only on the backbone polymer so that only graft polymer is produced. However, in practice, this is very rare and the object must be to reduce the amount of homopolymer formed to a minimum. To achieve this, G_R (PDMS) should be greater than G_{in} (VAc monomer). There is no definite G_R value for PDMS but $G_R = 3.6$ has been suggested for a high molecular weight PDMS (33) which does not compare too favourably with G_{in} (VAc) of 4 - 5 (26, 33, 34, 64, 80). Despite this, the grafting efficiency of vinyl acetate is very high. From Figure 5.2 it can be seen that complete polymerisation occurs very quickly (about 2 Mrad) and this is a consequence of PVAc being very reactive once a radical is present in the system. The speed of vinyl acetate polymerisation is shown by the fact that the rate of polymerisation has been estimated at 27% per 0.06 Mrad at 20°C (80).

The question of homopolymer formation and G values is not quite so simple since stray free radicals are formed in the initiation of the silicone backbone which will initiate polymerisation. In addition, the better the contact between polymer and monomer the less likelihood there is of homopolymer formation (8, 26, 64). Transfer from the growing chain to other materials is quite important for PVAc, especially in the later stages of polymerisation, since it has a strong tendency to branch by transfer from one part of the polymer to another. Hence it seems likely that the low homopolymer content is due, in part, to transfer from PVAc back to the PDMS backbone (33, 80, 122). Because of this transfer, vinyl acetate polymerisation is very susceptible to retardation by low molecular weight compounds, especially halocarbons, which reduce both the length of the side-chains and the rate of polymerisation.

When irradiated alone in vacuum (34, 44, 70) PDMS crosslinks through (Si - C) linkages :



The respective bond energies are (Si - C) 241 kJ mol^{-1}, (Si - O) 375 kJ mol^{-1}, (C - H) 366 kJ mol^{-1}. Consequently the (Si - C) bond is the normal one broken although the (C-H) bond is also broken, but to a lesser extent (25, 44), and hence this is the normal mechanism of initiation of graft copolymerisation. The (Si - O) bond, being more stable and less accessible, is never broken.

In the later stages of polymerisation, and in systems such as this in which the polymer is swollen with monomer, the viscosity of the system is high enough that diffusion within it is restricted. This means that the growing chains tend to stay apart, reducing termination and producing high molecular weight side-chains (8, 33, 34). As a result of this, the rate of polymerisation is enhanced, especially at high dose-rates where polymerisation is naturally rapid.

Thus mutual irradiation is expected to produce high molecular weight grafted side-chains with high efficiency with respect to the rate of polymerisation, monomer conversion and homopolymer formation.

5.1.3 Structure and Physical Properties

Since most polymers are incompatible when mixed together as blends or when forming graft and block copolymers, there are usually two phases present in such systems. From thermodynamics

$$\Delta G = \Delta H - T\Delta S \qquad \ldots.(5.1)$$

where ΔG, ΔH, ΔS are respectively the free energy, heat and entropy of mixing; phase separation occurs when ΔG is positive. This is determined mainly by the ΔH term which may be estimated from

$$\Delta H = V(\delta_A - \delta_B)^2 \phi_A \phi_B \qquad \ldots.(5.2)$$

where V is the total volume of the system, ϕ the volume fractions of components A and B, and δ their solubility parameters. If δ_A and δ_B are

different phase separation will occur, and the greater the difference the lower is the molecular weight of each component required before separation occurs. Equation (5.2) only predicts positive or zero values of ΔH. If the components were to interact strongly negative ΔH values follow. In general the polymer which is present in larger quantities tends to be the continuous phase with the other polymer dispersed in domains throughout the matrix. The domains may be of various shapes (spheres, spheroids or cylinders) and orientation (random, cubic- or face-centred lattices) (12). For block and graft copolymers the bonds between the components must lie in the surface regions of the domains (61), the size of which are determined by a minimisation of the surface to volume ratios providing that uniform density can be maintained throughout the domains (46). The shape of the domains is governed by the molecular weight of the grafted chains and the configuration changes from spheres to cylinders to spheroids as molecular weight increases. However the choice of solvent for the system can have a dominating effect.

These general observations for copolymers and blends are generally observed with the P(DMS - g - VAc) copolymers used in the present investigation. Scanning electron microscopy (Department of Material Science, Queen Mary College) has been applied to each of the copolymer samples to try to elucidate the structures present (the actual micrographs are shown in Appendix 8.1). The domains are spherical in shape and of fairly uniform size, the details of which are given in Table 5.1. After extraction in a mutual solvent, slow evaporation of solvent was achieved so as not to crack the samples which were highly swollen. This, in fact, ensured that the domains were of spherical shape, regularly spaced and of uniform size (51). Since PDMS is present initially as polymer, it is to be expected that this will form the continuous phase and any PVAc formed will be discontinuous. As the PVAc content increases it will at some stage become the continuous phase and phase inversion will occur. One would anticipate that this ought to occur in the middle of the composition range although the limits at which a phase can be continuous are 26 - 74%. Below this limit there is insufficient material to support another phase, and above the upper limit the dispersed spheres start to touch and hence some continuity arises. In these particular copolymers PDMS is present as a crosslinked polymer so that it may be expected that this will delay phase inversion to some extent and, perhaps, such that true phase inversion may never occur. The copolymer

Table 5.1

Scanning Electron Microscopy of P(DMS - g - VAc) Copolymers

Volume Fraction of PVAc	Average Domain Sizes Radius (nm)	Range (nm)
0.034	12.5	10 - 15
0.093	15	11 - 19
0.157	25	20 - 30
0.214	47.5	37 - 57
0.442	75	60 - 90

containing 44% volume PVAc is obviously getting towards phase inversion even though PVAc is still the discontinuous phase. However, despite separate domains, there is a tendency for these to come close together in some regions to form a kind of "pseudo-continuous" region expected before phase inversion actually occurs.

The composition of the PVAc domains is open to question as it has been suggested from the micrographs that they contain occlusions of PDMS (Figure 8.5 in Appendix 8.1). Despite the fact that energy considerations should favour domains of uniform composition and density this phenomenon can be found elsewhere in the literature, especially for impact poly(styrene) (96). The formation of occlusions in the styrene/butadiene system is quite feasible since styrene monomer is polymerised in the presence of poly(butadiene). After about 15% styrene had been polymerised, phase inversion occurs so that the rubber becomes the disperse phase. However each rubber domain consists of poly(butadiene) swollen with styrene monomer which, when polymerised, forms the inner core of the occlusion. If there is no agitation during polymerisation phase inversion does not occur and the poly (styrene) phase remains discontinuous. In the case under study, the monomer polymerises in a non-agitated system and phase inversion does not occur in this highly viscous medium. Hence it becomes difficult to postulate a mechanism whereby the polymerising medium remains discontinuous and occludes backbone polymer. This question will be left open and further attempts at clarification will be employed, though it seems unlikely that occlusion is present in this system.

Glass transition temperature, melting point and density data have been presented in Table 3.1. Both the glass transition (T_g) and melting point (T_m) of PDMS are changed very little by grafting. This is not unexpected (26, 126) since, in general, there are relatively few graft chains per backbone molecule so that the free volume available to the backbone polymer is not affected. The melting point shows a slight decrease (-44°C to -48°C; 0 to 44% PVAc) and the melting range broadens with increasing PVAc content as this impairs crystallite formation. The glass transitions of PVAc in the graft copolymers are at the same temperature as that of PVAc homopolymers of high molecular weight. Radiation grafting, as a rule, produces high molecular weight side-chains and this seems to be consistent with the thermal data. This is also in accord with the PDMS transition data since the longer the side-chains the less effect they will have on the T_g and T_m of the backbone polymer (64). The fact that the T_g's of the two components in the copolymers are the same as for the homopolymers seems to indicate that occlusions are not present. The presence of occluded PDMS must have some effect on the T_g of PVAc since PDMS crosslinks must be in the PVAc phase so as to connect the occluded and continuous phases.

The 3% PVAc copolymer does not show a transition for PVAc, even though it contains domains of PVAc like the rest of the copolymers. The probable explanation is that there is insufficient material there for the instrument to detect.

Density data also support the picture of two distinct phases and is presented in Table 3.1 and Figure 5.3. If the two polymers are completely incompatible then it is expected that the volumes of the components are additive (31, 32) such that

$$1/\rho = x_1/\rho_1 + x_2/\rho_2 \qquad \ldots.(5.3)$$

where ρ is the density of the copolymer, ρ_i and x_i are the density and mass fraction of each component respectively.

From Figure 5.3 it can be seen that this condition agrees very well with experiment. Thus, whilst the electron microscopy indicates that there is a certain amount of phase separation the thermal properties and density of the copolymers suggest that there is complete phase separation. In the light of this it seems unlikely that there are any occlusions present in the PVAc domains.

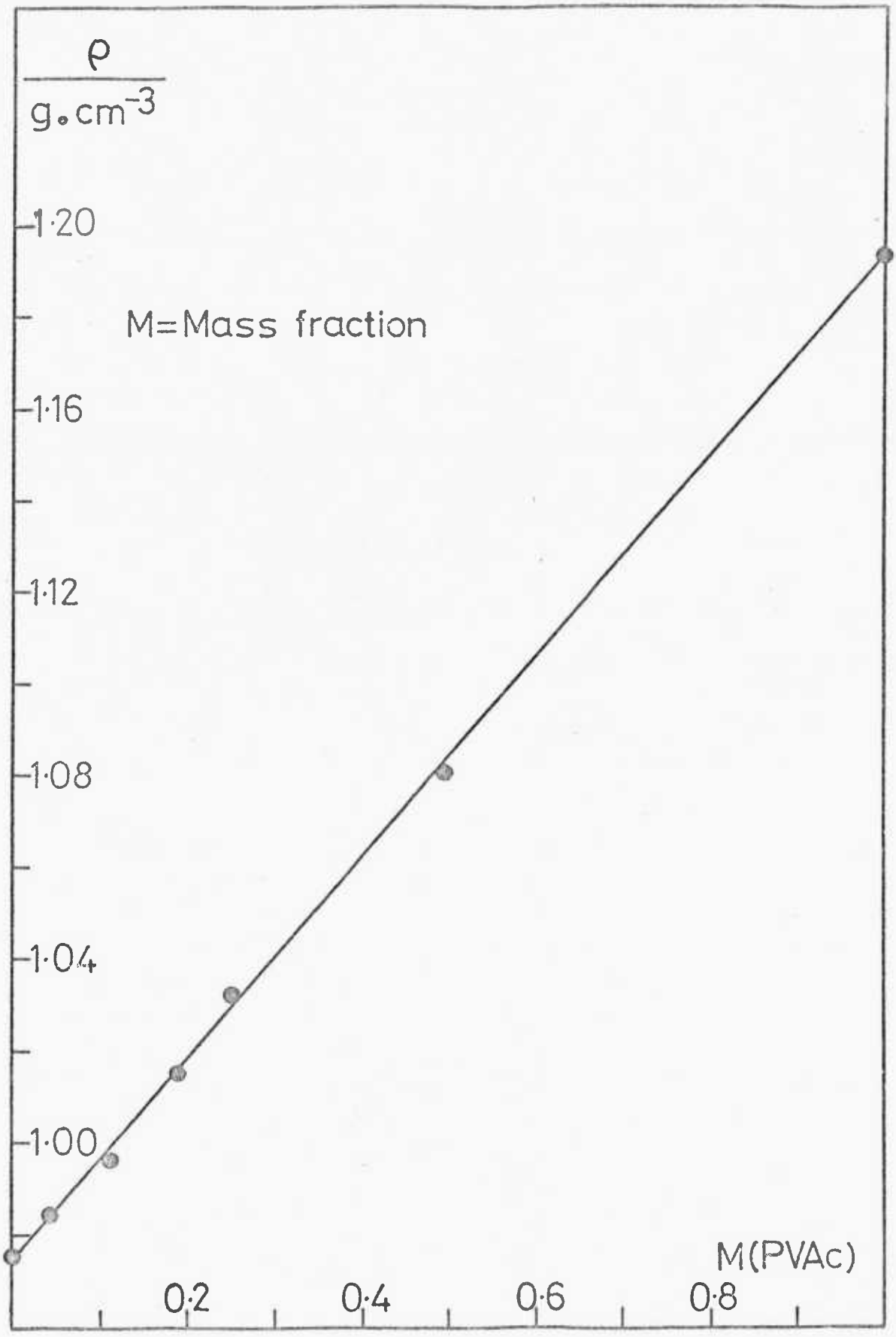


FIGURE 5.3 DENSITY MEASUREMENTS

5.2 Equilibrium Sorption Results

Equilibrium sorption isotherms for water vapour in PDMS, PVAc and P(DMS - g - VAc) copolymers containing 3.4%, 15.7%, 21.4% and 44.2% by volume of PVAc are given in Figures 5.4 - 5.10 respectively. Sample calculations are given in Appendix 8.3. All samples were above their respective glass transition in these experiments and no hysteresis was observed.

All results were obtained on the vacuum microbalance so that valid comparisons could be made, even though PVAc measurements could be obtained with a spring-sorption apparatus.

5.2.1 Sorptive Capacities of the Polymers

Since most of the isotherms are non-linear even at low concentrations, values of $\sigma_{c=o}$ for each polymer were determined as $\lim_{c\to o} (c/p)$ and are presented in Table 5.2 where ϕ(PVAc) denotes the volume fraction of PVAc in the polymer system.

Table 5.2

Limiting Henry's Law Solubility Coefficients $\sigma_{c=o}$ (cm^3(S.T.P.). cm^{-3} . cm Hg^{-1}) for water vapour

	Sample Temperature			
ϕ (PVAc)	35.0°C	42.0°C	49.0°C	55.0°C
0	0.112	0.097	0.080	0.071
0.034	0.348	0.273	0.206	0.168
0.093	0.730	0.554	0.424	0.340
0.157	1.119	0.800	0.623	0.485
0.214	1.415	1.082	0.759	0.622
0.442	2.908	2.145	1.579	1.258
1.00	6.529	4.647	3.484	2.775

The PDMS results agree to within 7% of previous results (20) and this level of agreement is satisfactory for different samples even though they were obtained from the same source. Previous work on the PVAc - water vapour system has been reported (73, 74, 81, 124) but no comprehensive study of sorption, permeation and diffusion was made.

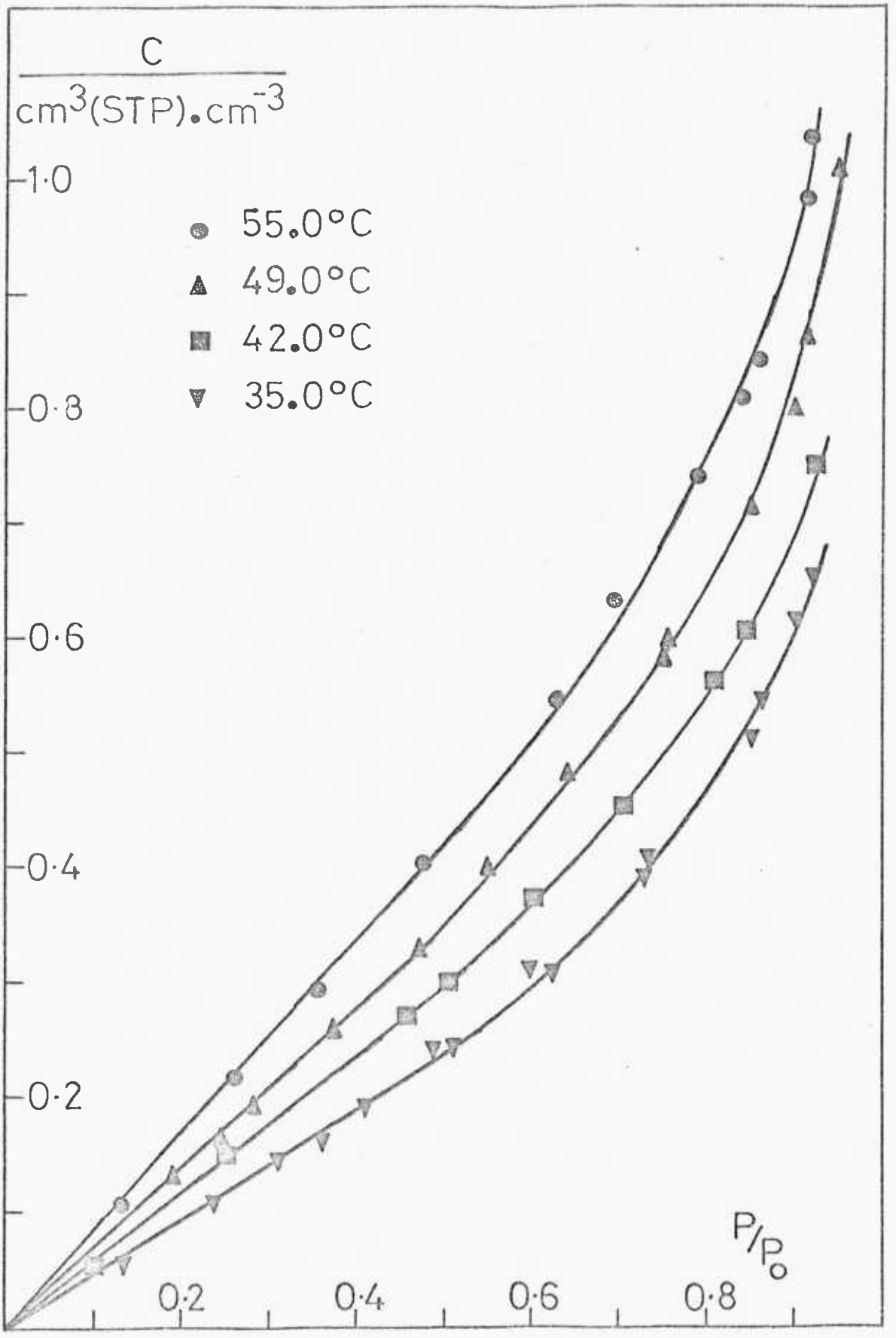


FIGURE 5.4

SORPTION ISOTHERMS

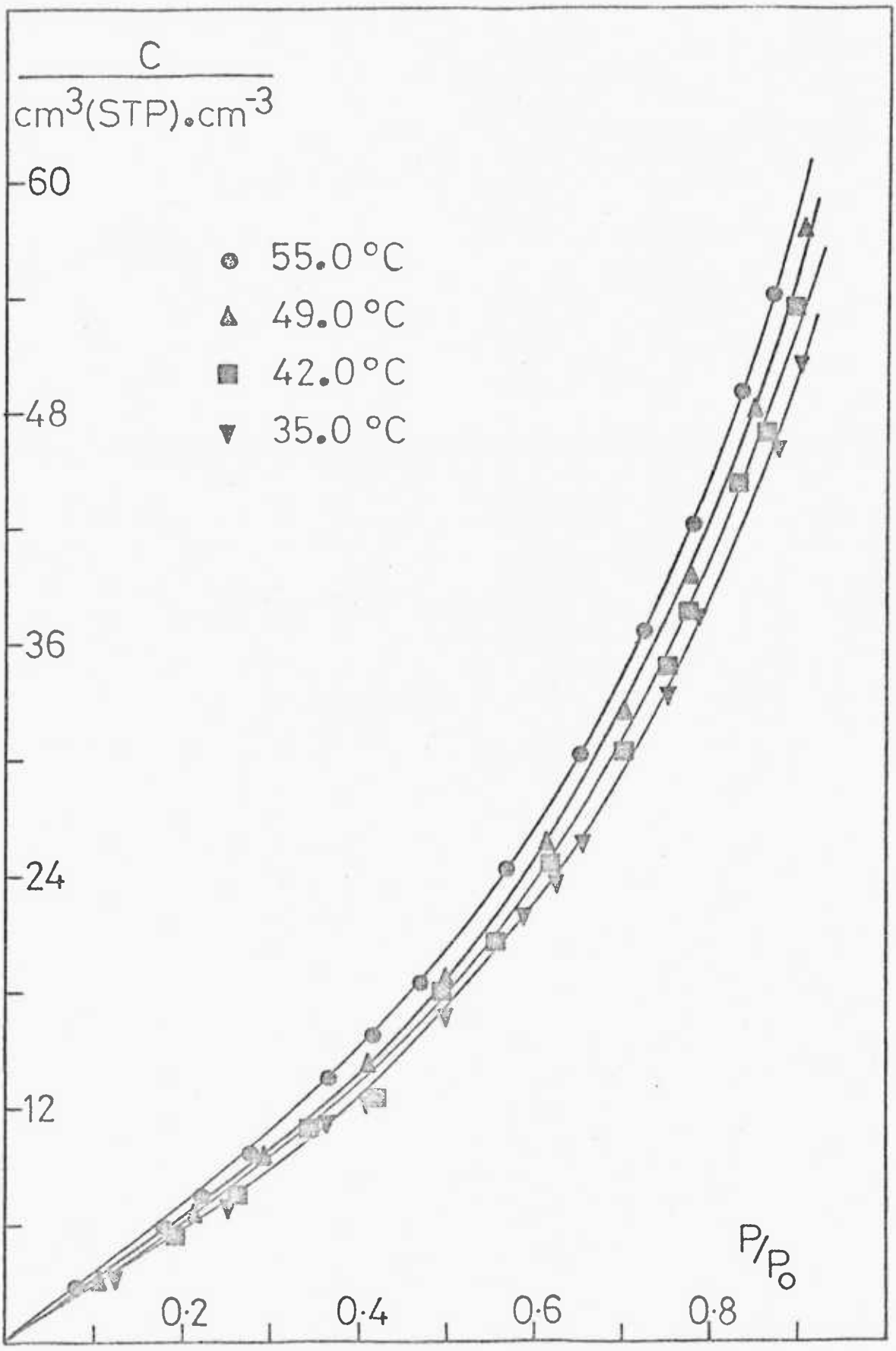


FIGURE 5.5 PVAc–H_2O

SORPTION ISOTHERMS

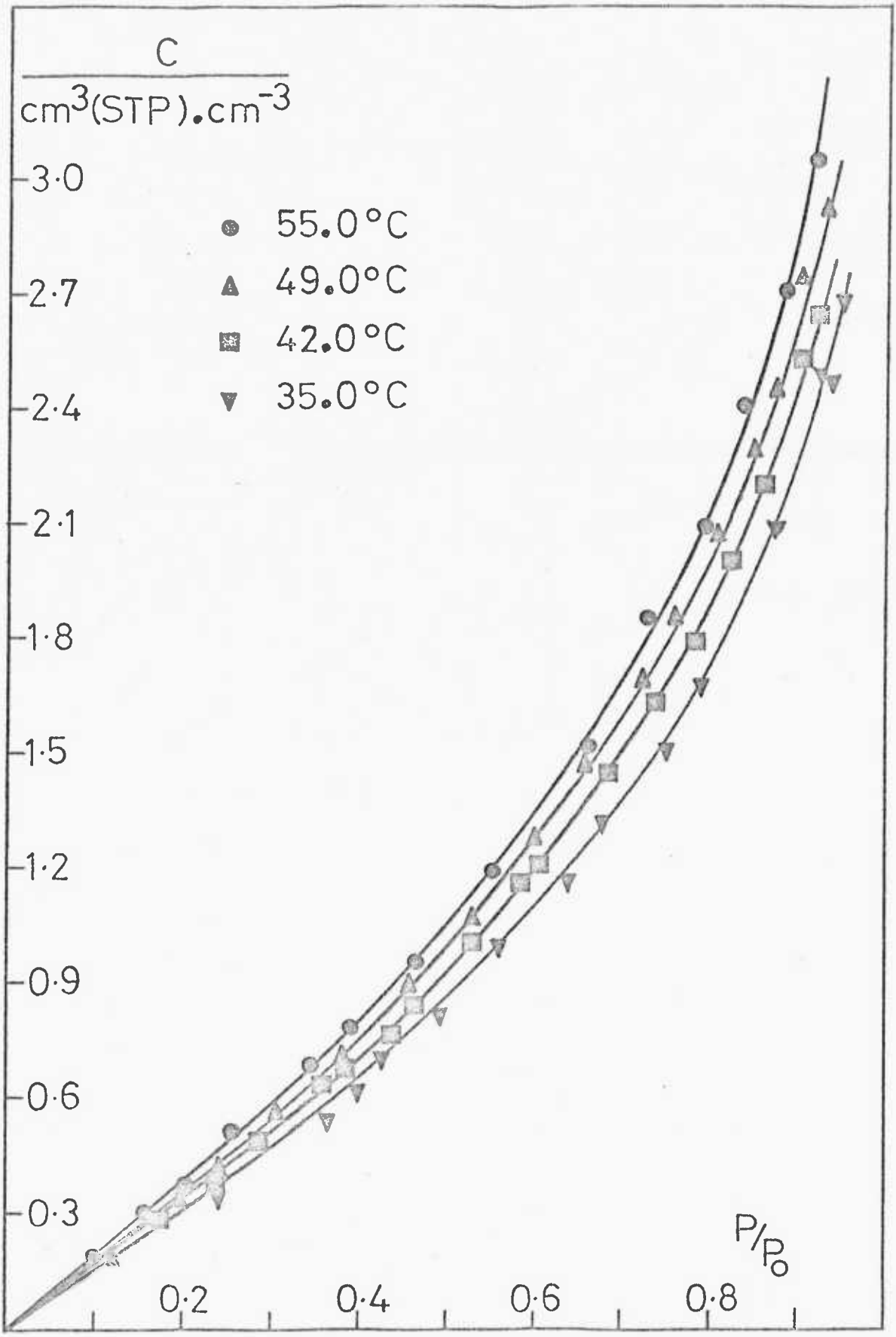


FIGURE 5.6 P(DMS-g-0·034VAc)-H_2O SORPTION ISOTHERMS

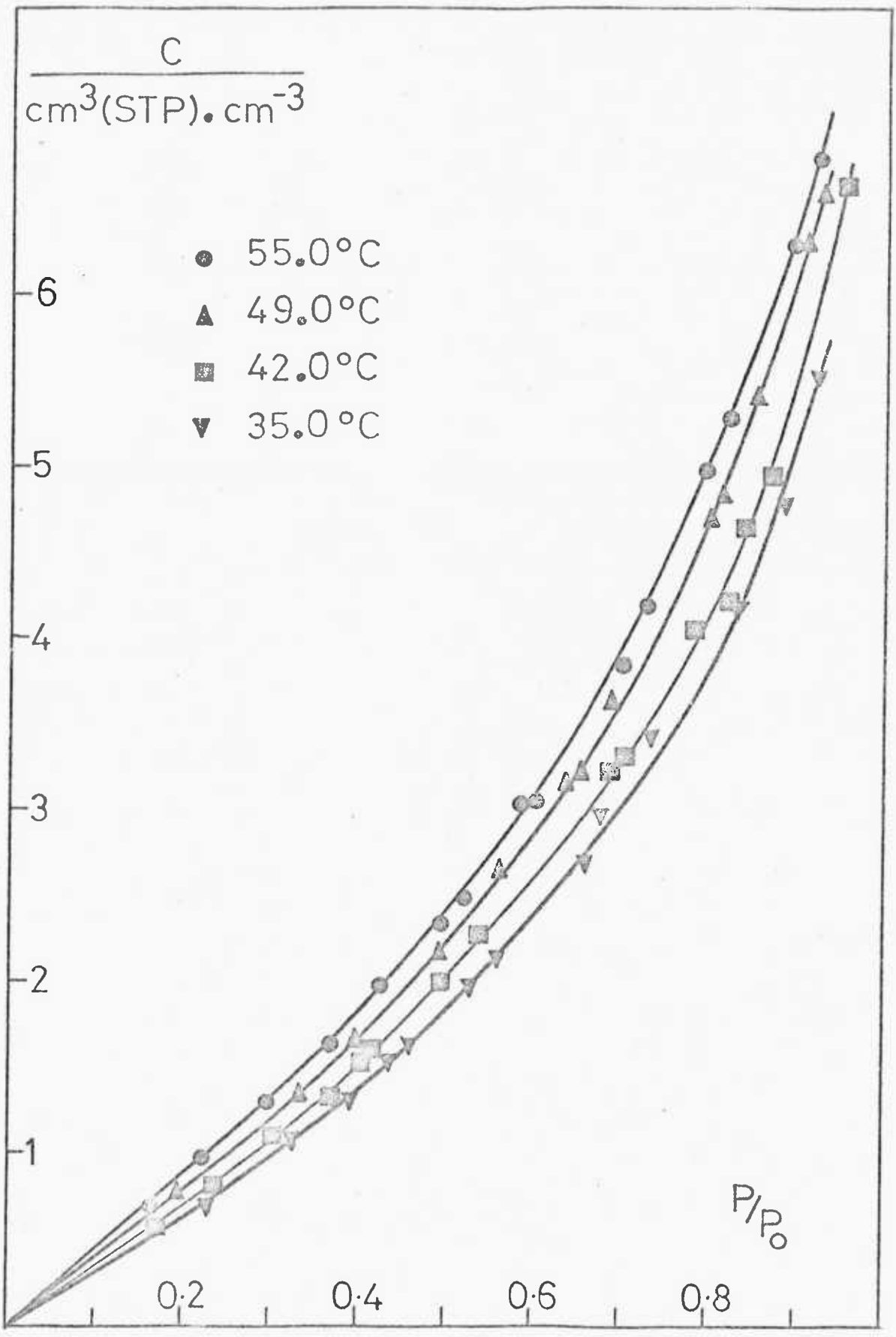


FIGURE 5.7 P(DMS-g-0·093VAc)-H_2O SORPTION ISOTHERMS

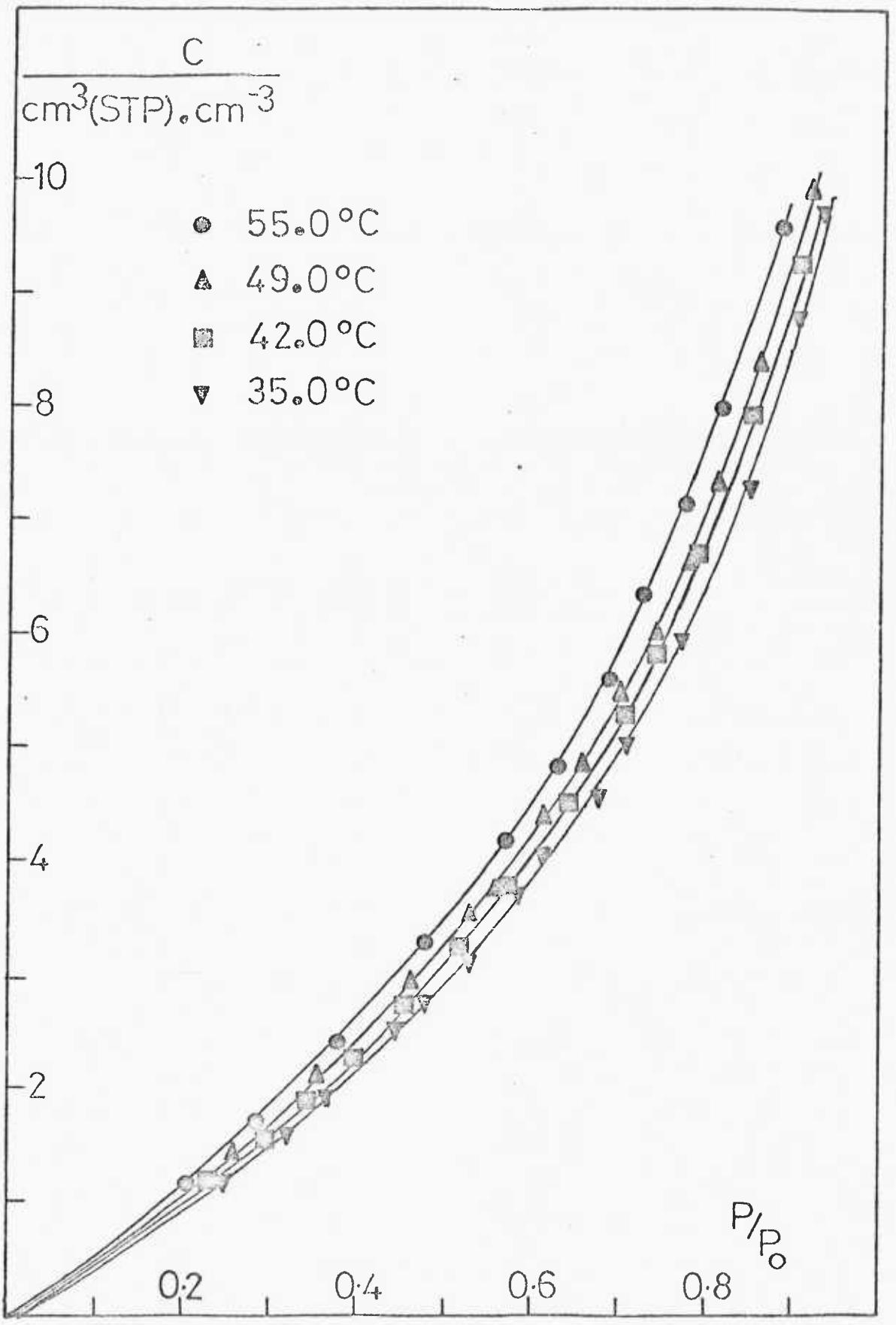


FIGURE 5.8 P(DMS-g-0·157VAc)-H_2O SORPTION ISOTHERMS

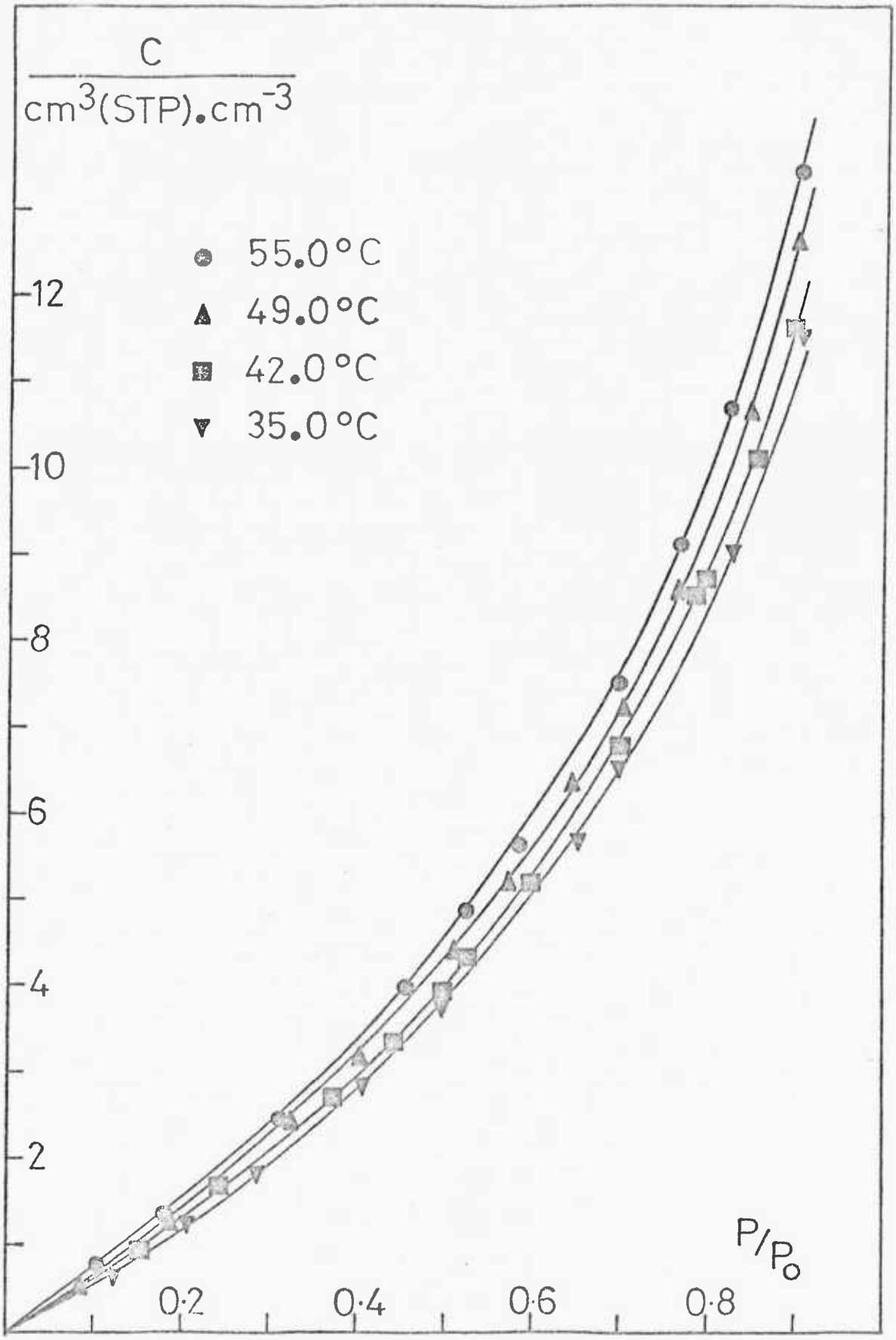


FIGURE 5.9 P(DMS-g-0·214VAc)-H_2O SORPTION ISOTHERMS

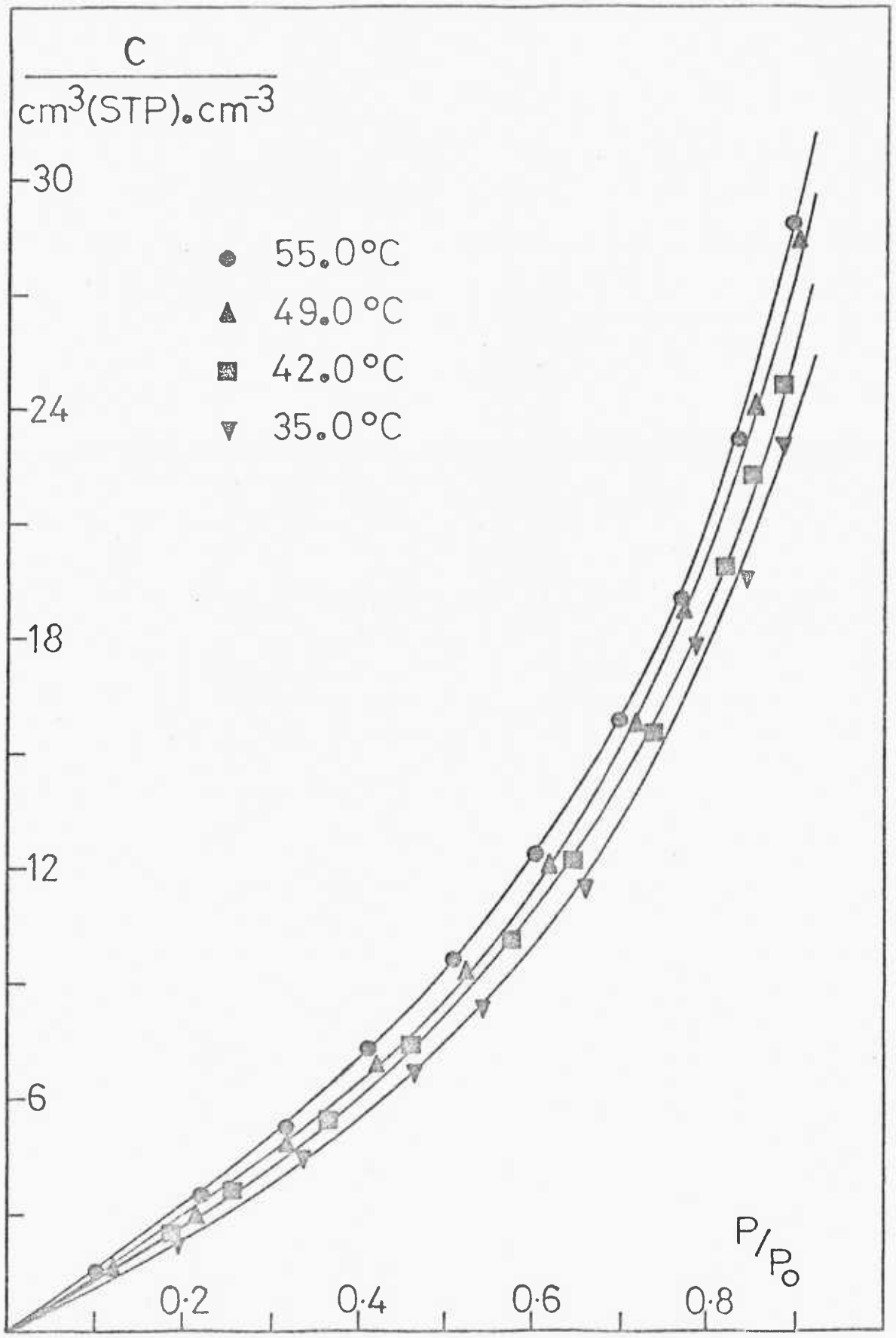


FIGURE 5.10 P(DMS-g-0·442 VAc)-H_2O SORPTION ISOTHERMS

The results of this investigation compare favourably with earlier measurements but there is some variation in the literature results.

The difference in solubility between the two components is large such that PVAc can be considered to be relatively hydrophilic and PDMS as very hydrophobic. The sorptive capacity of a polymer depends not only on the nature of the groups present but also on their positions on the polymer chains (17). Thus though the (Si-O) bond is partially ionic in nature it is effectively surrounded by the hydrophobic methyl groups of the side-chains which render the polymer, as a whole, hydrophobic. PVAc, on the other hand, possesses a relatively hydrophilic ester group in an accessible position on the side-chain which dominates the sorption behaviour of the PVAc polymer and the graft copolymers. For example, 83% of the total sorption of the 9.3% PVAc copolymer and 93% of that of the 15.7% PVAc copolymer is accounted for by the PVAc sorption. The dominance of the PVAc sorption is also reflected in the shapes of the isotherms for the copolymers. Of the graft copolymers, only the 3.41% PVAc sample shows the initial linear region, albeit reduced in length, associated with PDMS. The remainder of the copolymers show the continuously curving shape of the PVAc isotherm, even though there is always a slight doubt about isotherm shape in the very early stages of the isotherms. The departure from linearity of the PDMS sorption isotherm occurs at about the same relative pressure as that at which ionic salts dissolve in water. The most probably source of material causing the extra sorption is traces of ionic compounds obtained in the crosslinking reaction of PDMS by 2,4-dichlorobenzoyl peroxide in which benzoic acid is a by-product (25). This is difficult to remove by the reflux process and hence some remains within the sample. As a comparison, poly(ethylene) is as hydrophobic as PDMS (17) and obeys Henry's law at all pressures unless oxidative impurities are present when it behaves like PDMS. Hence it seems likely that impurities, or to a small extent the partially ionic (Si-O) bond, cause the deviation from Henry's law in the PDMS - water vapour system.

It can be seen from Figure 5.11 that the limiting solubilities of the copolymers are in good agreement with those expected from complete phase separation. Hence the solubility coefficient (σ) of the graft copolymers can be related to the volume fractions (ϕ) and solubilities of the two components :

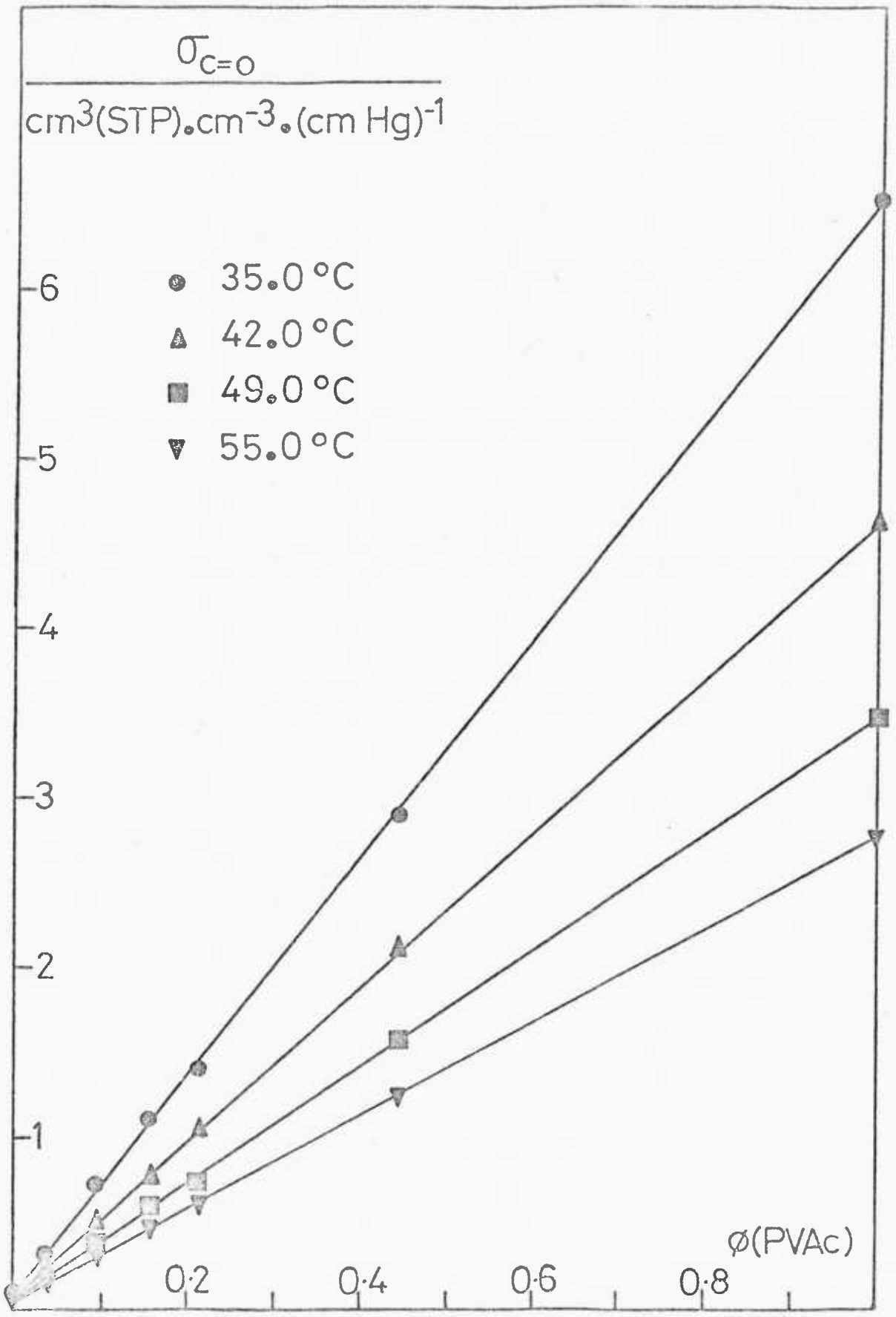


FIGURE 5.11 SOLUBILITY COEFFICIENTS

$$\sigma = \sigma_1 \phi_1 + \sigma_2 \phi_2 \quad \ldots.(5.4)$$

Whilst it is possible for occlusions to be present in a system with complete phase separation, it does not seem that this will be likely since there must be crosslinks through the PVAc regions linking the occluded and continuous PDMS phases.

5.2.2 Heats of Sorption

Heats of sorption ($\Delta\overline{H}_S$) in the limit (c→o) were calculated for each polymer and given in Table 5.3. Plots of log $\sigma_{c=o}$ vs. 1/T for water vapour in each copolymer are shown in Figure 5.12. In general the more water there is sorbed the more exothermic is the heat of sorption as a result of stronger interactions between the polymer and water.

Table 5.3

Heats of Sorption ($\Delta\overline{H}_S$, kJ mole^{-1}) in the limit (c→o)

ϕ (PVAc)	$\Delta\overline{H}_S$
0	- 19.6
0.034	- 30.9
0.093	- 32.0
0.157	- 34.6
0.214	- 35.4
0.442	- 35.4
1.00	- 35.9

The heat of sorption of PDMS is in reasonable agreement with a previous value (20) of ∿ 21 kJ . mole^{-1} for a similar sample (6% discrepancy). No value appears to be quoted in the literature for PVAc, even though the sorption isotherms have been determined.

The heats of sorption of the graft copolymers have been compared in Figure 5.13 with those expected from the two phase model. As expected from the solubility coefficient data agreement is very good. This clearly illustrates just how dependent the solubility process is on the presence of PVAc since the heat of sorption of the copolymers is

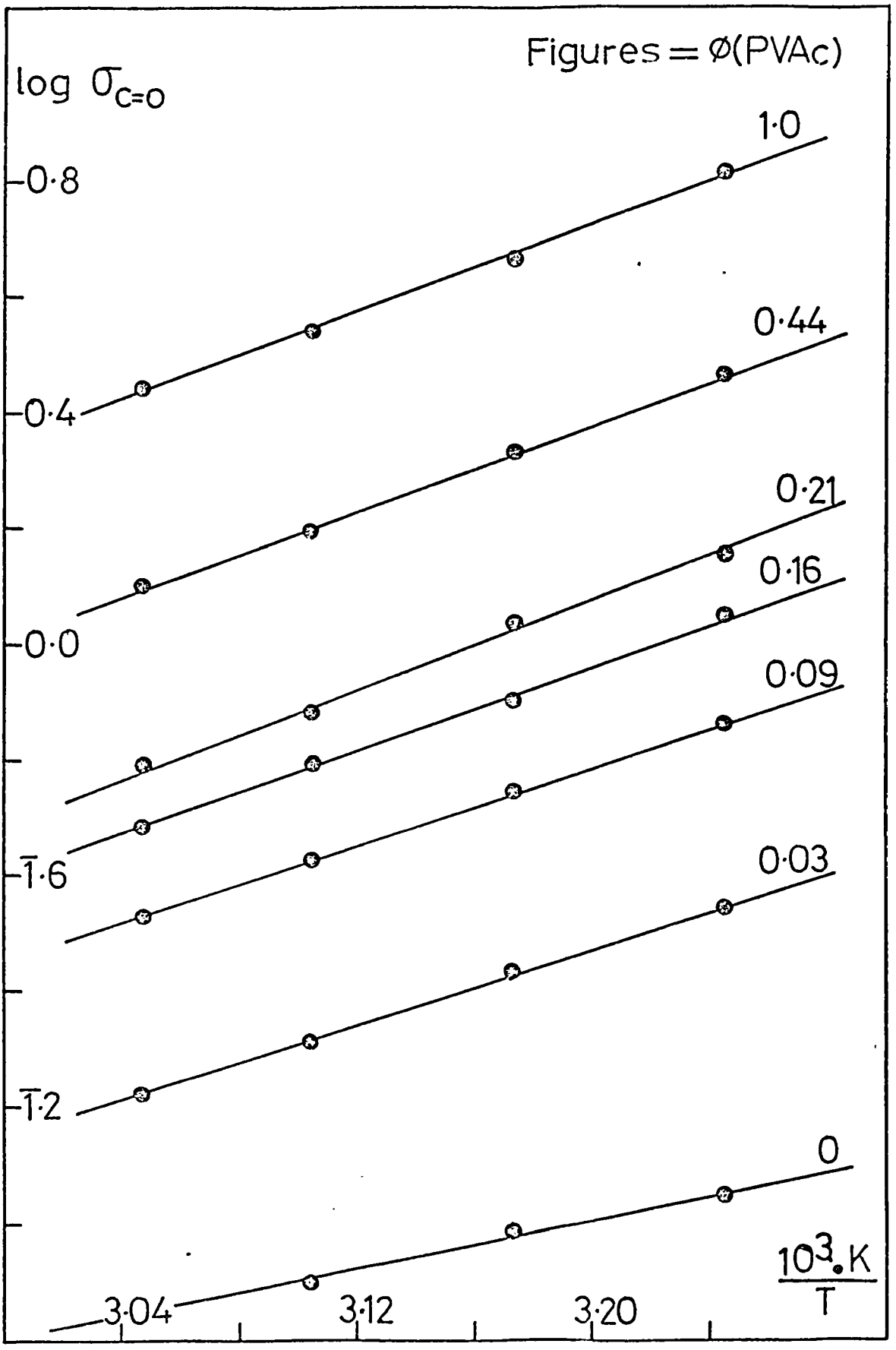


FIGURE 5.12 P(DMS-g-VAc)-H_2O
TEMPERATURE VARIATION OF SOLUBILITY

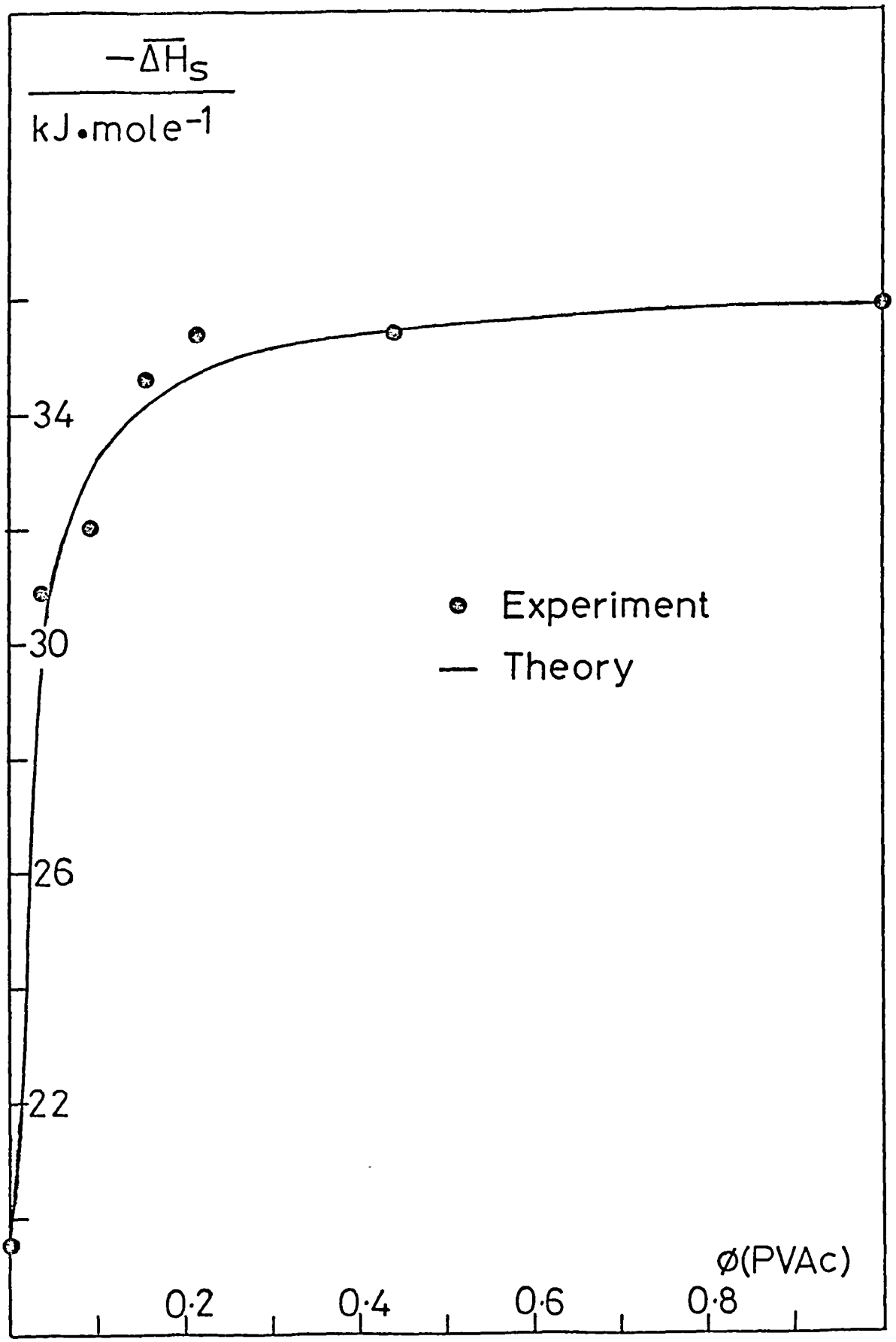


FIGURE 5.13 HEATS OF SORPTION

essentially that of pure PVAc when only about 25% PVAc is present.

5.2.3 Clustering Analysis

The clustering functions G_{AA}/V_A, $(1 + \phi_A G_{AA}/V_A)$ and $\phi_A G_{AB}/V_A$ will be referred to as X, Y, Z respectively and each was calculated for each polymer at various penetrant activities. Plots of a_A/ϕ_A vs. a_A and log ϕ_A vs. log a_A for PDMS and PVAc are presented in Figures 5.14 and 5.15 to illustrate the two possible extremes. The clustering functions derived from these are given in Table 5.4 for all polymers. It should be noted that since all these quantities are obtained from slopes of curves their accuracy is somewhat limited. The values of $X = -1$ and $Y = +1$ correspond to the initial regions of the isotherms for which clustering does not occur. This region is quite extensive for PDMS (up to $a_A \sim 0.45$) but much less so for the 3% PVAc copolymer (up to $a_A \sim 0.2$). For PVAc and the other graft copolymers there is no detectable linear region and the isotherm shapes are similar.

When comparing clustering of water in various polymers, it should be remembered that the actual magnitude of the X, Y, Z parameters depends upon the concentration of water sorbed. Thus, as more water is sorbed, X decreases and Y, Z increase for the same amount of clustering within the polymers. X is the clustering function ($X > 1$ indicates a tendency for penetrant to cluster), Y is the average size of a cluster and Z the mean number of solvent molecules in the neighbourhood of a point occupied by a polymer molecule in excess of the mean concentration of solvent molecules. Hence Y and Z tend to be similar in meaning.

As may be expected, X decreases with increasing PVAc content of the copolymers and hence as the volume fraction of water sorbed increases. However, to establish the relative clustering tendencies, the increase of X with water vapour activity is quite revealing. Thus, for PDMS, X varies from -1 to 2400 whilst that of PVAc increases only from 15 to 37. Hence the tendency to cluster is much more prominent in PDMS than PVAc. As suggested in the previous section, clustering in PDMS is probably initiated by ionic impurities remaining from the crosslinking reaction since clustering starts at a water vapour activity $a_A \sim 0.6$ and salts finally dissolve at $a_A = 0.73$ (68). PVAc is much less inclined to favour cluster formation since it sorbs more water vapour than PDMS and polymer - penetrant interactions are more frequent and more favourable than in PDMS. The graft copolymers show

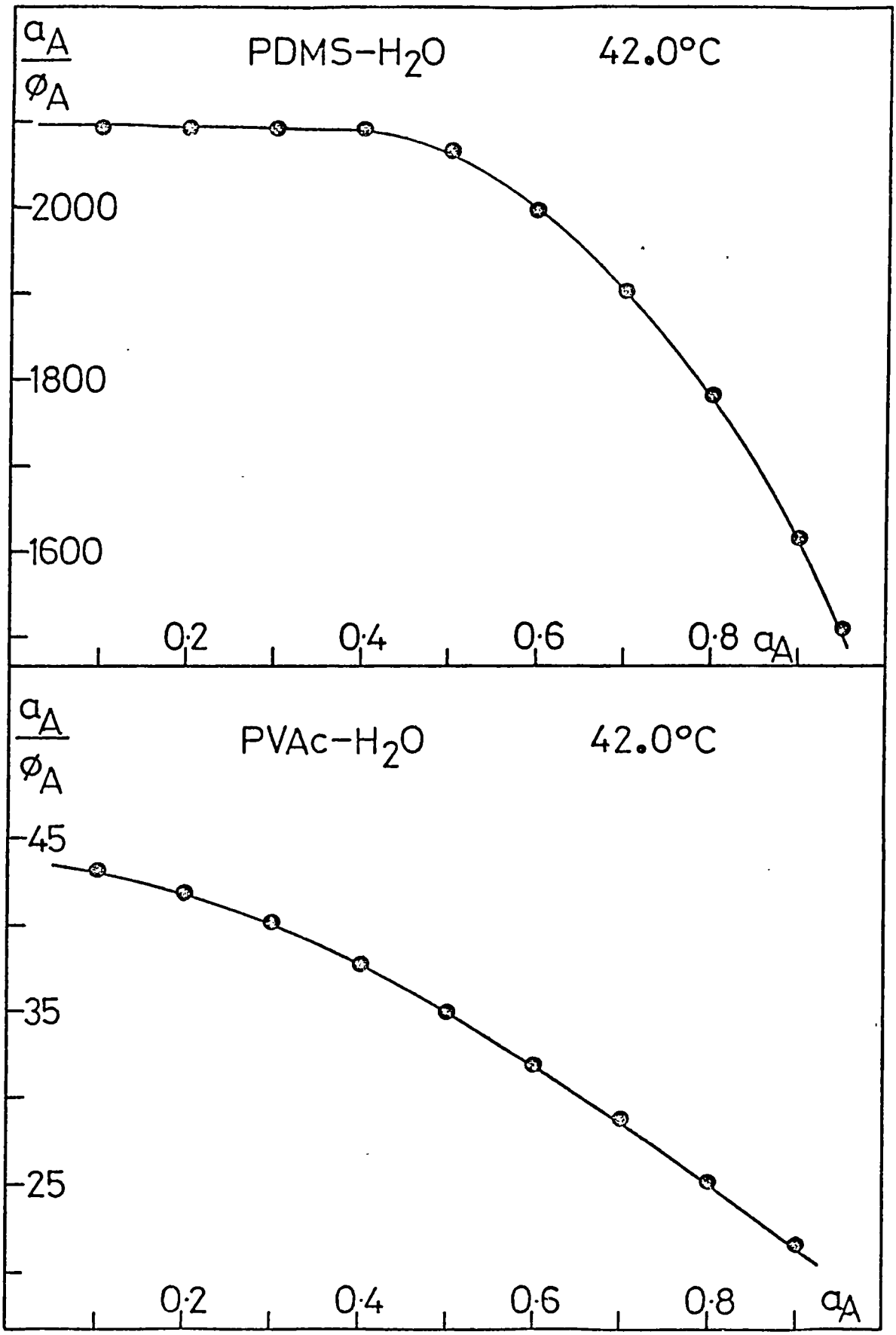
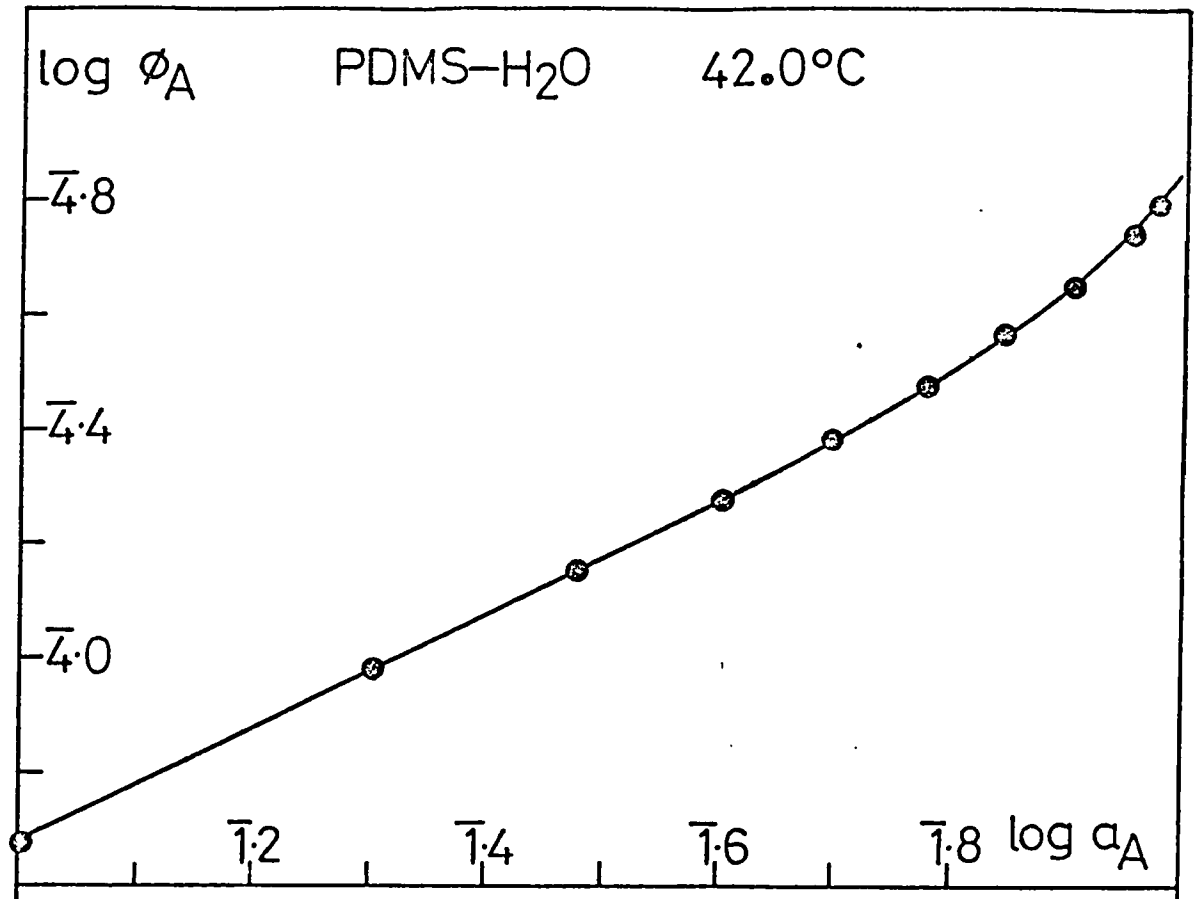


FIGURE 5.14 CLUSTERING ANALYSIS



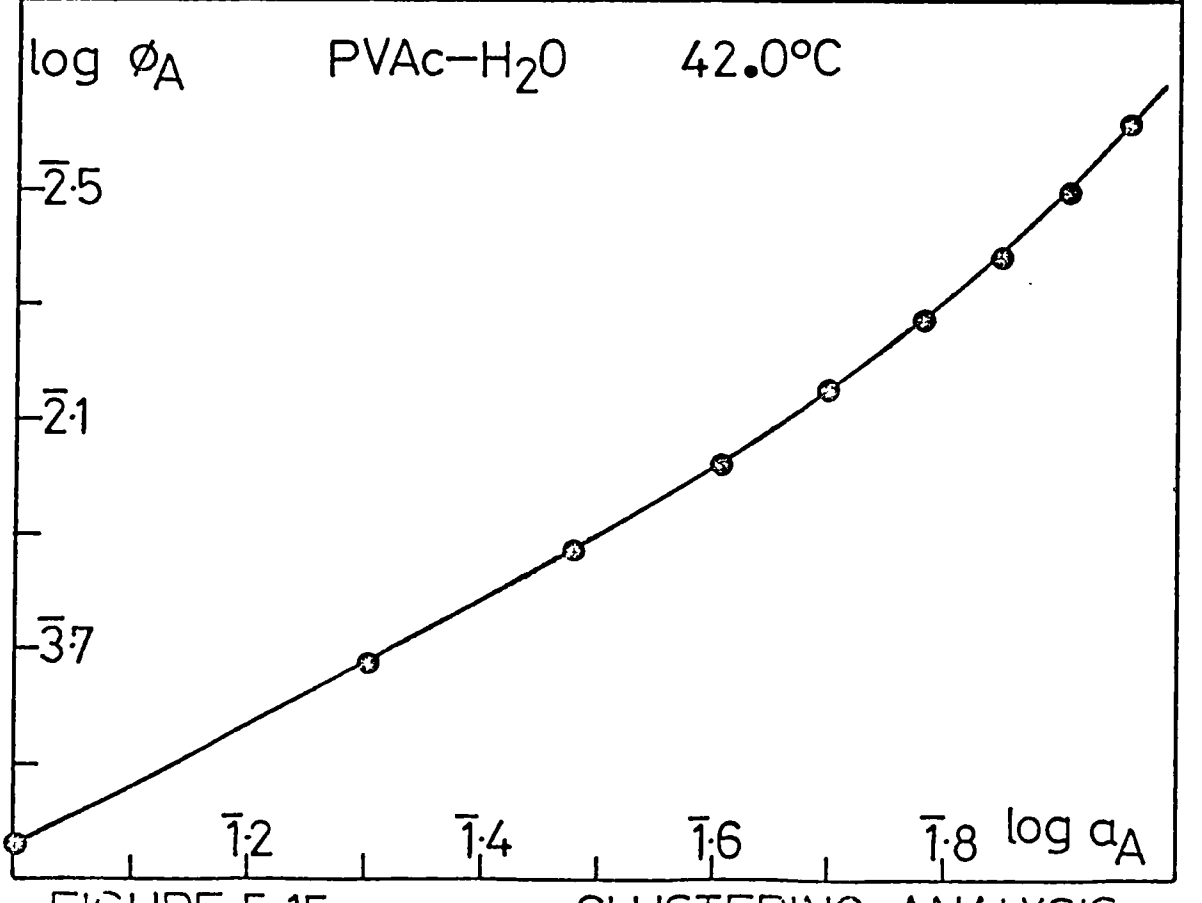


FIGURE 5.15 CLUSTERING ANALYSIS

Table 5.4

Clustering Functions for P(DMS - g - VAc) Copolymers
$(G_{AA}/V_A = X,\ (1 + \phi_A G_{AA}/V_A) = Y,\ \phi_A G_{AB}/V_A = Z$

ϕ		$a_A = 0.2$			$a_A = 0.5$			$a_A = 0.8$		
PVAc	T^oC	X	Y	$Z.10^3$	X	Y	$Z.10^3$	X	Y	$Z.10^3$
0	35.0	-1	1.00	-0.08	732	1.18	-0.23	2347	1.97	-0.74
	55.0	-1	1.00	-0.14	280	1.08	-0.37	823	1.52	-0.93
0.034	35.0	-1	1.00	-0.24	440	1.35	-0.91	687	2.00	-2.73
	55.0	-1	1.00	-0.32	332	1.30	-1.12	544	2.05	-3.59
0.093	35.0	139	1.09	-0.48	241	1.31	-1.64	411	2.13	-5.65
	55.0	70	1.04	-0.60	182	1.27	-2.07	294	2.00	-6.78
0.157	35.0	96	1.10	-0.80	161	1.40	-3.25	233	2.09	-10.8
	55.0	60	1.04	-0.99	129	1.40	-3.86	197	2.43	-14.7
0.214	35.0	108	1.13	-1.10	146	1.47	-4.43	164	2.04	-13.7
	55.0	48	1.03	-1.28	102	1.38	-5.01	152	2.16	-17.3
0.442	35.0	45	1.11	-2.20	67	1.44	-8.55	97	3.25	-44.3
	55.0	25	1.07	-2.71	49	1.40	-10.7	68	2.13	-35.9
1.00	35.0	15	1.05	-4.87	25	1.36	-18.7	37	2.26	-65.6
	55.0	12	1.04	-5.67	22	1.35	-21.9	29	2.03	-72.8

clustering behaviour intermediate between the two homopolymers such that there is a progressive change as the PVAc content of the copolymers increases.

From Table 5.4 it can be seen that the mean cluster size (Y) is approximately constant for all copolymers at any given penetrant activity. This also indicates the prevalent clustering trend since, although PVAc sorbs much more water, proportionately more water is much more clustered in PDMS. The excess mean solvent concentration (Z) shows essentially the same pattern.

In all cases clustering occurs to a lesser extent as the temperature is increased. This is not surprising since, at the higher temperatures, the penetrant molecules have more energy with which to break away from the clusters.

5.2.4 Heats and Entropies of Dilution

Heats ($\Delta\overline{H}_A$) and entropies ($\Delta\overline{S}_A$) of dilution were calculated for various penetrant concentrations using equations (2.33) and (2.34). Mean values of $\Delta\overline{H}_A$ and $\Delta\overline{S}_A$ over the temperature range studied are given in Table 5.5. Plots of log (p/p_o) vs. 1/T and log (p/p_o) vs. T for the PDMS - water system are illustrated in Figures 5.16 and 5.17.

It can be seen from Table 5.5 that $\Delta\overline{H}_A$ and $\Delta\overline{S}_A$ both decrease with increasing penetrant concentration. This is in accord with the fact that penetrant-penetrant interactions become more important at the higher concentrations. In addition, as the PVAc content of the copolymers increases from 0.157 ϕ (PVAc), the values of $\Delta\overline{H}_A$ and $\Delta\overline{S}_A$ are roughly constant consistent with sorption being primarily in the PVAc phase.

5.3 Steady-State Permeability Results

A sample calculation of permeability data is given in Appendix 8.3. Graphs of permeation rate against relative vapour pressure of water for PDMS, PVAc and the P(DMS-g-VAc) copolymers are illustrated in Figures 5.18 - 5.24. The plots are linear for PDMS and the graft copolymers, except for the 44.2% PVAc copolymer which shows a little curvature. This curvature is a scaled down version of that for PVAc and indicates that for this copolymer there may be a tendency to form continuous regions of PVAc. The shapes of the permeation curves for the two homopolymers are consistent with previous results. Because of the relatively large amount of water sorbed by PVAc some degree of plasticisation of the polymer matrix is anticipated and probably accounts for the curvature in the permeation isotherm.

5.3.1 Difficulties Associated with Water Vapour Permeation

Compared with gases and organic vapours water vapour is relatively strongly sorbed by the surfaces of the pressure measuring system. This feature renders accurate measurement of steady-state and in particular transient-state permeation difficult (19, 120, 135).

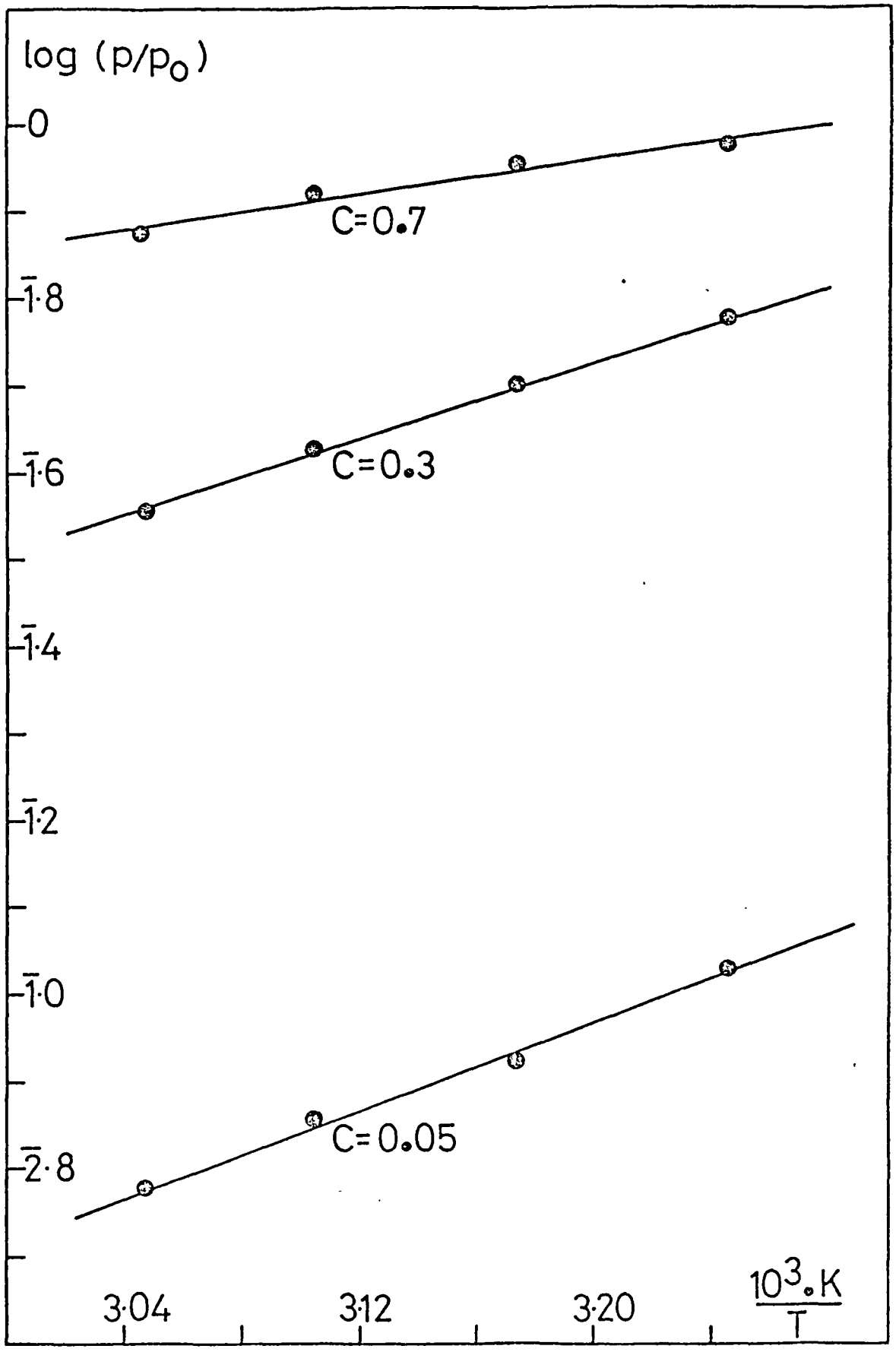


FIGURE 5.16 PDMS—H_2O

HEATS & ENTROPIES OF DILUTION

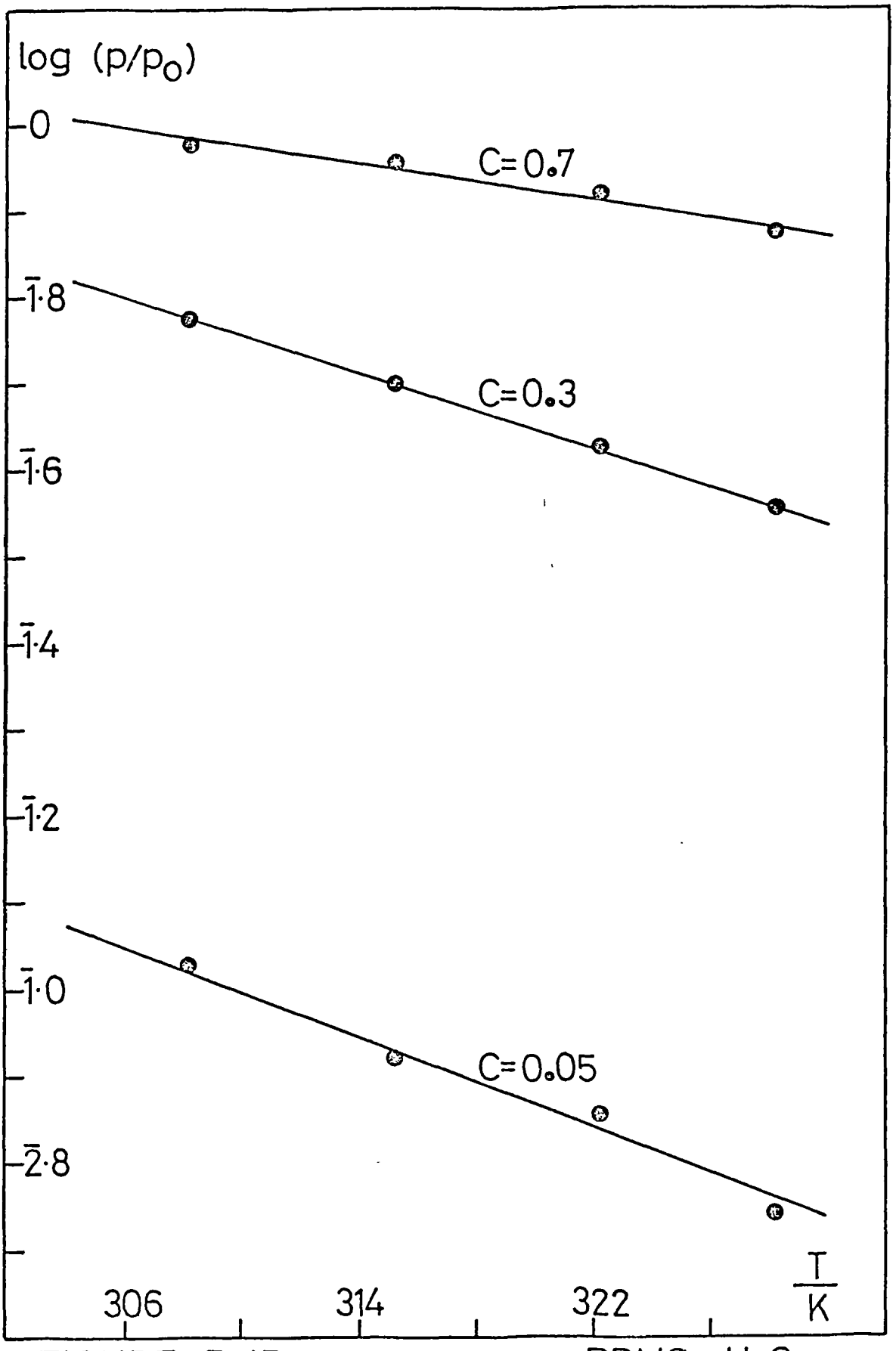


FIGURE 5.17 PDMS—H_2O

HEATS & ENTROPIES OF DILUTION

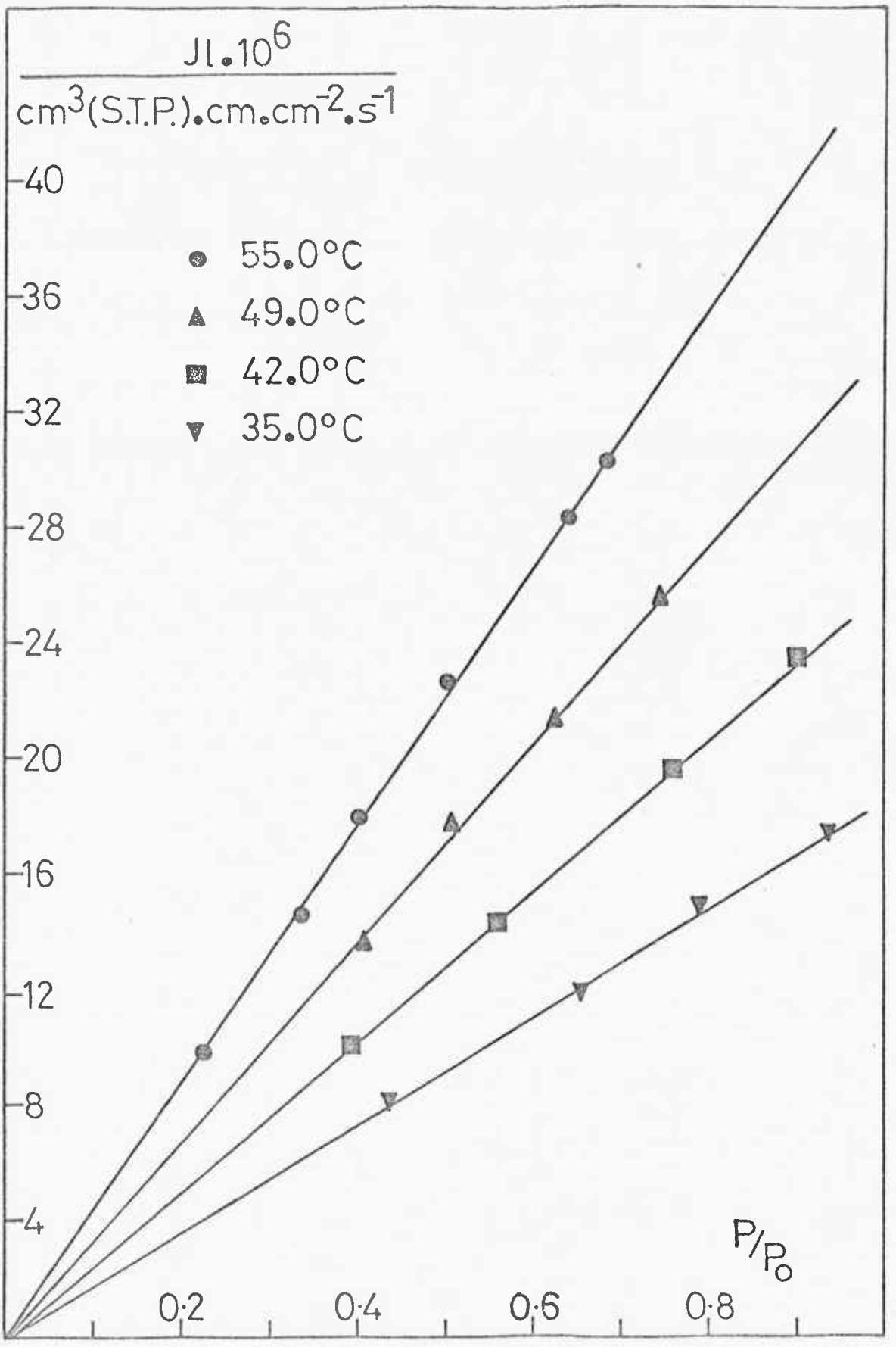


FIGURE 5.18 PDMS-H_2O

PERMEATION ISOTHERMS

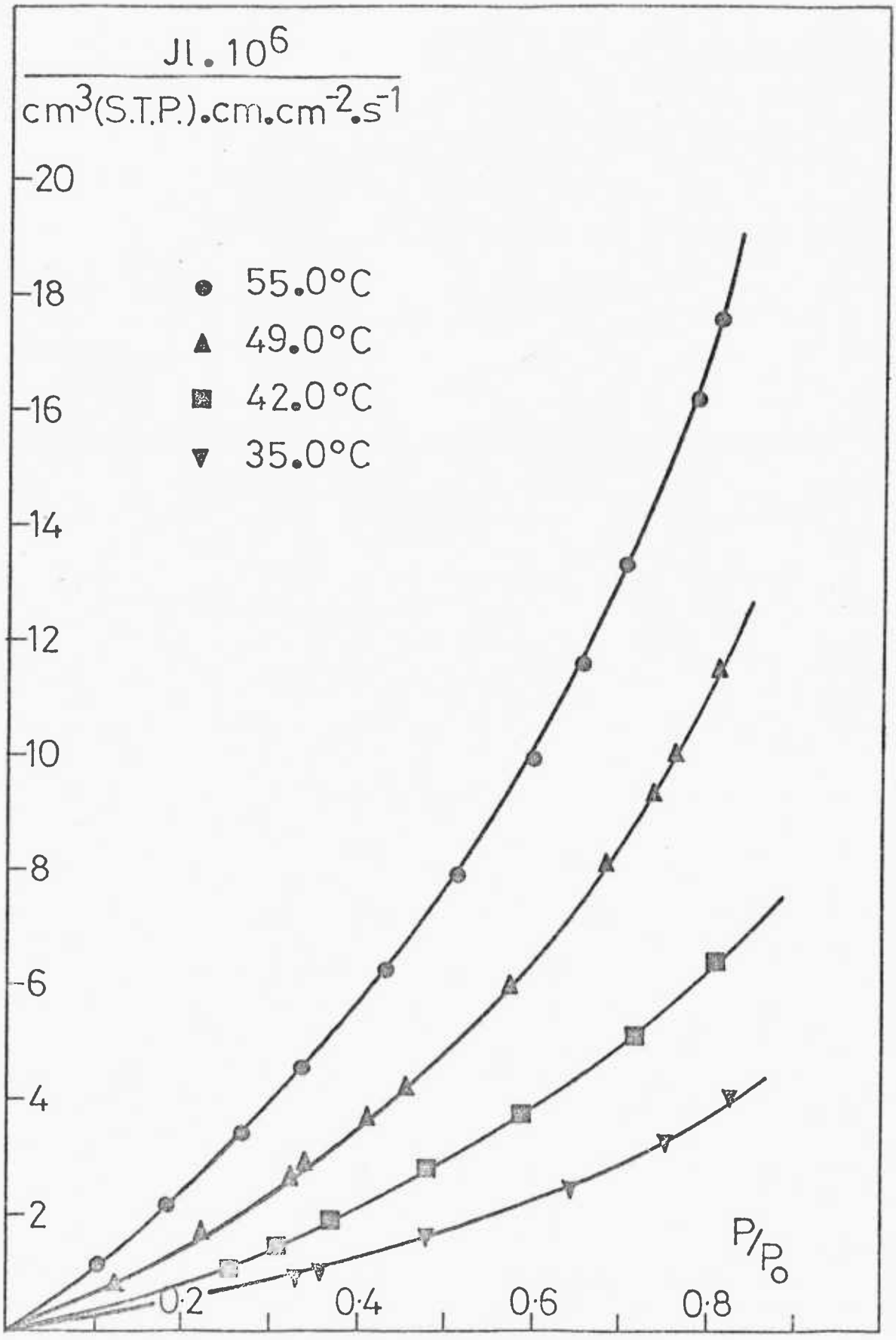


FIGURE 5.19 PVAc–H_2O

PERMEATION ISOTHERMS

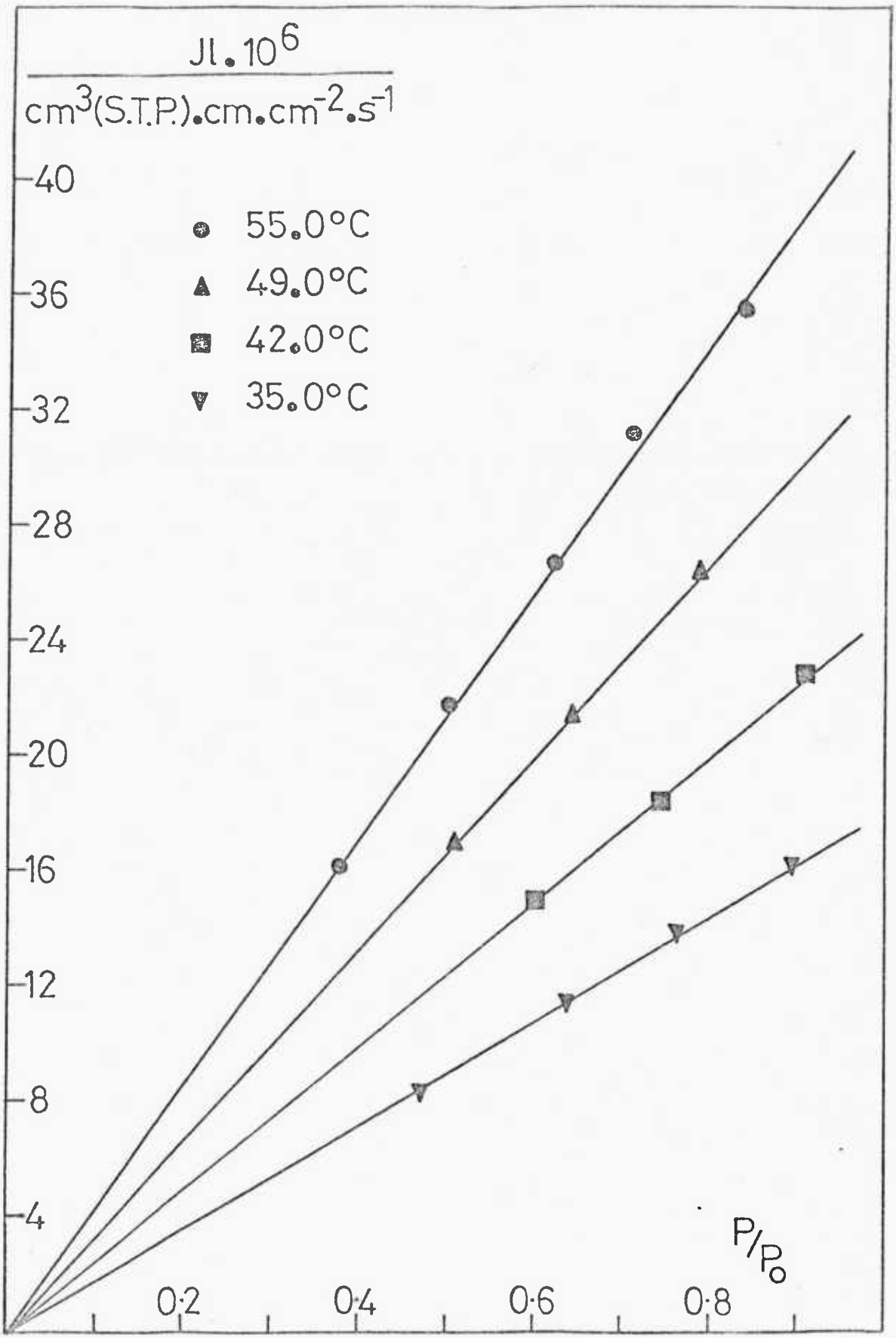


FIGURE 5.20 P(DMS-g-0·034 VAc)-H_2O

PERMEATION ISOTHERMS

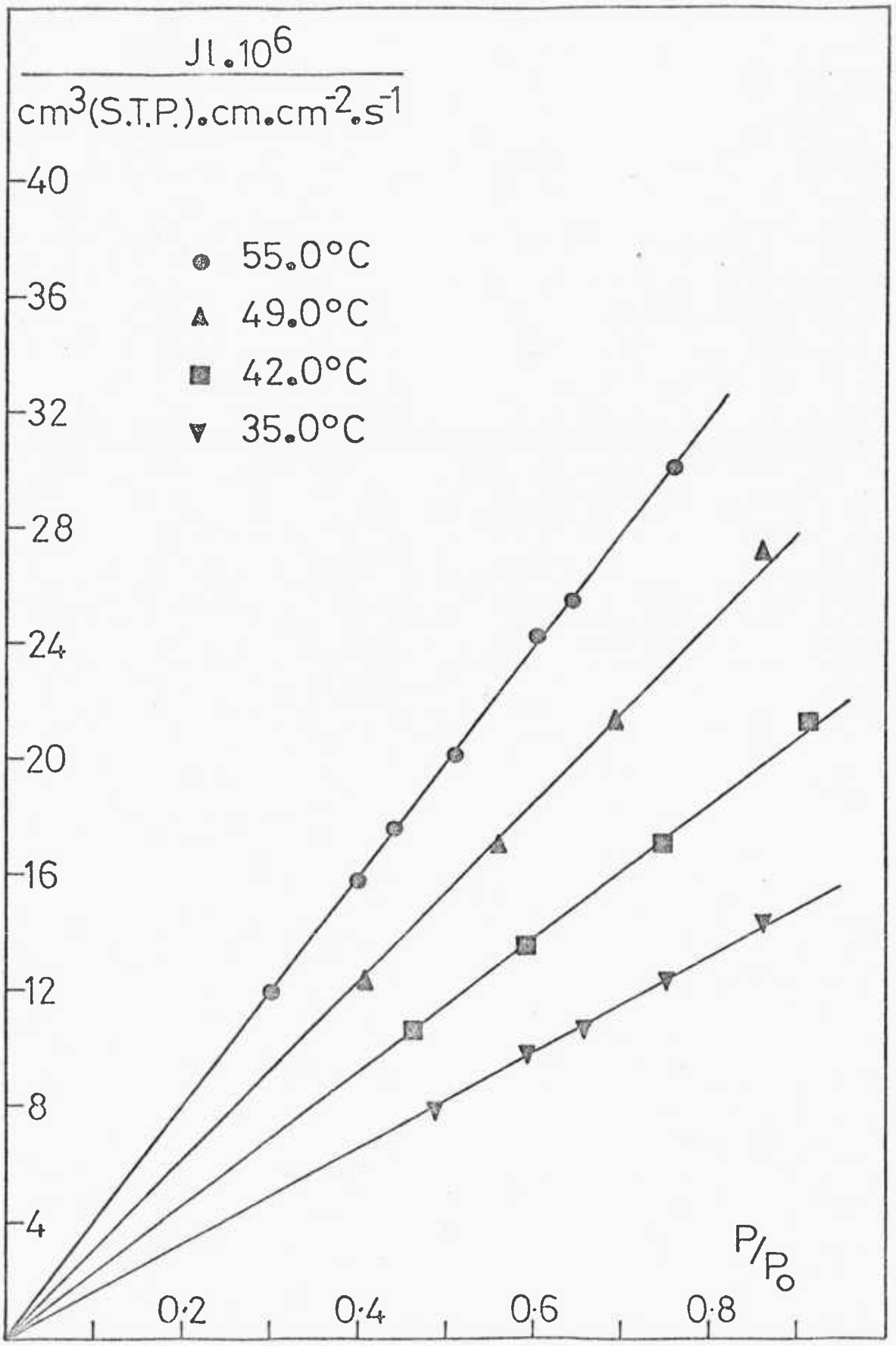


FIGURE 5.21 P(DMS-g-0·093 VAc)–H_2O PERMEATION ISOTHERMS

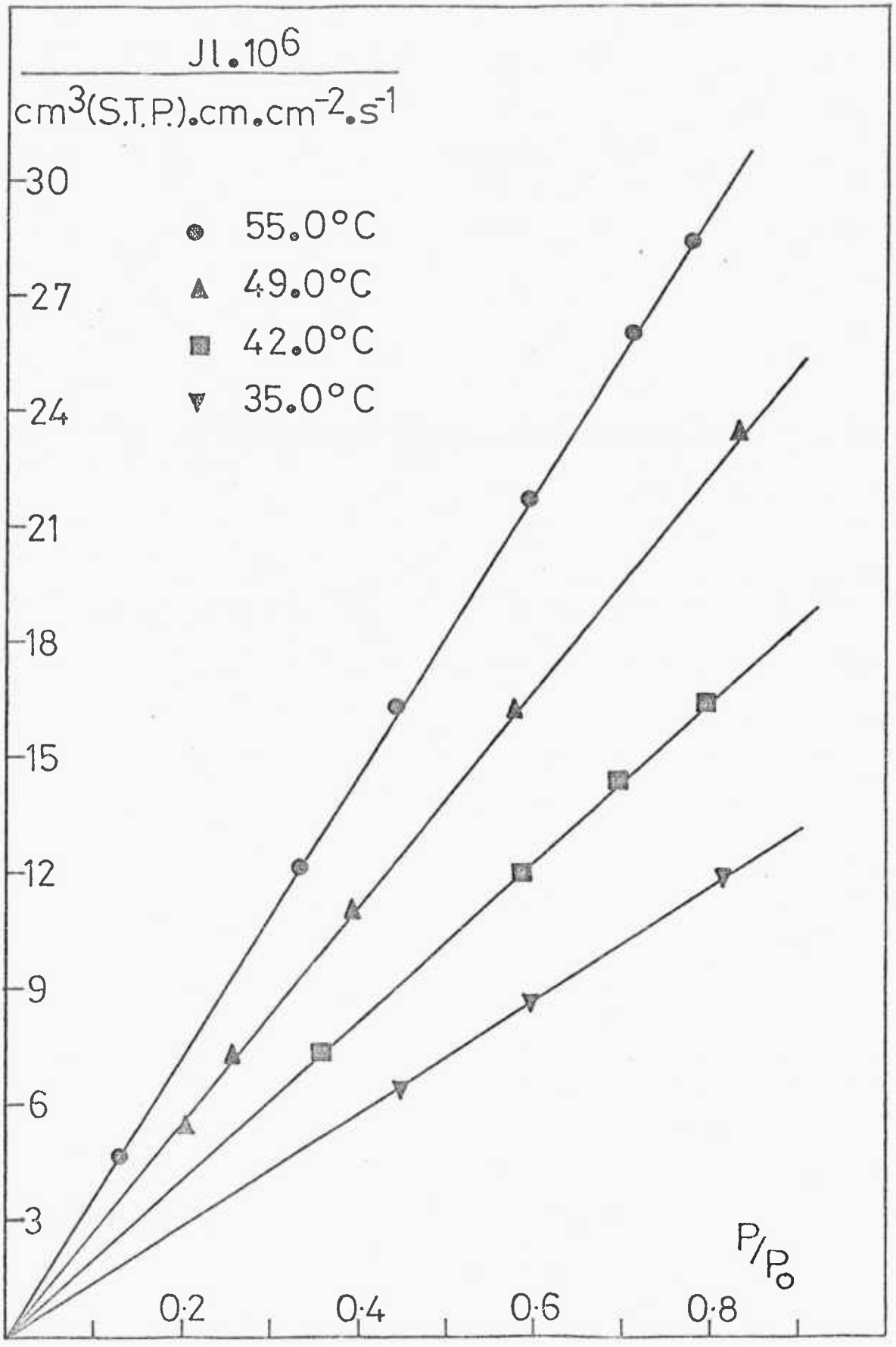


FIGURE 5.22 P(DMS-g-0·157 VAc)-H_2O

PERMEATION ISOTHERMS

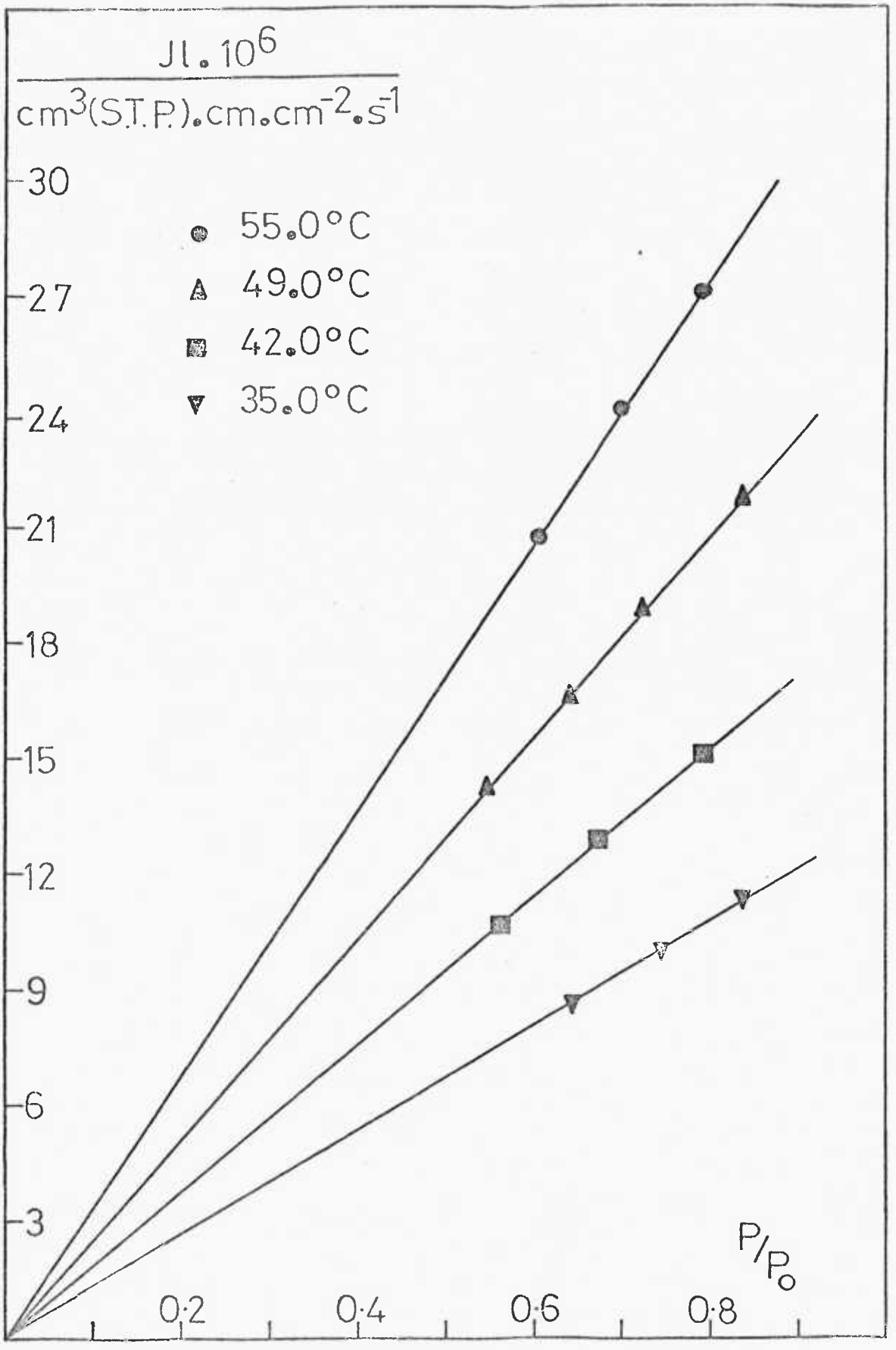


FIGURE 5.23 P(DMS-g-0·214VAc)-H_2O PERMEATION ISOTHERMS

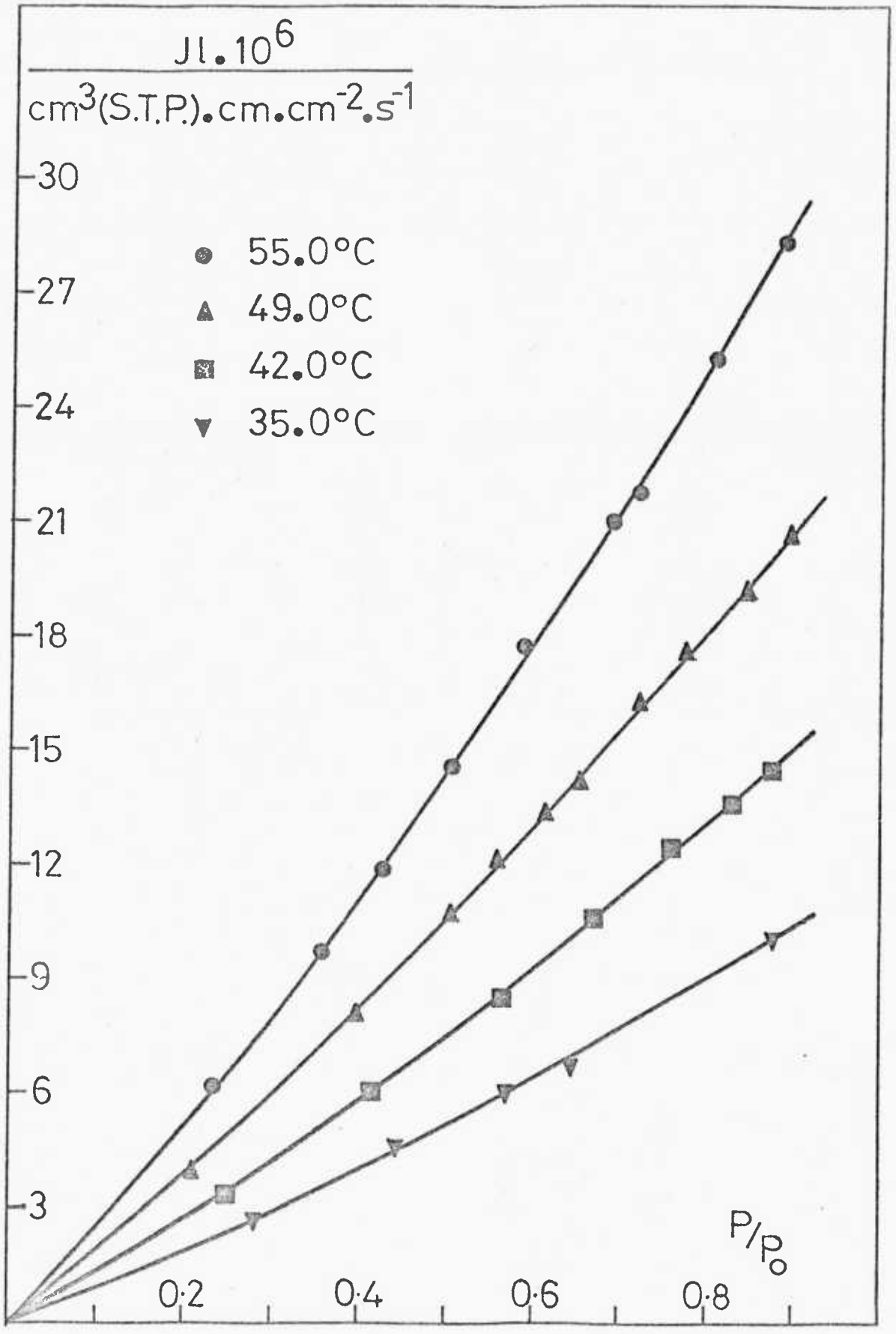


FIGURE 5.24 P(DMS-g-0·442 VAc)–H_2O PERMEATION ISOTHERMS

Table 5.5

Mean Heats ($\Delta\bar{H}_A$) and Entropies ($\Delta\bar{S}_A$) of Dilution in the Temperature Range 35 - 55°C

ϕ(PVAc)	cm^3(S.T.P.).cm^{-3} Concentration	$kJ.mole^{-1}$ $\Delta\bar{H}_A$	$J.K^{-1}.mole^{-1}$ $\Delta\bar{S}_A$
0	0.05	20.9	93.5
	0.3	18.8	75.4
	0.7	8.54	31.8
0.034	0.1	12.9	64.0
	1.5	6.32	23.6
	2.7	3.22	10.4
0.093	0.5	10.8	49.2
	2	8.67	32.4
	5	4.65	16.5
0.157	1	8.04	41.4
	6	3.27	12.1
	10	1.80	5.99
0.214	1	9.29	46.2
	6	4.15	16.8
	12	2.85	9.97
0.442	2	10.1	47.4
	10	6.57	25.4
	25	2.55	8.88
1.00	5	7.49	40.1
	20	4.90	20.4
	50	2.64	9.71

Thus transient diffusion data, as normally obtained by measurement of the time lag, are relatively unreliable (19, 135). For example some "time lag data" are given for the P(DMS-g-0.157 VAc) copolymer in Figure 5.25 which illustrates the difference between the measured time lags and those predicted from steady-state diffusion data (53). The lower

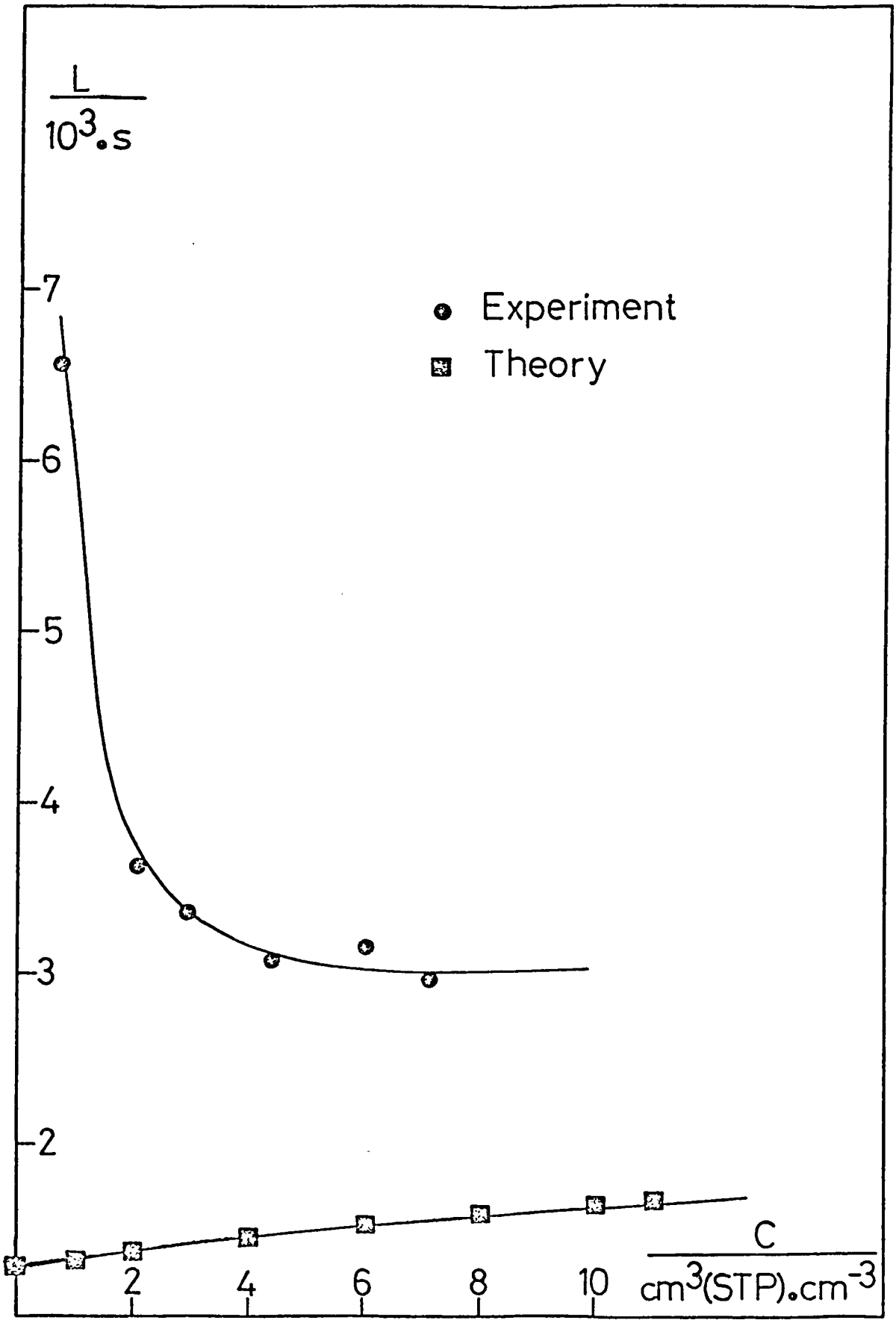


FIGURE 5.25 P(DMS-g-0·157 VAc)–H_2O
TIME LAG DATA

the flux-rate and the lower the magnitude of the pressures measured the more does sorption affect the results as the attainment of equilibrium sorption between the water vapour and the glass surfaces may take about 15 minutes (52). Some attempts have been made to overcome this problem (135) by pre-treating the "down-stream" part of the apparatus with a charge of water vapour. This reduces the discrepancy but agreement is still not good and hence it seems that sorption kinetics is a much more appropriate method of obtaining transient diffusion coefficients.

The effect of water vapour sorption on steady-state permeation is not so marked; however, it is not negligible and may be quite significant. It has been estimated that sorption effects cause a 3-4% drop in measured permeabilities (19, 84). However if, at the end of a set of measurements, the water vapour is pumped away and a new set of measurements taken then this 3-4% drop in permeability is recovered such that true permeabilities can be obtained. When however the Baratron manometer is used to monitor the pressure in the "downstream" section of the apparatus these effects may be even more pronounced. The design of the measuring head (type 90-H1) is such that one of the two sensing electrodes (measurement and reference) is placed on the sensing side of the diaphragm and hence is exposed to the penetrant vapour. These electrodes are supported on ceramic thermal insulators which are porous and capable of sorbing large quantities of water vapour. Consequently there is a serious reduction in the measured pressure which is difficult to circumvent. It was thus necessary to measure permeabilities by a different means so that a comparison could be made.

The alternative method employed was that a calibrated silica spring supporting a bucket containing molecular sieve (type 13X) was used. With this system the residual pressure of vapour in the measuring system is always relatively small. Calibration of the Baratron in this fashion was considered to be worthwhile as it affords a much more convenient method of measurement.

The spring chamber was incorporated into the permeation apparatus (Figure 3.2) such that either the spring, or the Baratron could be used during any particular experiment. Hence a direct comparison could be made under identical conditions.

It was found that permeabilities measured on the Baratron were lower than those measured on the spring. These results were reproducible and a calibration line was constructed for conversion of

Baratron fluxes to those of the spring as shown in Figure 5.26. Table 5.6 shows flux-rates measured by Baratron and the spring as well as the "ideal Baratron flux-rates" which would correspond to the flux measured by the spring. The discrepancy between Baratron and spring results is about 10%. To ensure that the spring results were themselves not affected by sorption effects flux-rates were measured with different outgoing volumes of about 1, 5 and 7 litres. It was found that both flux-rates and the residual vapour phase pressure were independent of the outgoing volume indicating that sorption effects did not affect these measurements. The calibration was found to depend only on the flux-rates through the membrane. The temperature of the membrane, pressure range measured (provided that this does not exceed 0.5% ingoing pressure), Baratron head temperature and outgoing volume (after the initial measurement) were found to make very little difference to the measured flux-rates and calibration.

5.3.2 Absolute Magnitudes of Permeabilities

Values of permeabilities (P) for each system are given in Table 5.7; those for PVAc and P(DMS-g-0.442VAc)refer to the lim(c→o) since permeabilities are concentration-dependent in these systems. The results obtained for PDMS are within 1% of earlier values (20). Permeability measurements have been reported in the literature for PVAc (74) but values of P are not given. The earlier PDMS results were obtained using the calibrated spring technique.

Various models have been proposed to predict the permeability of two phase systems such as are encountered with these copolymer systems. A brief outline of the form and conditions of use of some of these models has been given in Section 4.2 and only these will be considered further. For a fuller description several reviews of the subject are available (12, 39, 92) though none is entirely comprehensive.

Maxwell (87) considered a single sphere embedded in a continuum when the activity gradient is unidirectional and linear at great distances from the sphere. Subsequently it was assumed that the gradient in the continuous phase around the sphere is perturbed by the presence of the sphere. By considering the effect of this perturbation throughout all the continuous phase, Maxwell was able to formulate the model for the system as a whole (the mathematical formula is presented in Section 4.2.1). Hence, as only one sphere dispersed in a continuum

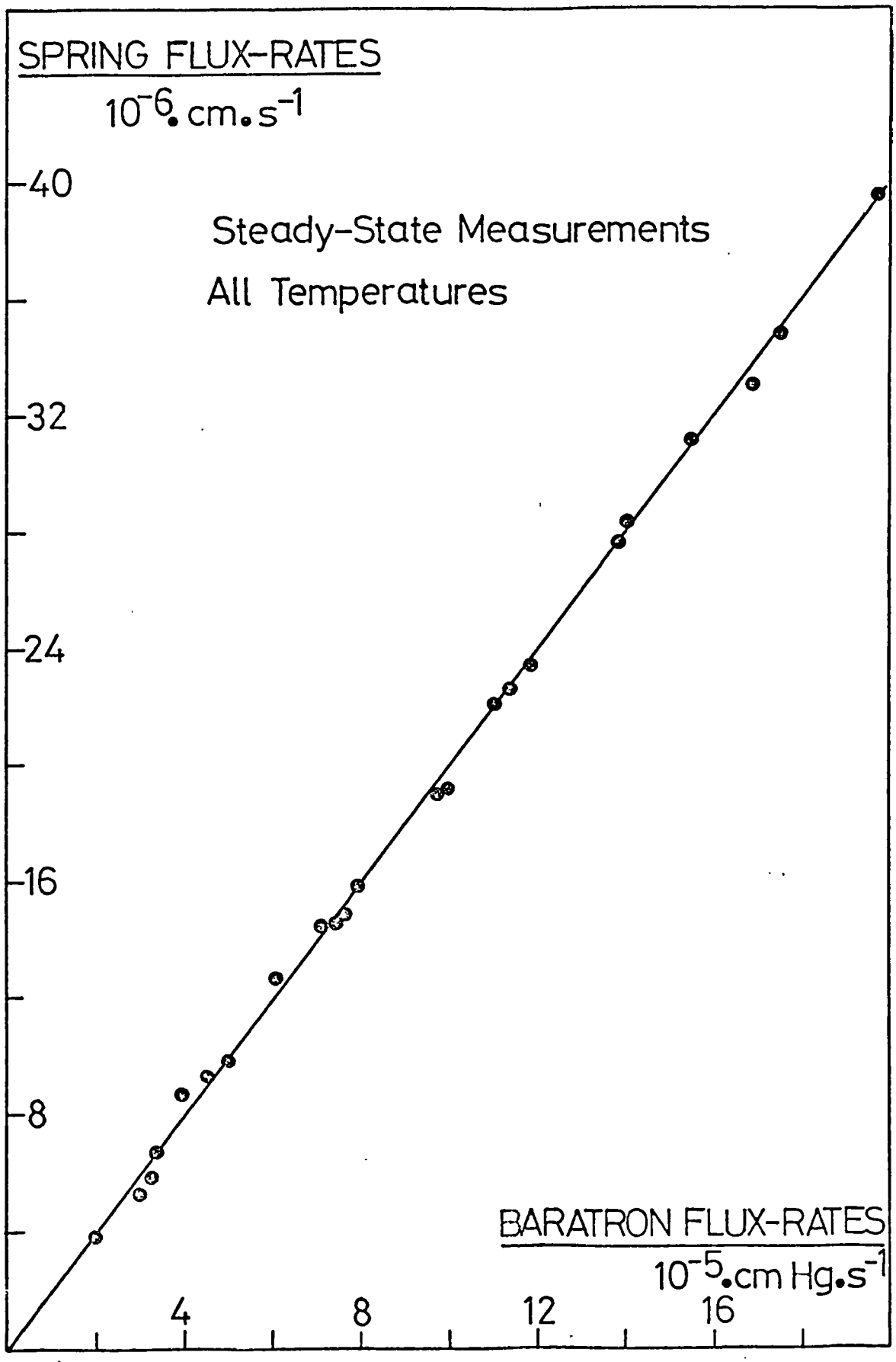


FIGURE 5.26
SPRING—BARATRON CALIBRATION

Table 5.6

Baratron and Spring Flux-Rates

Measured Baratron Rates 10^5.(cm Hg).s^{-1}	Measured Spring Rates 10^6. cm . s^{-1}	"Ideal" Baratron Rates 10^5.(cm Hg).s^{-1}
2.002	3.908	2.165
3.007	7.372	4.112
3.297	5.918	3.252
3.487	6.852	3.768
3.975	8.773	4.897
4.572	9.342	5.203
4.977	9.938	5.493
6.040	12.70	7.097
7.043	14.48	8.037
7.413	14.58	8.048
7.598	14.91	8.253
7.910	15.88	8.735
9.630	19.02	10.54
9.907	19.23	10.72
10.99	22.15	12.27
11.24	22.65	12.49
11.33	22.63	12.70
11.33	22.88	12.67
11.78	23.45	13.10
13.83	27.60	15.23
14.04	28.42	15.86
15.44	31.20	17.38
16.88	33.03	18.42
17.45	34.80	19.15
19.68	39.55	22.18

Table 5.7

Permeability Coefficients P(cm^3(S.T.P.).cm^{-1}.(cm Hg)$^{-1}$.s^{-1})

	P . 10^6			
ϕ (PVAc)	35.0°C	42.0°C	49.0°C	55.0°C
0	4.410	4.184	3.923	3.743
0.034	4.246	4.054	3.815	3.644
0.093	3.885	3.722	3.527	3.371
0.157	3.451	3.358	3.211	3.100
0.214	3.189	3.106	2.981	2.910
0.442	2.189	2.261	2.290	2.228
1.00	0.555	0.681	0.847	0.977

was considered, this model is applicable for dilute suspensions (20% dispersed phase by volume) of spheres.

Wagner (129) has attempted to simplify the Maxwell expression by expanding it in a Taylor's series about $V_D = 0$ (V_D = volume fraction of the dispersed phase) and neglecting all but the first two terms. However this treatment yields similar results to that of Maxwell but is applicable over a shorter range of suspension concentration and hence there is no advantage to be gained.

Several attempts have been made to extend the Maxwell model to greater concentrations of dispersed phase. Rayleigh (103) treats the situation of uniform spheres in a cubic lattice and introduces some "interaction" of the fields surrounding each sphere whereby, using the principle of superposition of potentials, he obtained expressions for the permeability of the continuous and dispersed phases in the form of series expansions. The overall permeability was than obtained by finding the relationships between the constant terms of the two expansions. It was found that this reduces to the Maxwell expression for very dilute suspensions and is applicable up to $V_D = 0.524$ at which point the spheres touch and form the continuous phase. The Rayleigh approach has been extended by Meredith & Tobias (93) who applied a different function for the activity gradient and considered higher terms in the series for the gradient in the continuous phase. This treatment is expected to be more realistic at higher concentrations (20-45%) of the disperse phase (92). (Both are formulated in Section 4.2.2).

Another adaptation of the treatment for concentrated suspensions has been proposed by Higuchi (62, 63) for a random distribution of uniform spheres. It is assumed that, for any sphere of the dispersed phase, the concentration gradient of penetrant in that sphere is induced by the overall gradient which is modified by the presence of the perturbations due to the neighbouring spheres. Since one cannot ascertain the magnitude and direction of the overall interactions in a random mixture it is necessary to introduce an empirical constant which fortuitously is found not to be a function of the volume fraction of dispersed phase (Section 4.2.3).

In concentrated suspensions Bruggeman (28) suggests that the gradient within any particular sphere is induced by the gradient of the system as a whole rather than that of the continuum. The most severe

limitation of this approach is that the model applies only to dispersions that have a wide distribution of particle sizes. This arises as a consequence of having to increase the dispersed phase concentration infinitesimally in order to evaluate the concentration gradient of the system. It is found that these successive additions require the size of the dispersed phase to be greater than any added previously. This approach has been adapted by Meredith & Tobias (94) to include the case of the dispersed phase being of uniform size. Only half the particles are added in a similar manner to that of Bruggeman and the procedure is then repeated with the other half so that there is a tighter control of particle size. These models are also formulated in Section 4.2.3.

Böttcher (27) considered the case where the gradient in a particle is related to the gradient in the system immediately around the particle. This surrounding area may contain other dispersed particles as well as continuum. However this approach has been criticised (94, 99, 101) as it applies only to spherical particles and only for very dilute suspensions similar to those for which the Maxwell expression is applicable.

These are the general outlines of the method of derivation and range of validity of each of the models that will be considered in this Section. The Maxwell model is perfectly satisfactory for systems containing dilute suspensions of dispersed phase. However the other models have all been proposed in order to extend the range of applicability. It is necessary, in this instance, to specify the distribution of dispersed phase throughout the continuum and the two common ones are random and cubic arrangements. It is reported (92) that ordered arrangements result in less average interaction between particles than random arrangements. Only the Higuchi (62, 63) Böttcher (27) and Bruggeman (28) models are derived for random arrangements and it may be anticipated that these may approach most closely the distributions found in practice.

It is necessary when interpreting experimental data in terms of these models to specify which component forms the continuous phase. Provided that the two components are incompatible and form two distinct phases then either component may be discontinuous and the models are applicable to both situations. The experimental data cover the composition range of 0 - 45% PVAc by volume and also both homopolymers

have also been studied. As previously stated (Section 5.1.3 and Appendix 8.1) PDMS forms the continuous phase in all the copolymers studied and hence the 0 - 50% PVAc region will form the basis of the comparison of experimental and theoretical permeabilities.

The 35.0°C isotherm has been chosen for comparison of experimental and theoretical permeabilities since this is the one that has the greatest difference in the permeabilities of the two homopolymers, and hence there is more chance to differentiate between the various models. The situation is illustrated in Figure 5.27 for PDMS as the continuous phase and where the circles represent smoothed experimental data. To a first approximation all the models, except the Series/Parallel, are a reasonable representation of the behaviour found experimentally. This is not unexpected as the continuous PDMS phase is the component with the higher permeability and hence the effects of increasing domain interactions tend to be of a secondary nature. However it is possible to differentiate between the various models to some extent and the Higuchi, Böttcher and Bruggeman (and its adaptation by Meredith and Tobias) models seem to fit the experimental data most closely. There are only small differences between the permeabilities predicted by the Maxwell, Rayleigh-Runge, and Meredith & Tobias models since they are variations of the same method. These differences will be more significant if there were a greater discrepancy between the permeabilities of the homopolymers. The simplified Wagner approach appears to over-compensate for the interactions between domains and predicts permeabilities that are significantly lower than found experimentally in the 20-50% PVAc range. On balance the Higuchi, Böttcher and Bruggeman approaches are probably the most realistic and the most appropriate representations of the experimental data.

In order to complete the comparison of experimental and theoretical permeabilities and to differentiate between the models, the complete composition range ought to be employed. However the 50-100% PVAc by volume range has not been covered as there were some experimental difficulties which made this region very hard to obtain. In order to make the copolymer containing 44% PVAc by volume it was necessary to prepare the membrane in two stages. After irradiation and extraction in the usual manner, the graft sample was swollen with more monomer and re-irradiated. However, in contrast to the initial irradiation, half of the monomer polymerised could be extracted so that it was not possible to increase the PVAc content within the graft copolymer very rapidly and

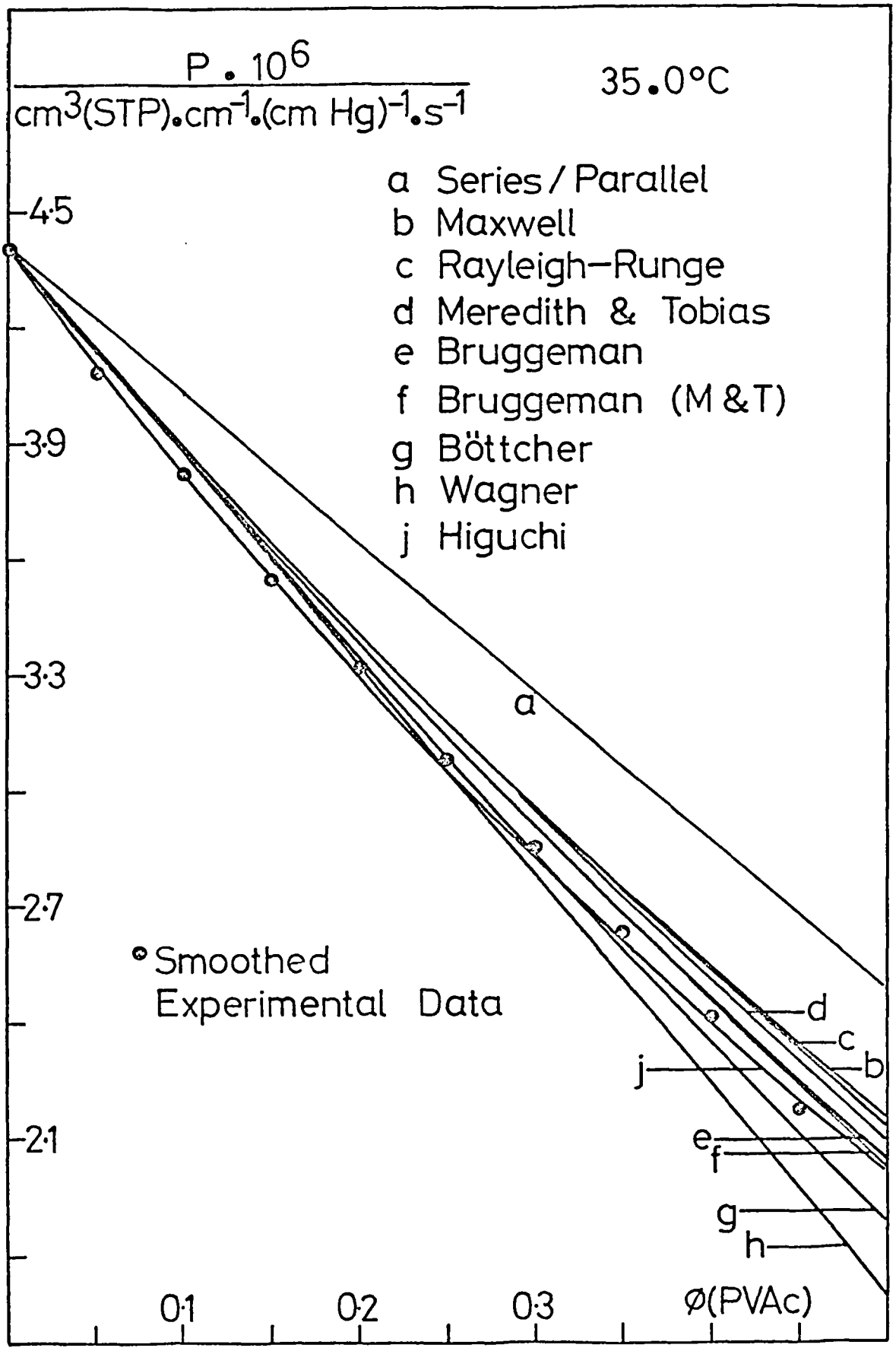


FIGURE 5.27
THEORETICAL P—Ø RELATIONSHIPS

hence further irradiation was not considered appropriate. One further consideration is that copolymers with PVAc as the continuous phase and of thicknesses similar to those found here would take a prohibitively long time to come to equilibrium and hence render low accuracy to the measurements. Further attempts to prepare membranes in the desired range of PVAc content were made by trying to form blends of the two homopolymers. However, as the two polymers are incompatible, homogeneous films of the polymer mixtures could not be cast from a mutual solvent since the minor component always came out of solution initially as large aggregates. Hence it is very difficult to obtain copolymers of these two polymers containing greater than 50% PVAc by volume.

However, the models have been used to calculate the overall permeability of the systems in the range 50-100% PVAc assuming that PVAc is the continuous phase. These are illustrated in Figure 5.28 for the 35.0^{o}C isotherm. Comparison of Figures 5.27 and 5.28 shows that the divergence of the permeabilities predicted by the various models is much greater in the latter. This is to be expected as the more permeable PDMS is contained within the disperse phase and this tends to exaggerate the differences caused by the methods of evaluation of domain-domain and domain-continuum interactions. It can be seen that this region (50-100% PVAc) in which the dispersed phase is more permeable than the continuum is the most appropriate test of the models. Although no experimental data is available for this region, a comparison with the 0-50% PVAc region yields that, again, the Higuchi, Bruggeman, and Böttcher models are probably the most appropriate. The Series/Parallel and Wagner approaches are shown to produce a large disparity with the remainder of the models and their shortcomings are highlighted. However both these models, especially the Series/Parallel one, may be of value in providing a rough and ready estimate since simple calculations ensure faster calculations. The variations of the Maxwell model, namely by Rayleigh-Runge and Meredith & Tobias, are shown more clearly here although they are quite small in the context of the difference between the other models. It is of interest that, as is found in the 0-50% PVAc region, all the models except that of Higuchi, tend towards the same permeabilities for small dispersions, a consequence of their methods of derivation. This should allow differentiation of the Higuchi model from the remainder to be comparatively easy although there is sufficient disparity in the 50-100% PVAc region to allow one to choose the most appropriate model.

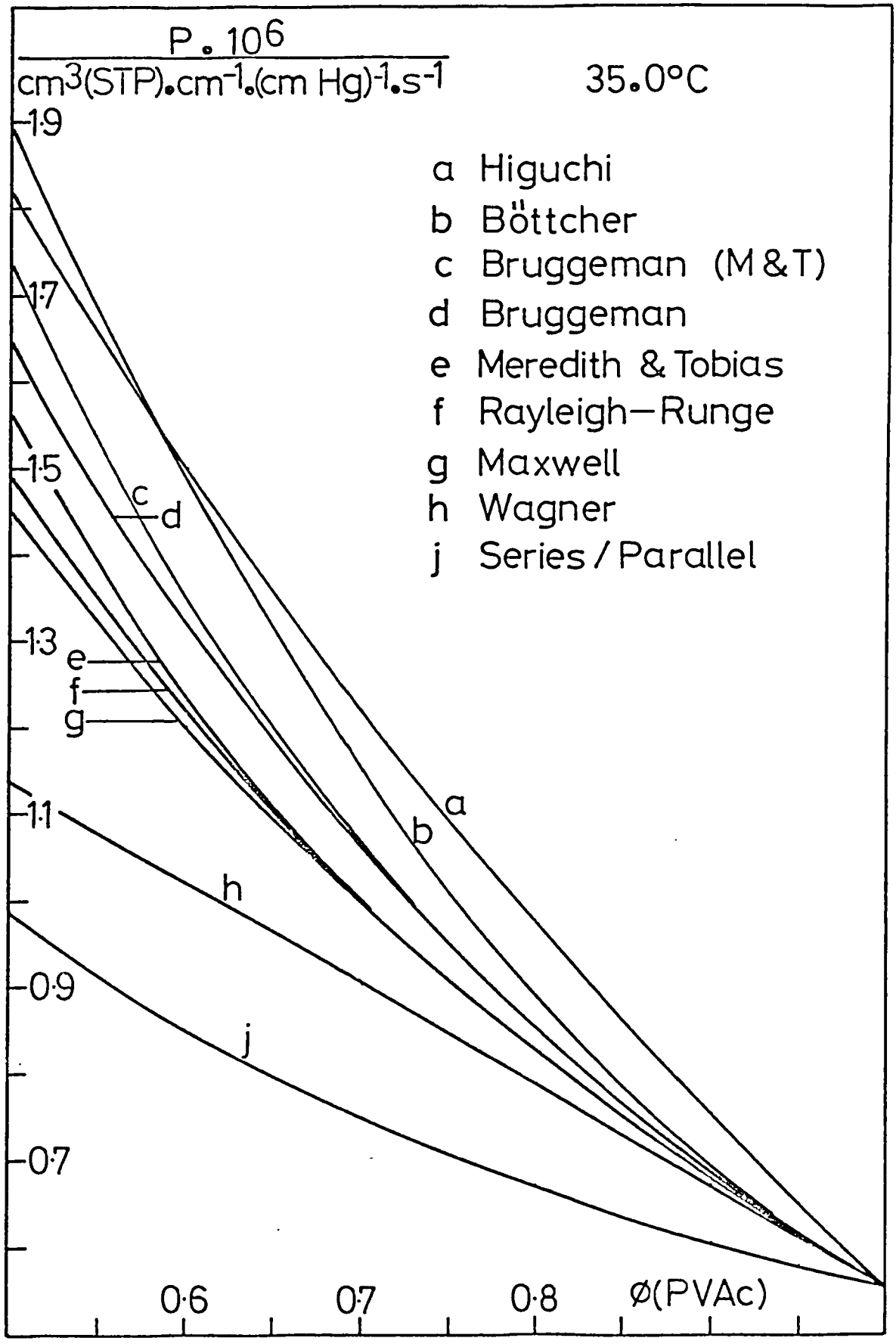


FIGURE 5.28 PVAc CONTINUOUS
THEORETICAL P—ø RELATIONSHIPS

In order to try to obtain data for the range of PVAc as the continuous phase it is tempting to try to extrapolate the experimental data into this forbidden range. A plot of log $D_{c=o}$ vs. ϕ(PVAc) yields a smooth curve within the experimental composition range which can be easily extended to cover the remainder of the composition range since the limit of the diffusion coefficient of PVAc has been experimentally determined. This is illustrated in Figure 5.29 for all temperatures. At first sight this procedure appears to be valid but it was felt that this could not be justified. The change in diffusion coefficient within the extrapolated region is much less than that covered by experiment and hence any difference between extrapolated and true permeabilities will be highlighted. However the greatest difficulty is associated with the phase inversion of the system whereby the PDMS phase changes from being continuous to discontinuous. It is anticipated that in the intermediate composition ranges (40-60% PVAc) that both phases will be continuous as interpenetrating networks so that the phase transition is not expected to be a sudden phenomenon. In the proposed extrapolation this is not taken into consideration since a smooth curve is used to connect the experimental data (0-45% PVAc) with the limit of the range (PVAc). However, in practice, this phase inversions appears naturally, even from a smooth extrapolation, and is illustrated for the 35.0°C isotherm in Figure 5.30. The smoothed and extrapolated "experimental" data are given in Table 5.8 for the four operating temperatures. Consequently the errors involved may not be as large as anticipated but the uncertainties involved mean that this may be valid as a means of estimating roughly the permeabilities of systems in the forbidden range but not valid as a real test of the applicability of the various models proposed. It is interesting, however, to note that if this extrapolated data is incorporated into Figure 5.28 for the region of PVAc continuous then this data follows very closely the permeabilities predicted by the Higuchi model. Although this may be fortuitous, it does seem that this confirms the Higuchi, Bruggeman and Böttcher models as most applicable since it may be expected that the true permeability data may lie close to the extrapolated. In this respect, this procedure may draw some justification.

The main weakness of the theoretical models is the fact that one must specify which component comprises the continuous phase and the models do not allow for the change from continuous to discontinuous for that component. This means, as can be seen from Figures 5.27 and 5.28,

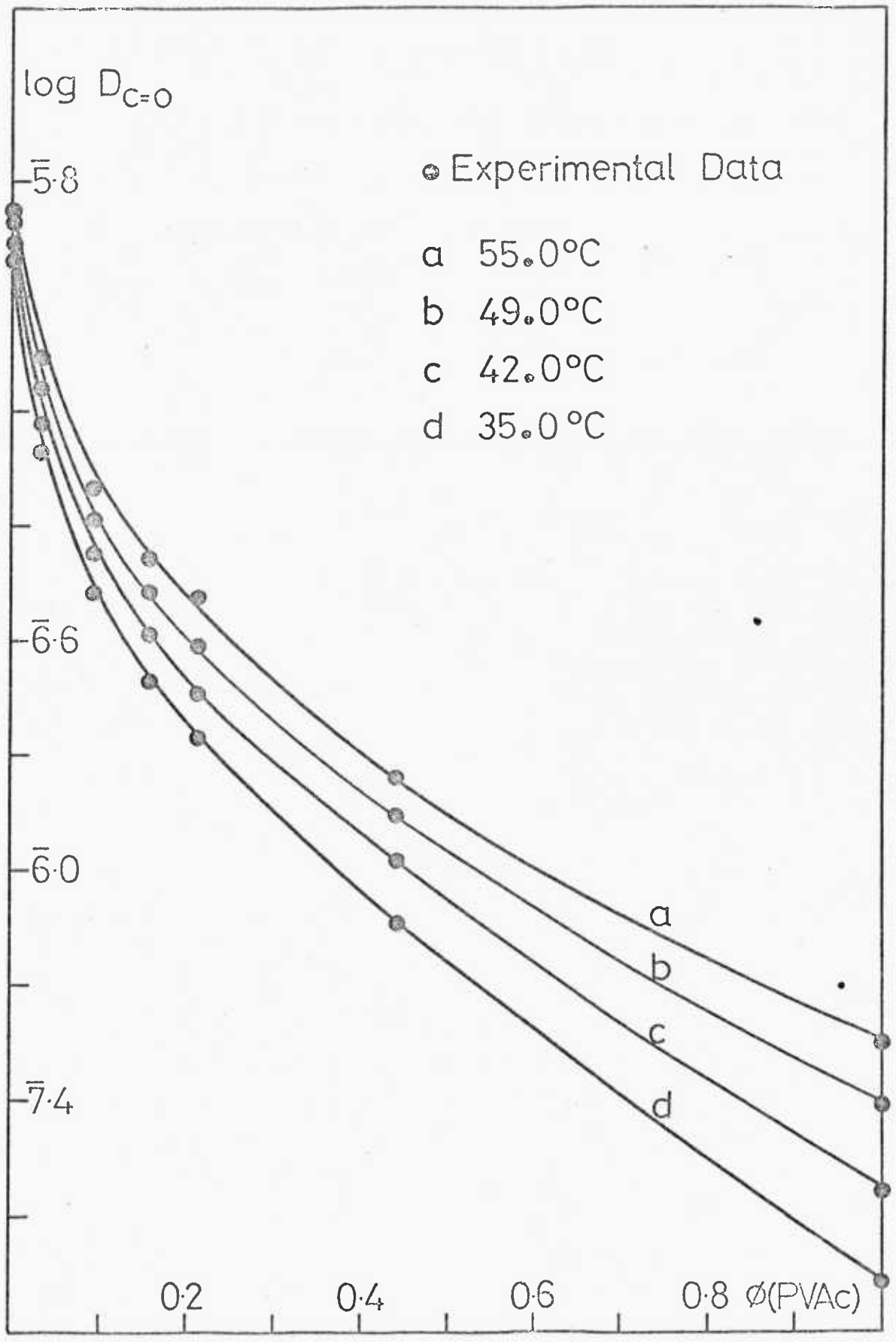


FIGURE 5.29
EXTRAPOLATION OF EXPERIMENTAL D-Ø DATA

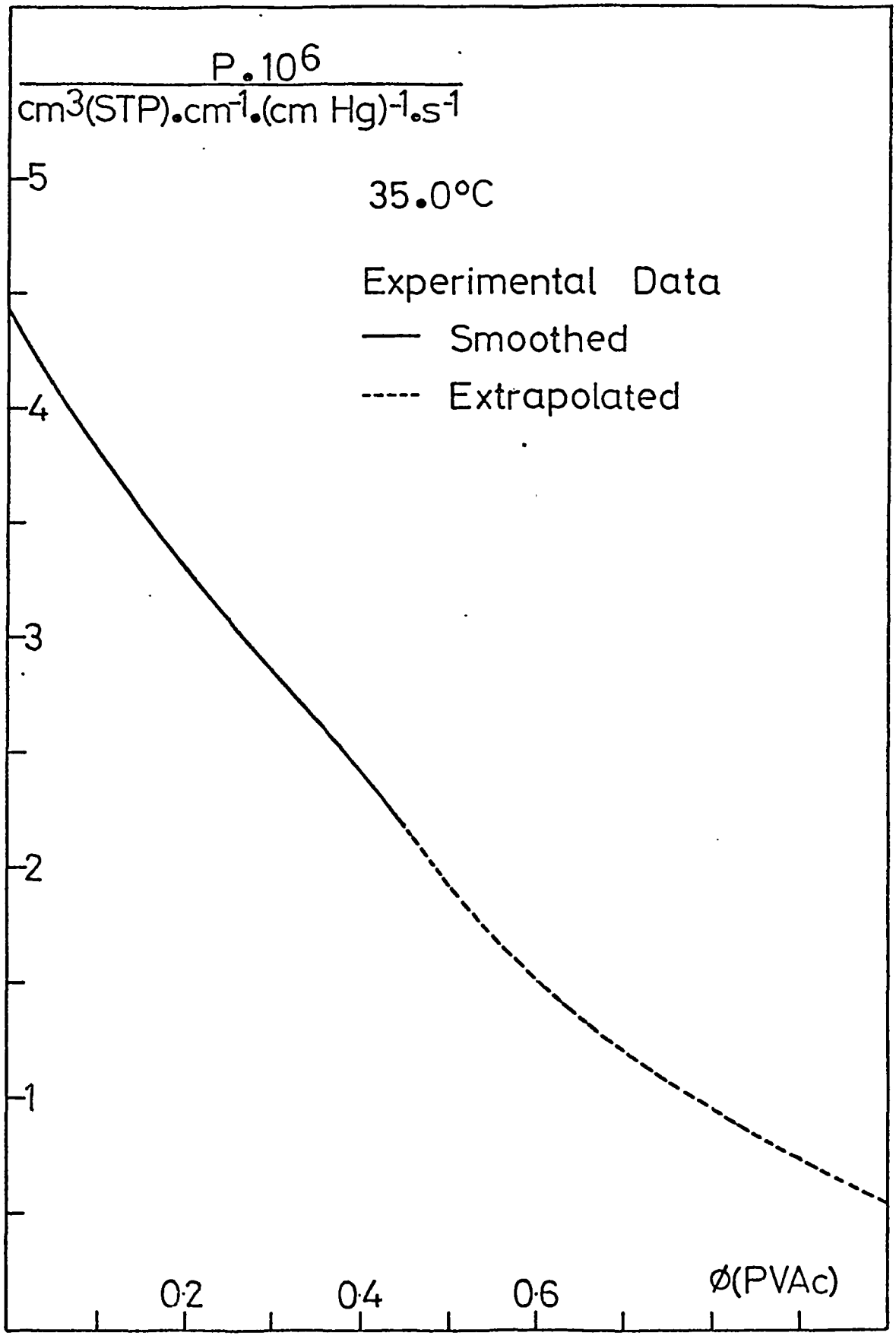


FIGURE 5.30
SMOOTHED & EXTRAPOLATED P DATA

Table 5.8

Smoothed and Extrapolated "Experimental" Permeabilities
(P, cm^3 (S.T.P.). cm^{-1} . $(cm\ Hg)^{-1}$. s^{-1})

	P . 10^6			
ϕ(PVAc)	35.0°C	42.0°C	49.0°C	55.0°C
		SMOOTHED DATA		
0	4.410	4.184	3.923	3.743
0.05	4.088	3.907	3.663	3.547
0.1	3.817	3.649	3.457	3.380
0.15	3.449	3.405	3.274	3.210
0.2	3.331	3.170	3.100	3.039
0.25	3.091	2.966	2.919	2.874
0.3	2.858	2.773	2.713	2.695
0.35	2.637	2.590	2.573	2.548
0.4	2.424	2.402	2.424	2.406
0.45	2.193	2.198	2.260	2.261
1.00	0.555	0.681	0.847	0.977
		EXTRAPOLATED DATA		
0.5	1.923	1.995	2.042	2.066
0.6	1.506	1.617	1.706	1.779
0.7	1.202	1.362	1.436	1.538
0.8	0.955	1.106	1.222	1.334
0.9	0.759	0.876	1.031	1.145

that the two composition ranges must be considered separately for meaningful results to be obtained. The phase inversion region, in which both phases are continuous to some extent, is completely inaccessible when dealing with the basic models and obviously the use of the models becomes restricted somewhat. In order to give some idea of the effect this has, some of the models have been employed outside the usual composition ranges. The models used in this section fall into two groups depending upon the composition range to which they may be applied (irrespective of the physical significance involved). Thus the Series/Parallel, Maxwell, Higuchi, Bruggeman and Böttcher models yield respectively the permeabilities of each polymer component in the limit

ϕ (dispersed phase) (ϕ_B) → 1 or 0 irrespective of which component is specified as continuous. The remainder of the models are applicable only up to ϕ_B = 0.524 whereupon the resultant permeabilities lie outside the range set by the two homopolymer permeabilities. It is interesting to note that this latter group comprise of those models derived for the domains set in a cubic configuration for which a composition containing 52% dispersed phase is the upper limit. The Higuchi, Bruggeman and Böttcher models are derived for random dispersions which can accommodate a composition of 74% dispersed phase. However if the dispersed phase contains spheres of different sizes, implicit in the Bruggeman derivation, it is possible to accommodate a disperse phase for which ϕ_B = 1 can be approached very closely (92). The Maxwell model, since it is defined for dilute dispersions, makes no mention of the geometry of the dispersed phase and hence suffers from no restriction although whether this is justified is debatable. The Series/Parallel model treats the system as laminae and consequently any composition is realistic.

Figure 5.31 illustrates the permeabilities predicted by the appropriate models for the complete composition range for the 35.0°C isotherm. It can be seen that, apart from the Böttcher model, all models are represented by two curves depending upon which component is specified as the continuous phase. Thus for these models, the two curves specify the limits of permeability for any composition, lying close to the most realistic line at each end of the composition range and somewhere intermediate for the middle regions of the range. The Böttcher model appears to be the most convincing in this respect since only one set of data can be generated irrespective of which phase is deemed continuous. This is the closest to fitting experimental data in that the troublesome intermediate region is covered as a consequence of the model. Objections to the model have been proposed (92) on the grounds that it is applicable only to spheres at low dispersions and to systems in which the permeabilities of the two components are close. However this model is able to work with any ratio of the permeability of the components except 0 and ∞ and yields the respective permeabilities for ϕ_B = 0 or 1 so that, in practice, there is no real restriction on the model. From Figure 5.31 it can be seen that the more interactions there are between domains the closer the two curves generated by each model become. Thus there are no interactions inherent in the Maxwell and Series/Parallel models and the Maxwell model is a better approximation than the Series/Parallel model since this is derived for a two-phase system as opposed to laminae. The Bruggeman,

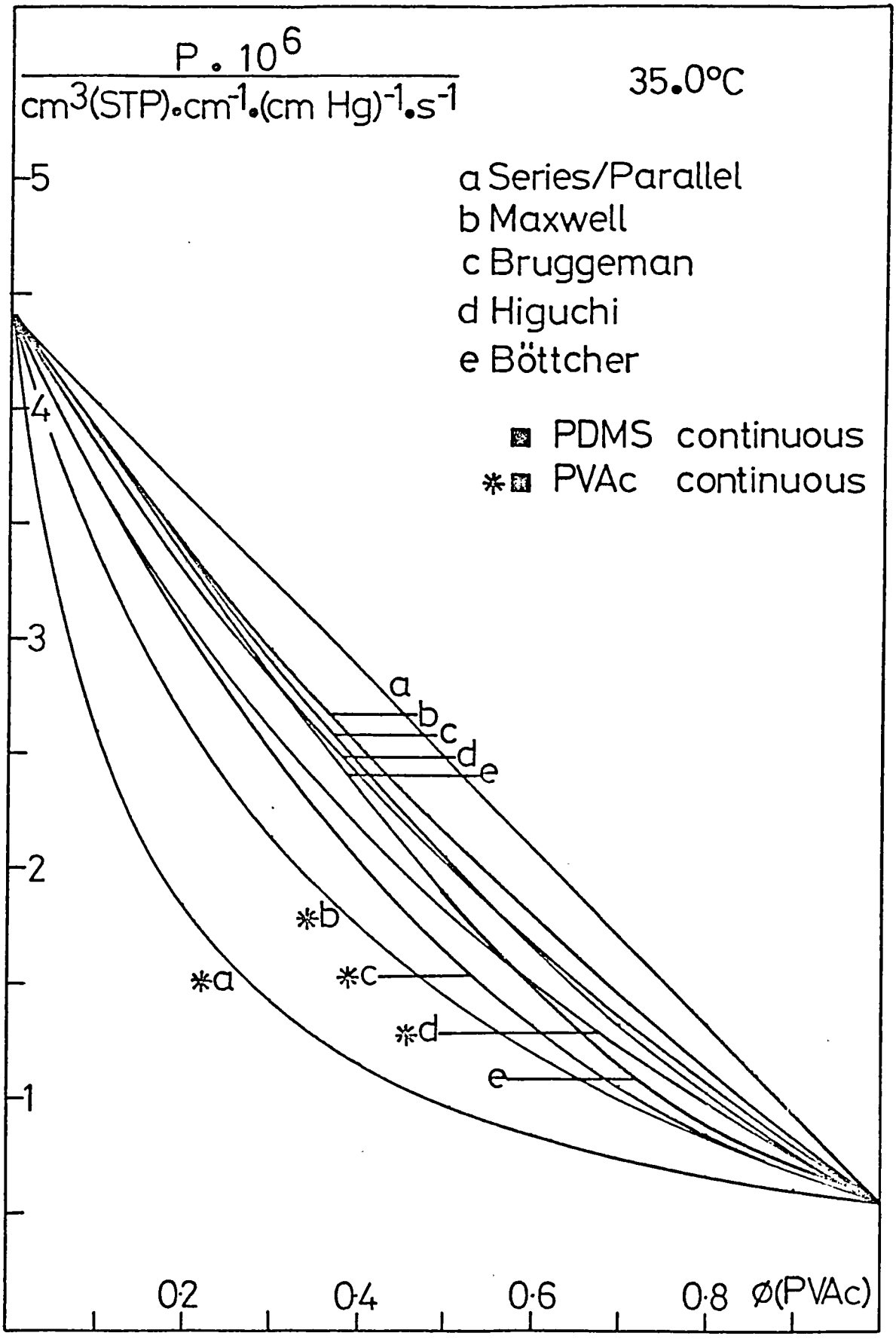


FIGURE 5.31
THEORETICAL P—ø RELATIONSHIPS

Böttcher and Higuchi models include the effect of domain interactions in their derivation and yield similar permeabilities which are closest to those found experimentally. If experimental data were to be included in Figure 5.31, the changeover of PDMS from continuous to discontinuous corresponds closely with that obtained by the Böttcher model and this ensures that this has advantages over the Bruggeman and Higuchi models. Agreement between the experimental permeabilities and those predicted by these models in the 0-40% disperse phase regions is good and probably favours the Higuchi model although the Böttcher and Bruggeman models predict permeabilities within experimental error similar to those found experimentally.

In order to adapt the models, except Böttcher, to encompass the whole range of composition a combination of predicted permeabilities for each component continuous has been suggested (105). This is really a method to try to cover the troublesome middle range (40 - 60% PVAc) which is generally not applicable for treatment by the simple models. In this region where phase inversion eventually occurs it is unlikely that the microstructure can be regarded as a discrete dispersion of one phase in another (95) and it would be unrealistic to apply the basic models in this region. Indeed the microstructure can be easily altered by the method of treatment of the copolymer (95). Despite this, it has been suggested that (105), for any given composition, a relationship ought to be applied such that

$$P = (P_A)\, X_A + (P_B)\, X_B \qquad \ldots.(5.5)$$

where P is the required permeability; (P_A), (P_B) are the permeabilities obtained for that composition from any appropriate model when A, B respectively are the continuous phases; and X_A, X_B are the fractional contributions (or weightings) of each computed permeability ((P_A) and (P_B)) at that composition such that $X_A + X_B = 1$. Mathematically this is justified as the curve in the intervening middle region must be between the curves of the extreme ends of the composition range. The parameter X is then arbitrarily chosen to give the best fit over the whole composition range. Physically this approach has no real meaning in terms of the microstructure of the system. However this approach, as it stands, offers no real advantages as the experimental data is required initially and the parameters X_A and X_B are unlikely to be constant for different systems. Perhaps a more realistic approach is to use arbitrary mixing coefficients only for the middle regions of composition (40-60% PVAc)

and apply the simple models outside this range.

One particular feature of this mixing feature has been suggested as a means of detecting the phase inversion point of the system, the disperse phase becoming continuous and vice versa. It has been suggested (105) that, with $X_A = X_B = 0.5$ in equation (5.5), the phase inversion point is that composition for which the experimental and calculated permeabilities (equation 5.5) are the same. This is illustrated in Figure 5.32 for the 35.0°C isotherm with the Higuchi and Maxwell models. Using "computed experimental" data (Table 5.8) the respective phase inversion points were found to be 51% PVAc for Higuchi and 62% PVAc for Maxwell. These are within the expected composition range and, in that respect, the method appears to be meaningful. However it was found that both the Böttcher and Bruggeman models could not be used in this way as the calculated and experimental permeabilities were never the same. Hence some reservation must be included in the analysis and this really only gives a general area within which phase inversion is likely to occur. In this particular system, there is some doubt whether true phase inversion would occur since the continuous phase (PDMS) of the experimental range is cross-linked so that truly dispersed domains are unlikely to be present.

In Section 5.1.3 the possibility of the presence of occlusions of PDMS within the PVAc domains was discussed. In view of the good agreement of the experimental data with permeabilities calculated for domains of PVAc only as well as the agreement of solubility and glass transition data, it seems unlikely that there are any occlusions present. However the effect of occluded material was tested using equations (4.14) and (4.4) which are the Higuchi and Maxwell models, respectively, adapted for the presence of an occluded disperse phase. It was decided to employ smoothed experimental data so as to eliminate any discrepancies in the data. However there is still the problem of interpolating domain sizes from those of the known copolymer compositions. The compositions chosen for this analysis are 5%, 20% and 40% PVAc by volume with respective domain radii of 13, 45 and 70 nm.

The electron micrographs (illustrated in Appendix 8.1), although showing some evidence of the possibility of occlusions, do not give any indication of the amount of occlusion present. If some PDMS is occluded within the domains, the amount of PDMS present in the

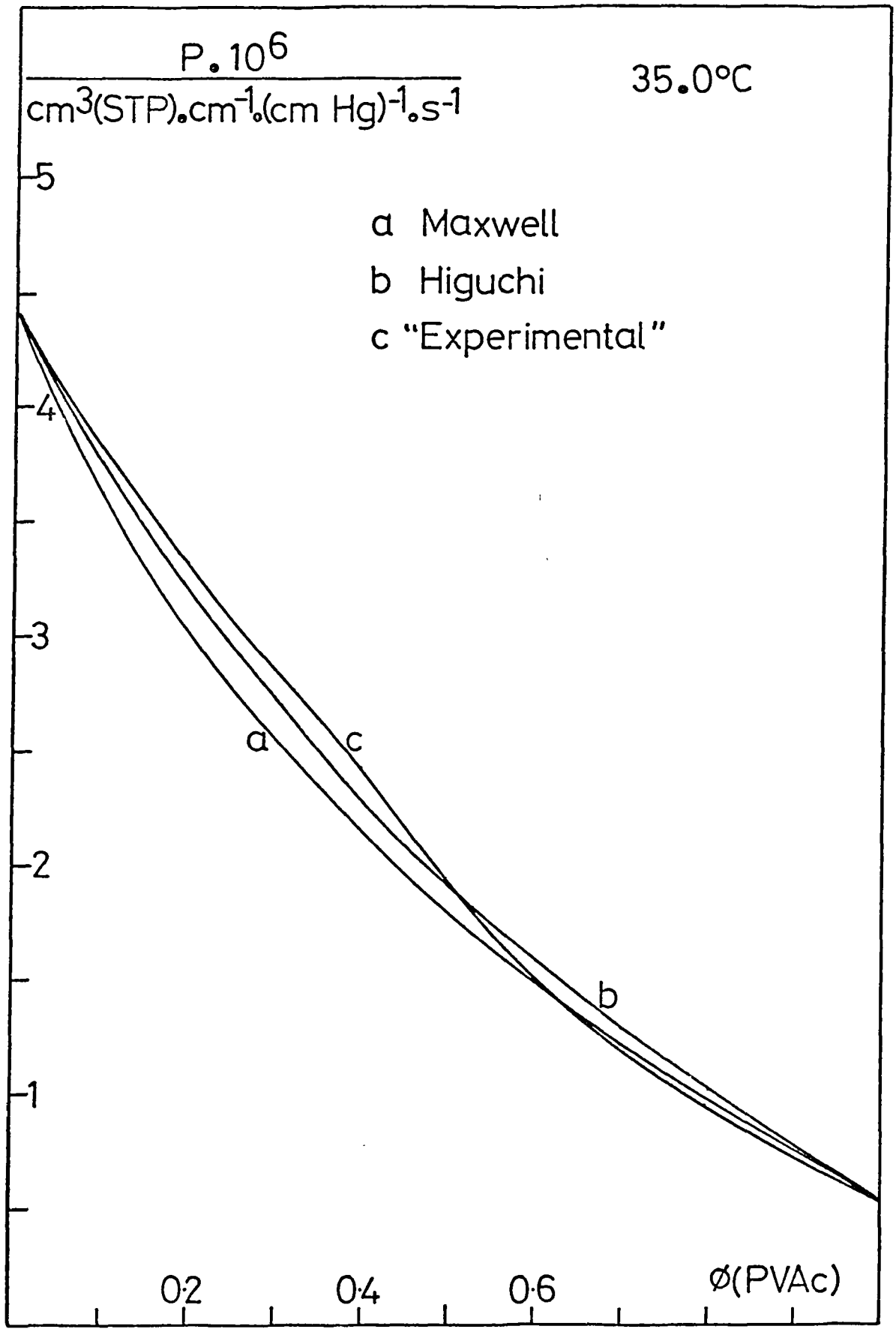


FIGURE 5.32
PHASE INVERSION ANALYSIS

continuous phase is less than that expected from the given composition, especially if large amounts of occluded PDMS are present. Some indication of this is given in Table 5.9, which shows the expected and calculated volume fractions at various degrees of occlusion.

Table 5.9

Effect of Occlusion on Volume Fraction and Occluded Radius of the Disperse Phase

Volume Fraction of PVAc

Initial ϕ (PVAc)	Occluded Volume 1%	10%	30%	50%
0.05	0.0505	0.055	0.065	0.075
0.20	0.202	0.22	0.26	0.30
0.40	0.404	0.44	0.52	0.60

Occlusion Radius (nm)

Initial ϕ(PVAc)	Domain Radius(nm)	Occluded Volume 1%	10%	30%	50%
0.05	13	2.8	6.0	8.7	10.3
0.20	45	9.7	20.9	30.1	35.7
0.40	70	15.1	32.5	46.9	55.5

The Maxwell and Higuchi analyses results are given in Table 5.10 for the various compositions and occlusions. The results obtained from the adapted Maxwell expression show that the dominant feature is the increase in permeability of the disperse phase. Obviously a relatively permeable inner core must increase the permeability of the disperse phase whilst this increased disperse phase composition means a reduction in net permeability. Hence the increased permeability of the copolymer as calculated from the Maxwell expression means that increased domain permeability is the dominating feature. The situation is more complex with the Higuchi relationship in that the overall permeability goes through a minimum. There is an initial decrease in permeability as occlusion occurs and an increase later as the large occlusions cause the increased domain permeability to dominate. In most

Table 5.10

Permeabilities P $(cm^3(S.T.P.) \cdot cm^{-1} \cdot (cm\ Hg)^{-1} \cdot s^{-1})$

ϕ (PVAc) = 0.05 Experimental $P = 4.088 \cdot 10^{-6}$

	Maxwell		Higuchi	
% Occluded	R_2/R_1	$P \cdot 10^6$	$P_D^* \cdot 10^6$	$P \cdot 10^6$
1	4.642	4.169	0.567	4.105
10	2.154	4.195	0.680	4.095
30	1.494	4.223	0.996	4.090
50	1.260	4.257	1.444	4.111

ϕ (PVAc) = 0.20 Experimental $P = 3.331 \cdot 10^{-6}$

	Maxwell		Higuchi	
% Occluded	R_2/R_1	$P \cdot 10^6$	$P_D^* \cdot 10^6$	$P \cdot 10^6$
1	4.642	3.494	0.567	3.292
10	2.154	3.590	0.680	3.258
30	1.494	3.691	0.995	3.237
50	1.260	3.819	1.444	3.308

ϕ (PVAc) = 0.40 Experimental $P = 2.424 \cdot 10^{-6}$

	Maxwell		Higuchi	
% Occluded	R_2/R_1	$P \cdot 10^6$	$P_D^* \cdot 10^6$	$P \cdot 10^6$
1	4.642	2.697	0.567	2.398
10	2.154	2.865	0.680	2.342
30	1.494	3.047	0.998	2.304
50	1.260	3.278	1.444	2.411

cases this results in better agreement between experimental and calculated permeabilities but the difference is not large and probably within experimental error. It would appear that the permeability of the system is not very sensitive to occlusions and consequently it is difficult from a permeability analysis to rule out completely the presence of these in the systems studied.

5.3.3 Permeability Temperature Dependence

Values of the temperature coefficient of permeability (E_p) were obtained from graphs of log P vs. 1/T shown in Figure 5.33 and are given in Table 5.11.

Table 5.11

Temperature Coefficients of Permeability (E_p, kJ . mole^{-1})

ϕ (PVAc)	E_p
0	-6.99
0.034	-6.49
0.093	-6.00
0.157	-4.57
0.214	-3.96
0.442	+0.91
1.00	+24.05

The value obtained here for PDMS agrees within 8% of previous values (20). It is a common feature of permeation through PDMS that E_p is small and negative whereas PVAc, in common with materials with lower permeabilities, has a positive E_p.

E_p data can be generated for the various models since permeabilities were calculated for each working temperature and for all compositions, even though only the 35.0°C isotherms have been illustrated. These are illustrated in Figure 5.34 for the 0-50% PVAc region (PDMS continuous) and in Figure 5.35 for the 50-100% PVAc region (PVAc continuous). As may be anticipated, E_p data closely follow the permeability behaviour from which they are derived. When considering the 0-50% PVAc region (for which the smoothed experimental data have been included) it can be seen that E_p data separates the models to a greater extent than the relevant permeability data. The Higuchi model appears to be the best representation of the experimental data in this composition range although the Wagner, Böttcher and Bruggeman models should not be ignored. A similar situation exists for the 50-100% PVAc region although no real experimental data can be used for comparison. The "computed experimental" data is in good agreement, like the permeability data from which it was derived, with that predicted by the Higuchi model, which appears to yield quite distinct E_p values in this region. The Bruggeman and Böttcher models and, to some extent, the

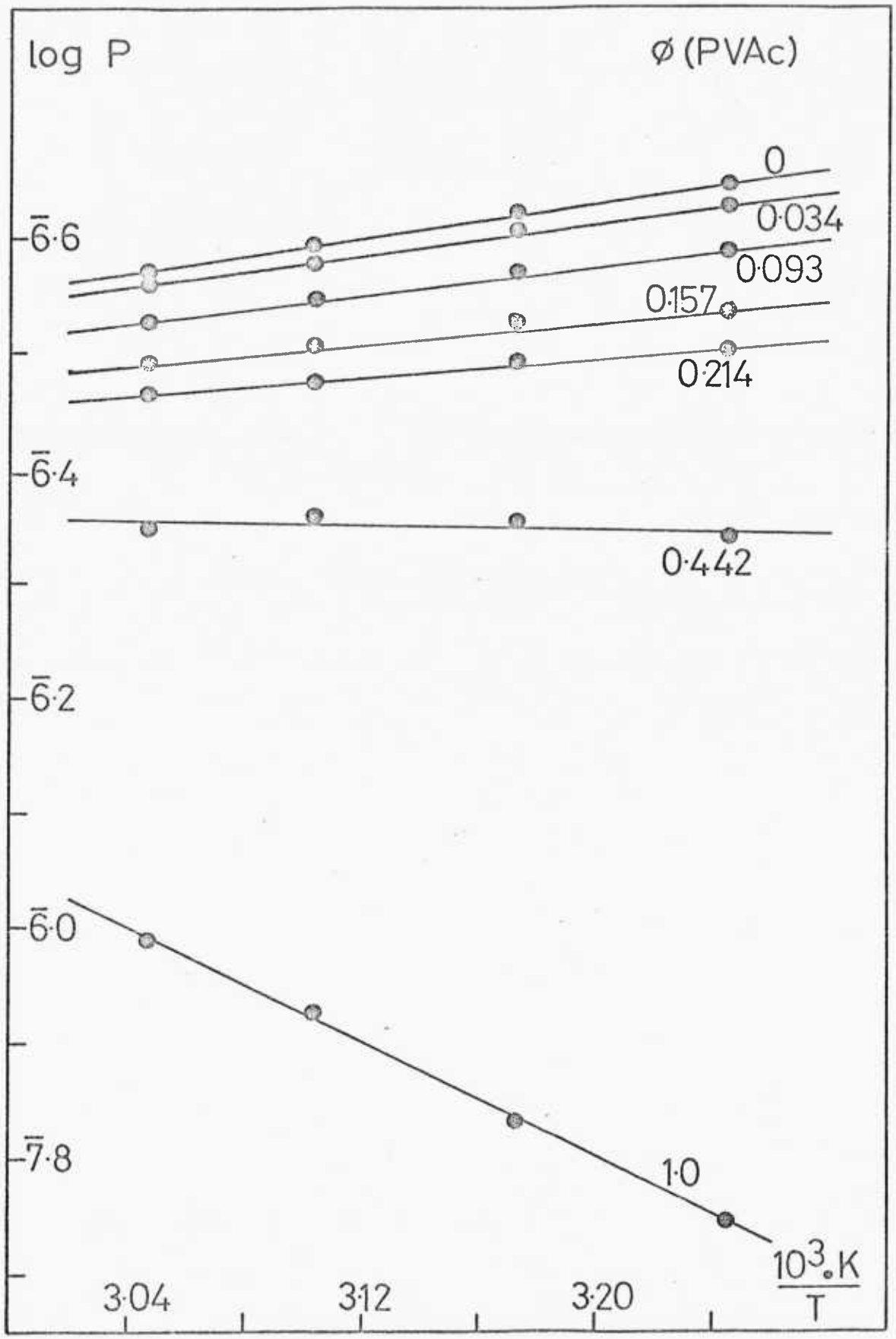


FIGURE 5.33
TEMPERATURE VARIATION OF PERMEABILITY

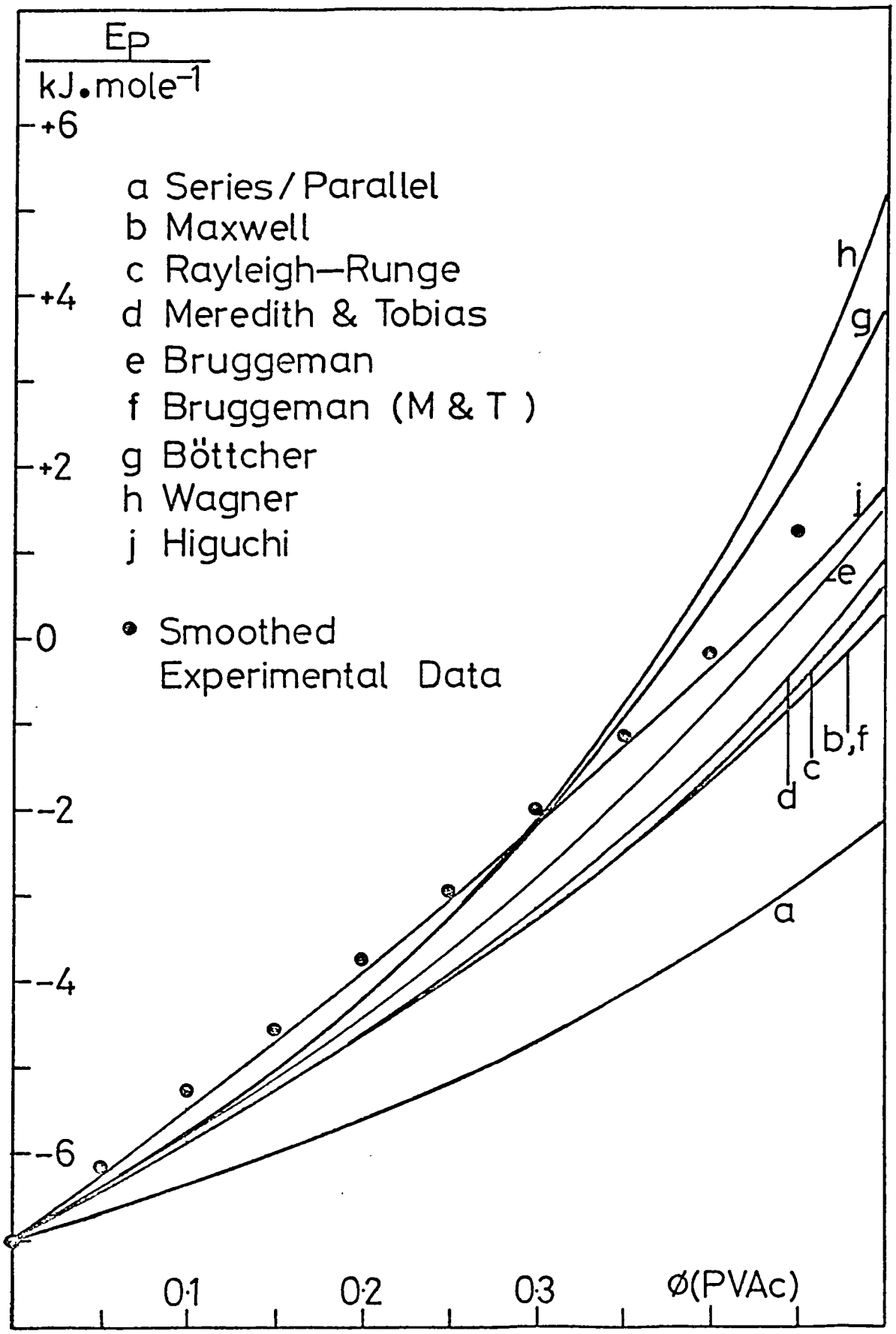


FIGURE 5.34
THEORETICAL Ep—ø RELATIONSHIPS

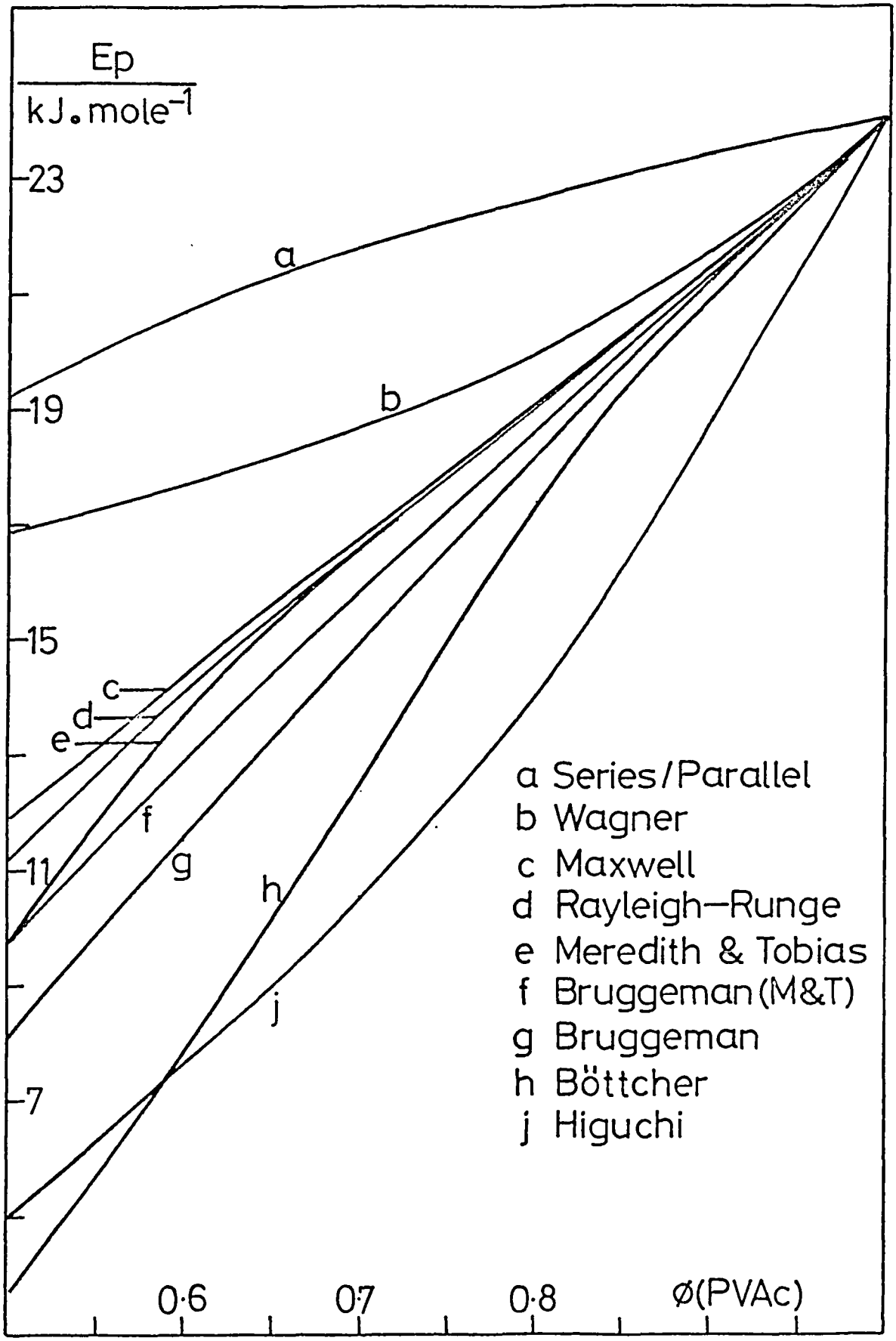


FIGURE 5.35
THEORETICAL E_p–ø RELATIONSHIPS

Maxwell model yield similar E_p values, although the Böttcher model appears to be the best representation of the data within this group.

The applicability of the Böttcher model is clearly seen when, from Figure 5.36, the whole of the composition range is considered. Once again this is the only model which appears to encompass to the greatest extent the experimental data over the composition range for which the change in permeability at the phase transition region is a natural consequence. In all probability the Higuchi model appears to be the most realistic at low dispersion concentrations although the Bruggeman model cannot be discounted.

5.4 Diffusion Results

Both steady-state and transient (sorption-kinetics) diffusion measurements have been obtained. Due to the difficulties described in Section 5.3.1 for permeation of water vapour, it was decided that no meaningful data could be obtained from time lag experiments.

5.4.1 Steady-State Diffusion

Steady-state diffusion coefficients were determined as described in Section 2.3 from solubility and permeability data.

(i) Values of $D_{c=o}$

Values of $D_{c=o}$ coefficients are given in Table 5.12. The agreement between these and earlier results is to within 4% for PDMS (20) and 7% for PVAc (74, 81). Previous PDMS values were obtained from both steady-state and transient measurements whilst those for PVAc are obtained from sorption-kinetic data only.

Table 5.12

Values of $D_{c=o}$ Coefficients ($cm^2 . s^{-1}$)

	$D_{c=o} . 10^6$			
ϕ (PVAc)	35.0°C	42.0°C	49.0°C	55.0°C
0	39.51	43.26	49.35	52.79
0.034	12.34	14.72	18.42	21.95
0.093	5.360	6.794	8.389	10.04
0.157	3.133	4.183	5.359	6.583
0.214	2.232	2.905	3.926	4.698
0.442	0.735	1.074	1.408	1.766
1.00	0.085	0.147	0.243	0.352

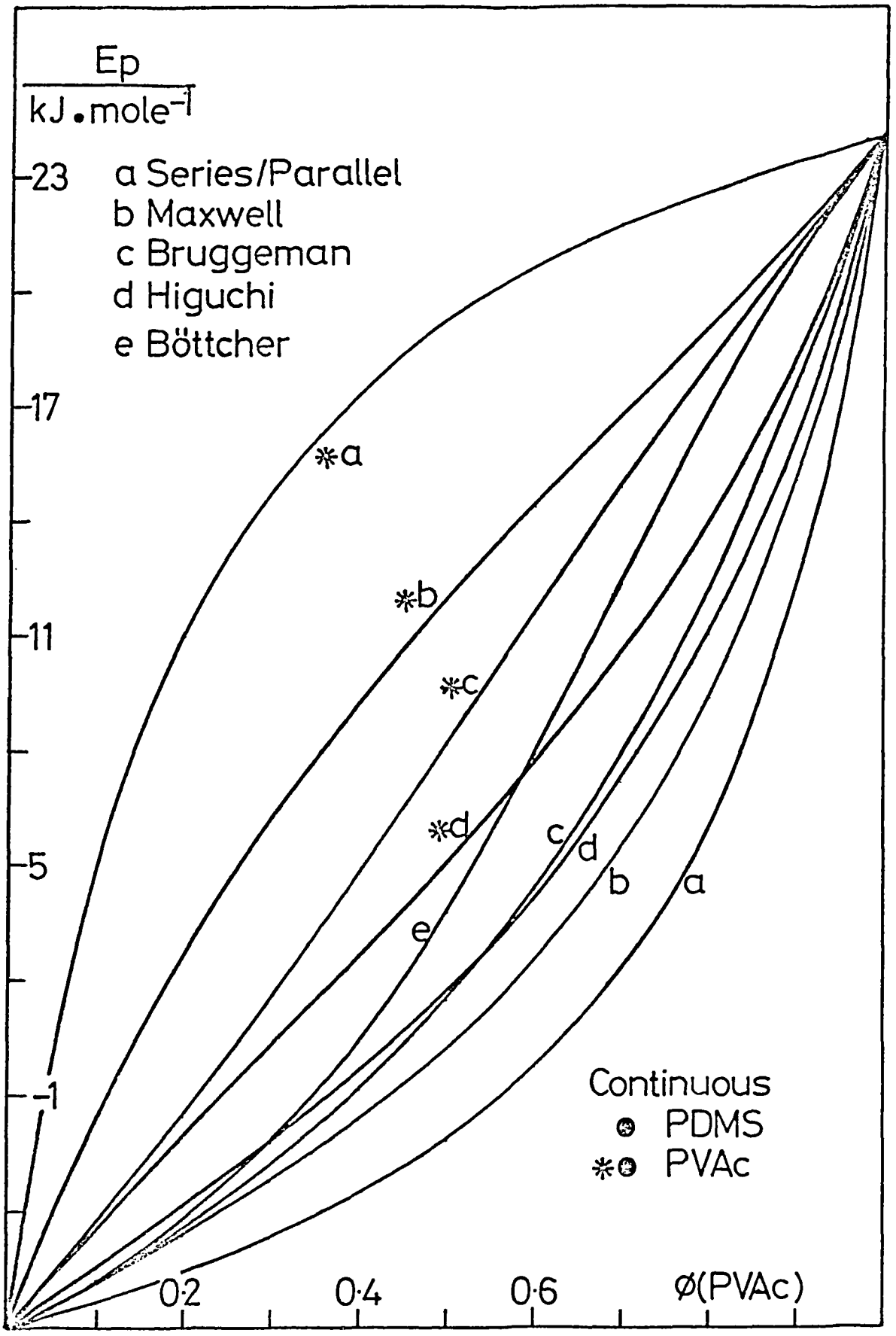


FIGURE 5.36
THEORETICAL E_p—ø RELATIONSHIPS

As the solubility data $\sigma_{c=o}$ varied linearly with ϕ (PVAc) over the complete range of composition then the behaviour of $D_{c=o}$ with ϕ (PVAc) will parallel that of the permeability behaviour. There is therefore nothing to be gained from an analysis of the $D_{c=o}$ vs. ϕ (PVAc) plot in terms of the previous models. In fact it is necessary to employ a log $D_{c=o}$ vs. ϕ (PVAc) plot to accommodate the large change in $D_{c=o}$ and this makes it very difficult to differentiate between the models.

However it is of interest to estimate the reliability of the method of extrapolation by a comparison with the diffusion coefficients obtained by the Bruggeman, Böttcher and Higuchi models as these are the best representations of the experimental data. Values of $D_{c=o}$ are given in Table 5.13 for the 35.0°C, the one expected to show the greatest difference between the $D_{c=o}$ values of the models. The most striking feature of the $D_{c=o}$ data is the drastic compression of the differences between the models as a result of the large variation in $D_{c=o}$ over the composition range. The Bruggeman and Higuchi models, because of their inability to follow phase transition changes, can be represented by some mixing of the values given for the 40-60% PVAc region but outside this region the simple models are sufficient to represent the data. The Böttcher model is free from this problem since, as has been shown in Section 5.3.2, the same permeability (diffusion) coefficients are generated irrespective of which component is specified as continuous. A log $D_{c=o}$ vs. ϕ (PVAc) plot was constructed (Figure 5.37) in order to ascertain whether this also was a smooth curve, as was drawn for the experimental data extrapolation (Figure 5.29). This also proved to be a smooth curve and very similar in outline with the experimental one. In fact if the diffusion coefficients obtained from Bruggeman and Higuchi models were also presented in Figure 5.37 it would be very difficult to separate them from the Böttcher data already given. The extrapolated experimental data falls within the bounds set by these models and hence this shows that the method is a valid means of estimating diffusion coefficients within the forbidden range. However, although these $D_{c=o}$ values are accurate to within a few percent, it is not possible to use them to differentiate between the models as the experimental data could be represented by any of the models depending upon how the extrapolation was drawn.

Hence the extrapolation technique confirms that the Bruggeman, Böttcher and Higuchi models are the best representations of the experimental data without being able to differentiate between them.

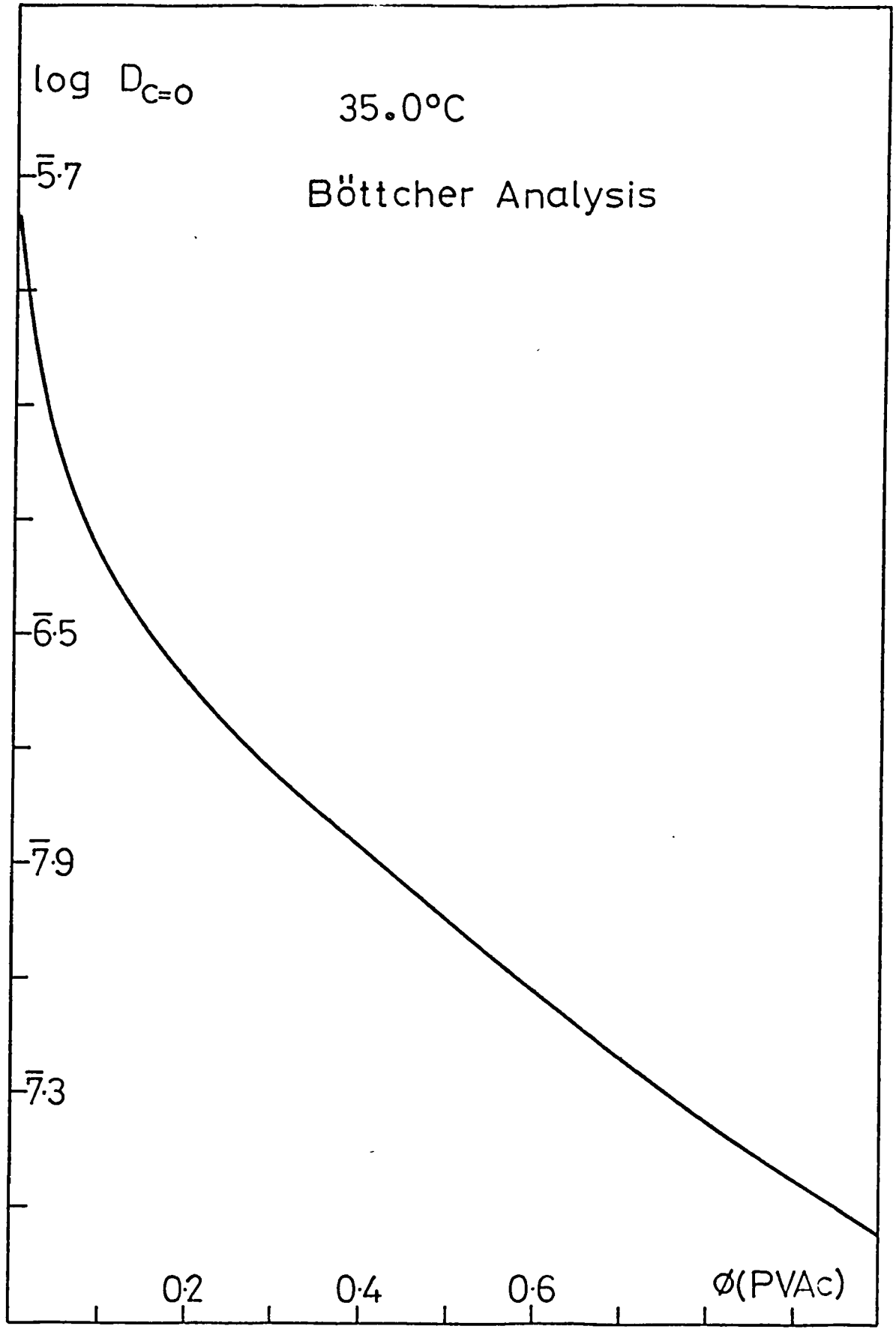


FIGURE 5.37
THEORETICAL D—Ø ANALYSIS

Table 5.13

Values of $D_{c=o}$ ($cm^2 \cdot s^{-1}$) from Experiment and the Permeability Models at 35.0°C.

	$D_{c=o} \cdot 10^6$			
ϕ (PVAc)	Experiment	Böttcher	Bruggeman	Higuchi
	Smoothed		PDMS cont.	PDMS cont.
0	39.51	39.51	39.51	39.51
0.05	9.441	9.559	9.564	9.483
0.1	5.062	5.134	5.145	5.066
0.2	2.388	2.396	2.420	2.363
0.3	1.403	1.389	1.425	1.388
0.4	0.905	0.874	0.918	0.898
0.5		0.569	0.617	0.609
0.6		0.375	0.422	0.423
	Extrapolated		PVAc cont.	PVAc cont.
0.5	0.579	0.569	0.495	0.547
0.6	0.380	0.375	0.333	0.379
0.7	0.261	0.250	0.230	0.265
0.8	0.182	0.169	0.162	0.185
0.9	0.129	0.118	0.117	0.128
0.95	0.104	0.100	0.099	0.105
1.00	0.0853	0.0853	0.0853	0.0853

(ii) Concentration-Dependence of D

At higher relative vapour pressures D decreases with increasing concentration for all systems except that of PVAc. The greatest decrease is shown by PDMS (20, 24) for which, at a relative pressure of 0.85, values of D are only $\frac{1}{4}$ - $\frac{1}{2}$ of the $D_{c=o}$ value. The decrease is largest at the lowest temperature; a consequence of the increased clustering tendency of the penetrant molecules. For PVAc, on the other hand, D is a constant for all concentrations (74, 81) even though clustering occurs (Section 5.2.3). However PVAc sorbs much more water than PDMS (about 4%) so that plasticisation of the polymer matrix is probable. A constant D may therefore be a consequence of a cancellation of two opposing factors; namely a decrease in D due to clustering and

an increase in D due to plasticisation. However it seems fortuitous that these unrelated factors should compensate exactly for all the measured concentrations and temperatures. The graft copolymers all exhibit diffusion coefficients which decrease with increasing concentration. The relative decrease in D is reduced as the volume fraction of PVAc increases since there is less clustering within PVAc than PDMS. These concentration-dependences are illustrated in Figures 5.38 - 5.44.

It can be seen from Figures 5.38 and 5.39 that for both PDMS and P(DMS-g-0.034 VAc) there is an initial region of constant D followed by a region in which D decreases with concentration at higher relative pressures. This behaviour has been reported previously (20) for PDMS and is a consequence of an initial linear region in the sorption isotherm and a permeability which is independent of relative pressure. With the 3.41% graft copolymer a significant part (37%) of the sorption occurs in the PDMS phase and this is reflected in the initial linear region of the isotherm and a region of constant D. For the other graft copolymers the sorption is almost entirely in the PVAc phase and hence no constant D region can be observed.

The decrease in D with increasing concentration for both PDMS and the graft copolymers is due to an increase of relative immobilisation of the penetrant molecules with increasing concentration. The mechanism of immobilisation in PDMS, and for that matter PVAc, is clustering of penetrant molecules thereby increasing the path length of diffusion and decreasing the concentration of free water. Thus, as concentration of sorbed water increases, a greater amount of penetrant is immobilised within the clusters and consequently there is a decrease in D. For the graft copolymers the prime mode of immobilisation is not clustering of penetrant molecules as such,but sorption of penetrant into the PVAc domains. As D for PVAc is much less than for PDMS (1/225) an increasing fraction of the water sorbed is relatively immobilised in the PVAc domains as concentration increases so that the apparent D for the system decreases with increasing concentration.

Since there is considerable swelling within these systems, one should take this into consideration by the use of intrinsic diffusion coefficients (see Section 6.4.2). These are illustrated in Figures 5.45 - 5.49 for PVAc and the copolymers containing 44.2%, 21.4%, 15.7% and 9.3% PVAc by volume. The graft containing 3.4% PVAc by volume is

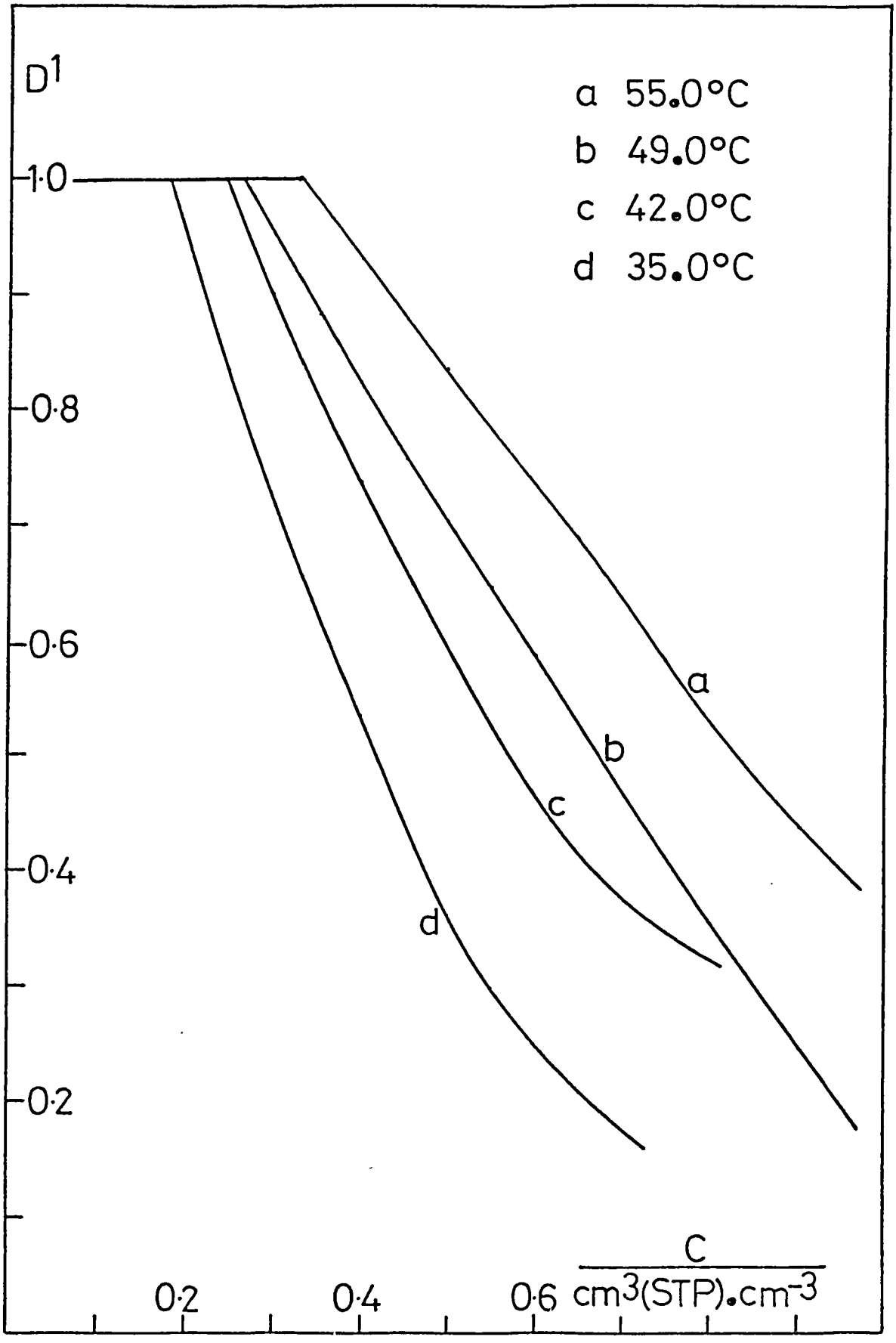


FIGURE 5.38 PDMS-H_2O

CONCENTRATION-DEPENDENCE OF DIFFUSION

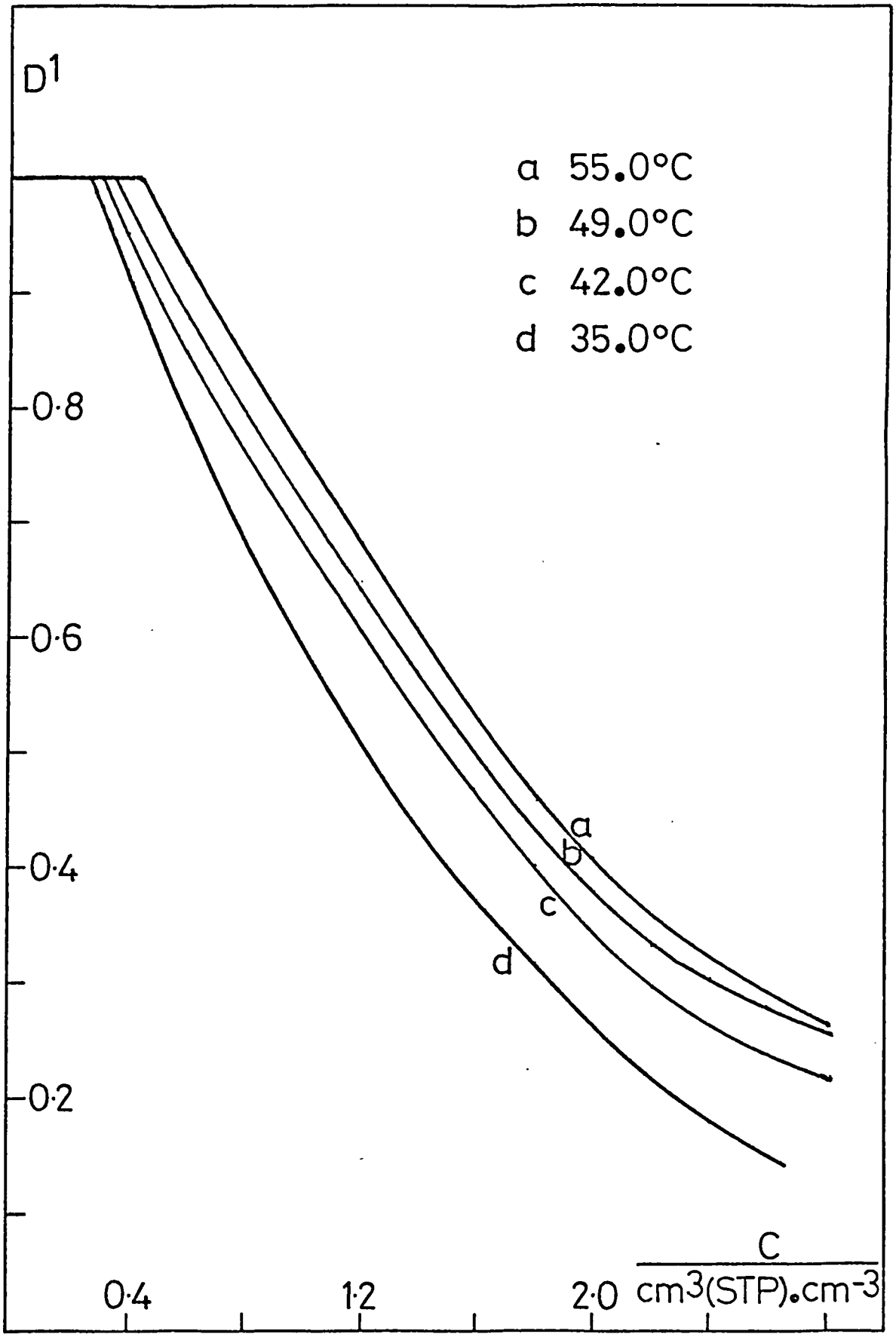


FIGURE 5.39 P(DMS-g-0·034 VAc)–H_2O

CONCENTRATION-DEPENDENCE OF DIFFUSION

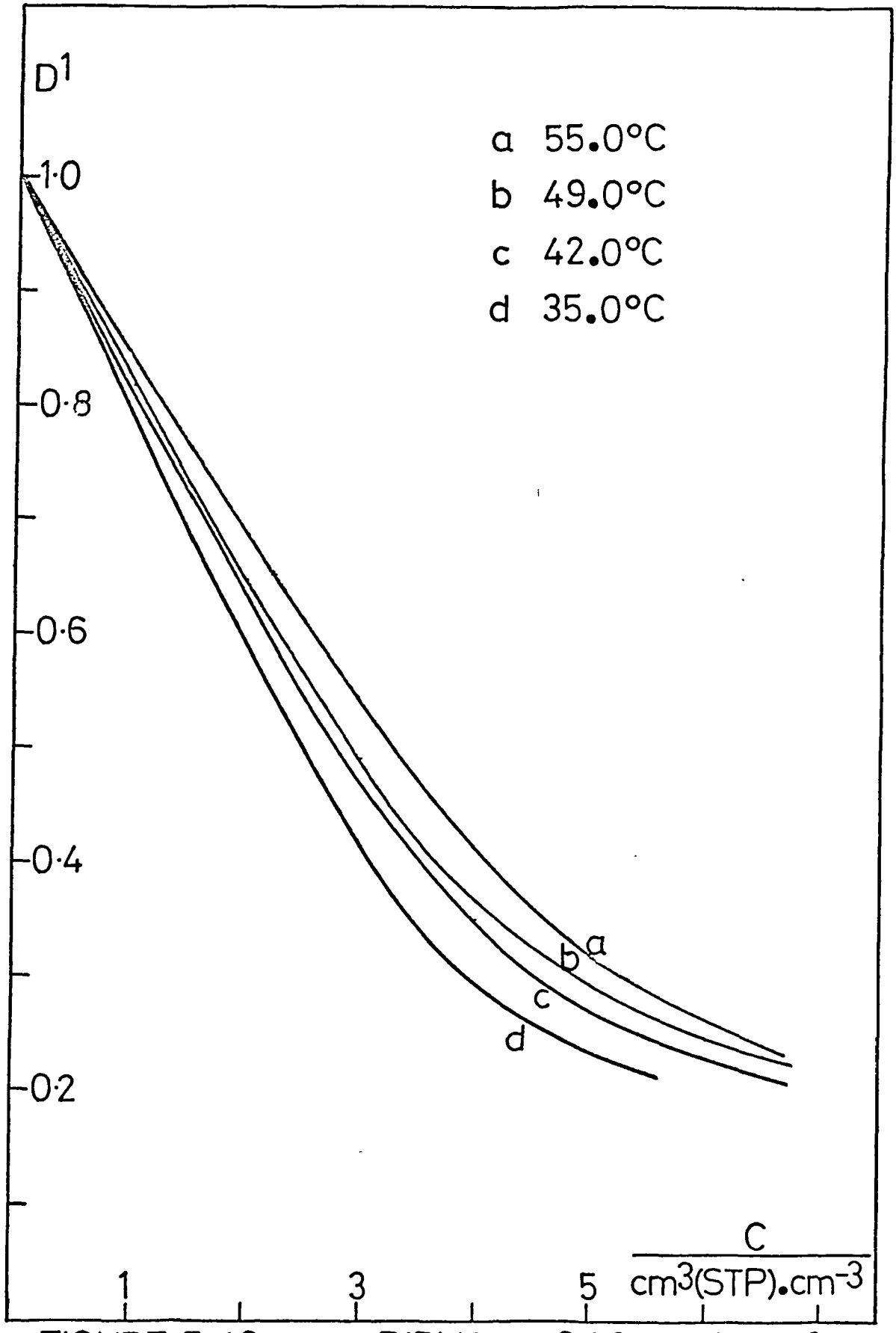


FIGURE 5.40 P(DMS-g-0·093 VAc)–H_2O

CONCENTRATION-DEPENDENCE OF DIFFUSION

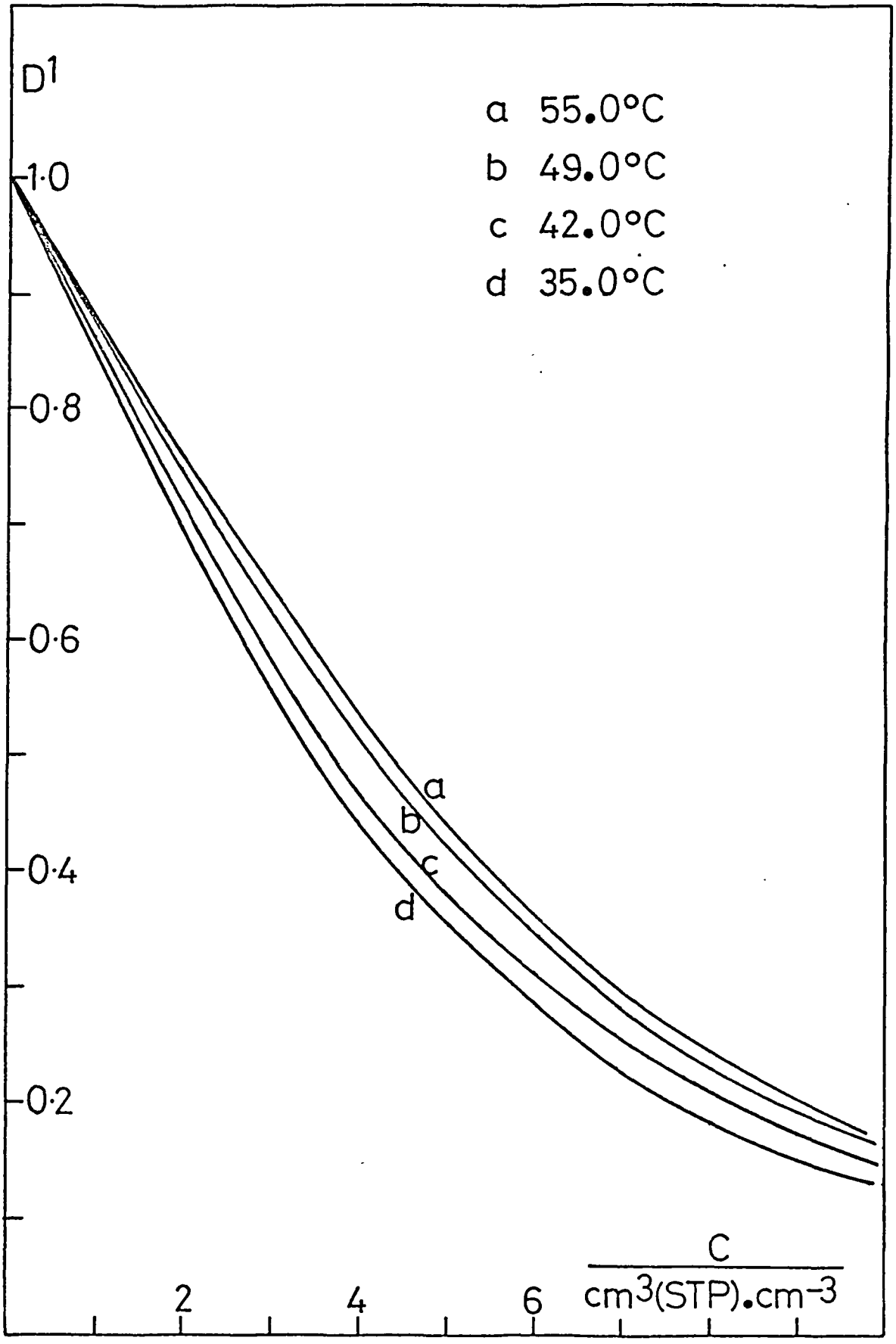


FIGURE 5.41 P(DMS-g-0·157 VAc)—H_2O
CONCENTRATION-DEPENDENCE OF DIFFUSION

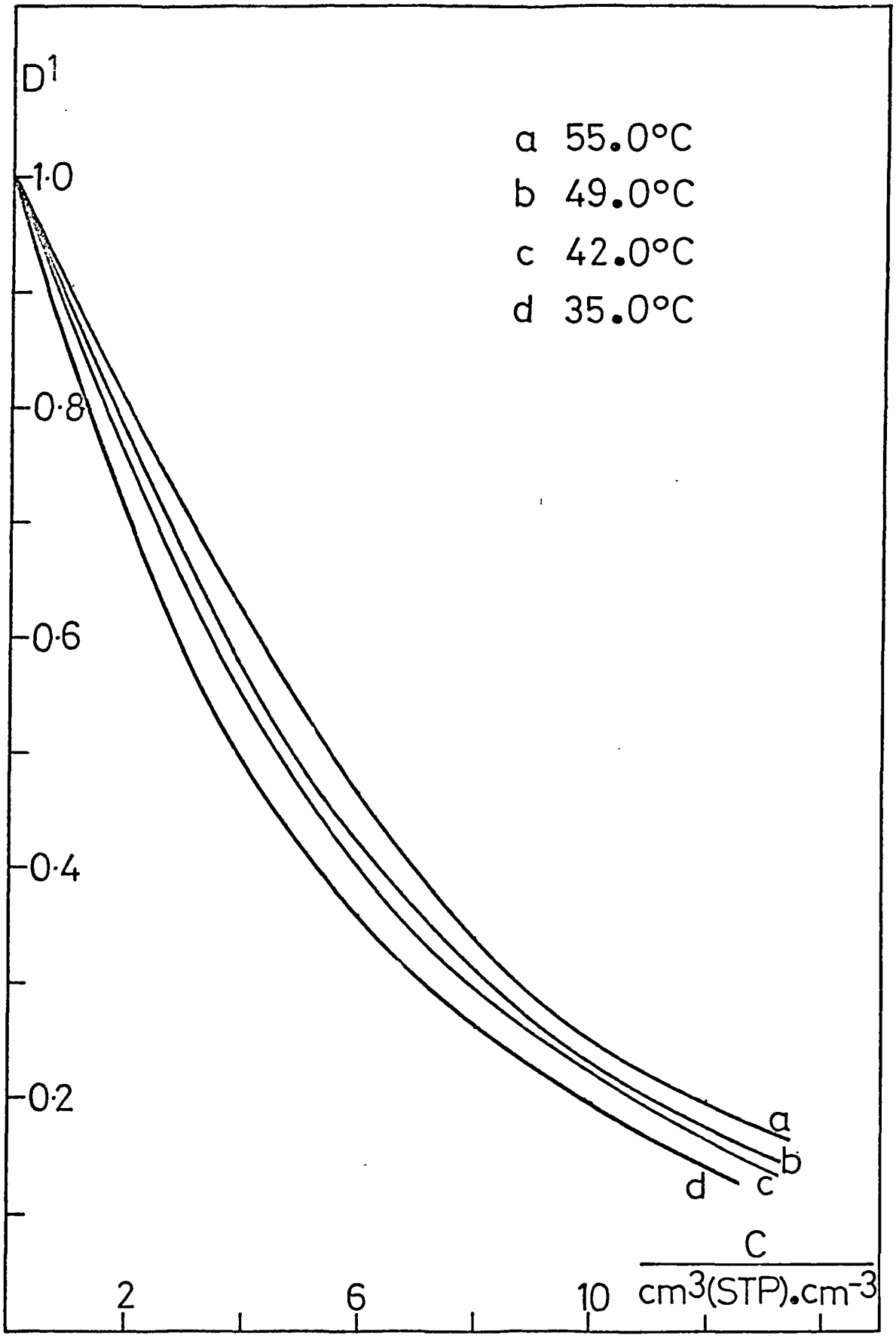


FIGURE 5.42 P(DMS-g-0·214 VAc)—H_2O
CONCENTRATION-DEPENDENCE OF DIFFUSION

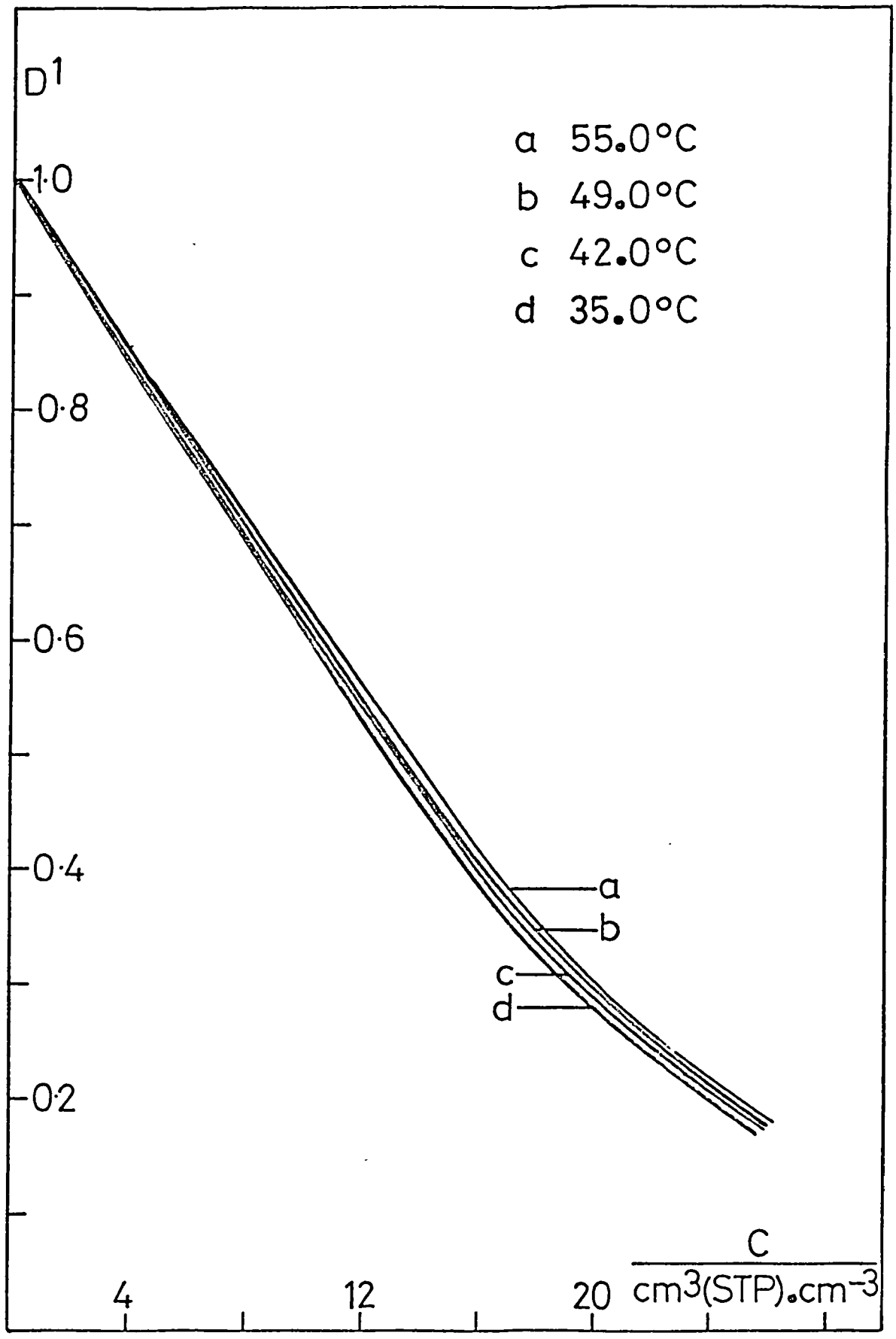


FIGURE 5.43 P(DMS-g-0·442 VAc)—H_2O
CONCENTRATION-DEPENDENCE OF DIFFUSION

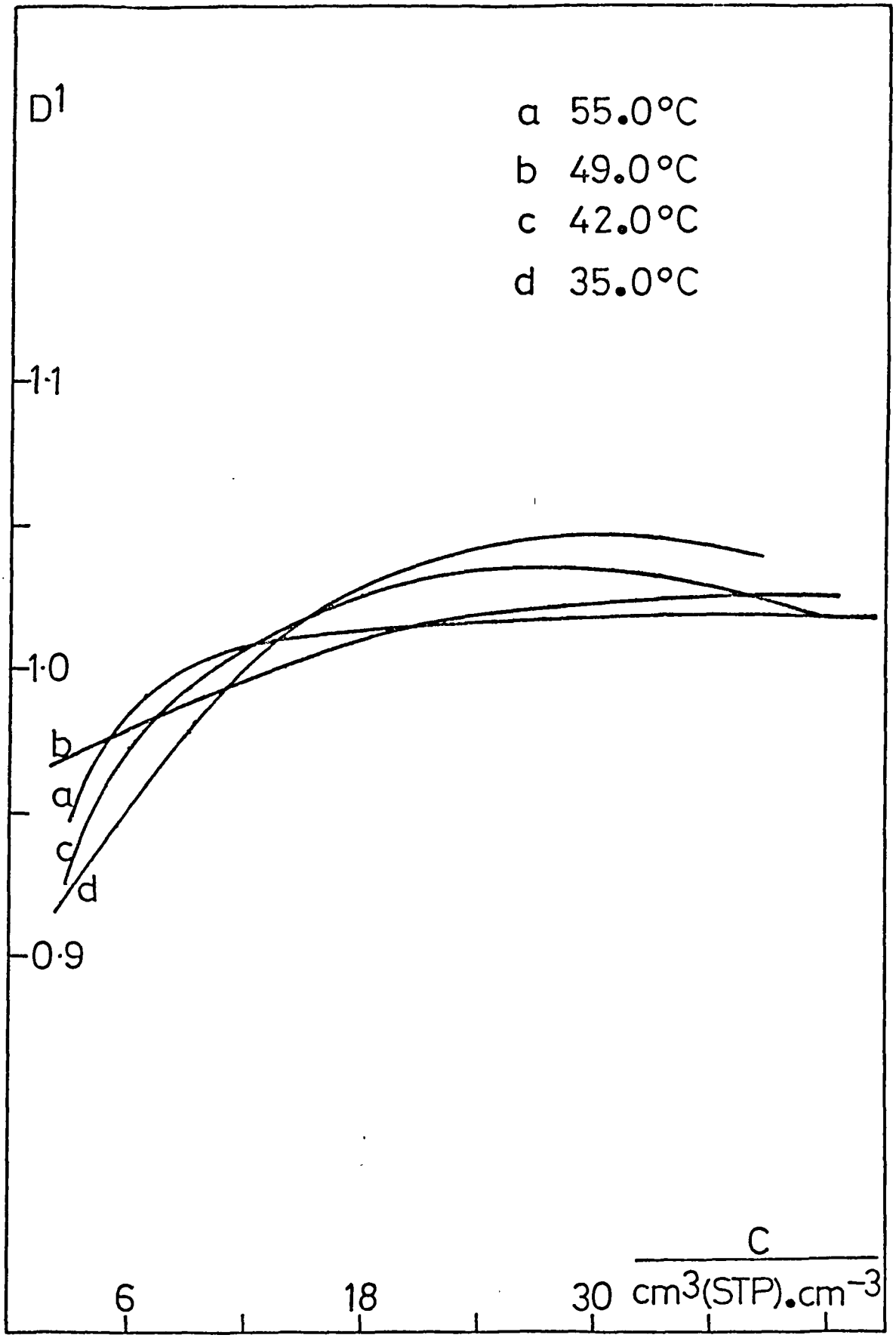


FIGURE 5.44 PVAc–H_2O

CONCENTRATION-DEPENDENCE OF DIFFUSION

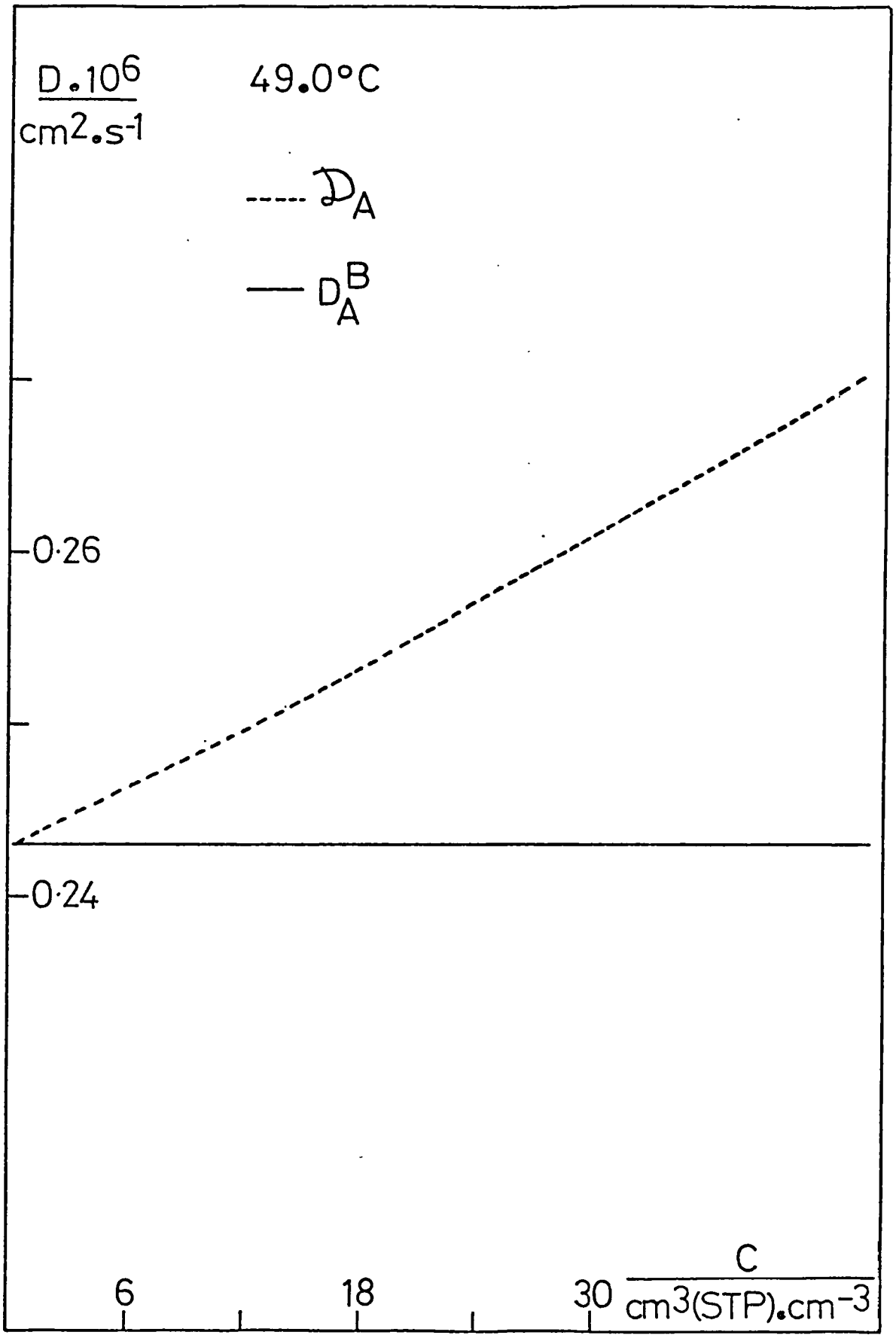


FIGURE 5.45 PVAc — H_2O

INTRINSIC DIFFUSION COEFFICIENTS

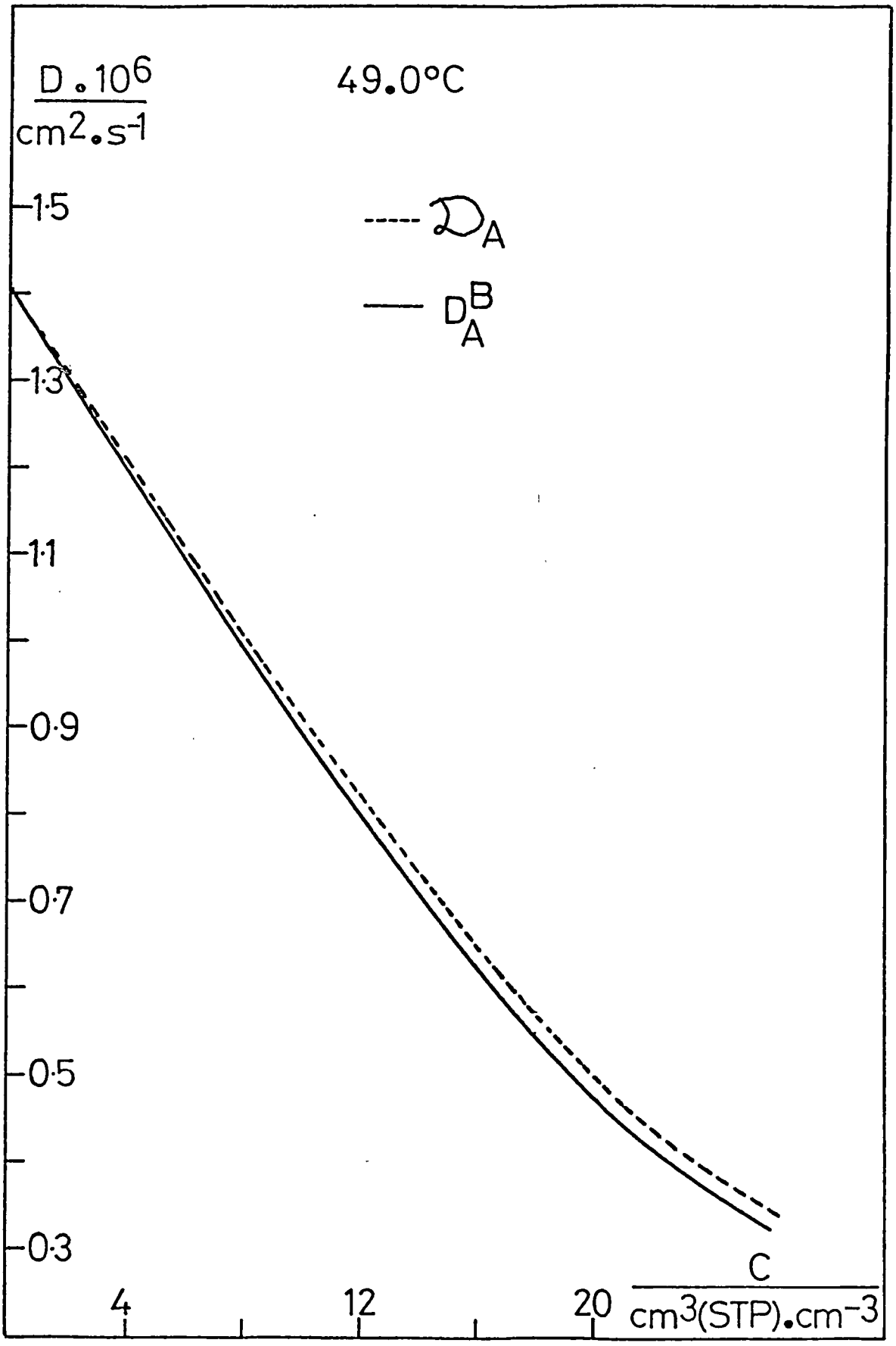


FIGURE 5.46 P(DMS-g-0·442VAc)—H_2O
INTRINSIC DIFFUSION COEFFICIENTS

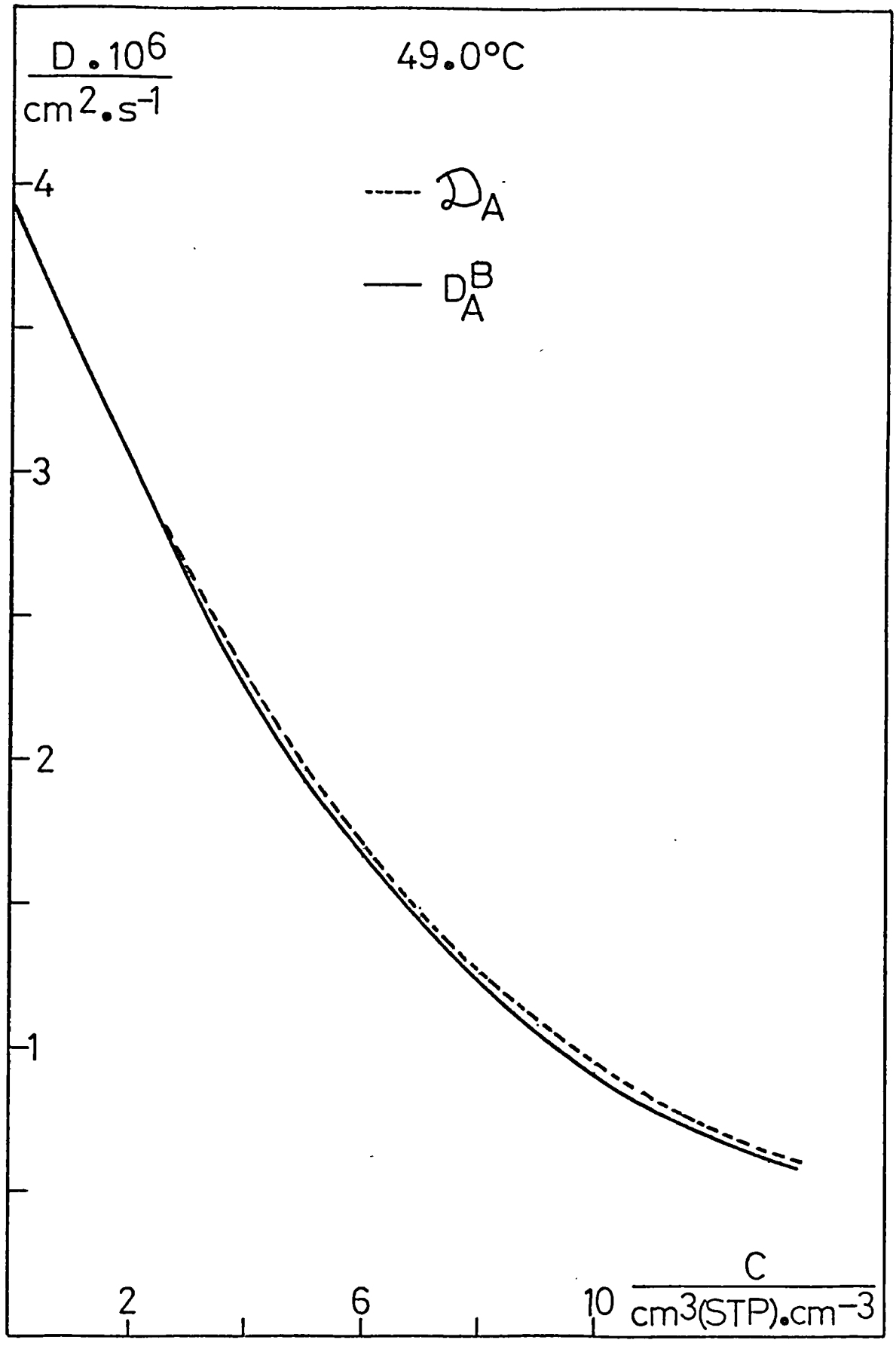


FIGURE 5.47 P(DMS-g-0·214VAc)—H_2O
INTRINSIC DIFFUSION COEFFICIENTS

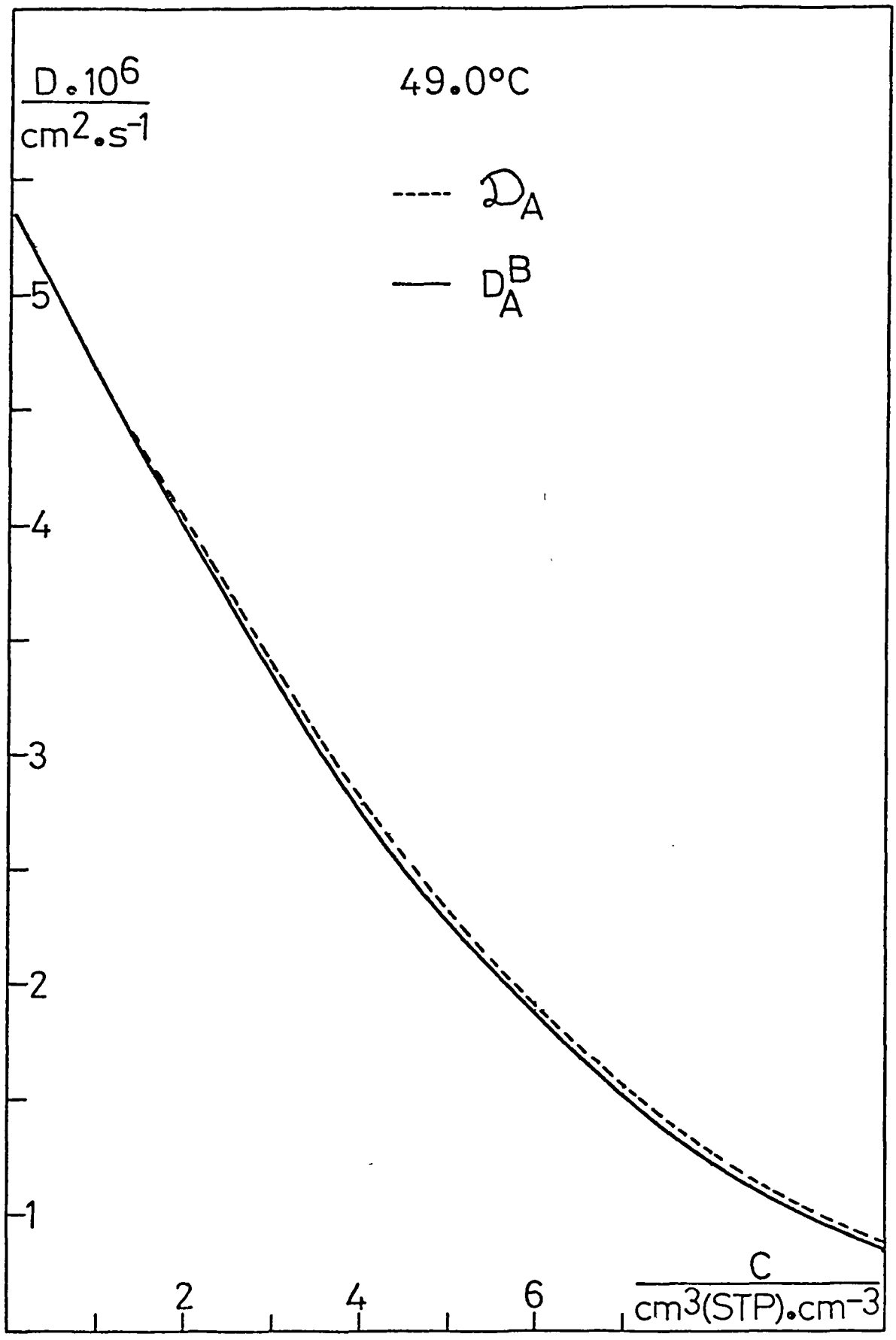


FIGURE 5.48 P(DMS-g-0·157VAc)—H_2O
INTRINSIC DIFFUSION COEFFICIENTS

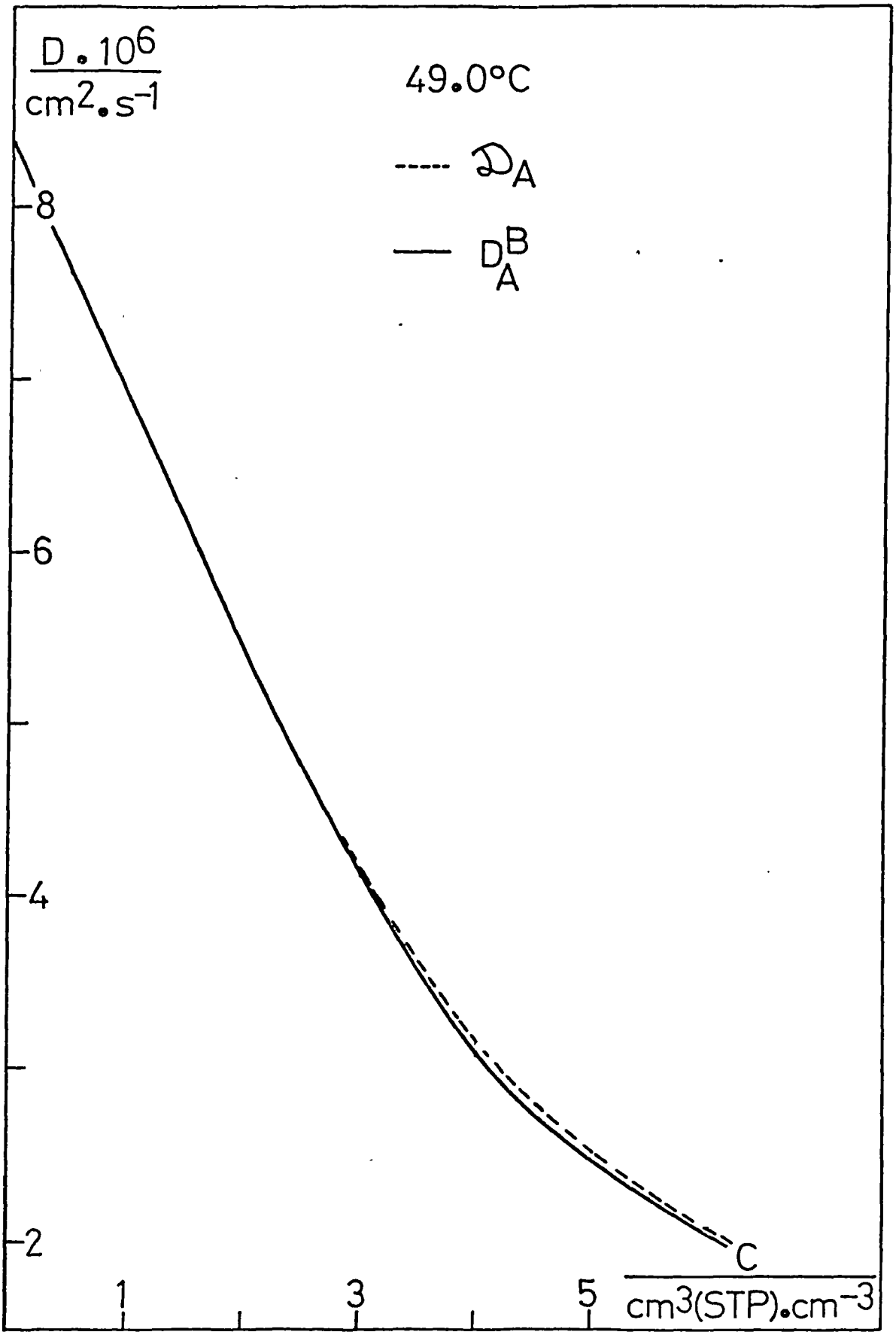


FIGURE 5.49 P(DMS-g-0·093VAc)–H_2O
INTRINSIC DIFFUSION COEFFICIENTS

not included since the swelling in this system is less than 1% so that mutual and intrinsic diffusion coefficients are the same. The intrinsic D results show that the net decrease of the mutual D with increasing concentration is reduced.

5.4.2 Transient-State Diffusion

Accurate time lag measurements were not possible for water vapour (see Section 5.3.1) but sorption-kinetics provided an alternative method of obtaining transient diffusion data. All copolymers and PVAc were studied but for PDMS the kinetics were too fast for D to be measured accurately with the sheet thicknesses available. The edges of the samples accounted for about 17% of the total surface area so that it was necessary to blank them off with aluminium foil. Sorption then took place through the two phase faces only, consistent with diffusion through an infinitely thin plane sheet. Several runs were performed for comparison purposes with the edge exposed.

(i) Sorption and Desorption Curves

Typical pairs of conjugate sorption-desorption curves are illustrated in Figures 5.50 - 5.52 for water vapour in the copolymers containing 3.4%, 21.4% and 44.2% PVAc by volume and are representative of the range of the time-scale and the sorption uptake involved. As can be seen from Figure 5.50 for the copolymer with the highest D, it takes about 150 seconds to reach the end of the kinetics region at $M_t/M_\infty = 0.5$. The initial stages of both sorption and desorption show uptakes which are always lower than one would expect from the later stages. This is a consequence of the fact that stable boundary conditions were not established quickly enough (around 20 seconds). In addition, this means that extrapolation of the sorption curve towards the $\sqrt{\text{time}}$ axis rarely went through the origin and usually intercepts the axis of M_t/M_∞. The slower the diffusion process the less noticeable is this effect which becomes relatively unimportant (Figures 5.51 and 5.52). The mathematics of this condition have been derived (37) and indicate that the rates of sorption and desorption increase initially and then decrease as equilibrium approaches when compared with the rates for a system in which attainment of stable boundary conditions is instantaneous. However, in this particular system, the discrepancy only amounts to 1-2% and hence the standard conditions and mathematics will be used.

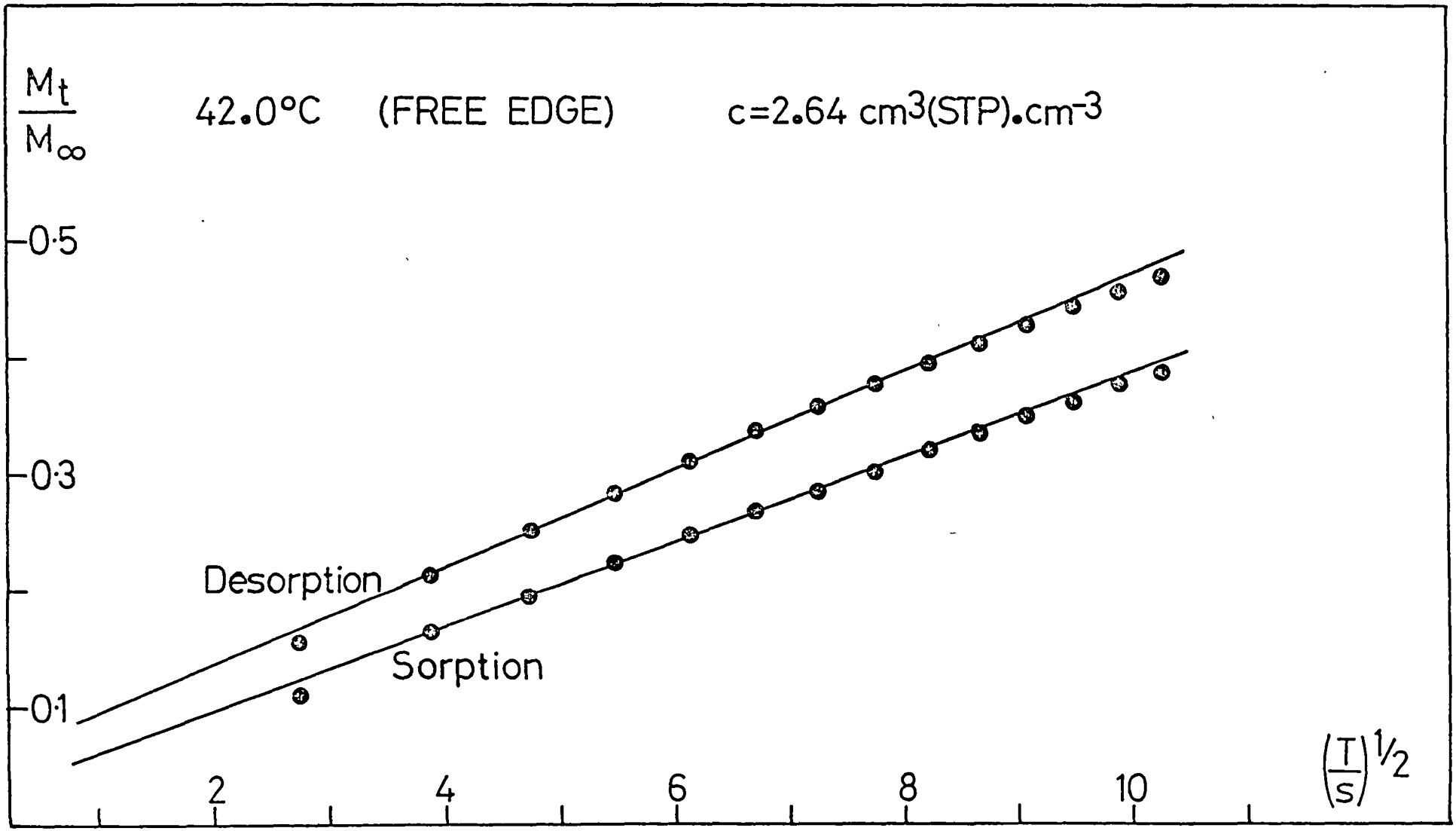


FIGURE 5.50 P(DMS-g-0·034 VAc)-H_2O CONJUGATE RATE CURVES

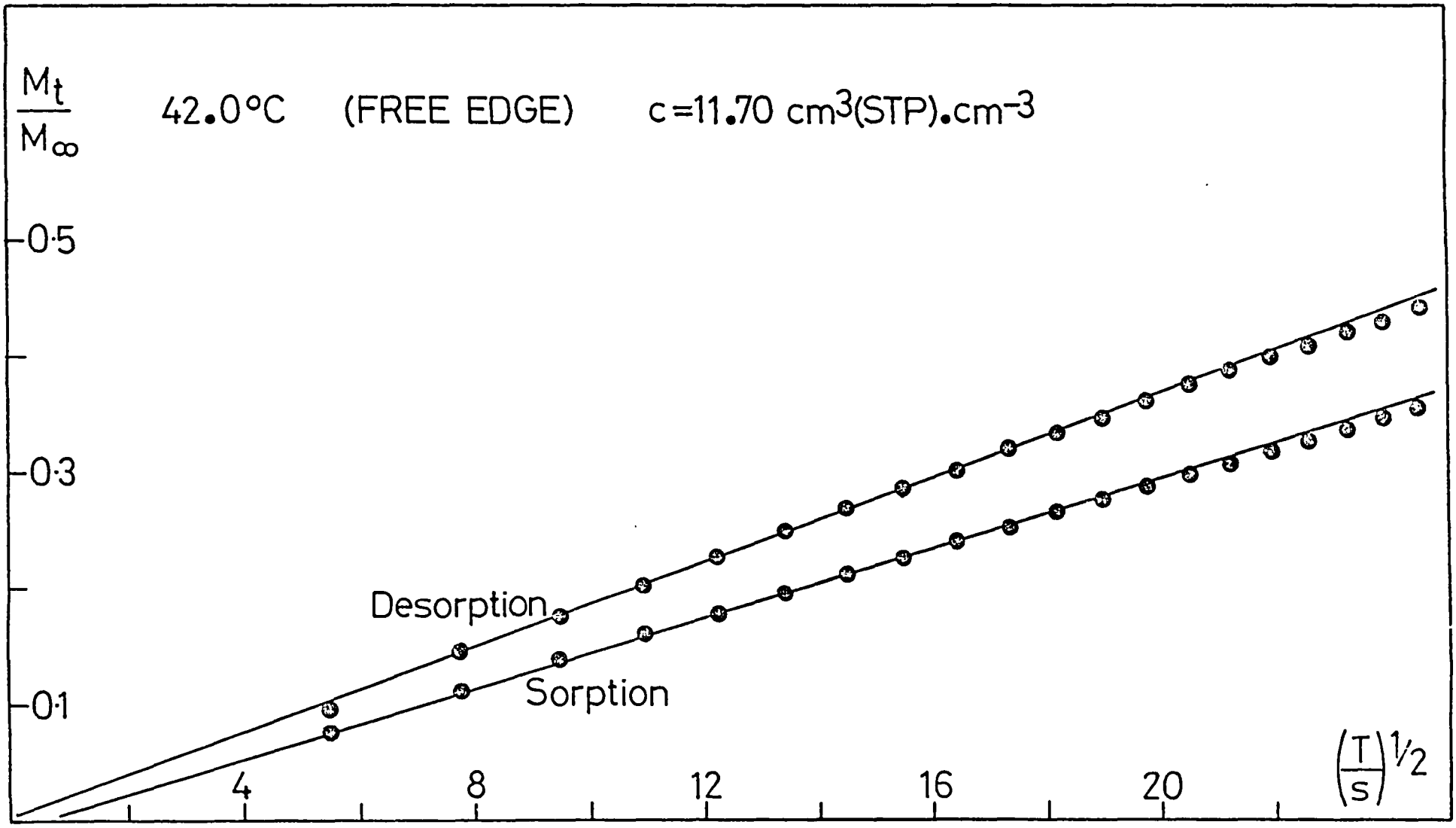


FIGURE 5.51 P(DMS-g-0·214 VAc)—H_2O CONJUGATE RATE CURVES

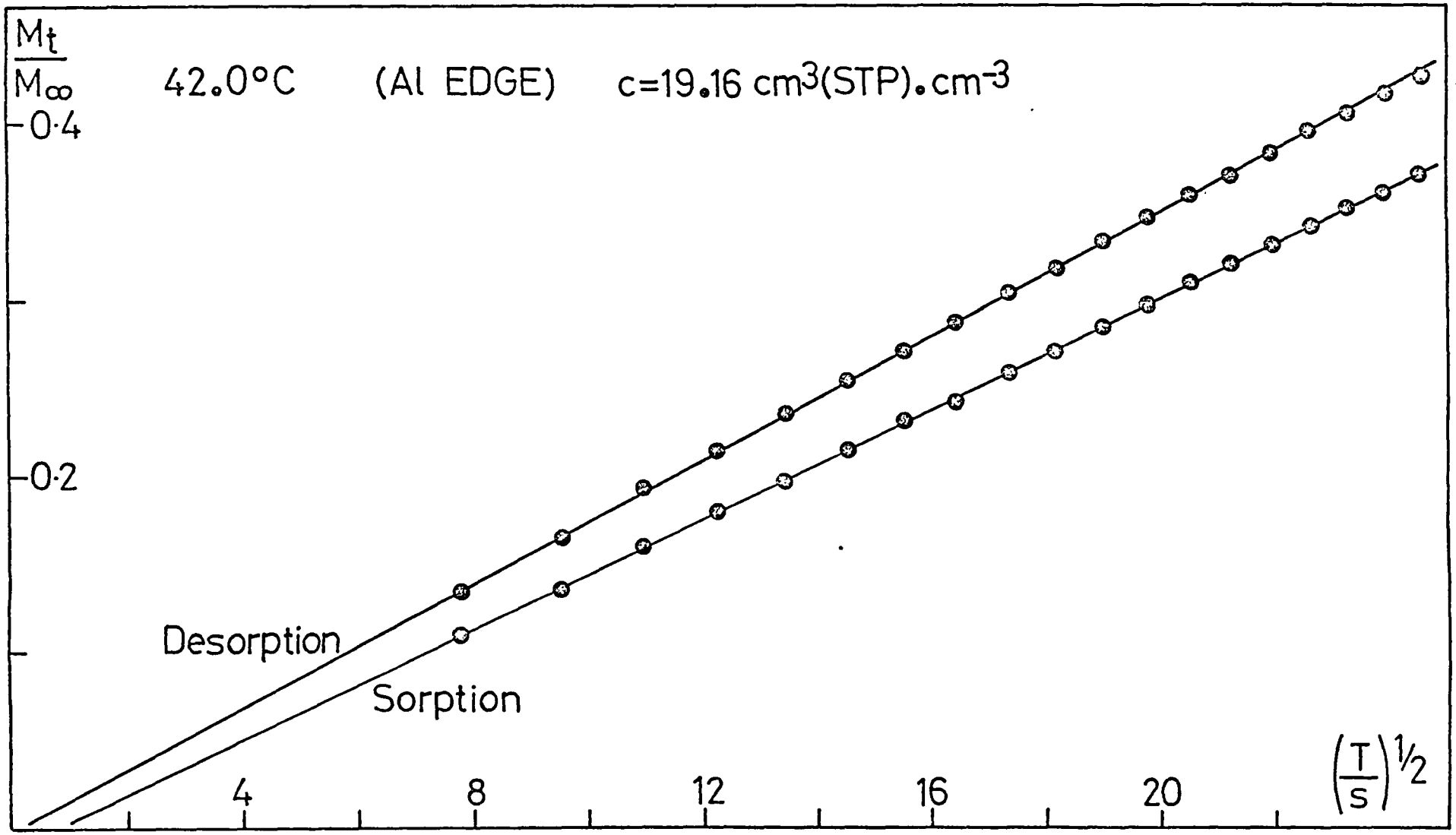


FIGURE 5.52 P(DMS-g-0·442 VAc)—H_2O CONJUGATE RATE CURVES

From these sorption-desorption curves average diffusion coefficients are obtained (see Sections 2.2.3 and 2.3.3) and these are illustrated in Figures 5.53 - 5.62.

(ii) Comparison of Transient and Steady-State Diffusion Coefficients

Steady-state and transient-state diffusion data are given in Table 5.14 for the same temperatures (42.0°C and 55.0°C). In all instances the diffusion coefficients are those at zero concentration.

It can be seen that, in general, there is reasonable agreement between the two methods considering the time scale of the transient diffusion measurements. For PVAc, which is an ideal in that it has a constant diffusion coefficient, agreement is within 3%.

Table 5.14

Steady-State and Transient Diffusion Coefficients ($D_{c=o}$, $cm^2 . s^{-1}$) in the limit ($c \rightarrow o$)

ϕ(PVAc)	T°C	% Area of Edges	Steady-State $D_{c=o} . 10^6$	Transient-State Al Edge $D_{c=o} . 10^6$	Transient-State Free Edge $D_{c=o} . 10^6$	* % Diff.
0.034	42.0	14.9	14.72	16.68	16.05	13.3
0.093	42.0	20.4	6.79	9.21	-	35.6
0.157	42.0	18.7	4.18	5.36	-	28.2
0.214	42.0	16.4	2.91	3.76, 3.60	4.04	23.7
0.442	42.0	10.2	1.07	1.03	-	3.7
1.00	42.0	2.2	0.147	-	0.151	2.7
0.093	55.0	20.4	10.04	-	11.32	12.8

* This is the difference between transient-state and steady-state D values, based on the steady-state values.

The results in Table 5.14 are puzzling in that there is little apparent effect when the edges of the samples are blanked off. The aluminium foil was found to adhere to the edges of the samples if these were treated with solvent such as 1,1,1-trichloroethane. In one instance

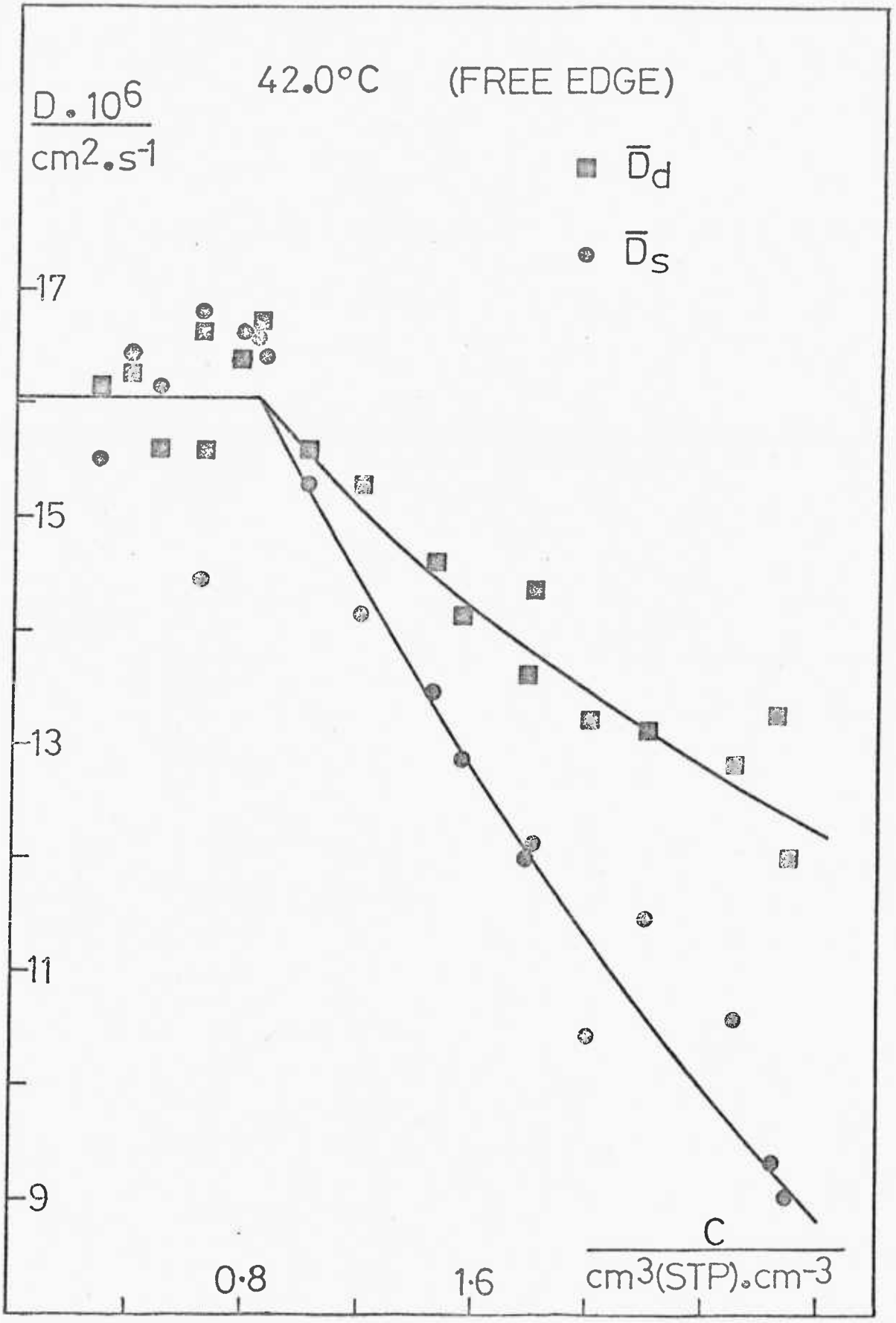


FIGURE 5.53 P(DMS-g-0·034VAc)-H_2O
SORPTION- & DESORPTION-KINETIC DATA

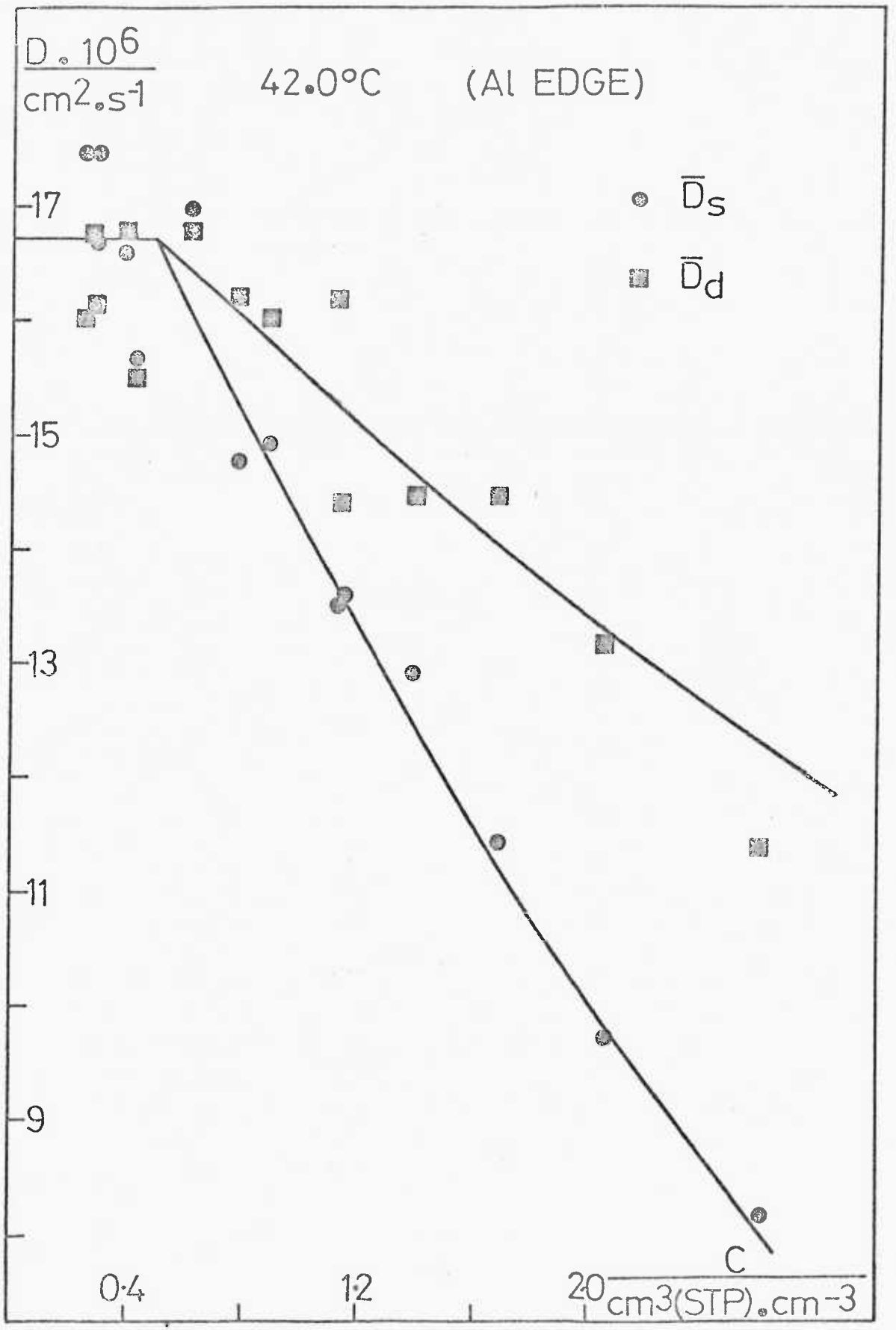


FIGURE 5.54 P(DMS-g-0·034VAc)–H_2O
SORPTION– & DESORPTION–KINETIC DATA

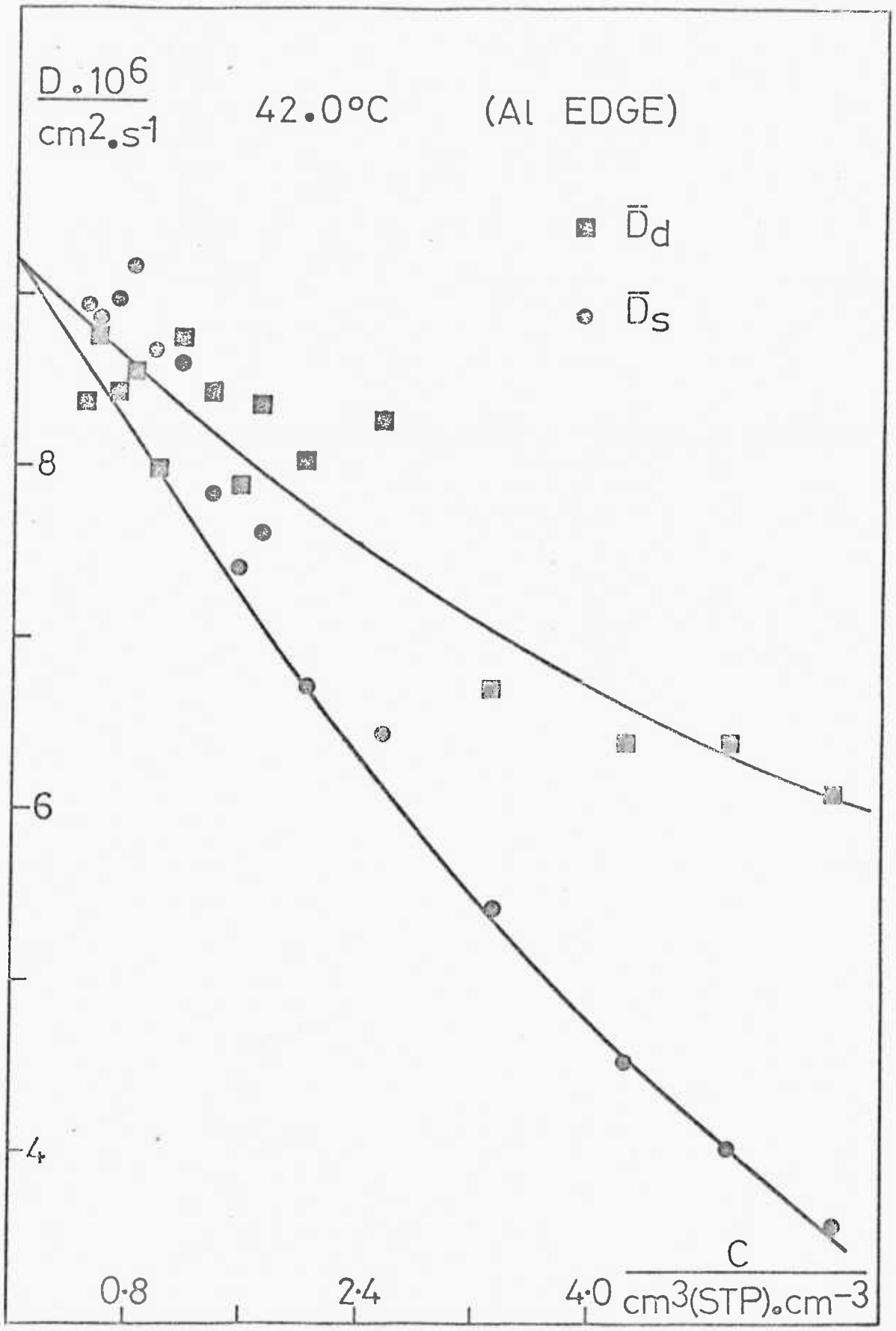


FIGURE 5.55 P(DMS-g-0·093VAc)–H_2O
SORPTION– & DESORPTION–KINETIC DATA

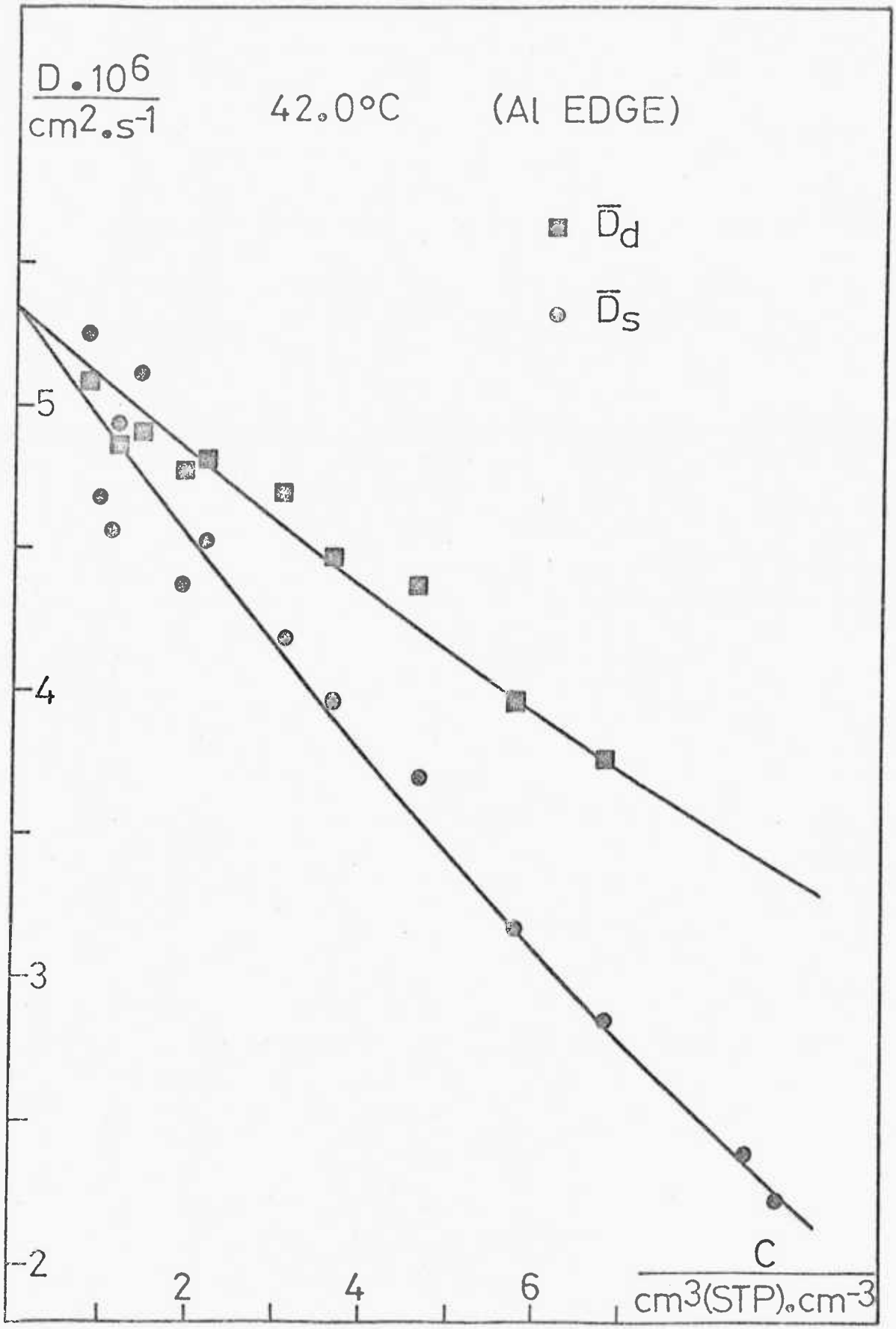


FIGURE 5.56 P(DMS-g-0·157 VAc)–H_2O
SORPTION– & DESORPTION–KINETIC DATA

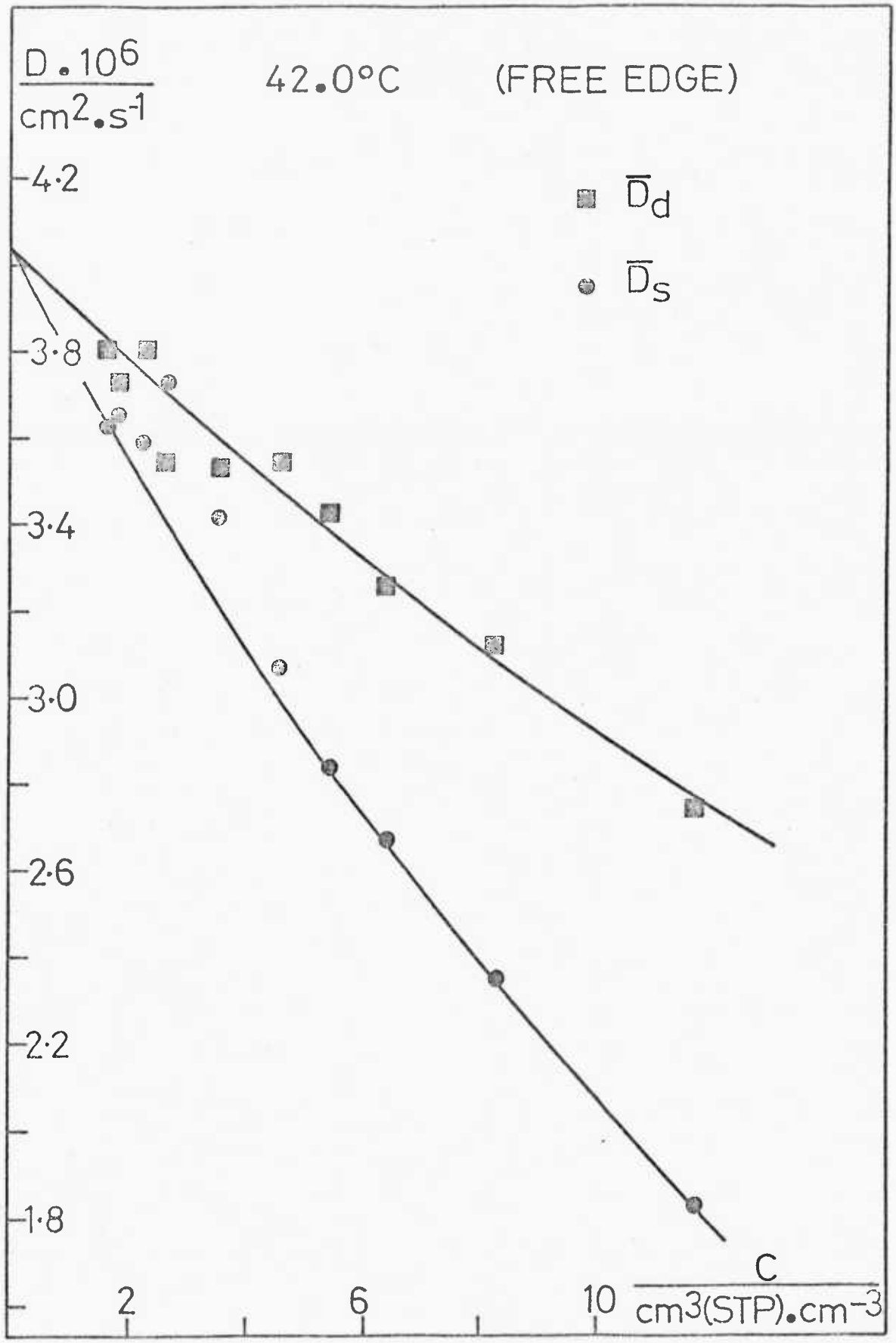


FIGURE 5.57 P(DMS-g-0·214VAc)—H_2O
SORPTION- & DESORPTION-KINETIC DATA

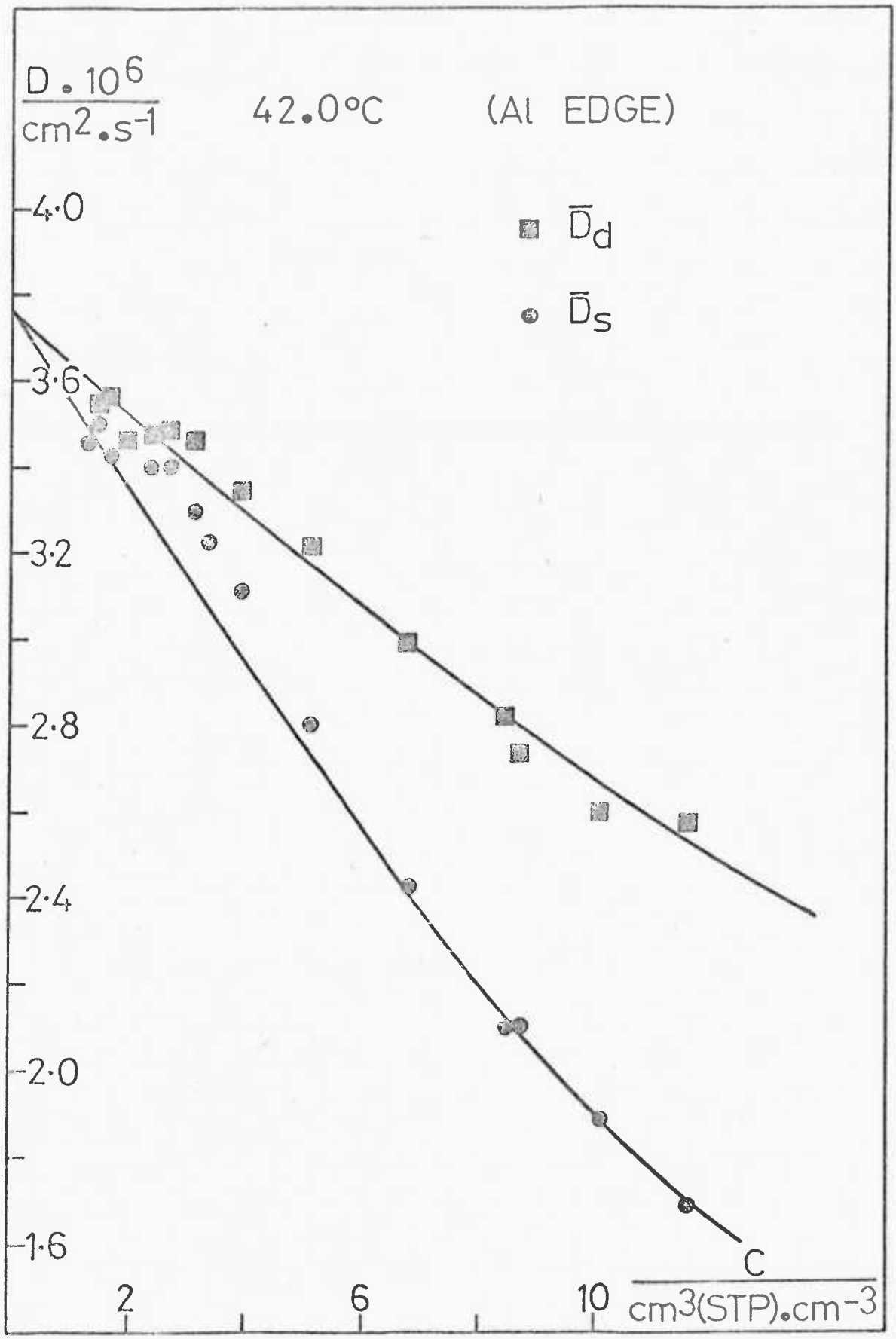


FIGURE 5.58 P(DMS-g-0·214VAc)-H_2O
SORPTION- & DESORPTION-KINETIC DATA

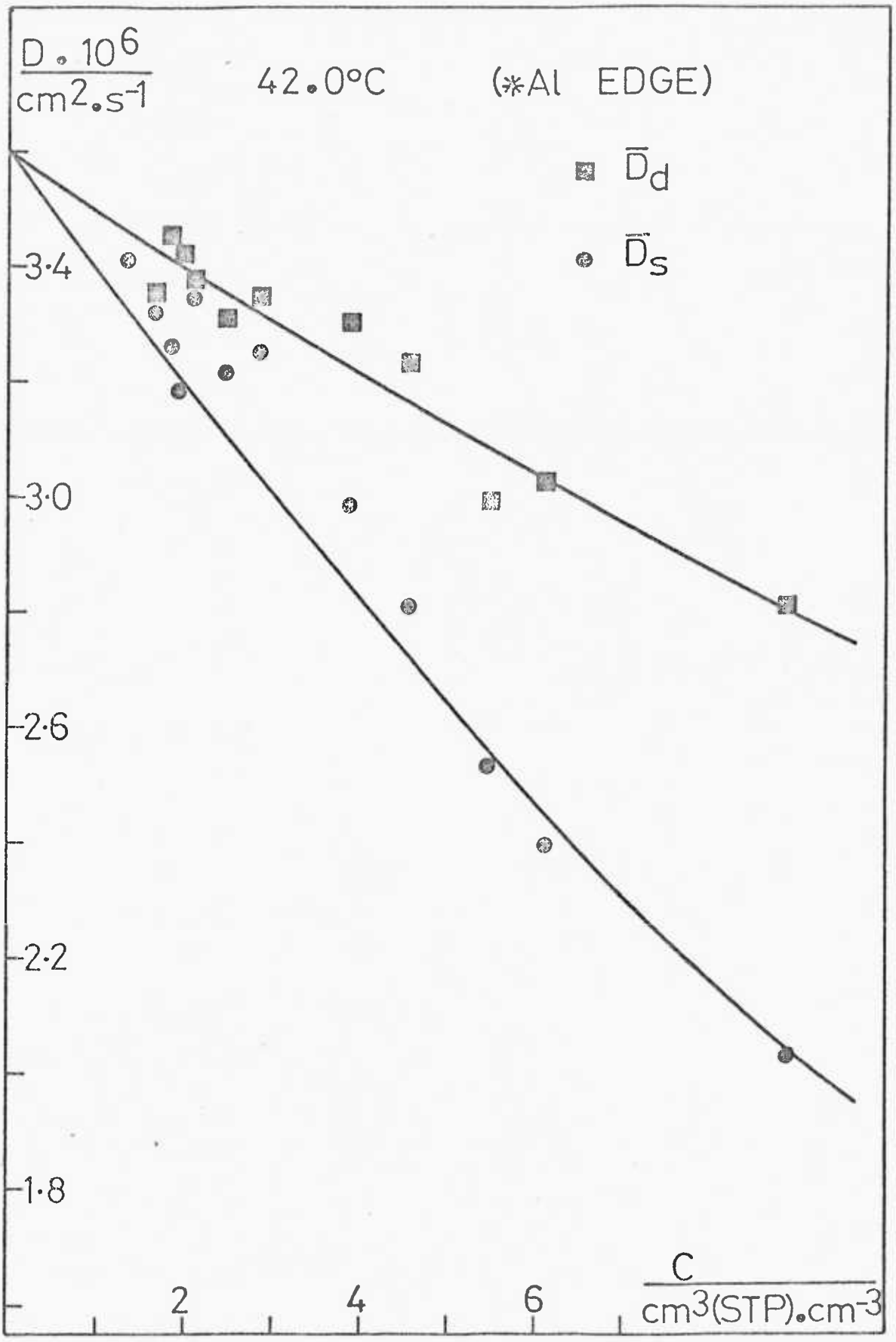


FIGURE 5.59 P(DMS-g-0·214VAc)–H_2O
SORPTION- & DESORPTION-KINETIC DATA

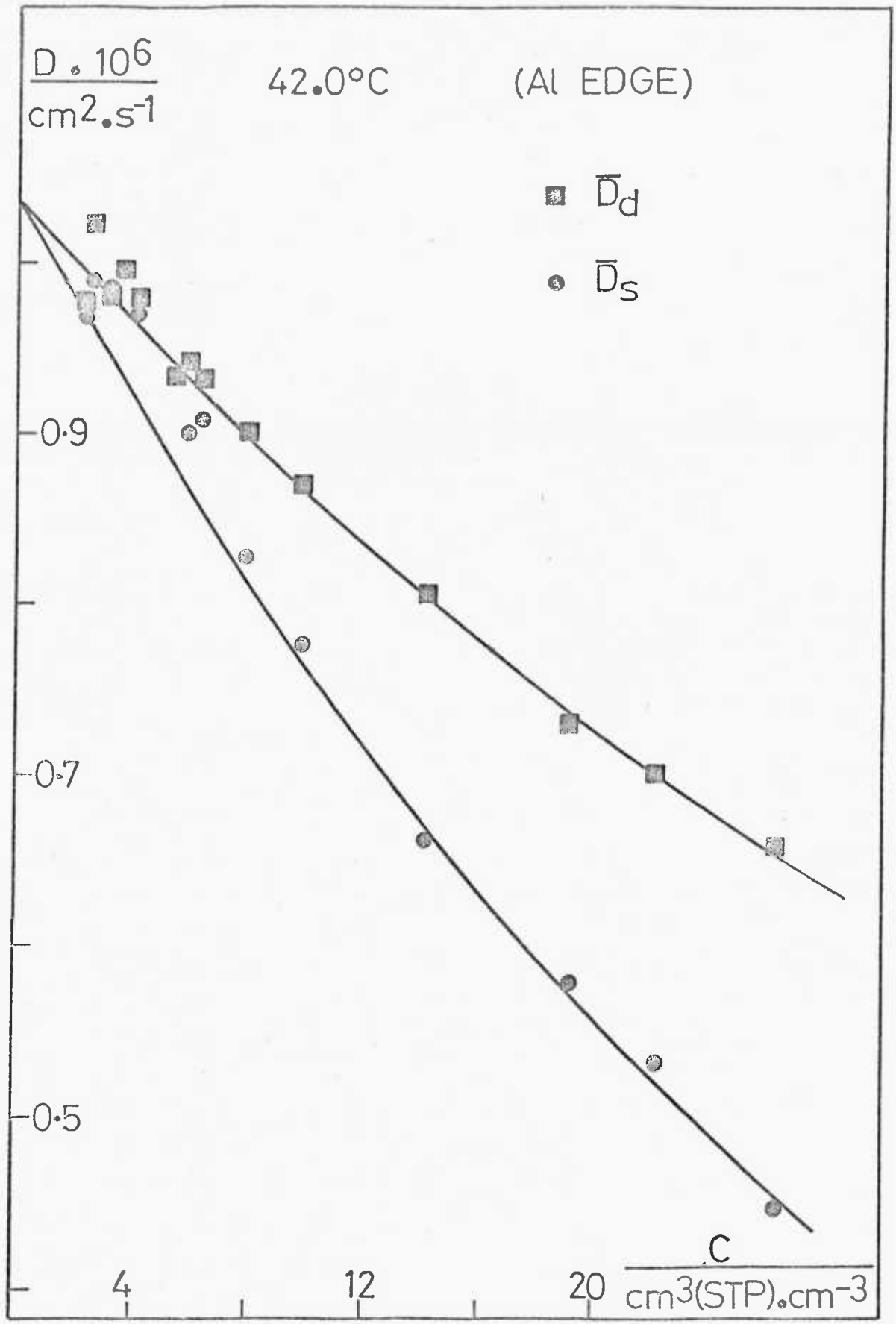


FIGURE 5.60 P(DMS-g-0·442VAc)–H_2O
SORPTION- & DESORPTION-KINETIC DATA

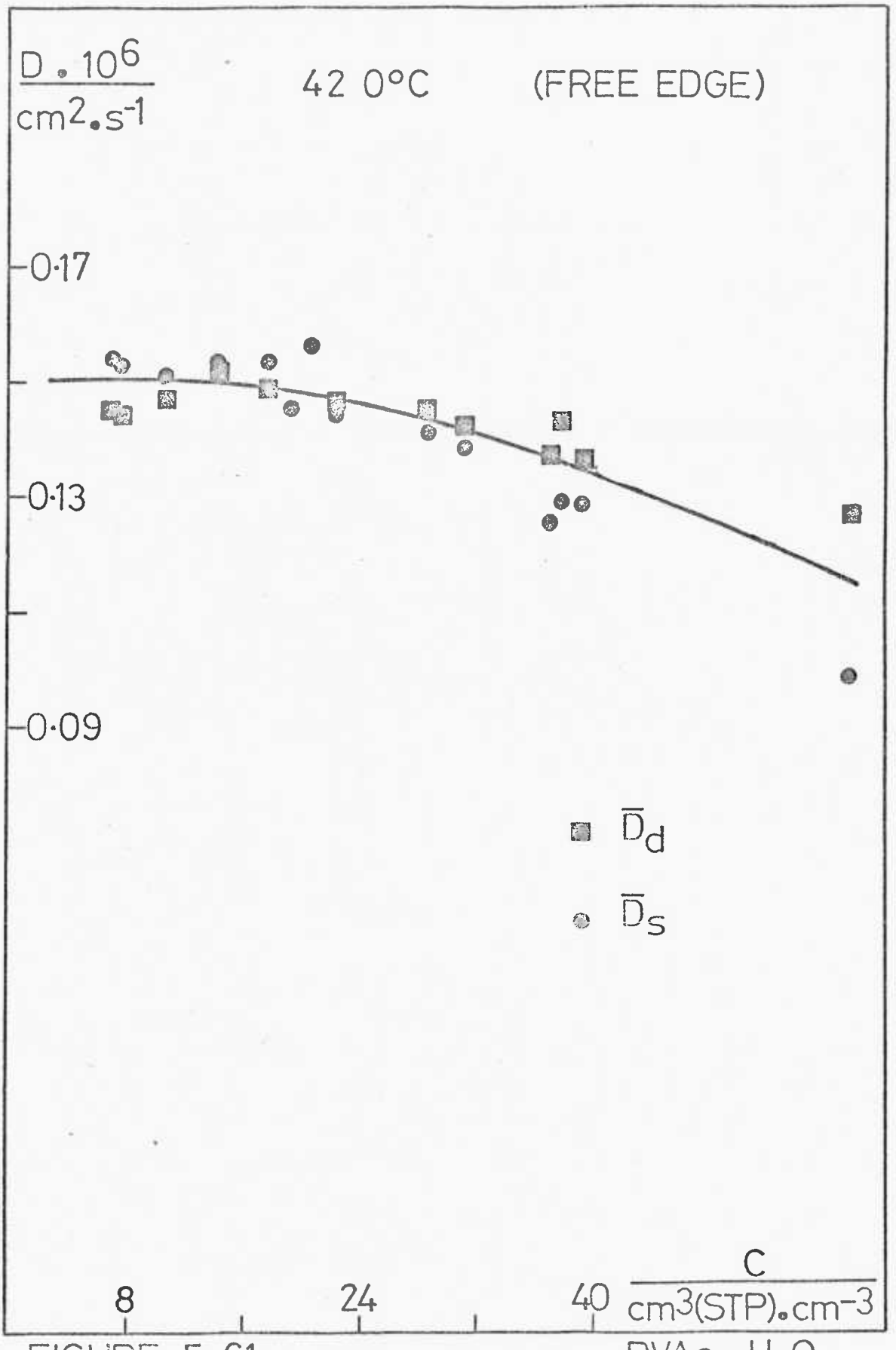


FIGURE 5.61
PVAc – H_2O
SORPTION– & DESORPTION-KINETIC DATA

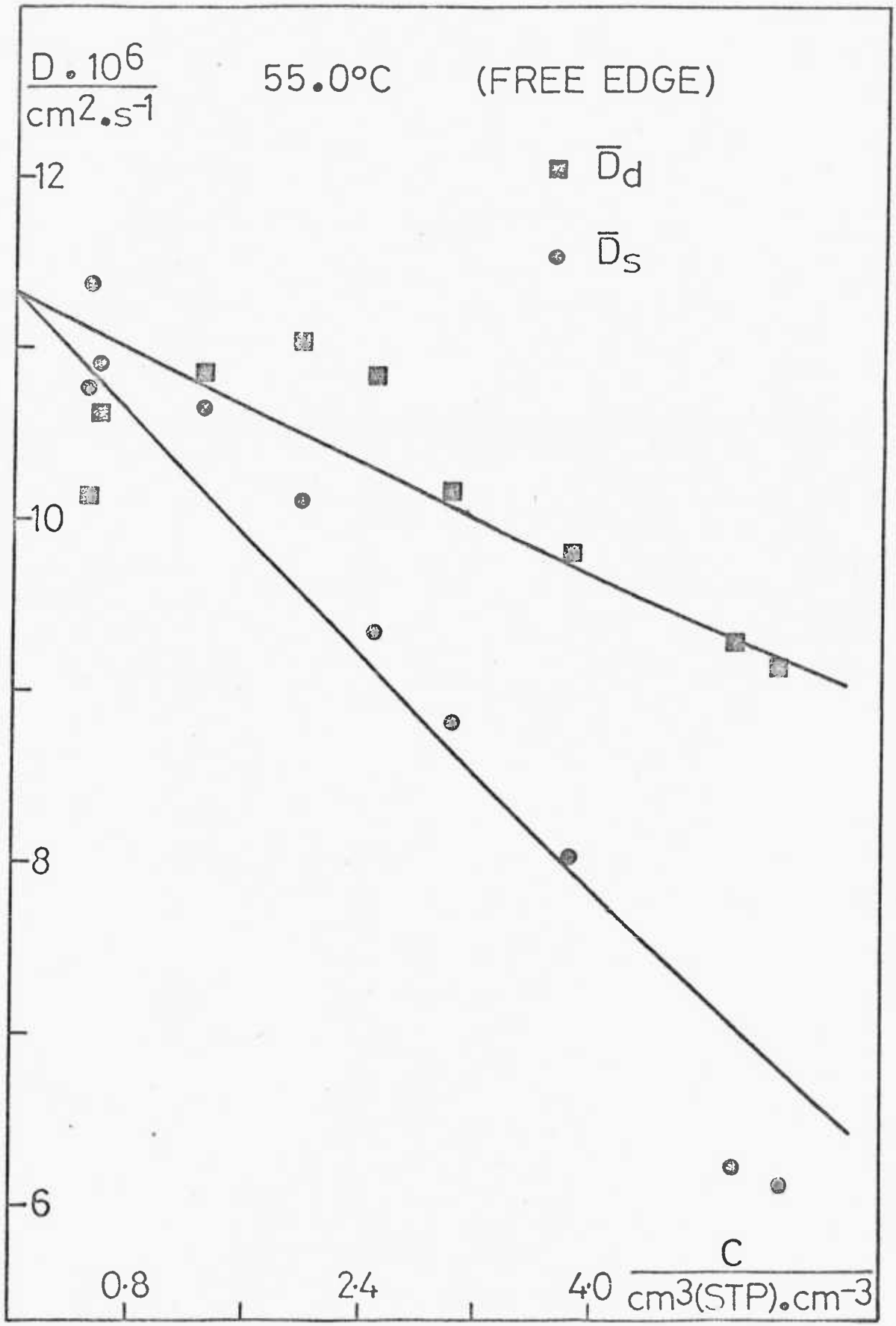


FIGURE 5.62 P(DMS-g-0·093VAc)–H_2O
SORPTION- & DESORPTION-KINETIC DATA

the adhesive "Silastic" gum was also used as a comparison. Since the difference between the two blanking procedures was small (P(DMS-g-0.214 VAc):- $D_{c=o}$ = 3.76 . 10^{-6} cm^2. s^{-1}(solvent) and $D_{c=o}$ = 3.60 . 10^{-6} cm^2 . s^{-1} (gum)) this does not account for all the difference between the steady-state and transient measurements. With PVAc much thinner films were used and the edge effect is relatively unimportant ($\sim$ 2%). The excellent agreement between steady-state and transient data for PVAc would indicate that the blanking off procedure was not very effective even though there appeared to be satisfactory adhesion.

For a two phase system both transient and steady-state analyses should yield the same diffusion coefficient provided that equilibrium is established between phases at all times in the process so that time effects are absent (63, 100). This means that the rate of diffusion of penetrant into the domain and through the external phase around that domain must be greater than the rate at which that region is penetrated by the penetrant (100). It is most convenient to transpose these rates into relaxation times, so that the time for steady-state attainment in the microscopic heterogeneous region is small compared to the time required for a unit change in concentration of penetrant in that region. There are two situations which contribute to the delay in the completion of partition of penetrant between the phases, namely diffusion into the domains and diffusion in the continuum for the penetrant molecule to reach the domain. The rate-determining process is the one with the longest relaxation time : τ_1 for the domains and τ_2 for the continuum. The relaxation times may be approximated to (63, 100) :

$$\tau_1 \sim \frac{r^2}{15 D_D} \qquad \tau_2 \sim \frac{2r^2}{D_M \phi_D^{2/3}} \qquad \ldots.(5.6)$$

where r is the average radius of the domain; D_M, D_D the diffusion coefficient of the membrane and dispersed phase respectively; and ϕ_D the volume fraction of the dispersed phase. It is anticipated that τ_2 will be the limiting feature in most instances, but the reverse is probable for systems in which the solubility is determined primarily by the disperse phase whose diffusion coefficient is much lower than that of the continuum. This is the situation for the system under study and hence it is necessary to evaluate both τ_1 and τ_2. For the copolymer containing 44.2% PVAc by volume (the one with the lowest D and the

largest domain size) the values of τ_1 and τ_2 are respectively $2.5 \cdot 10^{-5}$ s and $1.8 \cdot 10^{-4}$s. Hence, for all the copolymers, diffusion through the continuum is the limiting step in the attainment of the steady-state in the microscopic region. For equilibrium between the phases to be established at all times τ_2 must be very small compared to $(\partial t/\partial c)$, or for

$$R = \frac{2(\pi D_M)^{\frac{1}{2}} t^{2/3}}{\tau_2 S_M C_o x} \cdot \exp\left(\frac{x^2}{4D_M t}\right) >> 1 \qquad \ldots.(5.7)$$

where C_o is the concentration of penetrant in the membrane, t, x are specified as the time after the start of the experiment and distance within the membrane. Using appropriate values it was found that $R \sim 10^7$ so that equilibrium between the phases is established instantaneously and hence transient and steady-state analyses ought to yield the same diffusion coefficients.

However the situation is still not completely resolved since these comparisons are mainly at a temperature only 10^oC above the glass transition temperature of PVAc. Transient measurements in the transition region (88, 106) indicate a pseudo-Fickian type of transport. The characteristics of this mode of transport are that sorption and desorption curves resemble Fickian ones, show no inflexions, possess initial linear regions which do not extend to 50% uptake, have a slow approach to equilibrium, and give similar transient and steady-state diffusion coefficients at low concentrations but which diverge at high concentrations (106). This is especially true if measurements are taken near the glass transition for systems in which large uptakes take place rapidly. Most of these features are present in the transient measurements taken, especially that of the short linear regions. For a diffusion coefficient decreasing with increasing concentration the linear region ought to extend beyond 50% uptake whilst, in practice, it rarely extends beyond $M_t/M_\infty = 0.4$. As a comparison the copolymer containing 9.3% PVAc by volume was tested at 55.0^oC where these effects ought to be eliminated. A typical sorption-desorption curve is shown in Figure 5.63 in which the linear region certainly extends up to $M_t/M_\infty = 0.5$ after the initial stabilising of the boundary conditions. The agreement of steady-state and transient data is also much closer at 55.0^oC than at 42.0^oC. This may be fortuitous but it certainly seems that there needs to be some further work done to really establish whether the possibility of pseudo-Fickian behaviour is real.

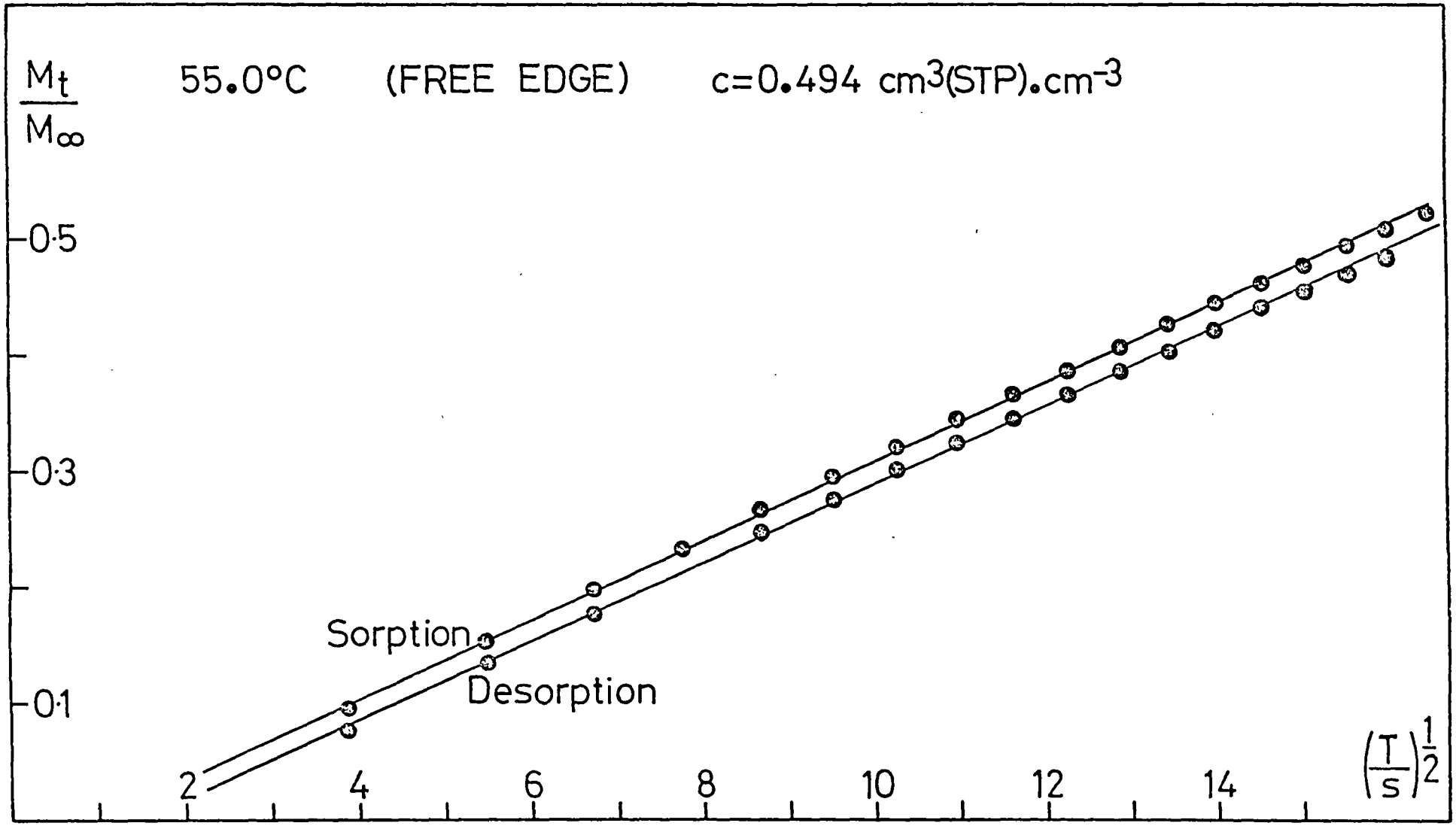


FIGURE 5.63 P(DMS–g–0·093 VAc)–H_2O CONJUGATE RATE CURVES

The concentration-dependence of the diffusion coefficients obtained by the two methods are shown in Figures 5.64 - 5.70. The transient data are obtained as averages of the two methods of analysis (Section 2.3.3); a weighted mean analysis of the sorption diffusion coefficients ($\overline{D}_s$) and a successive approximation analysis of the average diffusion coefficients ($\overline{D}_{av}$). In general the agreement between transient and steady-state results is quite reasonable, especially for PVAc even though one method indicates a D increasing slightly and the other D decreasing slightly with increasing concentration. Consequently these measurements support earlier analyses (74, 81) which indicated that D for PVAc was independent of concentration.

Hence transient and steady-state diffusion data yield similar results although there is some small discrepancy between the methods.

5.4.3 Temperature Dependence of D

Plots of log D vs. 1/T are given in Figures 5.71 - 5.77 for each of the systems. Values of E_D calculated from these plots are given in Table 5.15. These are all obtained from steady-state data only.

(i) Values of E_D at c=o

Values of E_D for the two homopolymers are in good agreement with previously reported data; within 4% for PDMS (20) and 5% for PVAc (81). The large difference in E_D for the two polymers is a consequence of the structures of the polymers and is reflected in their glass transition temperatures (-123°C for PDMS and + 33°C for PVAc).

Values of E_D for the graft copolymers are illustrated in Figure 5.78 which also shows the E_D values expected from the Higuchi, Böttcher, Bruggeman, Maxwell and Series/Parallel models. Like the diffusion coefficients from which they were derived, these theoretical values are composite quantities, calculated from $\Delta\overline{H}_s$ and E_P values. They serve as a useful check on E_D values although they essentially are a reflection of E_P data. It was decided not to include all the models in an analysis of this type as the wide range of E_D values ensures that the difference between the models is relatively small in the 0-50% PVAc region and hence comparisons are difficult.

As might be anticipated from the previous Sections, the Higuchi, Böttcher and Bruggeman models are the most realistic in representing experimental data. Overall the Higuchi model appears to show greater

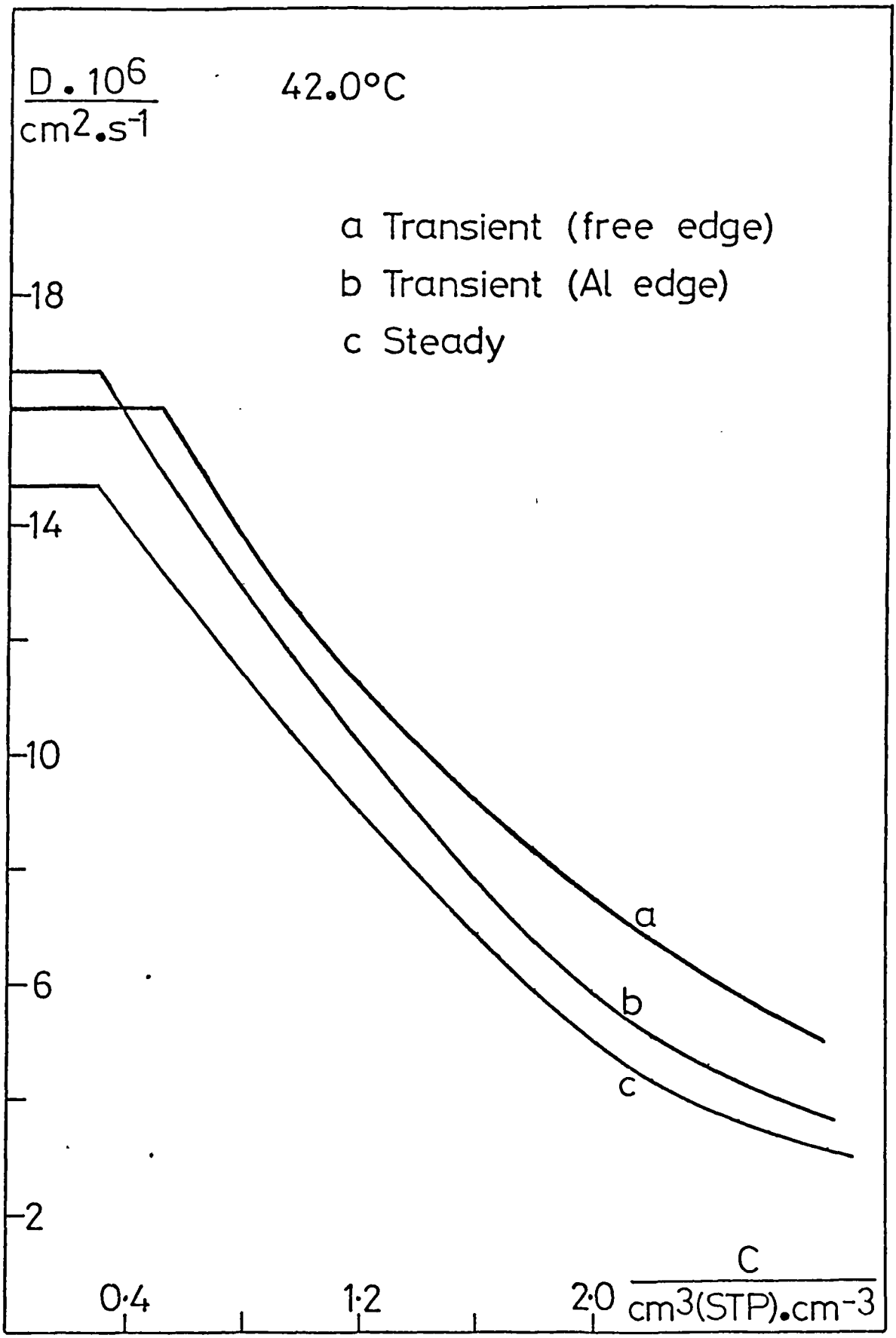


FIGURE 5.64 P(DMS-g-0·034VAc)–H_2O
TRANSIENT– & STEADY-STATE DIFFUSION

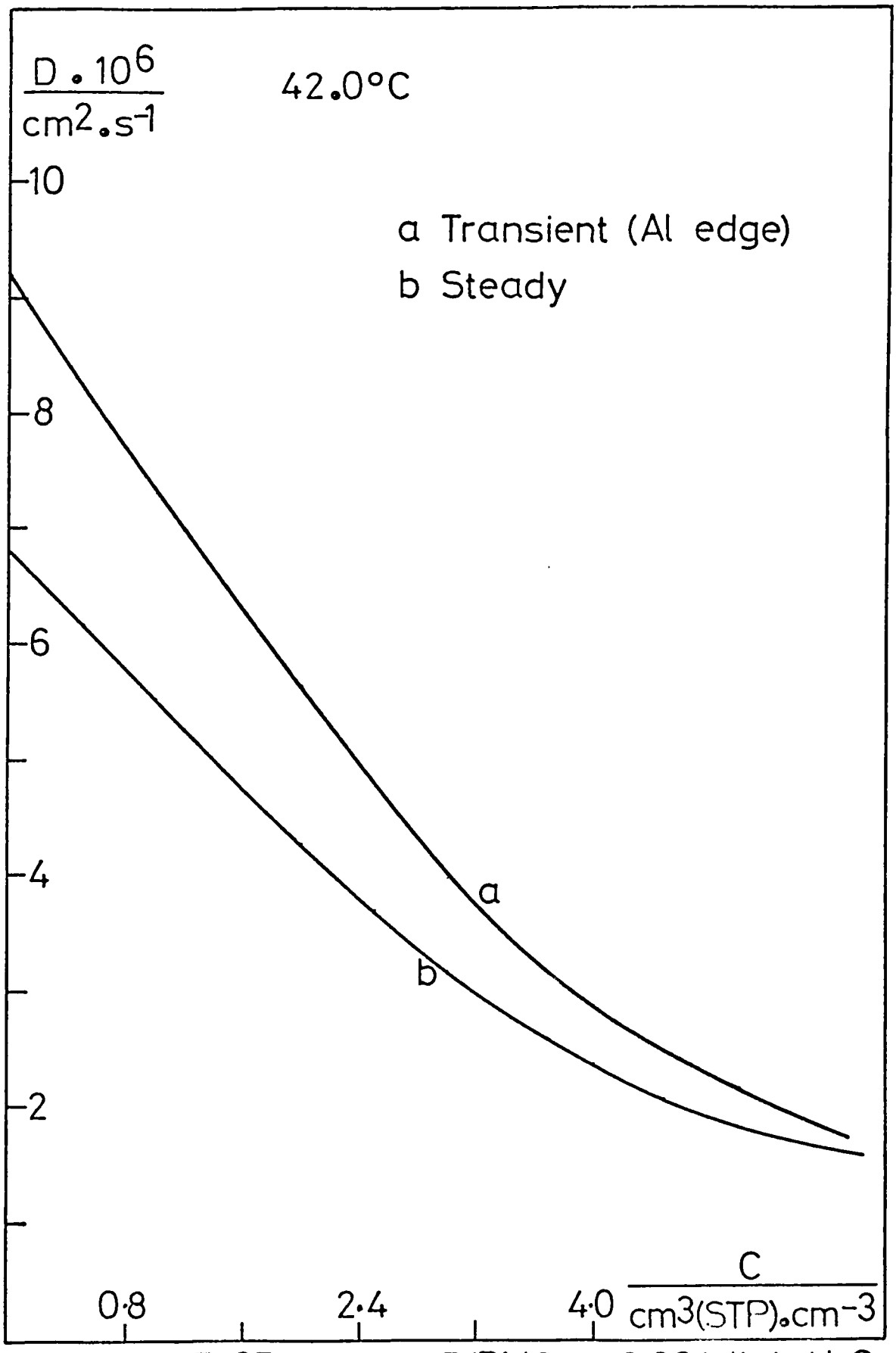


FIGURE 5.65 P(DMS-g-0·09 VAc)-H_2O
TRANSIENT- & STEADY-STATE DIFFUSION

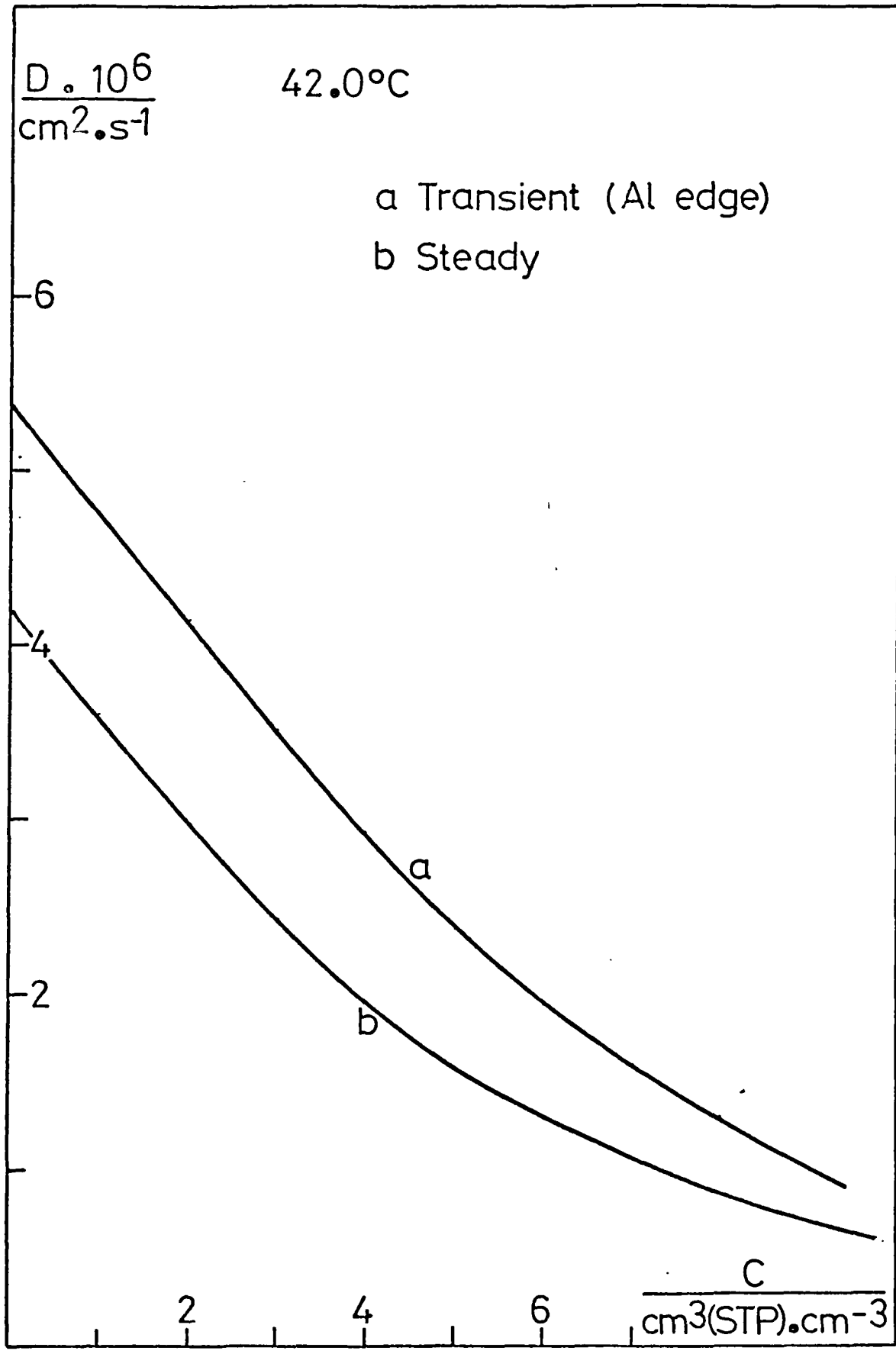


FIGURE 5.66 P(DMS-g-0·157VAc)–H_2O
TRANSIENT- & STEADY-STATE DIFFUSION

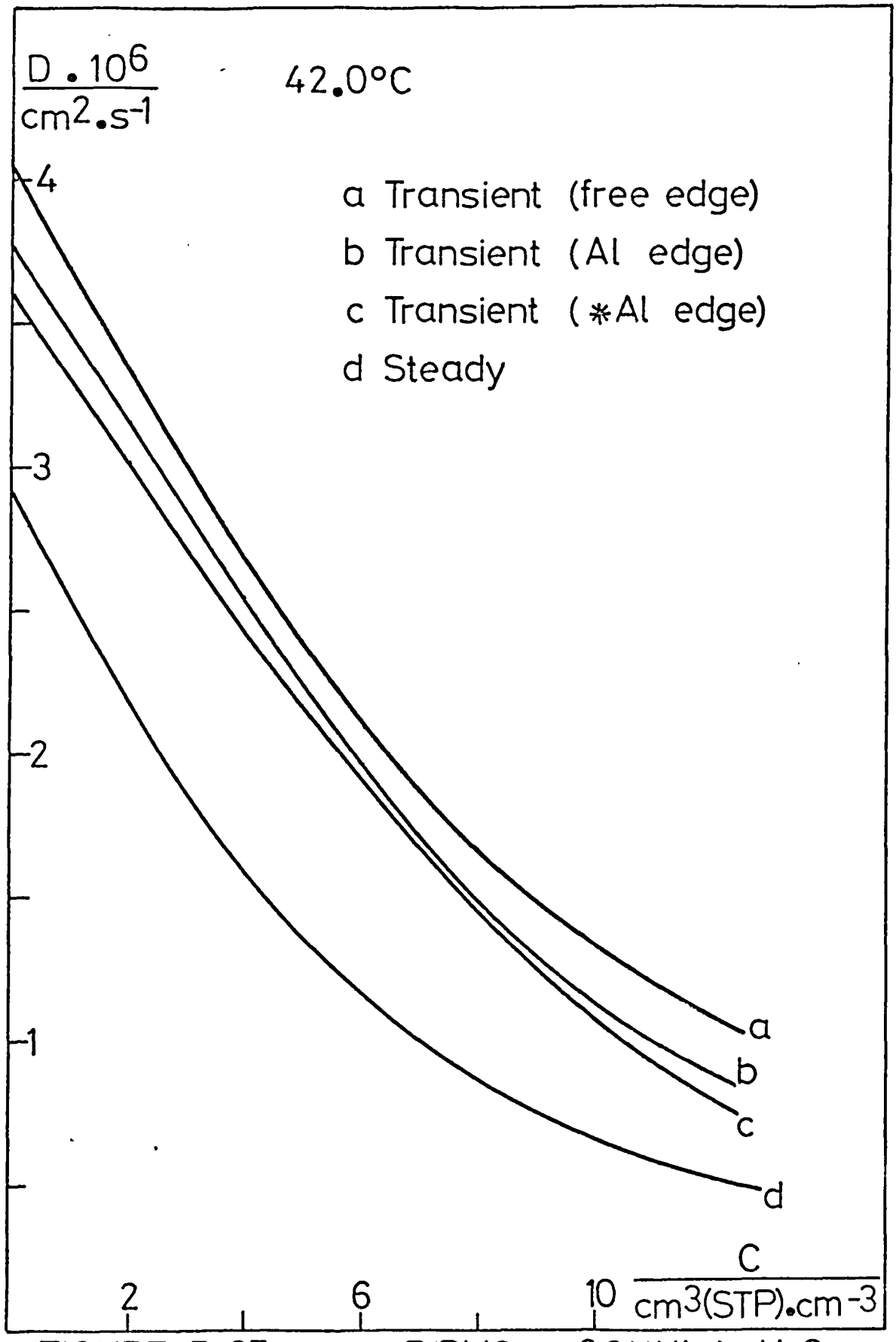


FIGURE 5.67 P(DMS-g-0·214VAc)–H_2O
TRANSIENT– & STEADY-STATE DIFFUSION

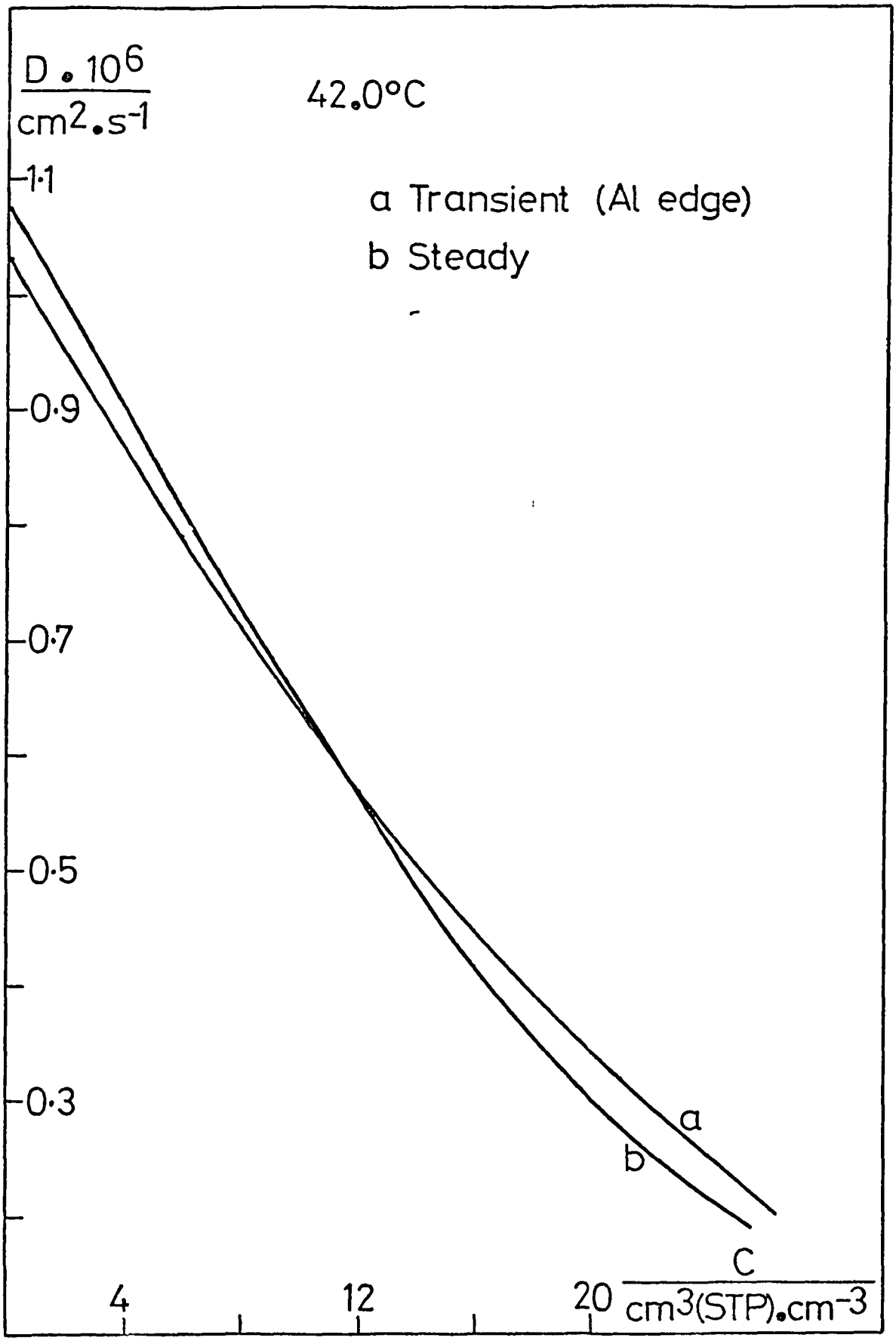


FIGURE 5.68 P(DMS-g-0·442VAc)—H_2O
TRANSIENT- & STEADY-STATE DIFFUSION

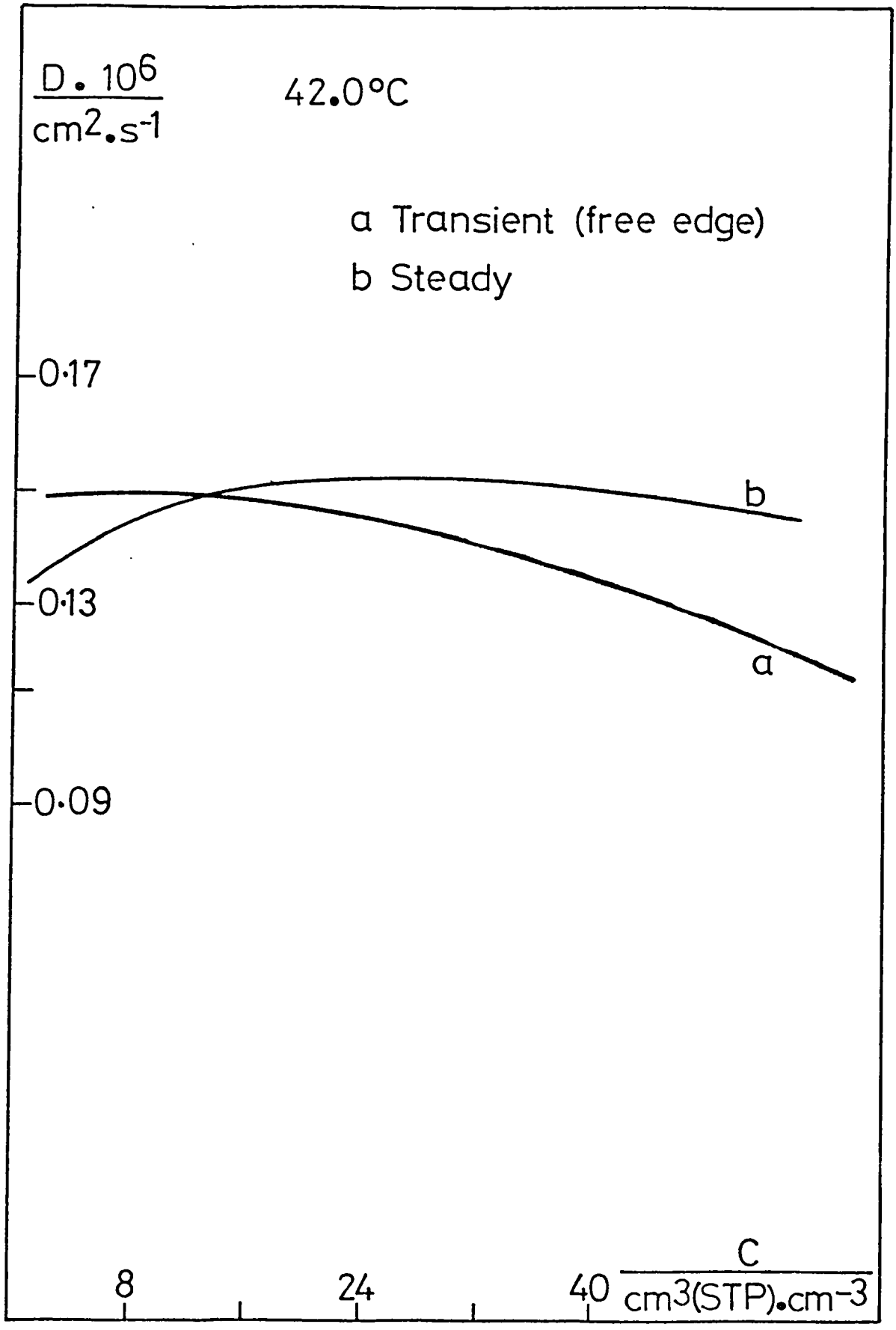


FIGURE 5.69 PVAc–H_2O

TRANSIENT– & STEADY–STATE DIFFUSION

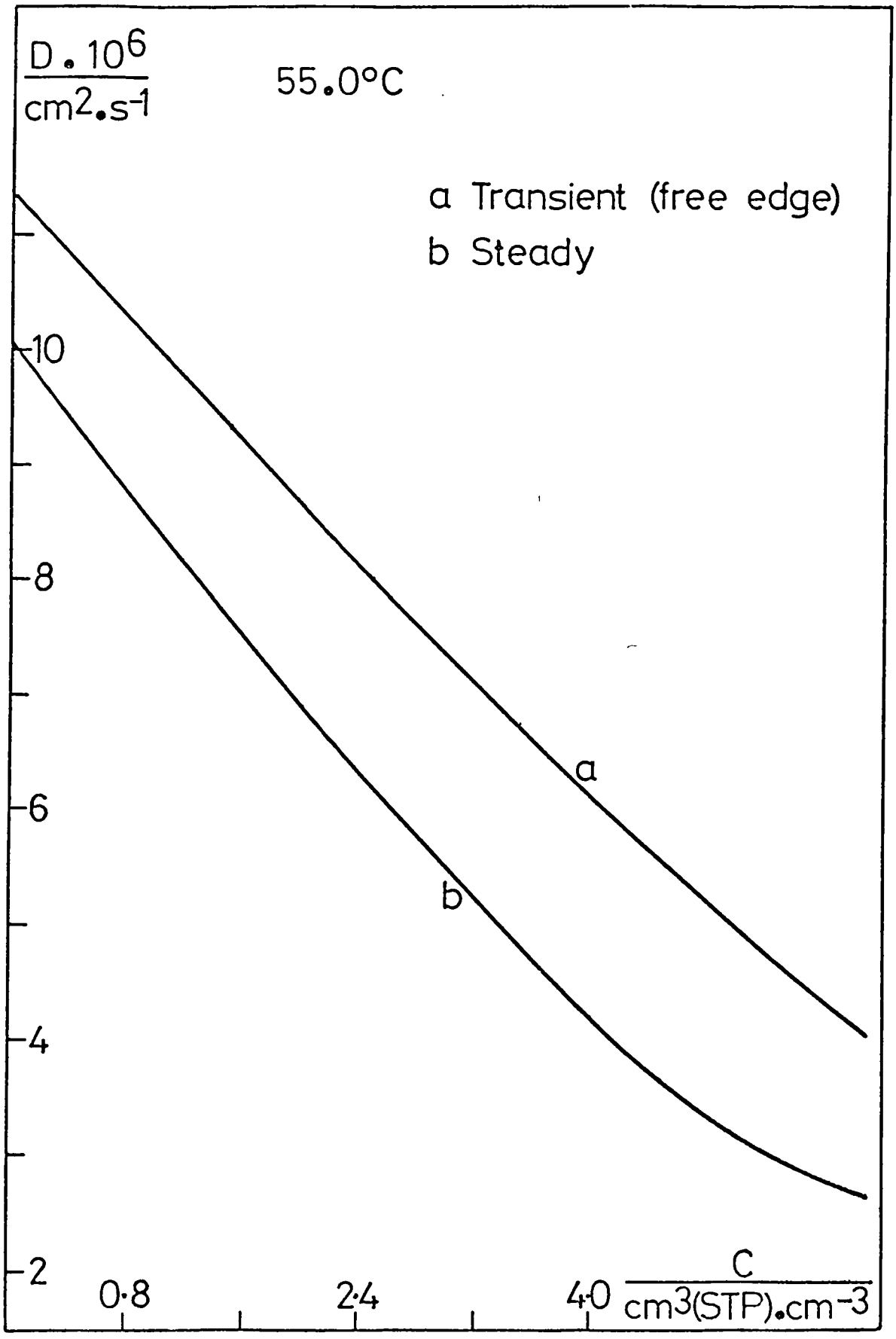


FIGURE 5.70 P(DMS-g-0·093VAc)-H_2O
TRANSIENT- & STEADY-STATE DIFFUSION

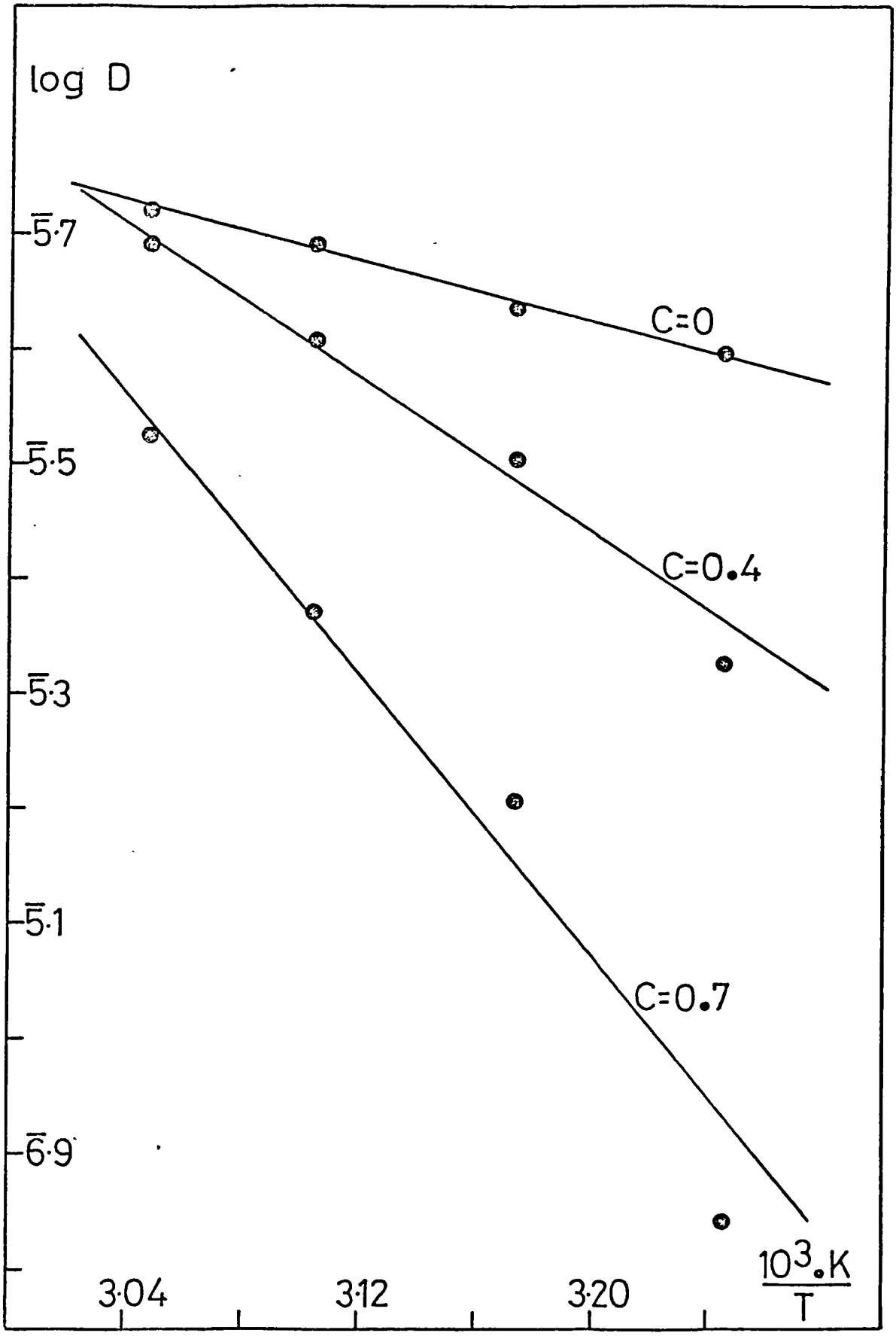


FIGURE 5.71 PDMS–H_2O

TEMPERATURE VARIATION OF DIFFUSIVITY

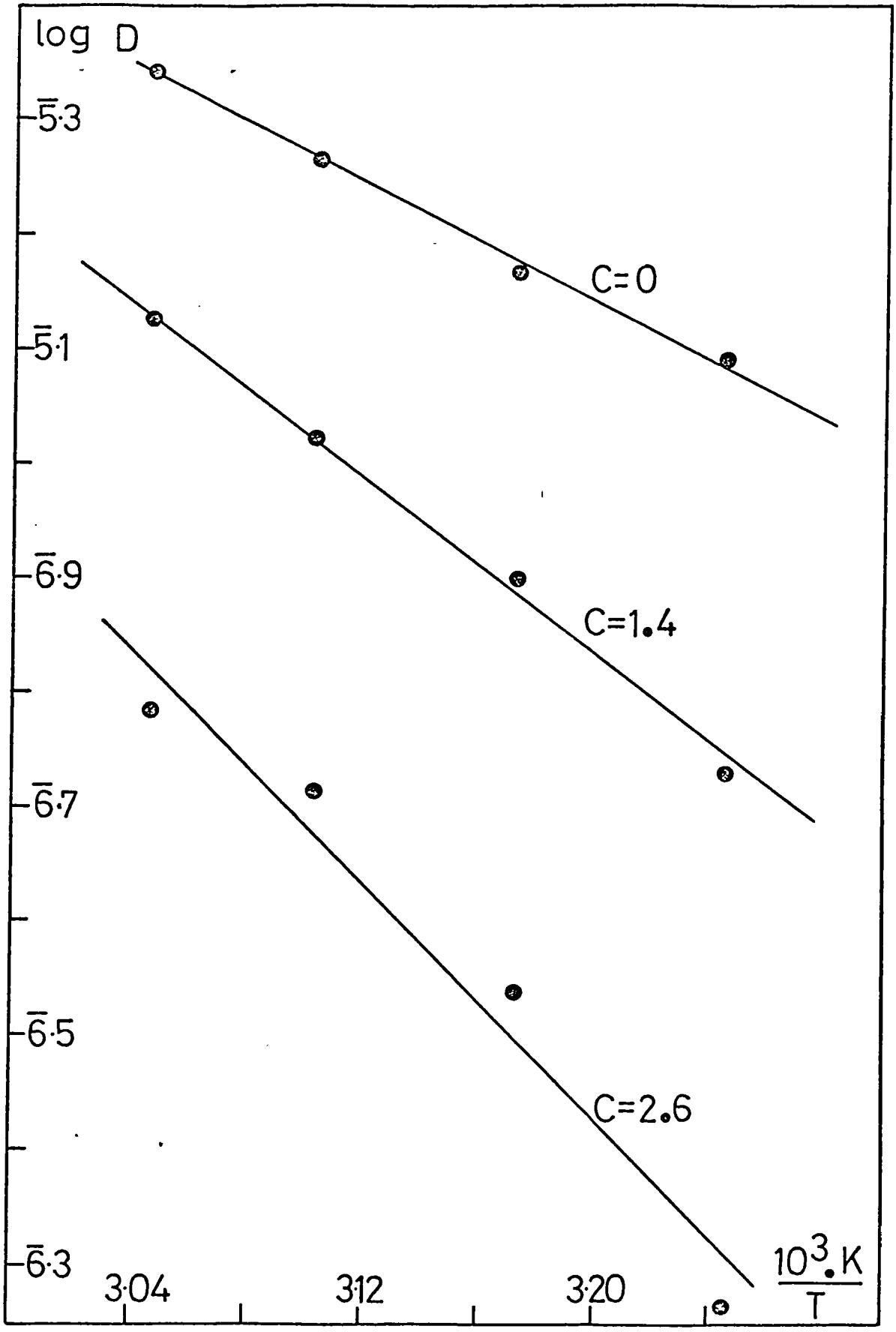


FIGURE 5.72 P(DMS-g-0·034VAc)—H_2O
TEMPERATURE VARIATION OF DIFFUSIVITY

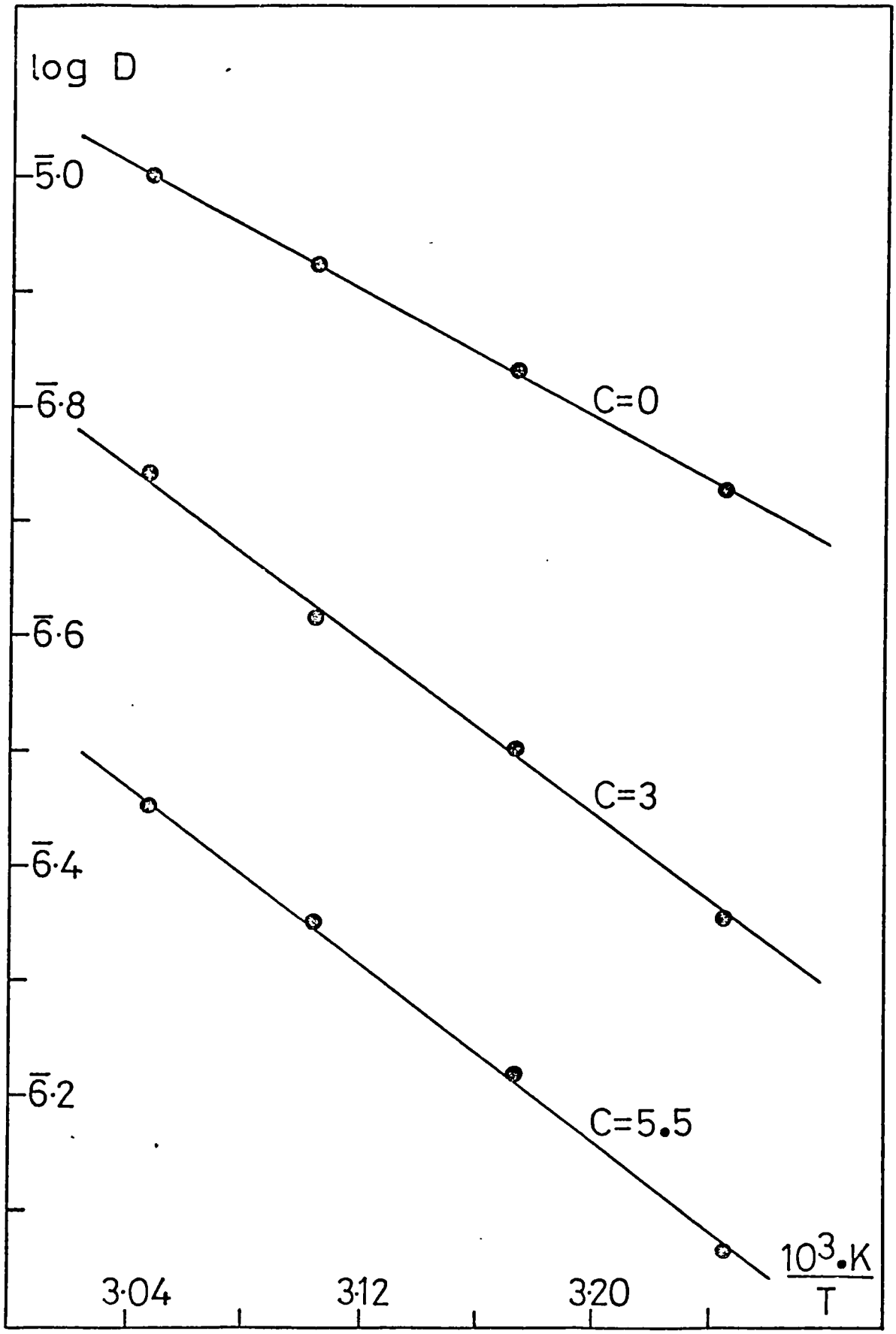


FIGURE 5.73 P(DMS-g-0·093VAc)—H_2O
TEMPERATURE VARIATION OF DIFFUSIVITY

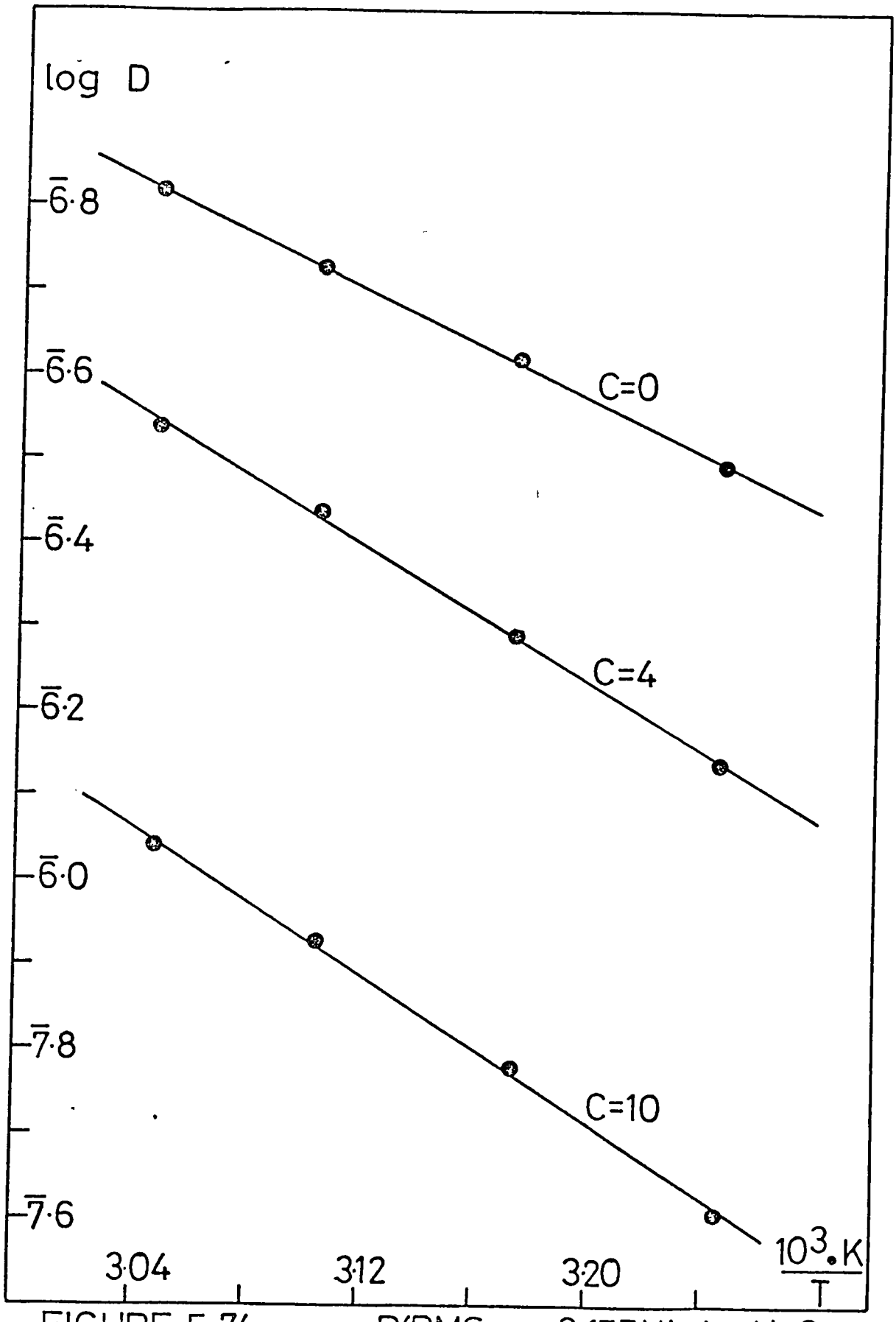


FIGURE 5.74 P(DMS-g-0·157 VAc)—H_2O
TEMPERATURE VARIATION OF DIFFUSIVITY

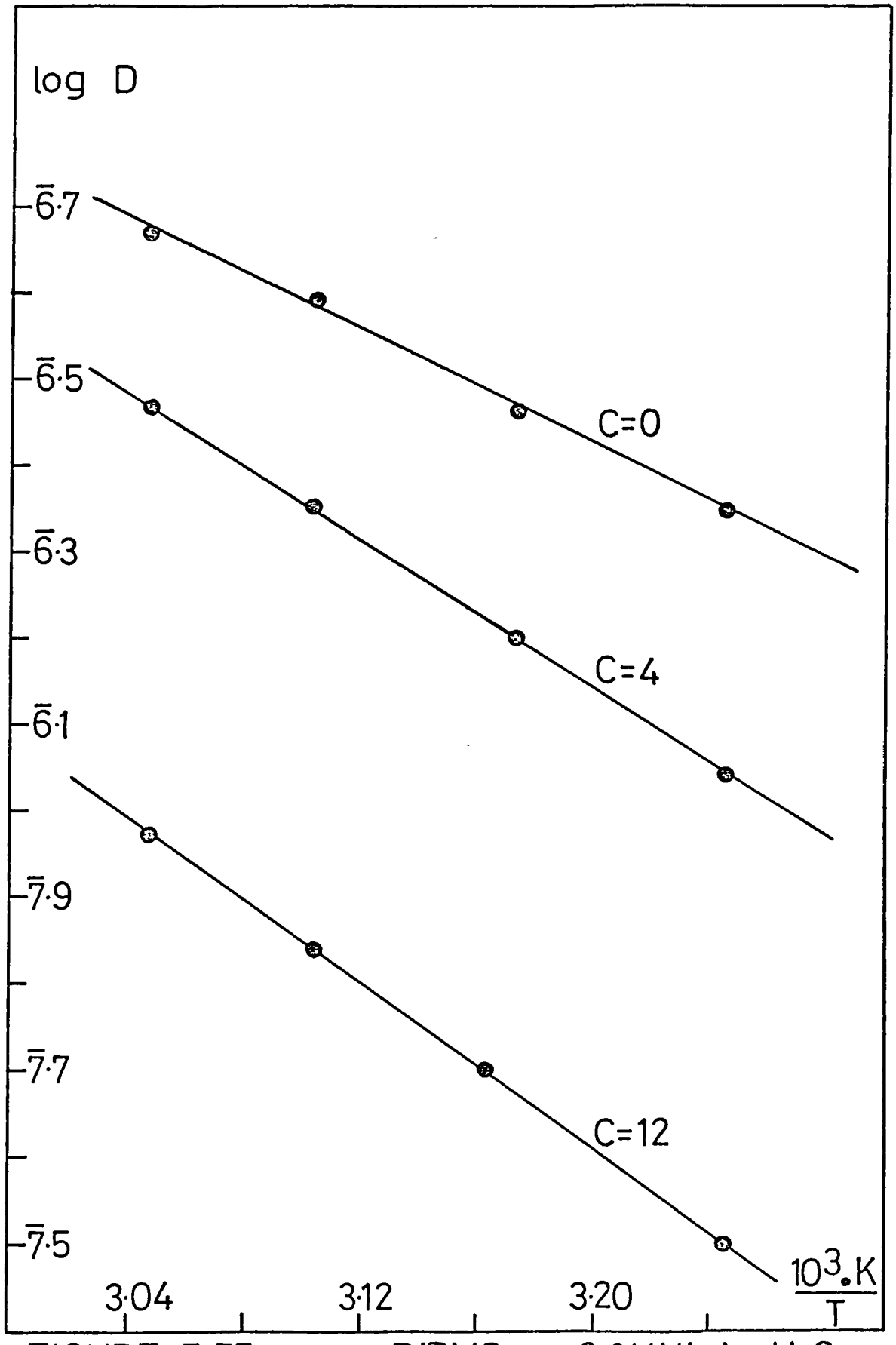


FIGURE 5.75 P(DMS-g-0·214VAc)—H_2O

TEMPERATURE VARIATION OF DIFFUSIVITY

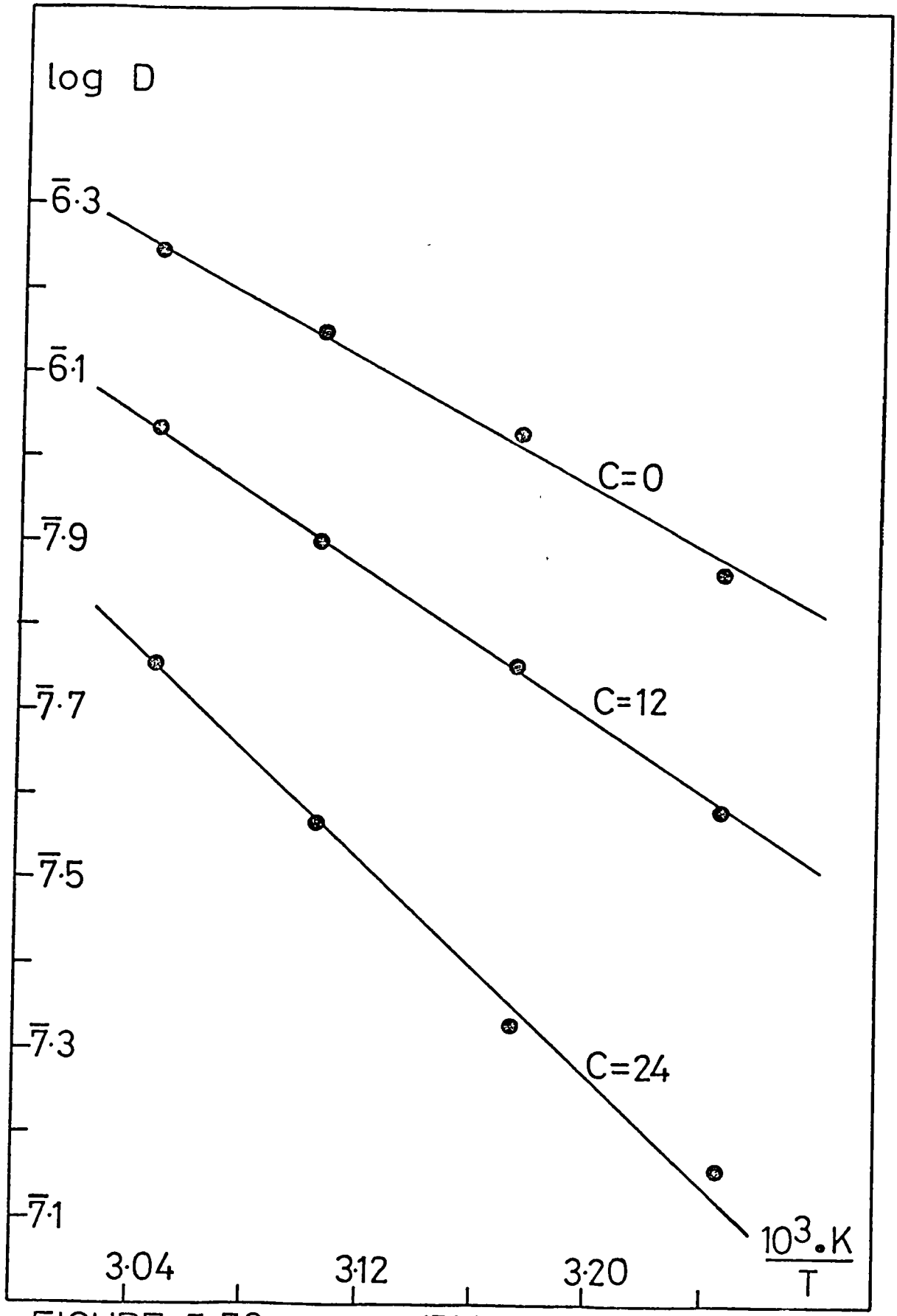


FIGURE 5.76 P(DMS-g-0·442VAc)—H_2O
TEMPERATURE VARIATION OF DIFFUSIVITY

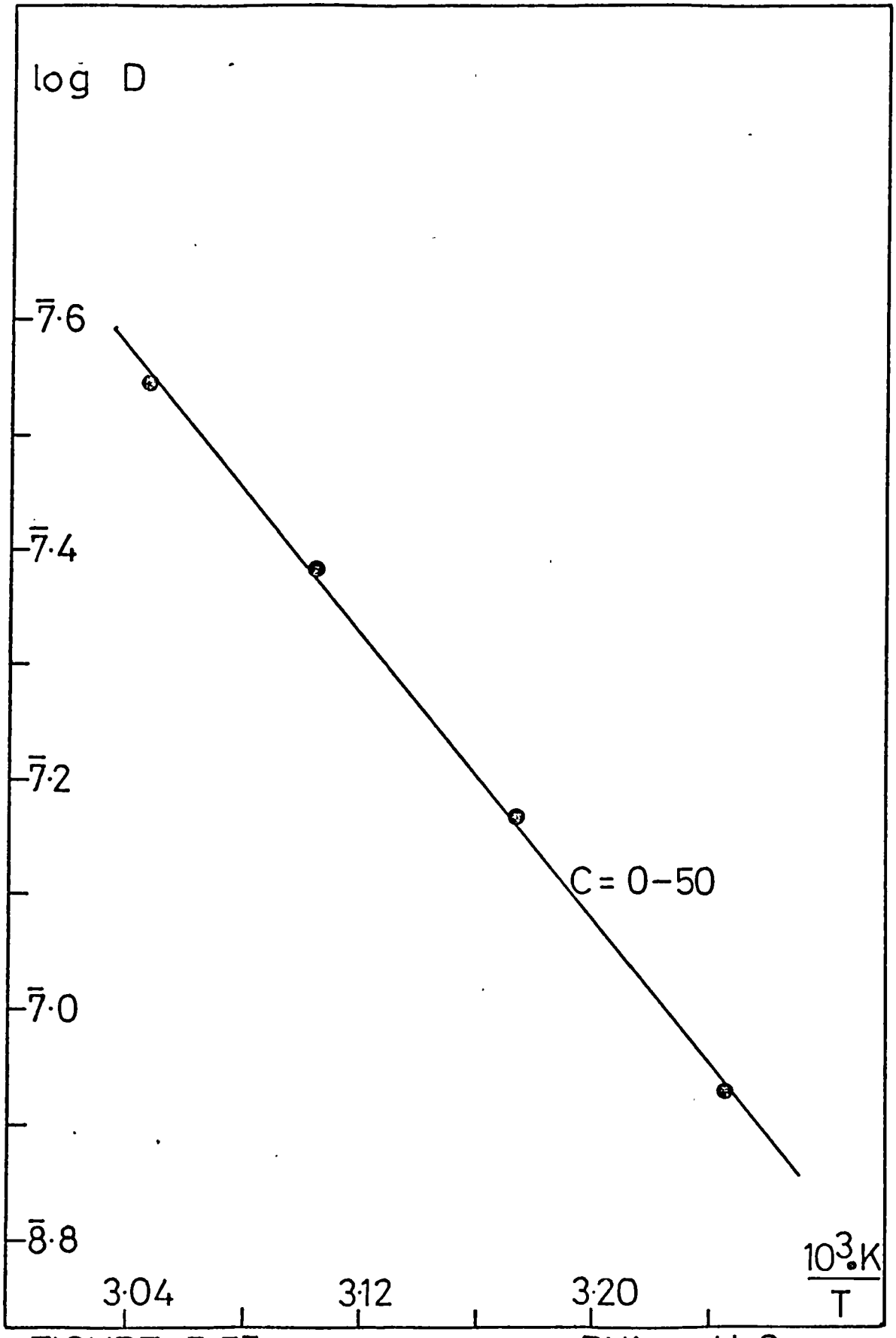


FIGURE 5.77 PVAc—H_2O

TEMPERATURE VARIATION OF DIFFUSIVITY

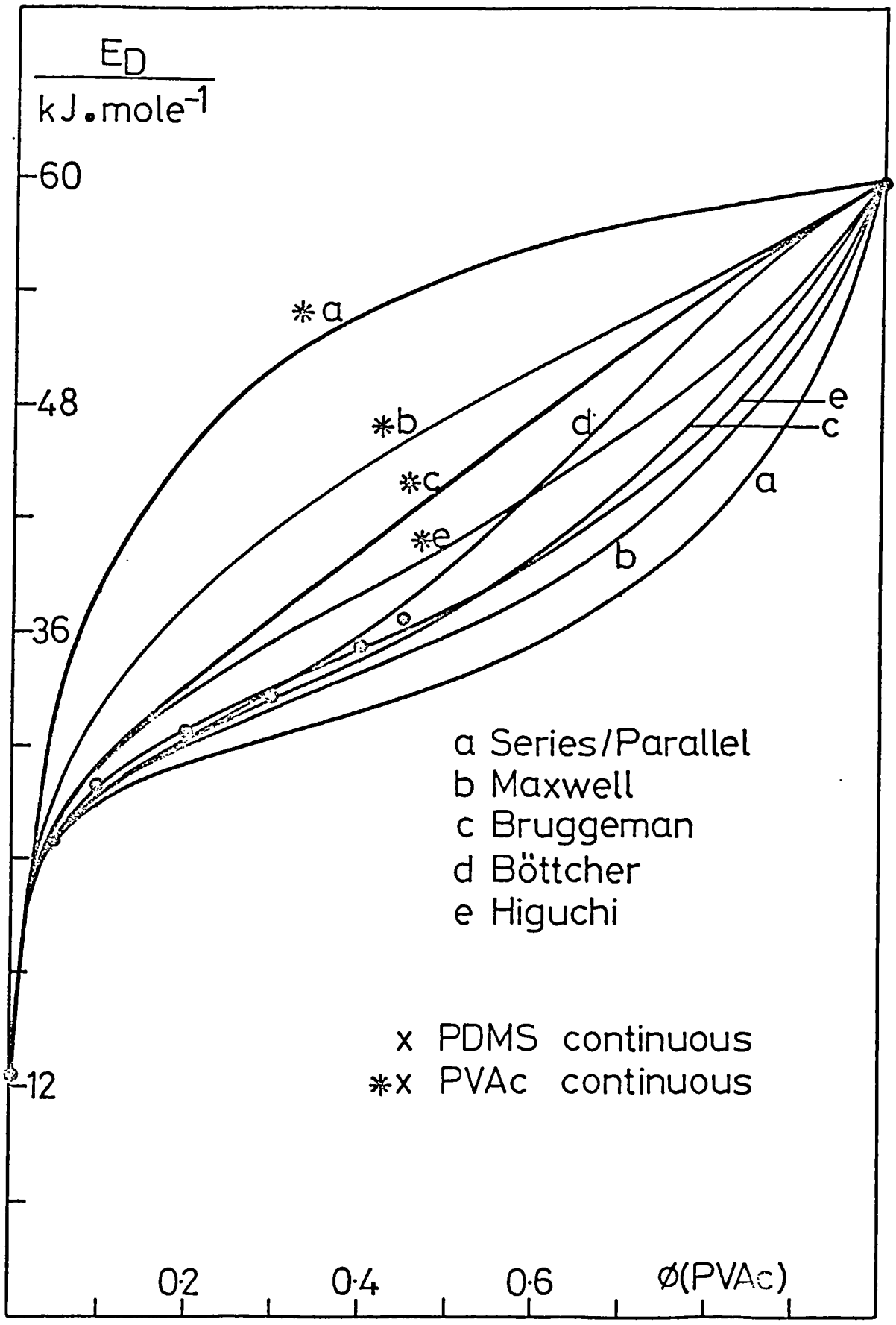


FIGURE 5.78
THEORETICAL E_D–Ø RELATIONSHIPS

Table 5.15

Values of E_D (kJ . mole^{-1}) at Various Penetrant Concentrations

ϕ (PVAc)	cm^3(S.T.P.) . cm^{-3} Concentration	kJ . mole^{-1} E_D
0	0	12.57
	0.4	35.0
	0.7	64.5
0.034	0	24.44
	1.4	38.2
	2.6	50.8
0.093	0	26.28
	3	36.6
	5.5	37.3
0.157	0	31.09
	4	39.0
	10	42.1
0.214	0	31.86
	4	41.4
	12	42.3
0.442	0	36.50
	12	43.3
	24	58.2
1.00	0 - 50	59.93

agreement in the 0-40% PVAc region whilst the Böttcher model is the best representation over the whole composition range.

(ii) Concentration-Dependence of E_D

Values of E_D are given in Table 5.15 for each polymer at various penetrant concentrations. There is an increase of E_D with increasing concentration which is consistent with the D-C behaviour and is due to

increased penetrant immobilisation. As its concentration increases a greater proportion of penetrant is immobilised within the PVAc phase and hence greater energy is needed for diffusion to occur.

CHAPTER 6

RESULTS AND DISCUSSION : ALCOHOLS

The aim of this Section was to investigate the effects of increasing plasticisation on penetrant clustering. Thus the transport of methanol, ethanol, and 2-propanol vapours in PDMS and 2-propanol vapour in FMS was studied. Increasing the hydrophobic hydrocarbon chain of the penetrant molecule entails more plasticisation of the polymer matrix and this opposes the clustering of penetrant.

6.1 Equilibrium Sorption Results

Equilibrium sorption isotherms for methanol (MeOH), ethanol (EtOH) and 2-propanol (2-PrOH) in PDMS and for 2-propanol in FMS are shown in Figures 6.1 - 6.4 respectively. Sample calculations and basic data are given in Appendix 8.3 and 8.2.1 respectively. No hysteresis was observed in any of the isotherms.

Because of the relatively large amounts of penetrant sorbed and also because of the possibility of interaction of alcohol vapours with the aluminium stirrups in the microbalance, it was decided that these measurements were to be made using a calibrated spring.

6.1.1 Sorptive Capacities of the Polymers

Since these isotherms are initially non-linear, values of $\sigma_{c=o}$ for each polymer were determined as the $\lim_{c \to o} (c/p)$ and presented in Table 6.1.

There are no reliable values reported in literature for comparison although water and methanol vapour sorption results have been determined for FMS (20, 84). The PDMS - MeOH system has been studied previously (18) but no solubility coefficients have been reported.

It can be seen that solubility coefficients for PDMS increase with increasing hydrocarbon chain length. PDMS consists of a partially ionic (Si - O) backbone effectively surrounded by the hydrophobic methyl side-groups which render the polymer hydrophobic as a whole. Therefore, as the principle of "like dissolves like" usually applies, the more hydrophobic the penetrant the greater is its solubility in PDMS. It has been reported (88) that there is a linear relationship between $\log \sigma_{c=o}$ and molar volume of penetrant (there is a similar one for $\log D_{c=o}$). This is illustrated in Figure 6.5 for solubilities at 35.0°C

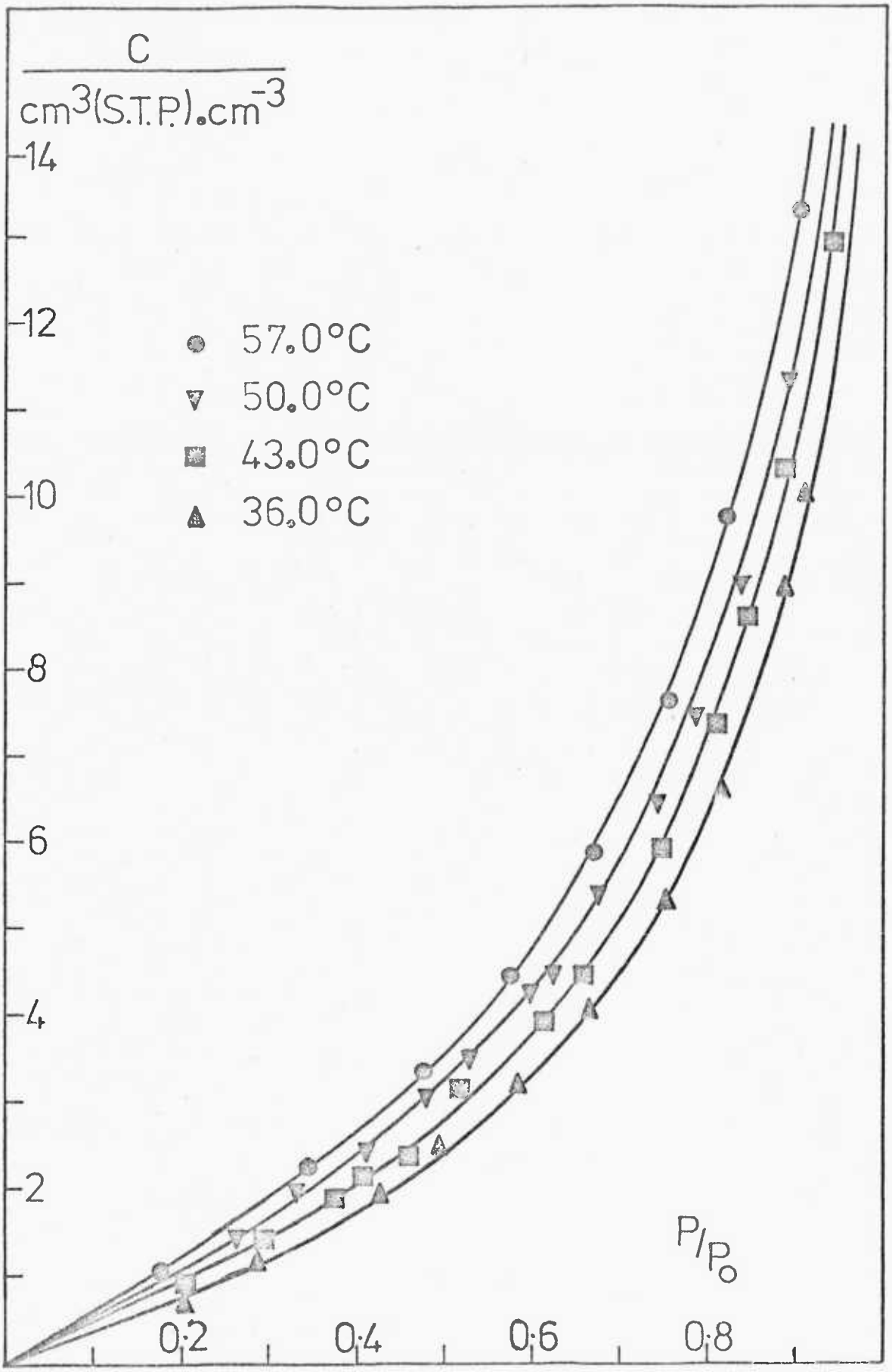


FIGURE 6.1 PDMS–MeOH SORPTION ISOTHERMS

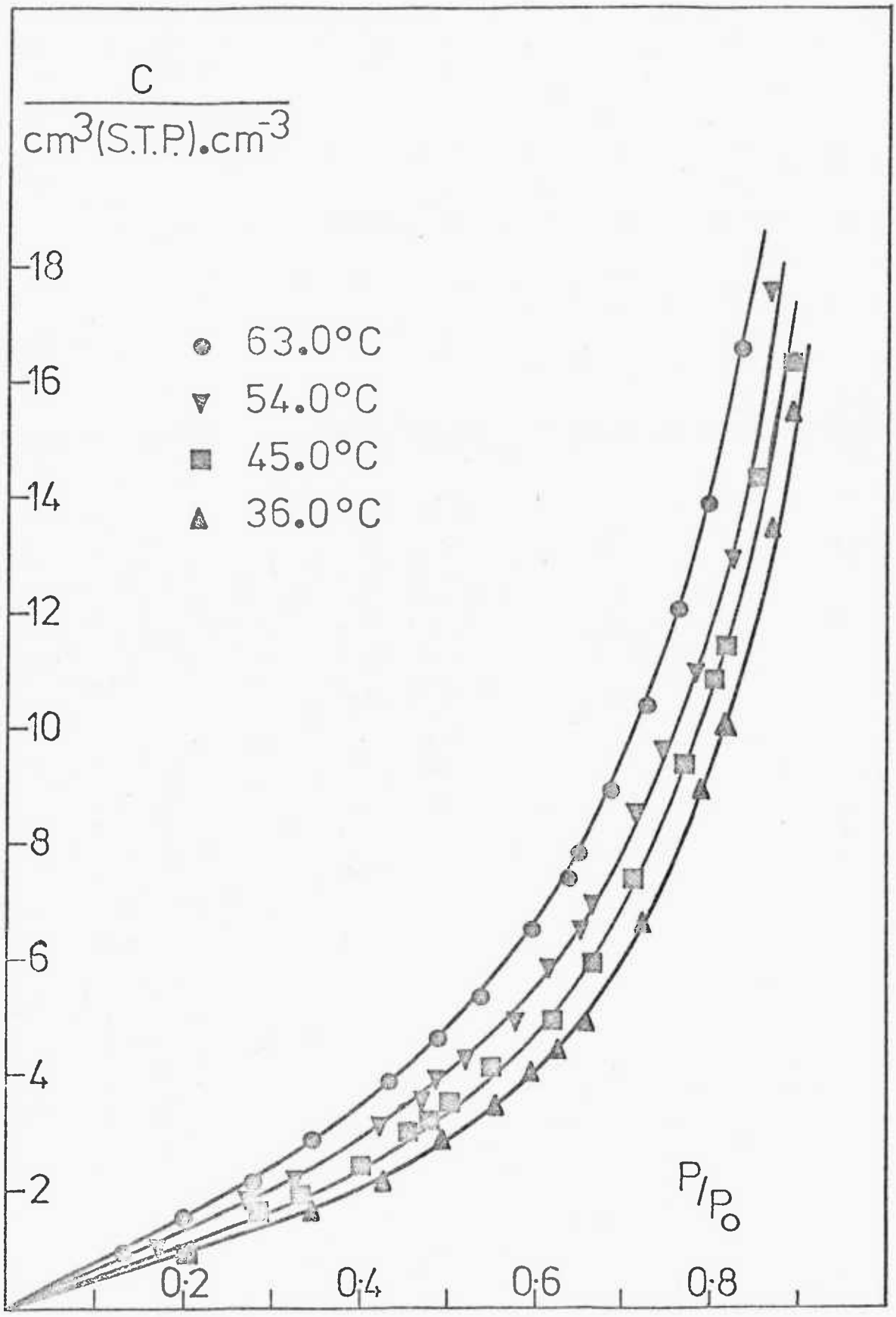


FIGURE 6.2 PDMS – EtOH SORPTION ISOTHERMS

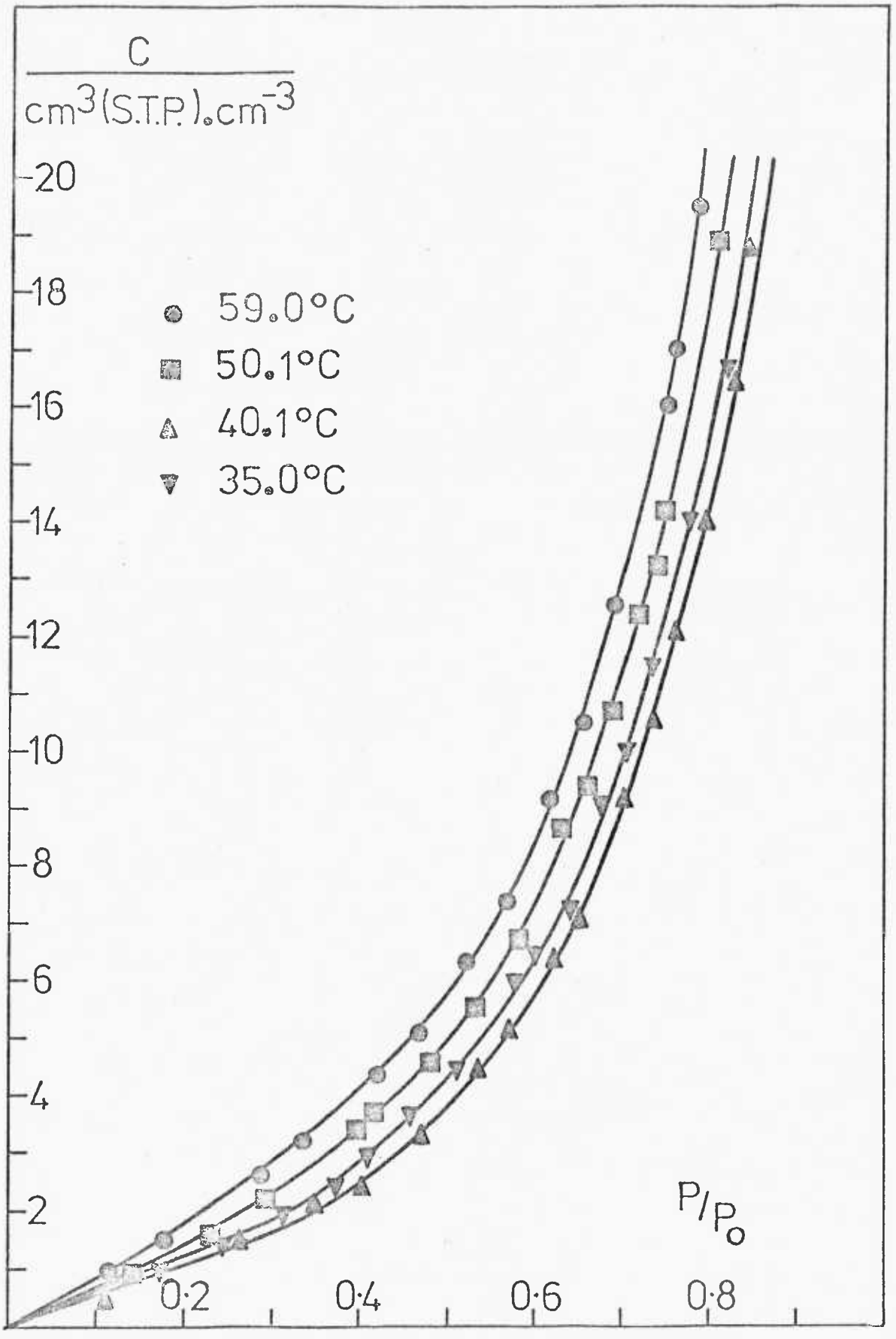


FIGURE 6.3 PDMS–(2-PrOH)
SORPTION ISOTHERMS

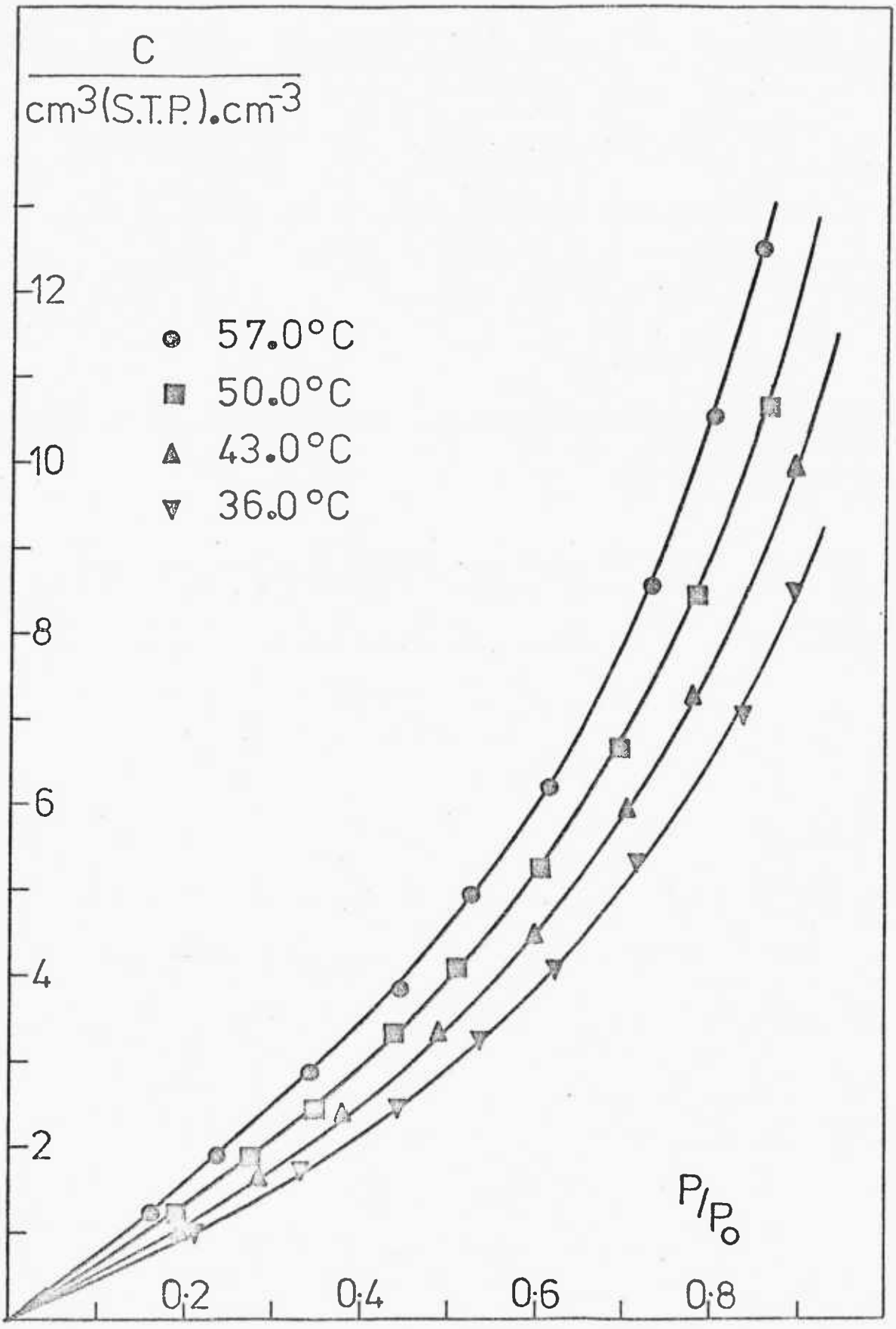


FIGURE 6.4 FMS—(2-PrOH)
SORPTION ISOTHERMS

and 50.0°C. Solubilities for each system at each temperature were interpolated from the temperature dependence of experimental solubility data. The slopes of the lines for each temperature are the same, a fact one might qualitatively expect for a polymer much above its glass temperature. The solubilities of water vapour in PDMS, obtained from Section 5.2.1, are included in the graphs since water is the lowest member of the homologous series. The good correspondence of solubilities implies that the interactions in each system are the same throughout the series.

Table 6.1

Limiting Henry's Law Solubility Coefficients
$\sigma_{c=o}$ (cm^3(S.T.P.) . cm^{-3}. (cm Hg)$^{-1}$)

System	T°C	$\sigma_{c=o}$	System	T°C	$\sigma_{c=o}$
PDMS -	36.0	0.180	PDMS -	35.0	0.572
MeOH	43.0	0.147	(2-PrOH)	40.1	0.489
	50.0	0.127		50.1	0.358
	57.0	0.105		59.0	0.289
PDMS -	36.0	0.355	FMS -	36.0	0.541
EtOH	45.0	0.281	(2-PrOH)	43.0	0.464
	54.0	0.223		50.0	0.369
	63.0	0.175		57.0	0.307

A similar situation exists for solubilities in FMS of water and methanol vapours (20, 84) and of 2-propanol vapour. This is illustrated in Figure 6.6 for the two temperatures, 35.0°C and 50.0°C. Again there is a linear relationship with both lines parallel but of different slope to those of PDMS. This is to be expected as the slightly electronegative trifluoropropyl group of FMS must encourage hydrogen-bonding of penetrant to polymer to some extent. Thus the solubility of water vapour is considerably greater in FMS than in PDMS (20, 84), whilst methanol solubilities are also greater but to a lesser degree. When 2-propanol is the penetrant the solubilities of the two polymers are similar since the hydrophobic hydrocarbon chain dominates the solubility.

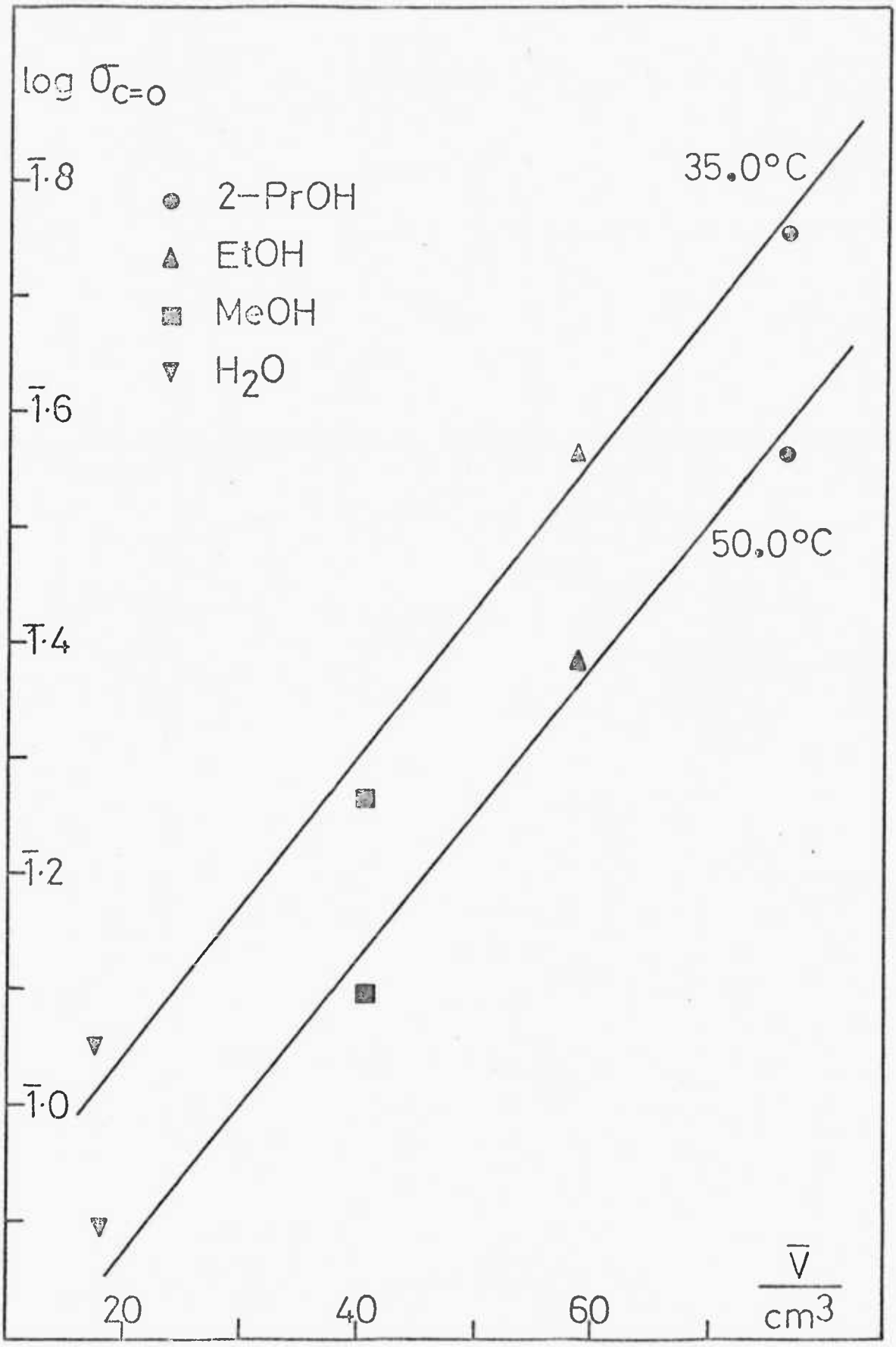


FIGURE 6.5 PDMS-ALCOHOLS

THE EFFECT OF SIZE ON SOLUBILITY

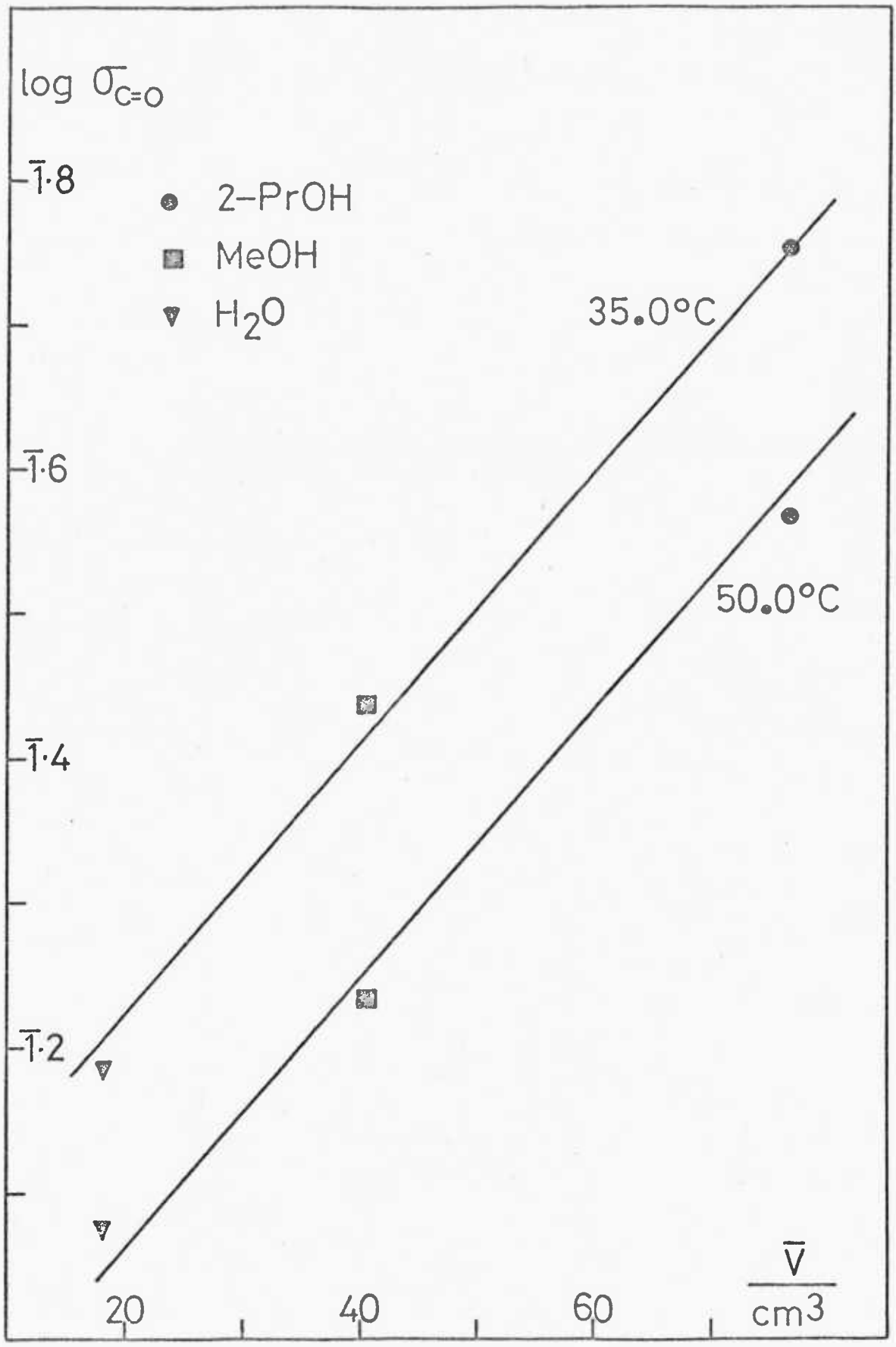


FIGURE 6.6 FMS-ALCOHOLS

THE EFFECT OF SIZE ON SOLUBILITY

Thus it is possible to establish the trend of solubilities of the alcohol penetrants in the two polymers and, not surprisingly, these polymers behave quite similarly.

6.1.2 Isotherm Shapes

Unlike the PDMS - H_2O vapour system, the sorption isotherms show no initial linear regions and are convex to the pressure axis at all relative pressures.

(i) Clustering Functions

The clustering functions were calculated for each system at various penetrant activities. The clustering functions G_{AA}/V_A, $(1 + \phi_A G_{AA}/V_A)$, and $\phi_A G_{AB}/V_A$, referred to as X, Y, and Z respectively for convenience, were calculated from plots of $(a_A/\phi_A$ vs. $a_A)$ and $(\log \phi_A$ vs. $\log a_A)$ and these are similar to those of the graft copolymers. Typical plots, for the FMS - (2-PrOH) system, are illustrated in Figure 6.7. Values of the clustering functions X, Y and Z are given in Table 6.2 along with some values for the PDMS - H_2O (Section 5.2.3), FMS - H_2O and FMS - MeOH systems (20, 84).

The values of X = -1 and Y = +1 correspond to the linear regions of the isotherms when clustering does not occur. It was found that mean cluster sizes (Y) are roughly constant for the alcohols in each polymer though they are greater for PDMS than FMS. Since the penetrant solubility increases with increasing hydrocarbon chain length the clustering tendencies must decrease through the series. This is to be expected as the clustering agent (the -OH group) occupies a smaller proportion of the penetrant molecule as the hydrocarbon content increases. This increasing hydrophobic content means that there are more polymer-penetrant interactions which favour plasticisation of the polymer and oppose penetrant clustering. Clustering of the penetrants in FMS is less than in PDMS since, as stated previously, the slightly electronegative trifluoropropyl group of FMS increases the possibility of polymer-penetrant interactions through hydrogen-bonding and hence opposes clustering of the penetrant molecules.

A similar situation occurs when the clustering functions X and Z are considered. Increasing penetrant solubility overshadows everything but a decrease in clustering with increasing alcohol size can be seen. Thus whilst the magnitudes of the cluster integrals (X) decrease with increasing solubility as the hydrocarbon chain increases,

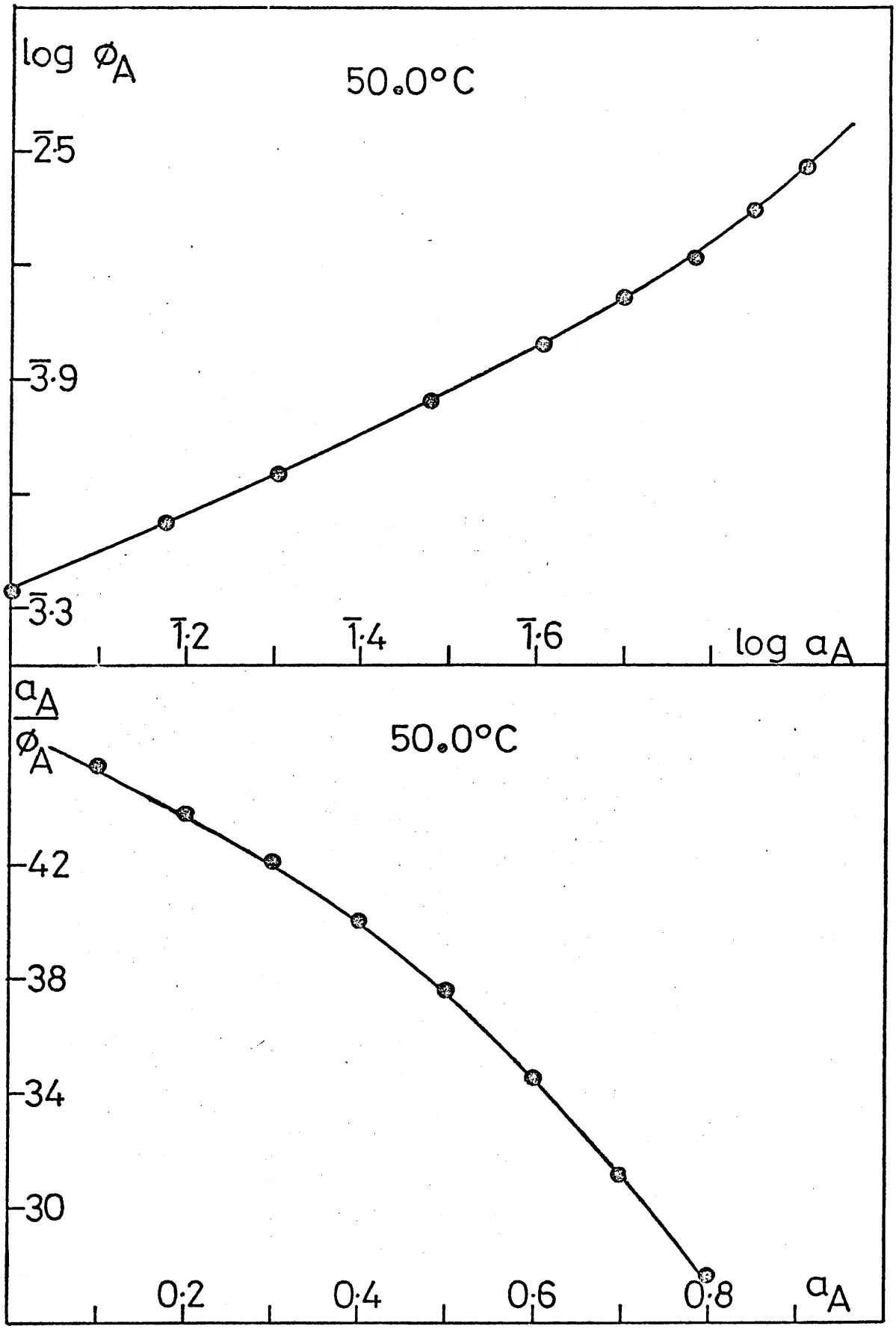


FIGURE 6.7 FMS-(2-PrOH)

CLUSTERING ANALYSIS

the increase of X with concentration at any temperature is slightly less as the size of penetrant increases.

Table 6.2

Clustering Functions : $X = G_{AA}/V_A$,

$Y = (1 + \phi_A G_{AA}/V_A)$, $Z = \phi_A G_{AB}/V_A$

		$a_A = 0.3$			$a_A = 0.5$			$a_A = 0.7$		
System	T^oC	X	Y	$Z.10^3$	X	Y	$Z.10^3$	X	Y	$Z.10^3$
PDMS -	36.0	76.5	1.22	- 2.87	101.2	1.49	- 6.81	128.1	2.24	- 18.3
MeOH	50.0	45.0	1.18	- 3.59	74.9	1.46	- 8.48	99.7	2.12	- 21.7
PDMS -	36.0	70.7	1.26	- 4.67	88.6	1.64	-12.6	104.4	2.77	- 44.4
EtOH	54.0	31.7	1.18	- 6.03	50.8	1.58	-16.1	74.3	2.31	- 47.5
PDMS-	35.0	48.8	1.22	- 7.4	64.6	1.82	-23.5	84.9	3.02	- 94.0
(2-PrOH)	40.1	34.1	1.28	-10.0	50.7	1.90	-32.1	56.2	2.75	-104.9
FMS-	36.0	32.9	1.14	- 5.94	38.3	1.37	-13.7	46.0	1.75	- 29.8
(2-PrOH)	50.0	17.8	1.14	- 8.15	25.0	1.34	-17.9	36.0	1.78	- 40.8
PDMS-	35.0	-1	1.00	- 0.11	732	1.18	- 0.23	1801	1.51	- 0.45
H_2O*	55.0	-1	1.00	- 0.20	280	1.08	- 0.37	631	1.30	- 0.66
FMS-	30.1	-1	1.00	-	-1	1.00	-	2800	1.9	-
H_2O**	50.3	-1	1.00	-	-1	1.00	-	1300	1.8	-
FMS -	30.0	3.0	1.0	-	51	1.3	-	93	1.7	-
MeOH**	40.0	14	1.1	-	65	1.4	-	110	2.2	-

* Section 5.2.3 ** Ref (20, 84)

Although there is a decrease in the extent of clustering with increasing hydrocarbon chain length, this is quite small in the context of the total amount of clustering present. Clustering in FMS is much less than in PDMS for any particular penetrant due to the enhanced polymer-penetrant interactions. Clustering also decreases with increasing temperature as there is additional thermal energy in the system which will break some of the hydrogen bonds of the clusters.

6.1.3 Comparison with Theoretical Isotherms

One model that has been proposed to reproduce experimental sorption isotherms in which clustering is the dominant feature is the polycondensation model (18, 20, 22, 24, 84). In formulating the model it has been postulated that there are no specific polymer-penetrant interactions only penetrant-penetrant ones, a situation which strictly is not accurate. Hence clustering is the prime model of interaction and the penetrant molecules can be considered as "monomer" which polymerises by hydrogen-bonding to form clusters of penetrant molecules. Alcohols are considered as AB_2 type "monomers" as there is one hydrogen atom and two lone pairs of electrons available for hydrogen-bond formation.

One can derive a relationship to predict sorption isotherms:

$$p = (C/\sigma_{c=o}) \cdot (1 - \alpha)^2 (1 - 2\alpha) \qquad \ldots.(6.1)$$

where

$$\alpha = \frac{1}{4}(3 + \frac{K}{C}) - \left(\left[\frac{1}{4}(3 + \frac{K}{C})\right]^2 - 0.5\right)^{1/2} \qquad \ldots.(6.2)$$

and where C is the concentration of sorbed penetrant, 2α is the fraction of hydroxyl groups reacted, and K is the equilibrium constant for the breakage of a hydrogen-bond.

It is necessary to obtain a value for K, and it was found, for this type of "monomer", that no specific value of K could be fixed. Hence K is treated as an adjustable parameter which has theoretical limits to its value and which is used to give the best fit between the experimental and theoretical isotherms. These isotherms are illustrated in Figures 6.8 - 6.11 for the systems studied. The fit of the theoretical model is not particularly good considering the adjustable nature of the isotherm and in fact shows up the inadequacy of the model as polymer-penetrant interactions are significant. However it is of some value in that it gives some indication of the dominance of clustering within any particular system.

The value of K chosen for each system shows the prevalent clustering trend. Thus for the systems studied the values and ranges of K are : PDMS - MeOH, K = 35 ($20 < K < 47$); PDMS - EtOH, K = 35 ($24 < K < 54$); PDMS - (2-PrOH), K = 30 ($25 < K < 57$); and FMS - (2-PrOH), K = 50 ($26 < K < 59$). Thus K values for PDMS are near the lower limit of the range and are nearer as the penetrant size increases. FMS, on the

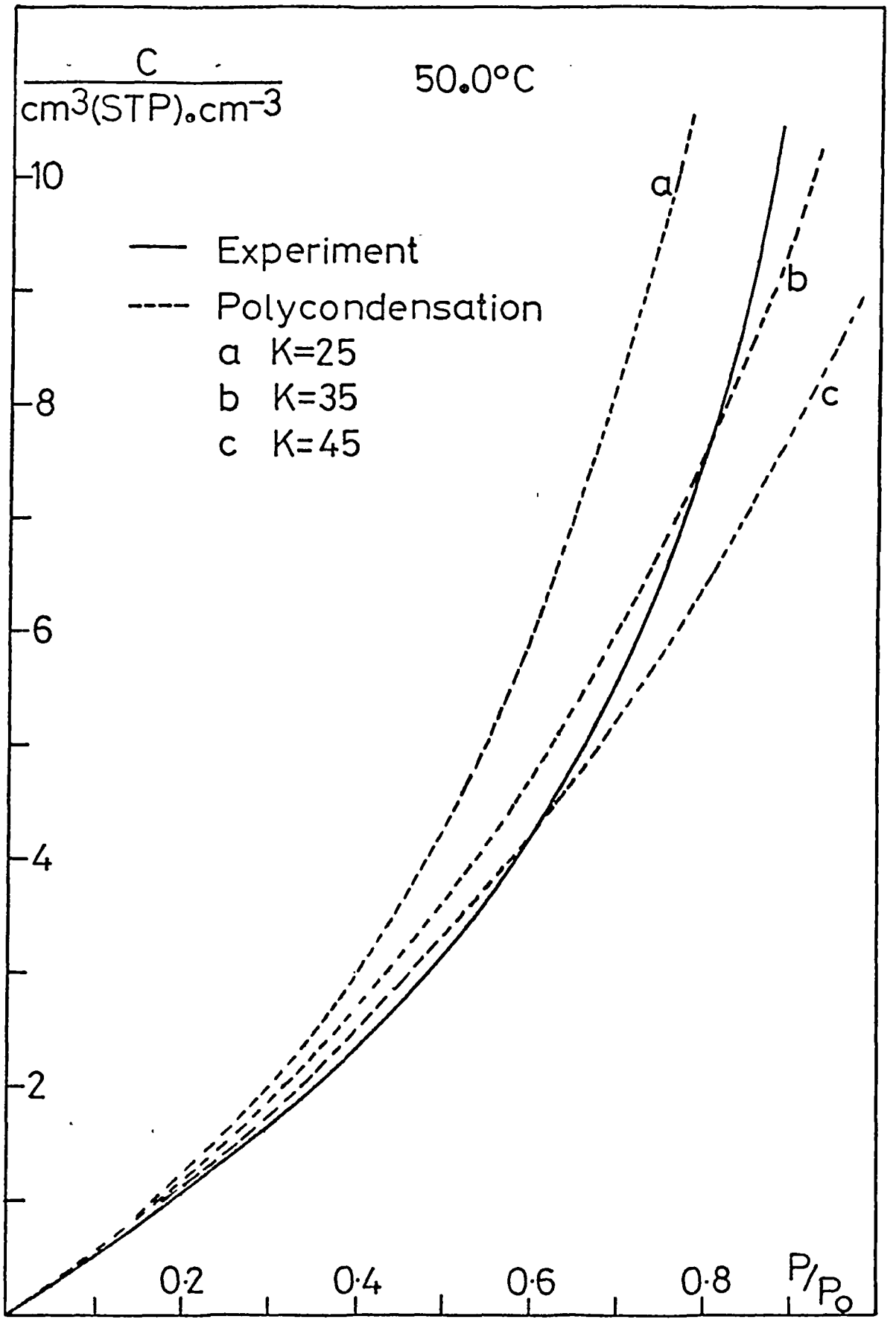


FIGURE 6.8 PDMS–MeOH
EXPERIMENTAL & THEORETICAL ISOTHERMS

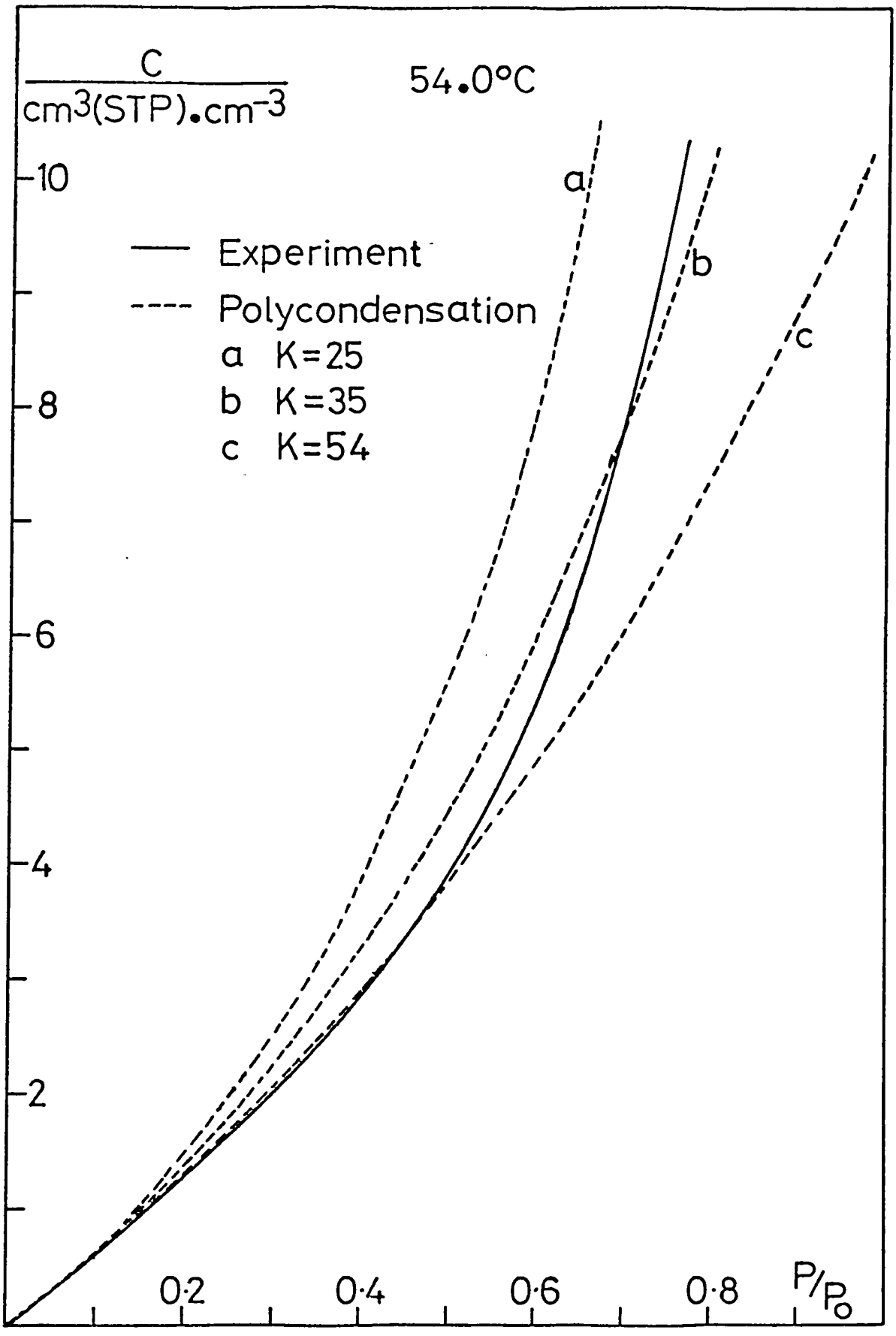


FIGURE 6.9 PDMS-EtOH
EXPERIMENTAL & THEORETICAL ISOTHERMS

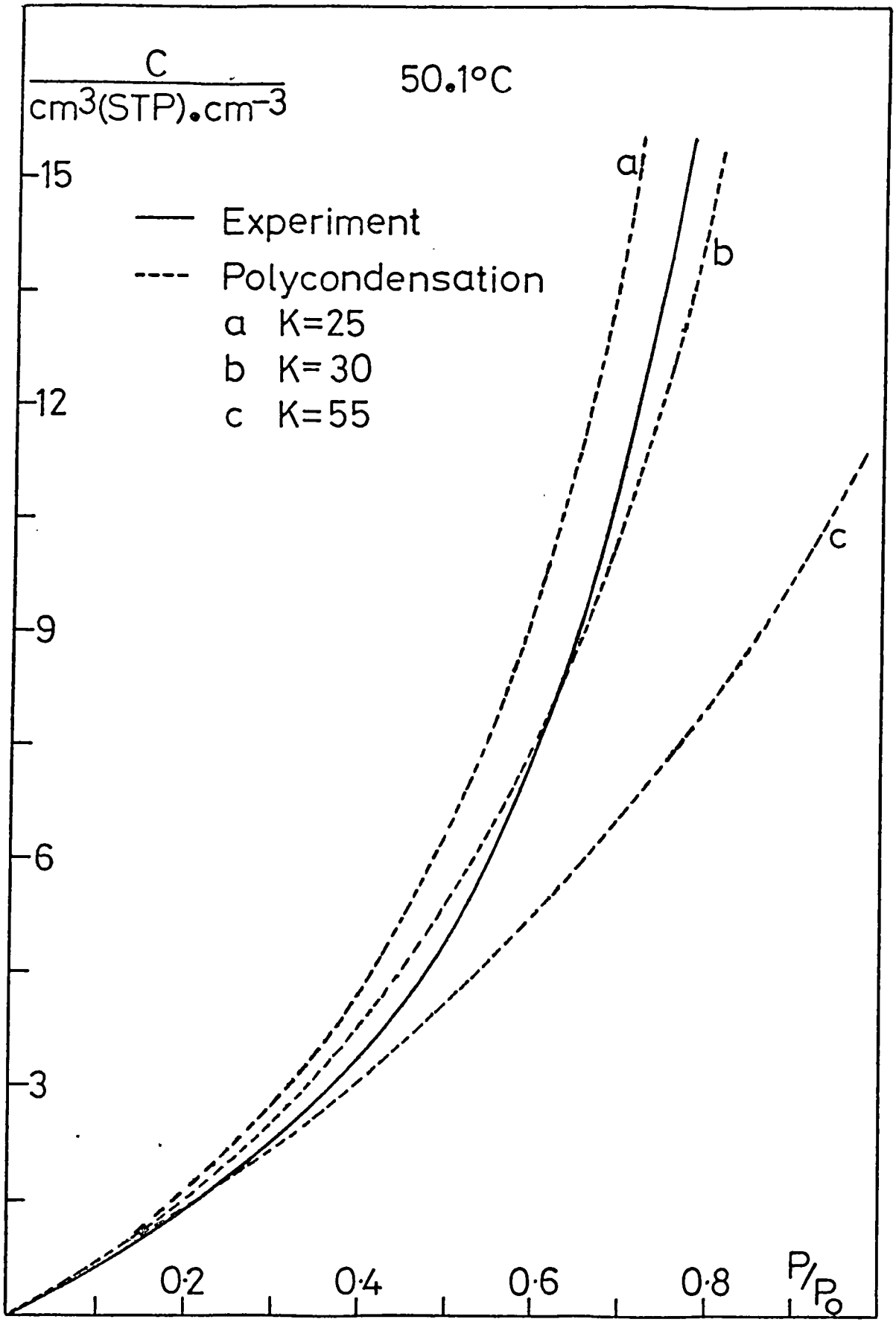


FIGURE 6.10 PDMS-(2-PrOH)
EXPERIMENTAL & THEORETICAL ISOTHERMS

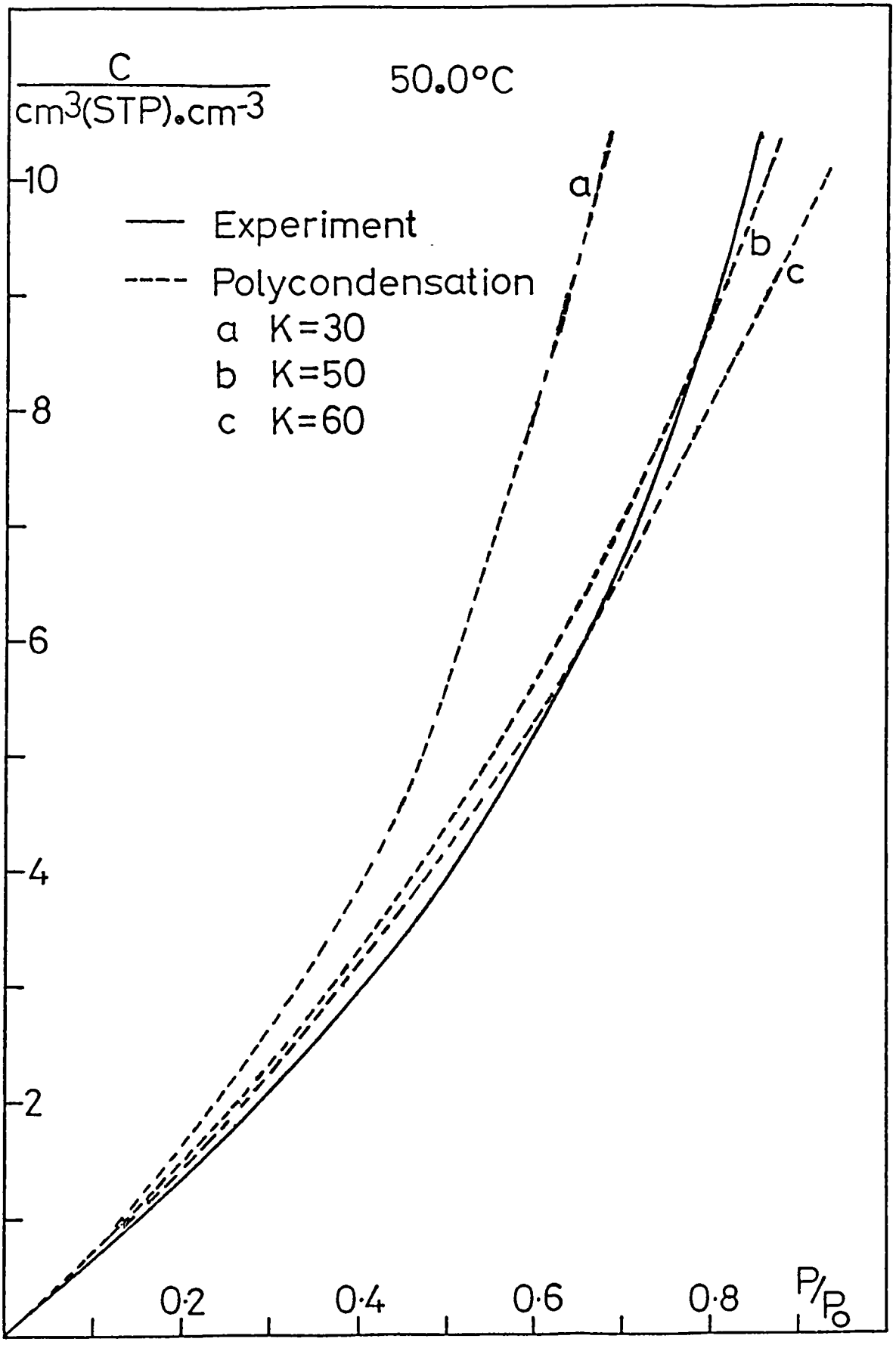


FIGURE 6.11 FMS-(2-PrOH)
EXPERIMENTAL & THEORETICAL ISOTHERMS

other hand, has K values at the other end of the range and similar throughout (using the data for FMS-MeOH from (20, 84)).

6.1.4 Heats of Sorption and Dilution

Heats of Sorption ($\Delta\overline{H}_s$) in the limit (c→o) were calculated for each system and presented in Table 6.3. Plots of log $\sigma_{c=o}$ vs. 1/T for each system are shown in Figure 6.12.

Table 6.3

Heats of Sorption ($\Delta\overline{H}_s$, kJ . mol^{-1}) in the limit (c→o)

System	$\Delta\overline{H}_s$
PDMS - MeOH	- 21.4
PDMS - EtOH	- 22.7
PDMS-(2-PrOH)	- 24.8
FMS -(2-PrOH)	- 23.4

The values of $\Delta\overline{H}_s$ are all very similar as may be anticipated for penetrants of similar structures. There is a slight trend for $\Delta\overline{H}_s$ to become more exothermic as the penetrant size increases as there are more polymer-penetrant interactions and hence greater solubilities. This increase is approximately linear with molar volume of penetrant, although an exponential type fit appears to be equally applicable over this short range of values of $\Delta\overline{H}_s$.

Heats of Sorption can theoretically be split into two components, the heat of condensation of vapour and the heat of dilution. The heats of condensation for water and the alcohols studied here are all approximately constant at 39 - 42 kJ . mol^{-1}.

Heats ($\Delta\overline{H}_A$) and entropies ($\Delta\overline{S}_A$) of dilution have been calculated for various concentrations using equations (2.33) and (2.34). Mean values over the temperature ranges of study are given in Table 6.4 and were calculated from plots of (log (p/p_o) vs. 1/T) and (log (p/p_o) vs. T). These are similar in nature to those illustrated (Figures 5.16 and 5.17) for the graft copolymers and hence need not be repeated here.

It can be seen that, for all systems studied, both $\Delta\overline{H}_A$ and $\Delta\overline{S}_A$ decrease with increasing concentration. This is in accord with an increase of clustering within the polymer, thereby reducing the degree of mixing of penetrant and polymer.

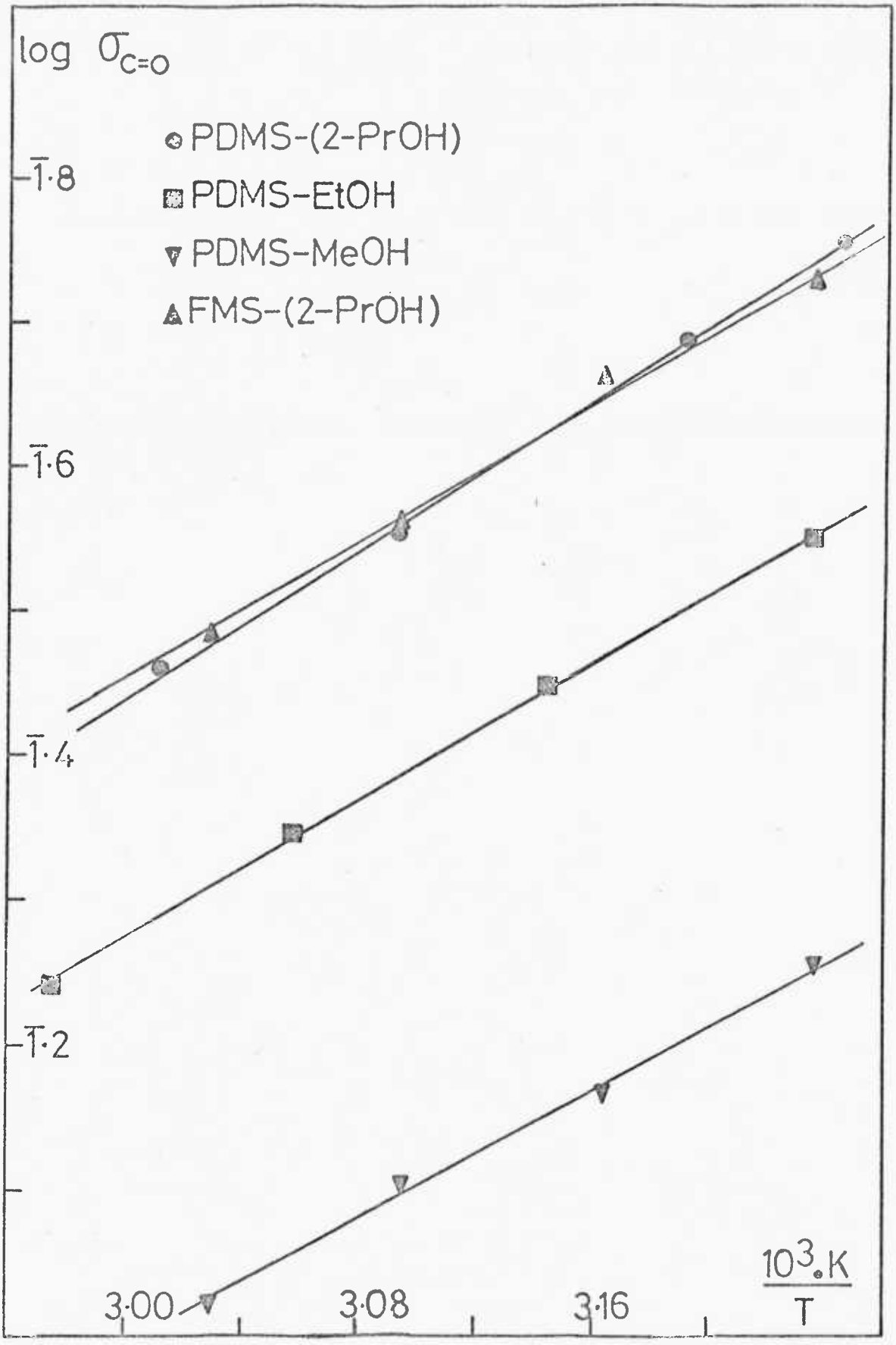


FIGURE 6.12
TEMPERATURE VARIATION OF SOLUBILITY

Table 6.4

Mean Heats ($\Delta\bar{H}_A$, kJ . mol^{-1}) and Entropies ($\Delta\bar{S}_A$, $J.K^{-1}.mol^{-1}$) of Dilution at various concentrations (C, cm^3(S.T.P.). cm^{-3})

System	C	$\Delta\bar{H}_A$	$\Delta\bar{S}_A$
PDMS - MeOH	1	14.0	24.9
36 → 57°C	2	11.6	19.4
	6	5.95	9.21
	10	3.22	4.90
PDMS - EtOH	1	16.2	64.1
36 → 63°C	2	13.0	46.9
	5	7.41	26.9
	11	3.60	12.9
PDMS - (2-PrOH)	2	13.4	52.0
35 → 59°C	4	8.80	35.1
	8	4.61	18.5
	16	2.76	10.8
FMS - (2-PrOH)	1	20.6	33.2
36 → 57°C	3	14.0	21.4
	7	8.71	13.5
	11	7.00	9.88

$\Delta\bar{H}_A$ varies little with chain length whilst $\Delta\bar{S}_A$ increases which is consistent with the relative degree of clustering in these systems. A comparison of the $\Delta\bar{H}_A$ data for 2-propanol in FMS and PDMS is also consistent with the relative degrees of clustering in these two polymers.

6.2 Steady-State Permeability Results

The data used to calculate permeabilities are presented in Appendix 8.2.3. Flux rates for each system at various temperatures and pressures are shown in Figures 6.13 - 6.16. These results were obtained using a Baratron to monitor the "down-stream" pressure. For comparison purposes, two isotherms of the PDMS - (2-PrOH) system were repeated using zeolite hanging from a calibrated spring to monitor the pressure (see Section 5.3.1). These results are presented in Figure 6.17, and

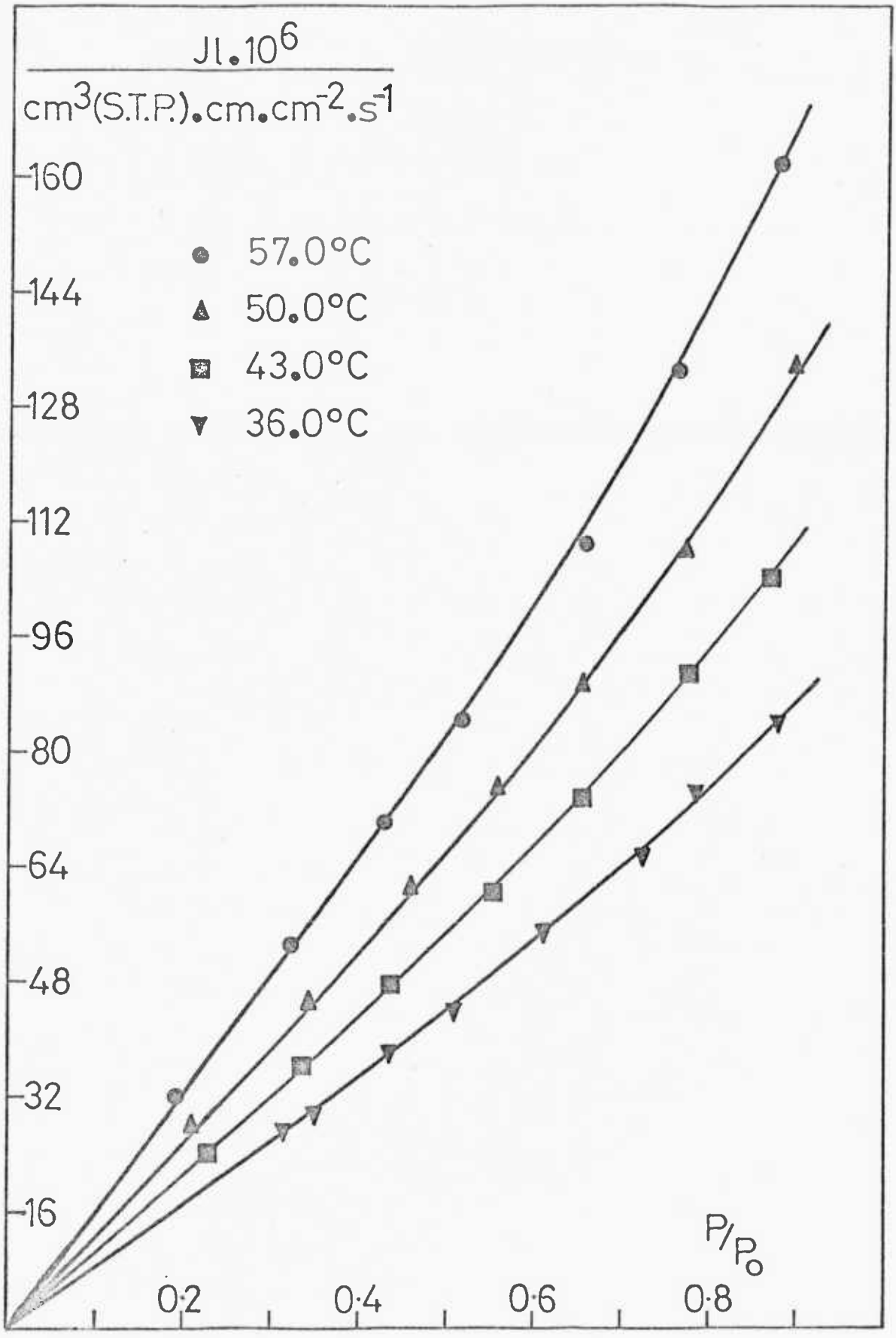


FIGURE 6.13 PDMS-MeOH PERMEATION ISOTHERMS

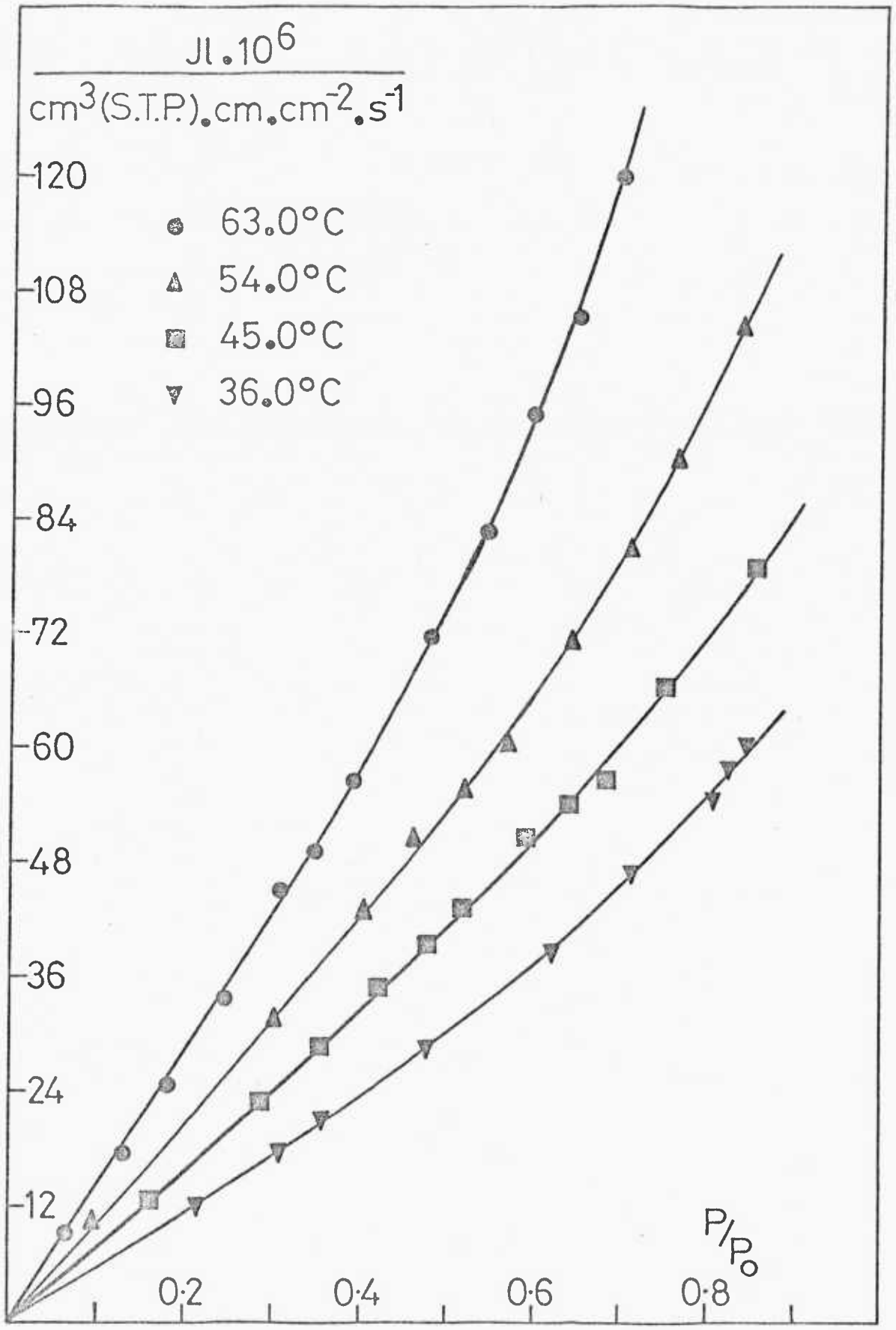


FIGURE 6.14 PDMS-EtOH PERMEATION ISOTHERMS

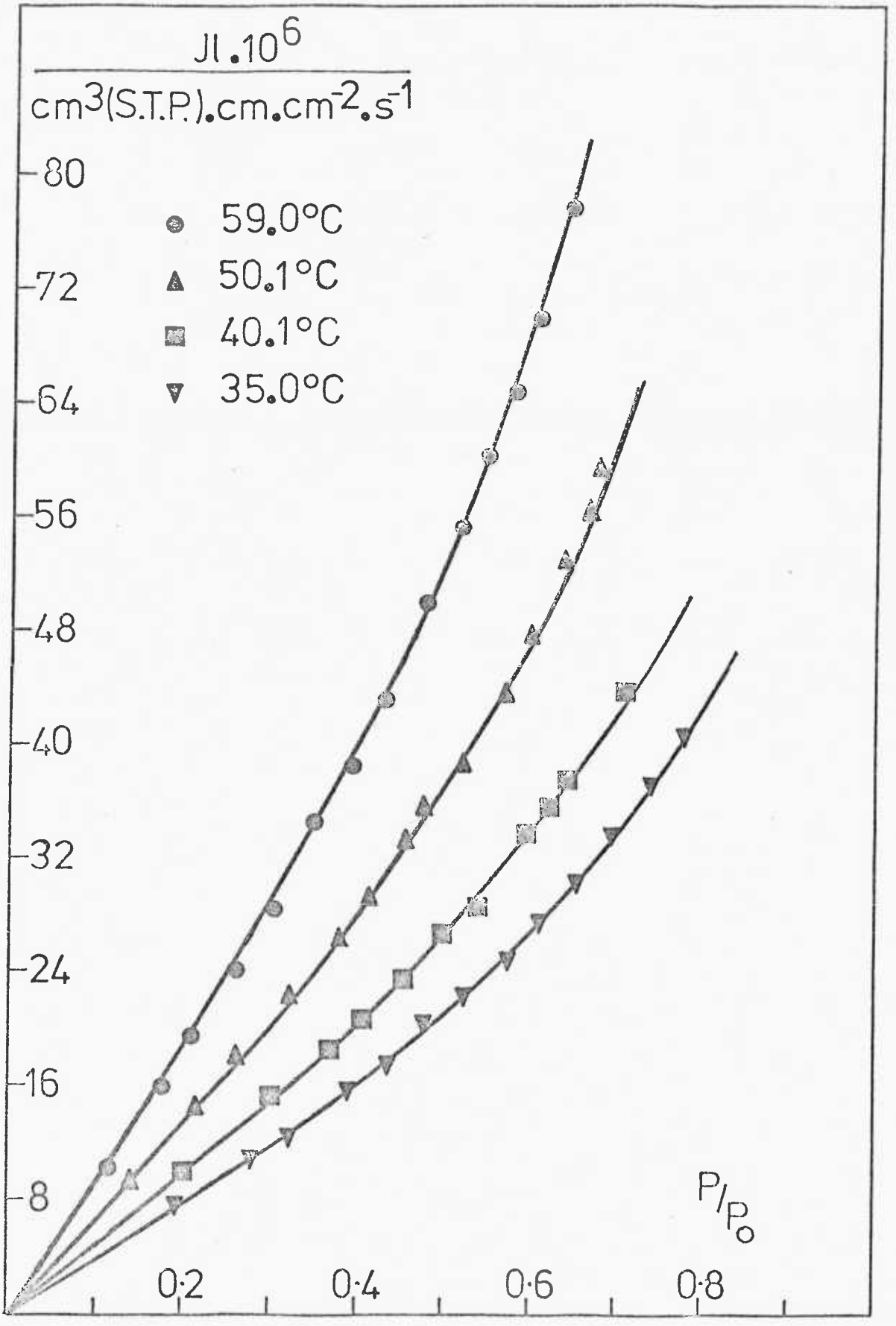


FIGURE 6.15 PDMS-(2-PrOH) PERMEATION ISOTHERMS

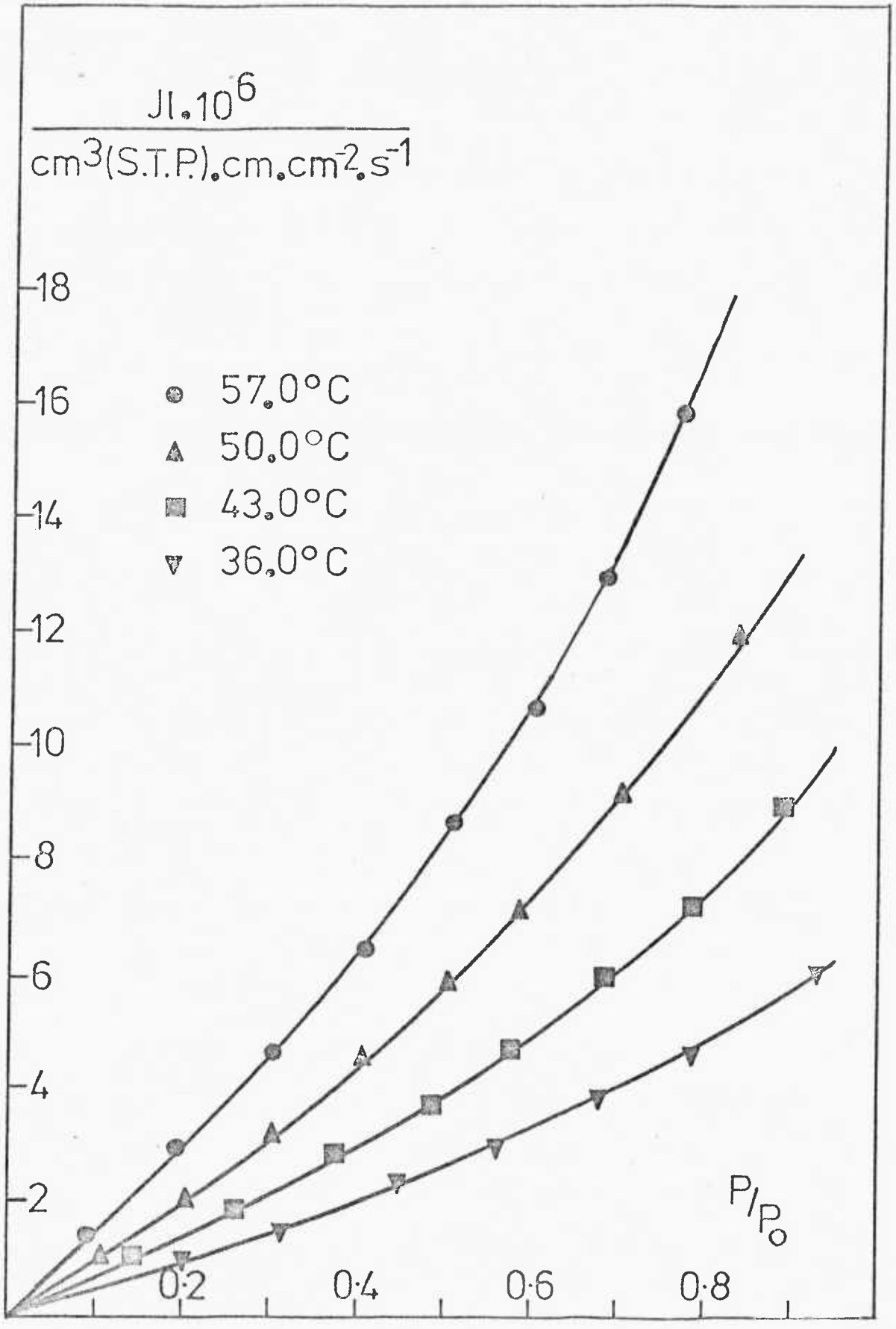


FIGURE 6.16 FMS-(2-PrOH)
PERMEATION ISOTHERMS

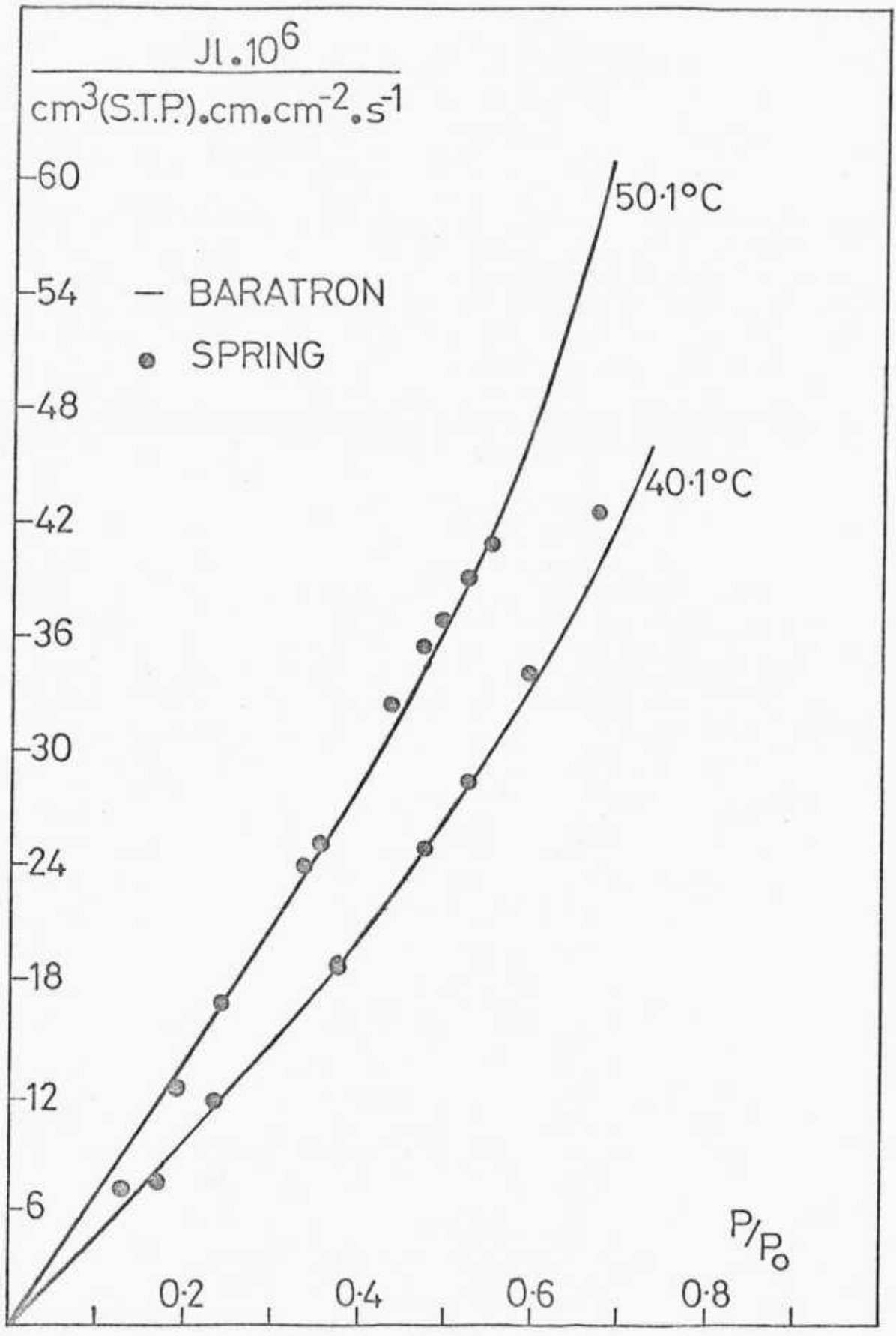


FIGURE 6.17 PDMS—(2-PrOH)
BARATRON & SPRING PERMEATION

agreement was found to be excellent.

The plots of flux rates for various pressures were all non-linear in contrast to the PDMS - H_2O system (Section 5.3). As the penetrant size and solubility increase this deviation from linearity becomes more marked since plasticisation of the polymer matrix occurs.

6.2.1 Absolute Magnitudes of P

Values of P (in the limit (c→o)) for each system are given in Table 6.5.

Table 6.5

Permeability Coefficients P (cm^3(S.T.P.). cm^{-1}. s^{-1}. $(cm\ Hg)^{-1}$) in the limit (c→o)

System	T°C	P.10^6	System	T°C	P.10^6
PDMS -	36.0	3.984	PDMS -	35.0	4.759
MeOH	43.0	3.555	(2-PrOH)	40.1	4.331
	50.0	3.290		50.1	3.750
	57.0	2.960		59.0	3.267
PDMS -	36.0	5.069	FMS -	36.0	0.565
EtOH	45.0	4.400	(2-PrOH)	43.0	0.574
	54.0	3.881		50.0	0.581
	63.0	3.375		57.0	0.594

For permeation in PDMS there appears to be a maximum at ethanol. This is a consequence of the fact that permeabilities are composite quantities of solubilities and diffusivities. As solubilities of these penetrants increase exponentially (Section 6.1.1) and diffusivities decrease exponentially with penetrant molar volume (Section 6.4.1), a combination of these is expected to produce a maximum at some point depending upon the relative magnitudes of the exponential dependences.

The values of P for the PDMS - MeOH system are in good agreement with previous data (18) for which a value of $P = 3.7 \cdot 10^{-6}$ cm^3 (S.T.P.) . cm^{-1} . s^{-1} . $(cm\ Hg)^{-1}$ at 30°C has been reported. No maximum is to be found for the FMS - alcohol systems if previous data are included (20, 84) : at 31°C, $P(H_2O) = 2.07 \cdot 10^{-6}$ and $P(MeOH) = 0.86 \cdot 10^{-6}$ cm^3 (S.T.P.) . cm^{-1} . s^{-1}. $(cm\ Hg)^{-1}$. Thus the bulky trifluoropropyl group of FMS causes the diffusion dependence to dominate as is also found from E_P data. Thus the relative magnitudes of P are :

P(PDMS)/P(FMS) :- 2, 4.5, 8 for H_2O, MeOH, 2-PrOH.

6.2.2 Temperature Dependence of P

Values of the temperature coefficient of permeability (E_P) are given in Table 6.6 and were calculated from graphs of log P vs. 1/T as illustrated in Figure 6.18.

Table 6.6

Values of E_P $(kJ\ .\ mol^{-1})$

System	E_P
PDMS-MeOH	-11.64
PDMS-EtOH	-12.77
PDMS-(2-PrOH)	-13.44
FMS-(2-PrOH)	+ 1.93

The negative values of E_P for PDMS indicate that $\Delta\bar{H}_S$ is numerically larger than E_D for these systems. This is in common with previous data for other small molecules in PDMS (20, 24, 84) for which permeabilities are quite large. FMS differs from PDMS in that E_D is the dominating feature, a fact that is usually true for systems that are much less permeable than PDMS (74, 81, 124).

6.3 Transient-State Permeation

As stated in Section 6.2, it is possible to measure steady-state fluxes directly using the Baratron, unlike water vapour. This is a consequence of the fact that alcohol vapours must sorb only the surface

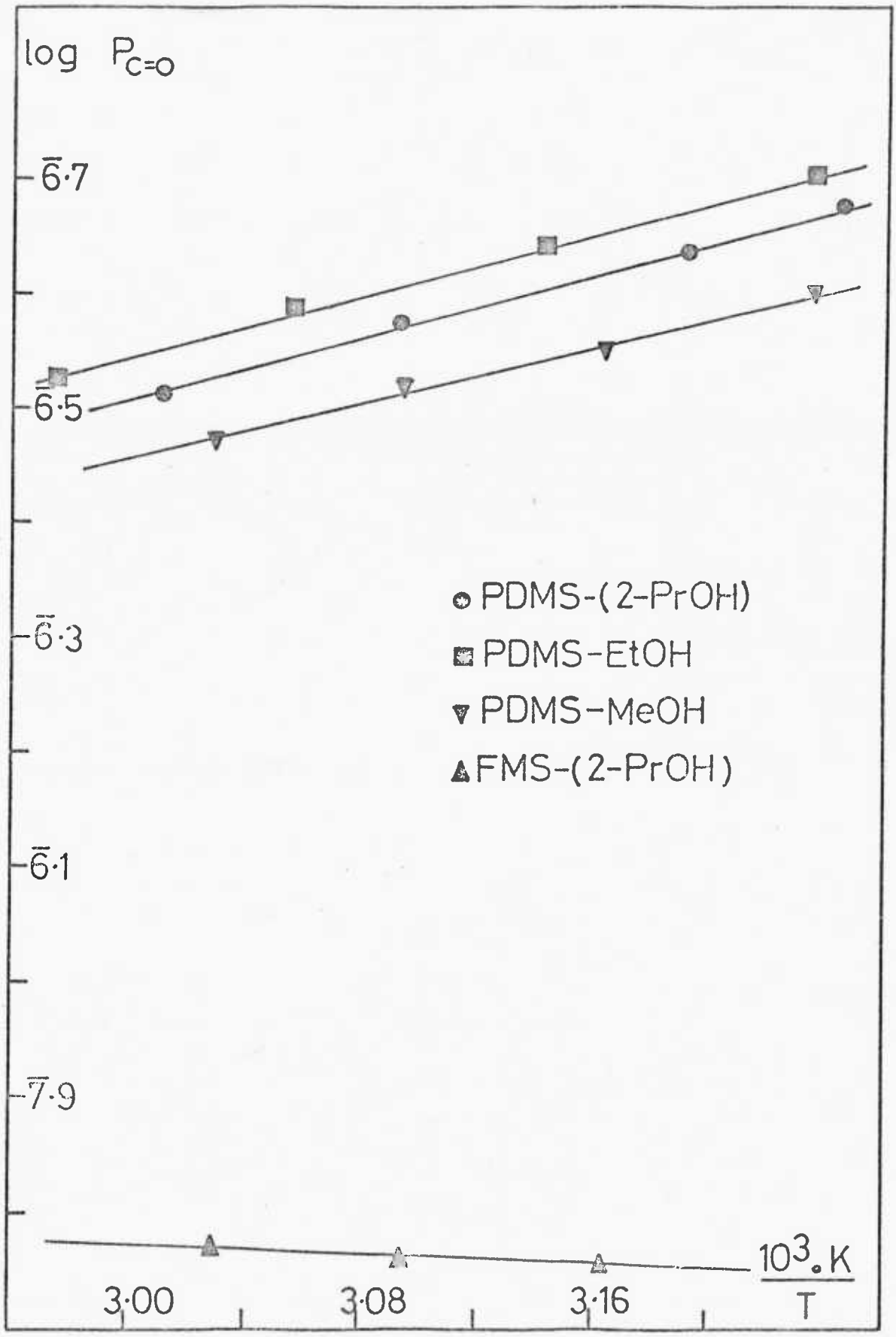


FIGURE 6.18
TEMPERATURE VARIATION OF PERMEABILITY

of the ceramic supports for the capacitance electrodes. Thus alcohol vapour is not continuously removed from the system by sorption inside the Baratron, although there is some sorption onto the glass and metal of the apparatus. Hence it may be anticipated that it is possible to measure time lags which have some meaning, even though agreement with steady-state results may not be exact.

6.3.1 Magnitudes of Time Lags

Time Lag (L) measurements were taken for the PDMS - EtOH and PDMS - (2-PrOH) systems at all the measured temperatures. This data is presented in Appendix 8.2.4 and illustrated in Figures 6.19 - 6.24. Perhaps the most striking feature of these results is the increase of the time lags with increasing concentration of sorbed penetrant. This is one of the very few systems in which this behaviour has been reported and is applicable to systems in which the diffusion coefficient decreases with increasing concentration. Previous literature of such systems (17) reported time lag data yielding a constant D in contrast to the D decreasing with increasing concentration obtained from steady-state measurements. However the penetrant in these systems was water vapour which sorbs on the surfaces of the apparatus to a much greater extent.

The actual magnitudes of the time lags are all greater than those calculated from steady-state diffusion data (53) by about 30% for EtOH and 20% for 2-PrOH. Whilst, in general, there is often some discrepancy between time lag and steady-state results, this difference can be explained to some extent. Ideally the membrane should have no edge around the area available for permeation and obviously this is impossible. Hence some penetrant diffuses into and through this "edge" and hence creates an additional path length, causing an increased time-lag. Another contribution arises from the sorption of vapour on the glass and metal of the "down-stream" volume. This causes the measured pressures to be less than the true pressure and hence again an increased time lag is observed. Despite this, it was felt to be justifiable to measure time lags for these particular systems and agreement with steady-state results is quite reasonable.

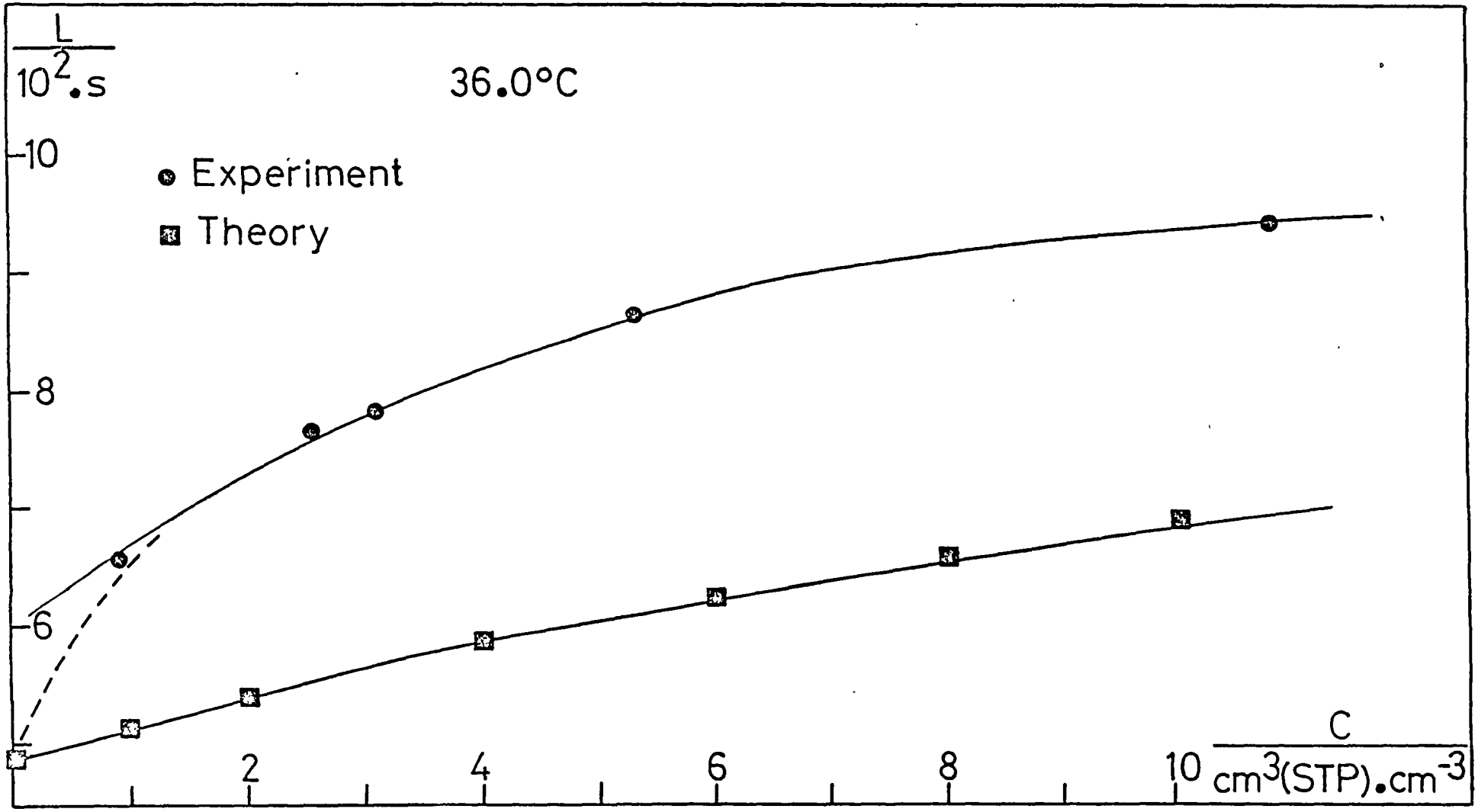


FIGURE 6.19 PDMS–EtOH TIME LAG DATA

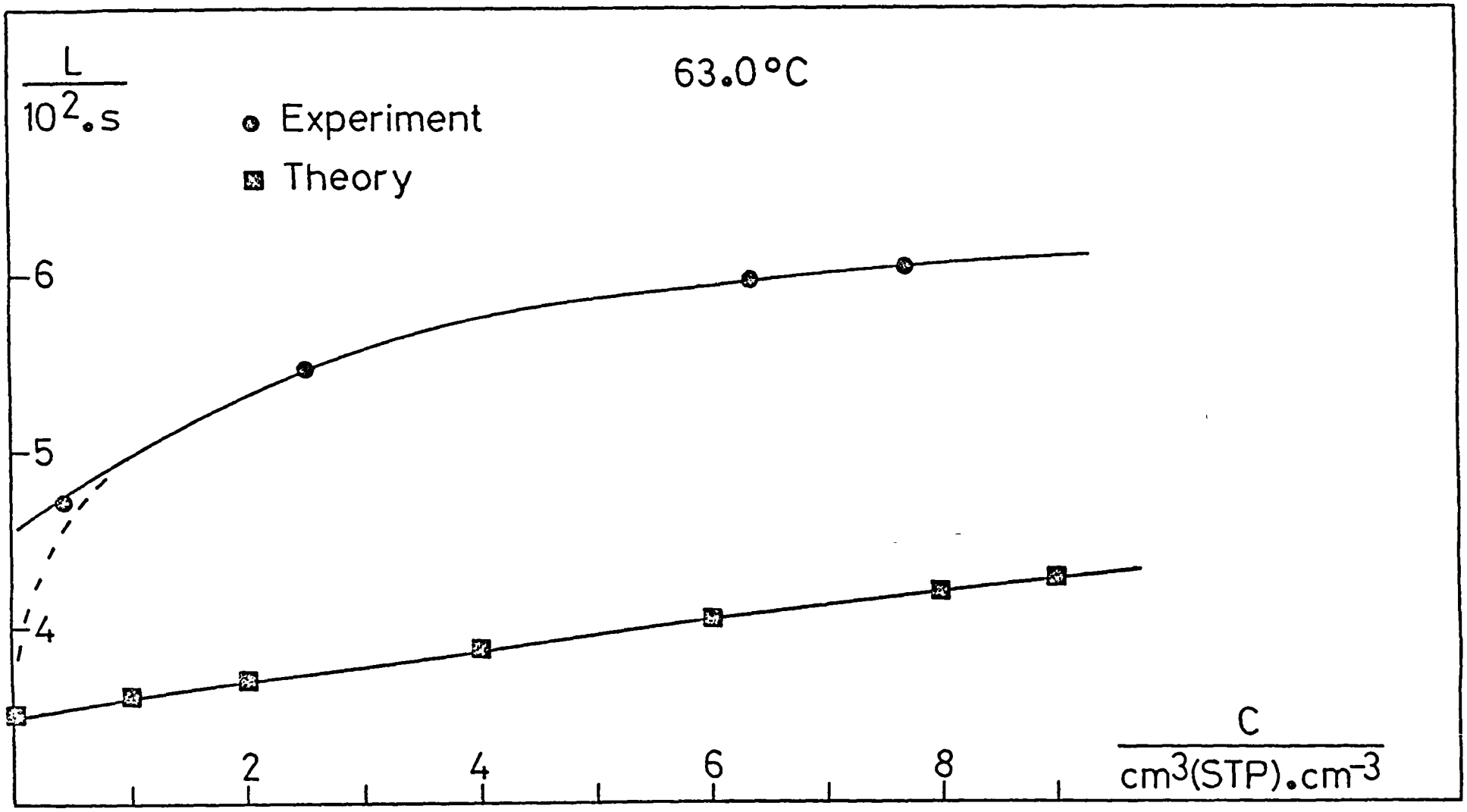


FIGURE 6.20 PDMS–EtOH TIME LAG DATA

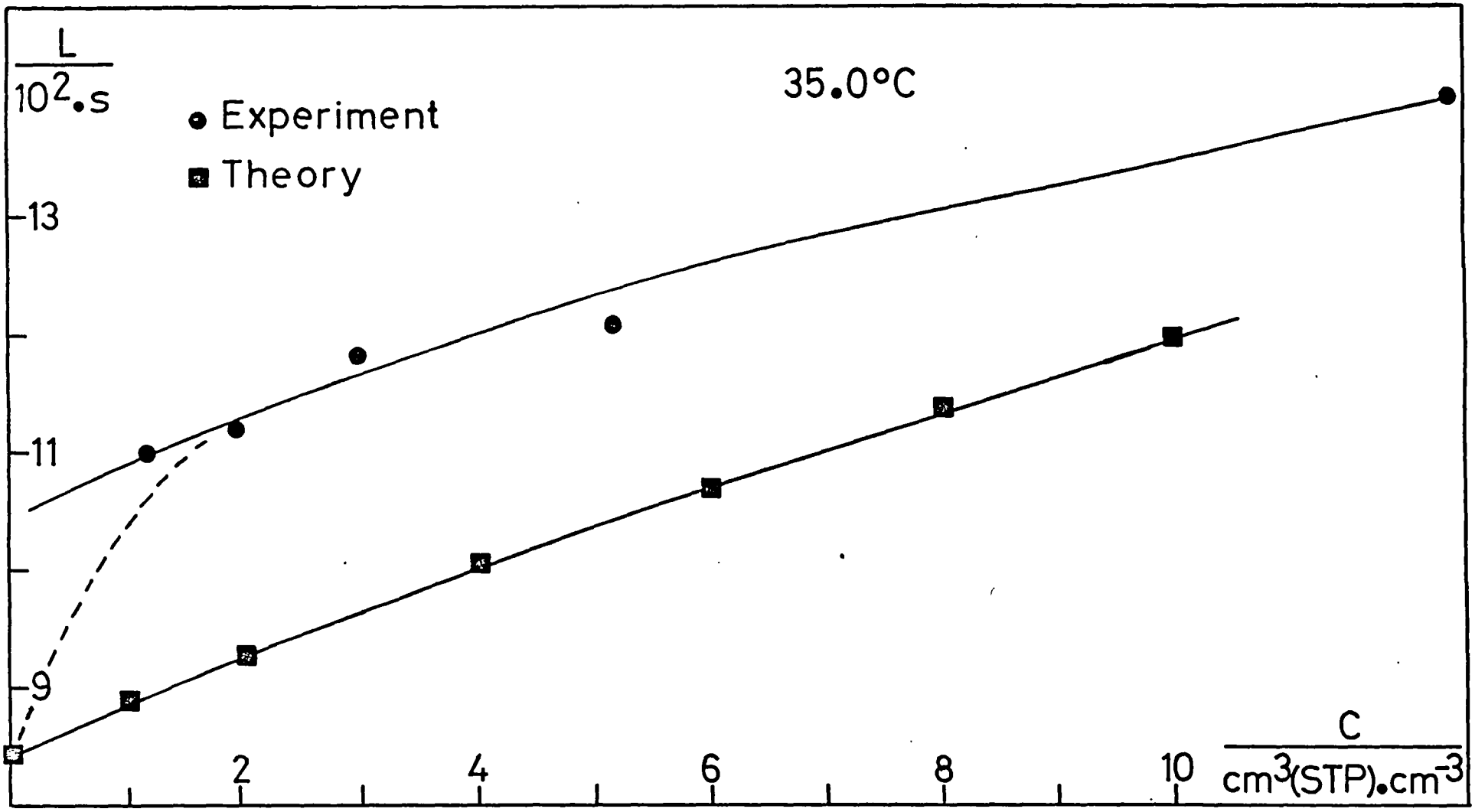


FIGURE 6.21 PDMS-(2-PrOH) TIME LAG DATA

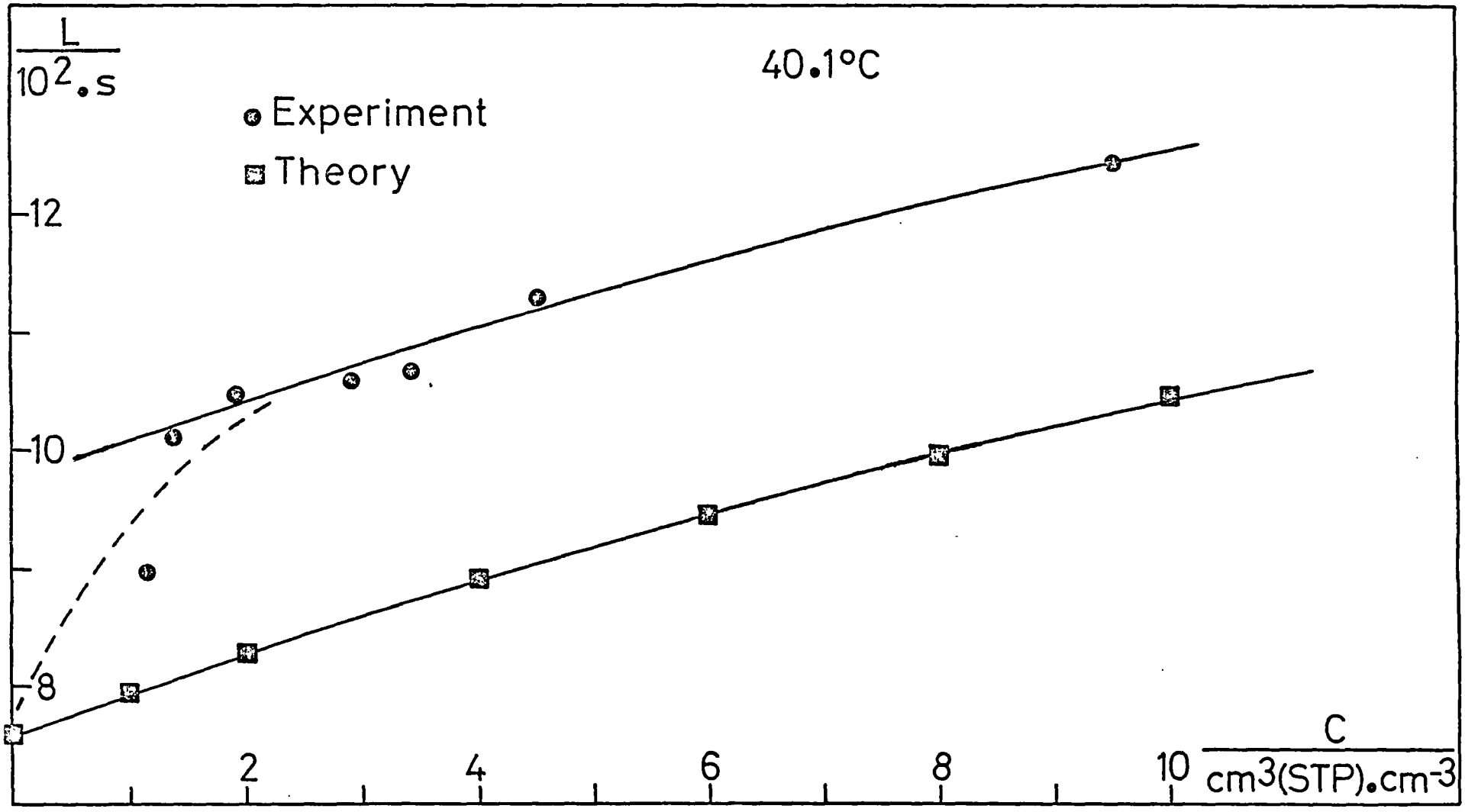


FIGURE 6.22 PDMS-(2-PrOH) TIME LAG DATA

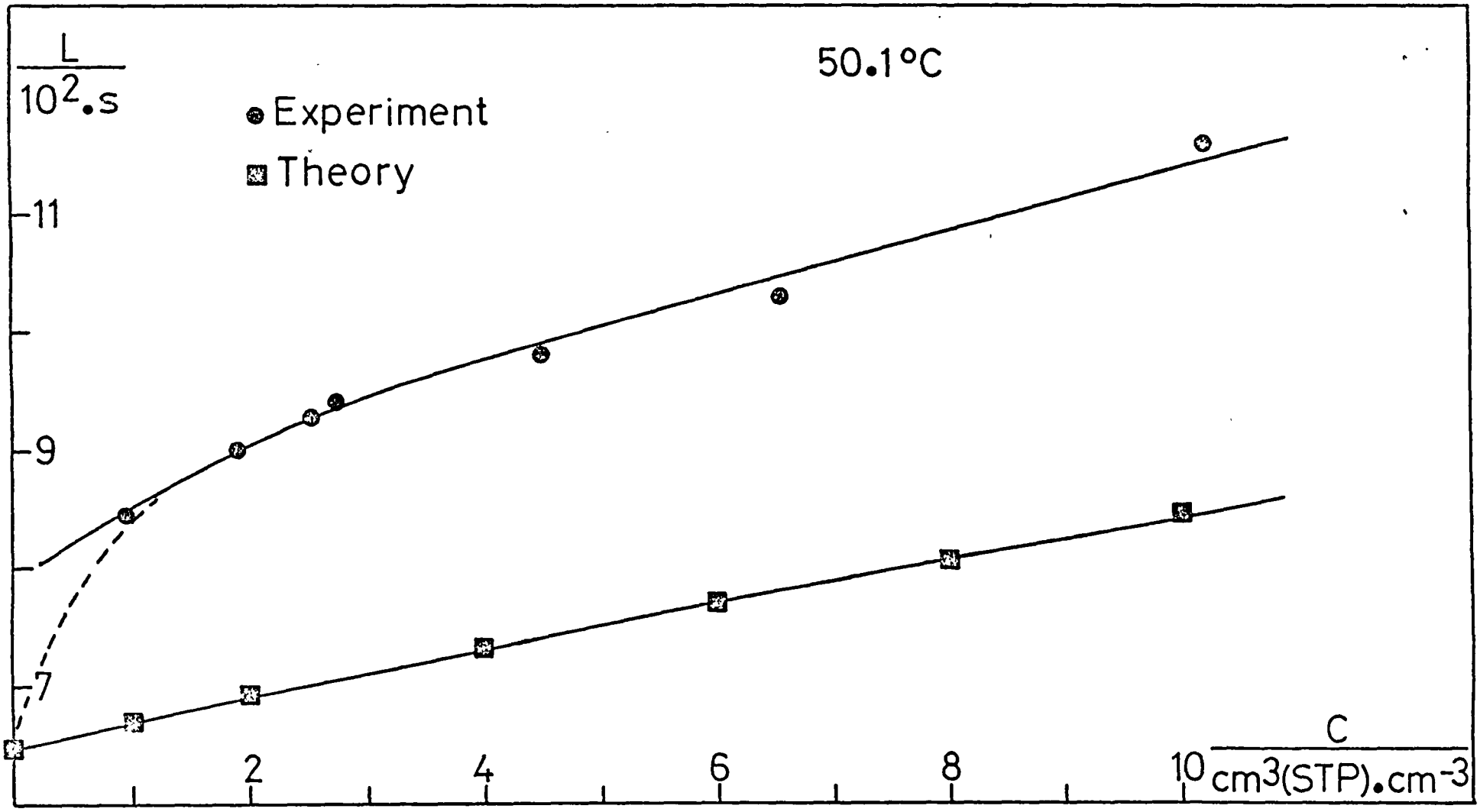


FIGURE 6.23 PDMS-(2-PrOH) TIME LAG DATA

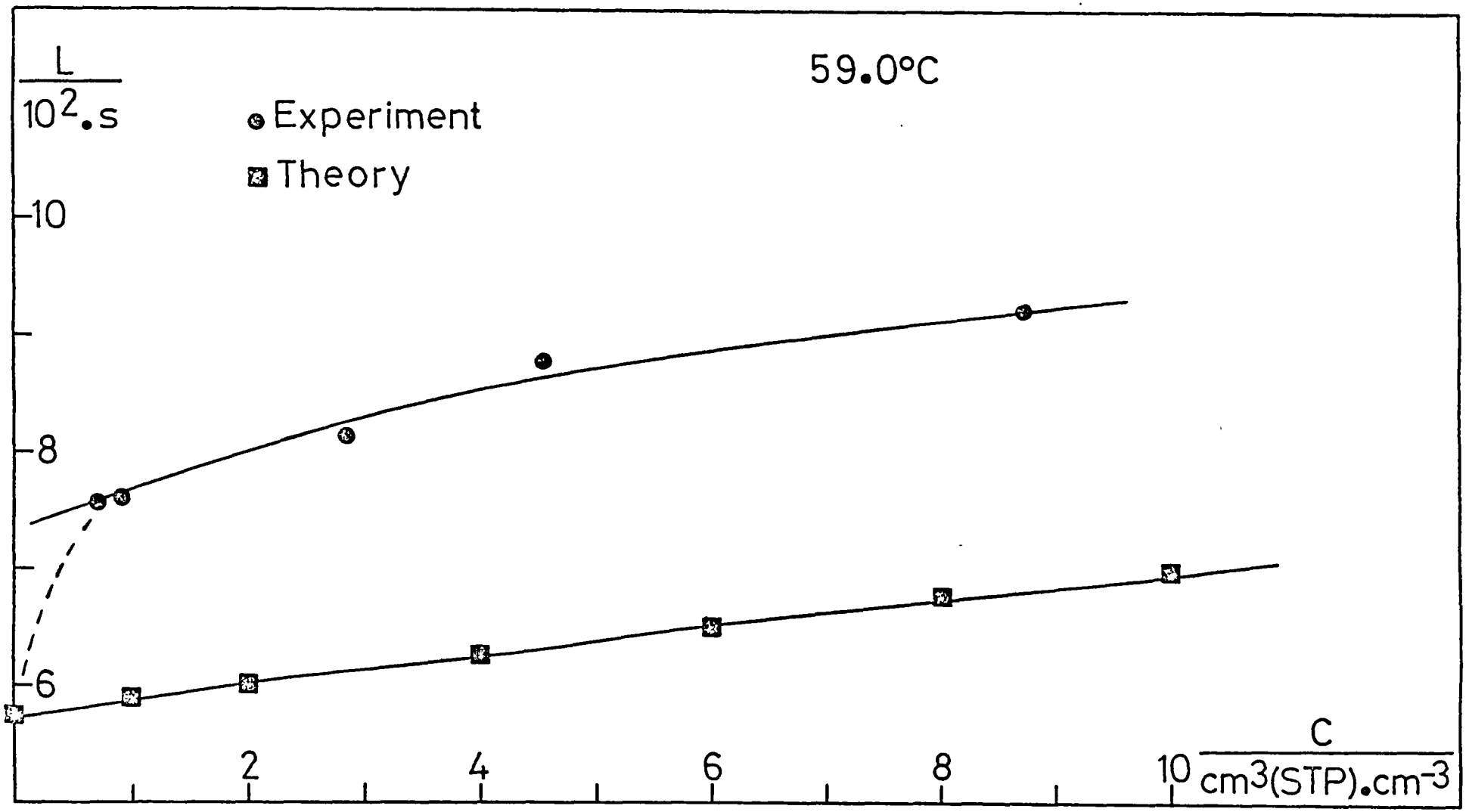


FIGURE 6.24 PDMS-(2-PrOH) TIME LAG DATA

Sorption on the walls of the "down-stream" volume probably accounts for the difference between the results for the two penetrants. Since neither ethane nor propane sorb on glass, sorption of the alcohol vapours is due to interaction of the -OH group with the glass. Hence, as the alcohol group is a smaller component of 2-PrOH than EtOH, sorption of 2-PrOH on glass is less than that of EtOH and hence there should be less discrepancy with the steady-state results.

The biggest difficulty with the experimental data is to decide on the time lag at zero concentration. Extrapolation of the time lags at high concentrations of sorbed penetrant give the limit greater than the steady-state results by the same difference as the experimental time lags although, in most instances, it is equally possible to extrapolate back to the "steady-state" time lags (dotted lines in Figures 6.19 - 6.24). As it is difficult to establish the time lag at zero concentration, it was decided not to attempt to extract any diffusion coefficients from this data. Indeed the variation of time lags with concentration for these types of systems is very much less than that of the diffusion coefficients derived from them and hence extraction of diffusion data is approximate at the very best.

6.4 Steady-State Diffusion Results

No realistic transient diffusion data could be obtained for these systems and hence only steady-state diffusion coefficients are to be considered. The difficulties of time lag measurements have been illustrated in Section 6.3 and it was found, using the spring-sorption apparatus, that adequate control of the vapour pressure could not be maintained. Thus, in any sorption-kinetic experiment, the pressure in the balance was never constant as there was no buffer volume present, and hence stable boundary conditions could not be obtained.

Steady-state diffusion coefficients were determined as described in Section 2.3.1 by graphical differentiation of $J\ell$ vs. C plots.

6.4.1 Values of $D_{c=o}$

Values of $D_{c=o}$ for each system are given in Table 6.7. The values of $D_{c=o}$ for the PDMS - MeOH system are in reasonable agreement with those previously reported (18) : at 30°C, $D_{c=o} = 16.0 \cdot 10^{-6}$ $cm^2 \cdot s^{-1}$. No previous literature values are available for the other systems studied.

Table 6.7

Values of $D_{c=o}$ ($cm^2 \cdot s^{-1}$)

System	T°C	$D_{c=o} \cdot 10^6$	System	T°C	$D_{c=o} \cdot 10^6$
PDMS -	36.0	22.04	PDMS -	35.0	8.09
MeOH	43.0	23.86	(2-PrOH)	40.1	8.92
	50.0	25.89		50.1	10.50
	57.0	28.26		59.0	11.86
PDMS -	36.0	14.00	FMS -	36.0	1.038
EtOH	45.0	15.73	(2-PrOH)	43.0	1.262
	54.0	17.53		50.0	1.640
	63.0	19.40		57.0	1.989

In conjunction with the values for the PDMS - H_2O system, these illustrate the high D values for small penetrant diffusion in silicone rubbers. This is due to the very flexible (-Si-O-) linkage of the main-chain whereby there are no side-chains on the oxygen atoms. This drastically reduces steric hindrance within the polymer so that hole formation is relatively easy.

Using the data presented in Table 6.7 and that for the PDMS-H_2O system (Section 5.4.1) and the FMS-H_2O and FMS-MeOH systems (20, 84) it is possible to construct plots similar to those for solubility data (Figures 6.5 and 6.6) to illustrate the effects of penetrant size on diffusion coefficients. These are shown in Figures 6.25 and 6.26 for PDMS and FMS respectively. Thus, as penetrant size increases, diffusion coefficients decrease due to the need to create larger holes for diffusion to take place. The bulky trifluoropropyl group of FMS hinders penetrant diffusion much more than the methyl side-chains of PDMS and hence diffusion coefficients in FMS are considerably lower than

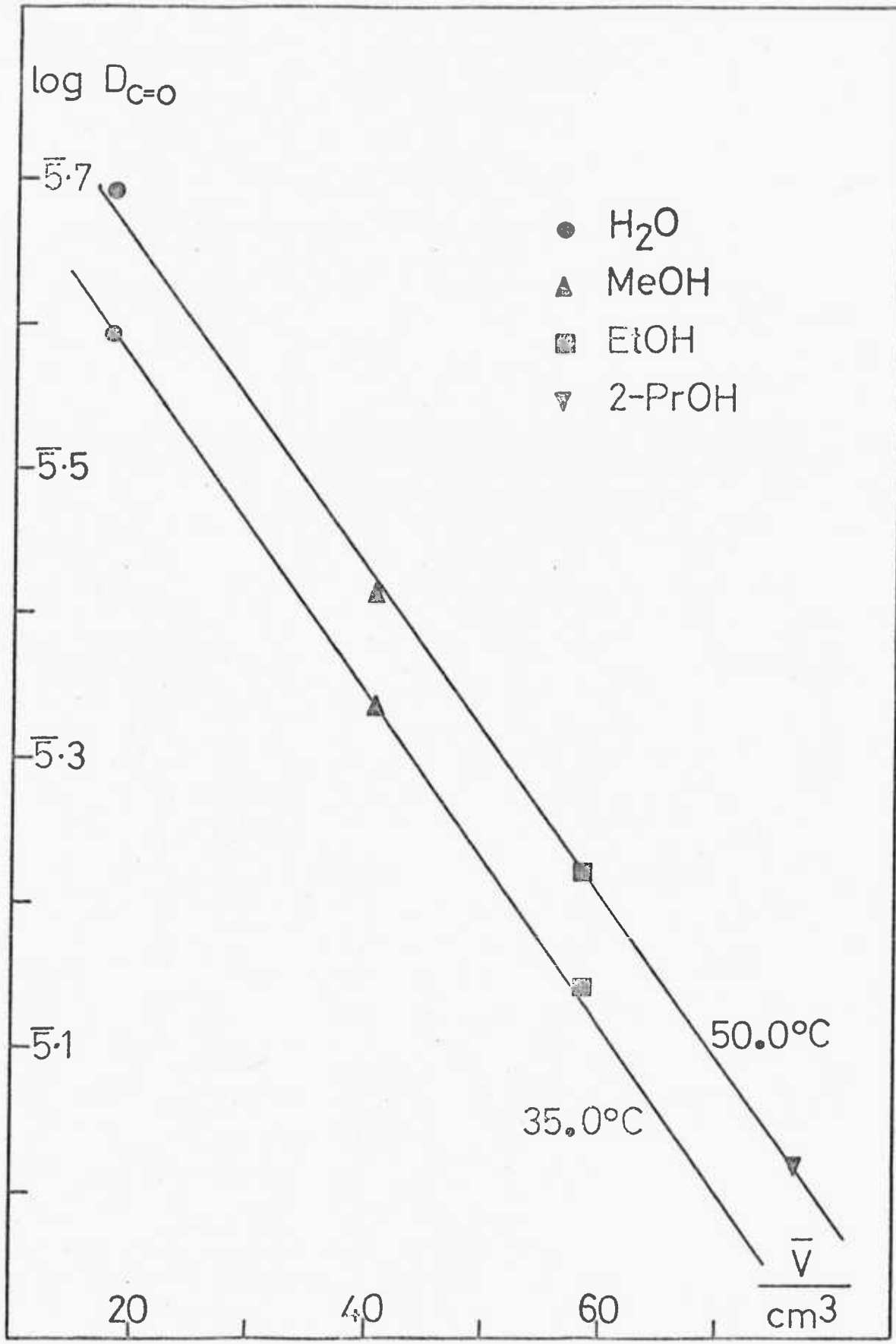


FIGURE 6.25 PDMS–ALCOHOLS
THE EFFECT OF SIZE ON DIFFUSIVITY

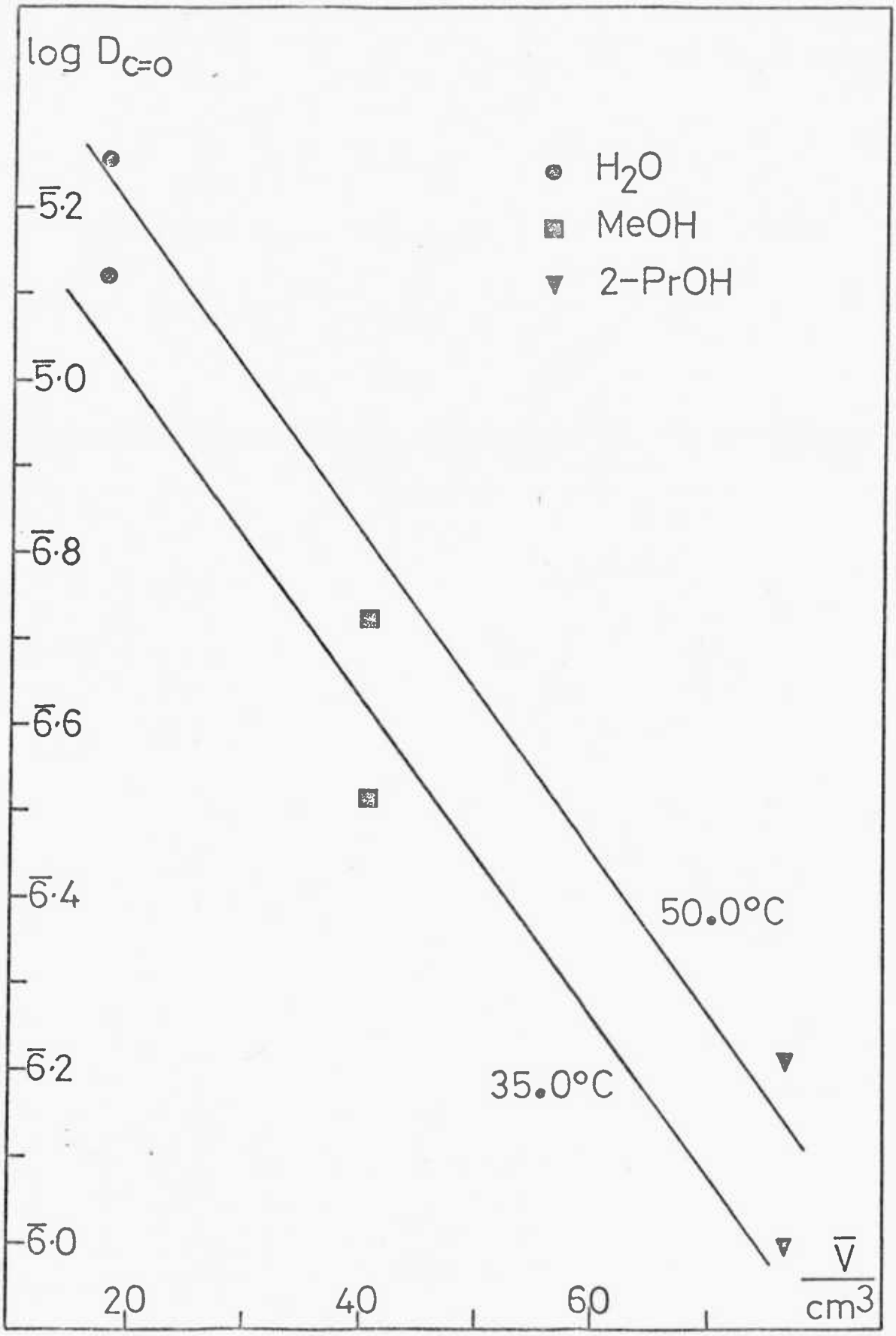


FIGURE 6.26 FMS-ALCOHOLS
THE EFFECT OF SIZE ON DIFFUSIVITY

in PDMS and the slope of the plots in Figure 6.26 is greater than those of Figure 6.25 for PDMS.

6.4.2 Concentration-Dependence of D

In all the systems studied D decreases with increasing concentrations and for all concentrations. The concentration-dependences of D are illustrated in Figures 6.27 - 6.30 where a relative diffusion coefficient (D^1) is defined as $D^1 = D/D_{c=o}$.

The behaviour of these systems is quite different from that of the PDMS - H_2O (Section 5.4.1), FMS - H_2O and FMS - MeOH systems (20, 84) in that there is no initial constant D region. This is due, in part, to the greater solubility of the alcohols in PDMS and FMS so that there is a greater possibility of penetrant contacts and hence clustering. Previous data (18) of the PDMS - MeOH system indicates that this continually decreasing D is a real feature even though the initial regions of the sorption isotherms cannot be determined very accurately.

The relative reduction in D with C decreases with increasing penetrant size for both polymers. This is a consequence of the decrease in clustering of penetrant as the increasing hydrocarbon chain encourages more polymer-penetrant interactions. In addition, for any particular penetrant, the reduction of D for PDMS is much greater than for FMS as the slightly electronegative trifluoropropyl group allows greater penetrant-polymer interactions with an associated decrease in clustering.

It is possible to estimate the D-C dependence of any system using the polycondensation model (Section 6.1.3). Thus by fitting the theoretical to the experimental sorption isotherm using a variable K value, it is possible to predict the D-C dependence by using the same K value (18, 20, 22, 24). Thus

$$D = D_{c=o} \cdot \left(\frac{K}{2C} \left[\frac{\alpha\,(1-\alpha)^2 + (1-2\alpha)(1-\alpha)}{\alpha - 1/4\,(3 + K/C)} \right] + (1-\alpha)^2(1-2\alpha) \right)$$

This model assumes that only monomeric water undergoes diffusion and the remainder within the clusters is immobilised. The theoretical D-C dependences are compared with the experimental in Figures 6.31 - 6.34 for one temperature only. The agreement, as may be expected from the

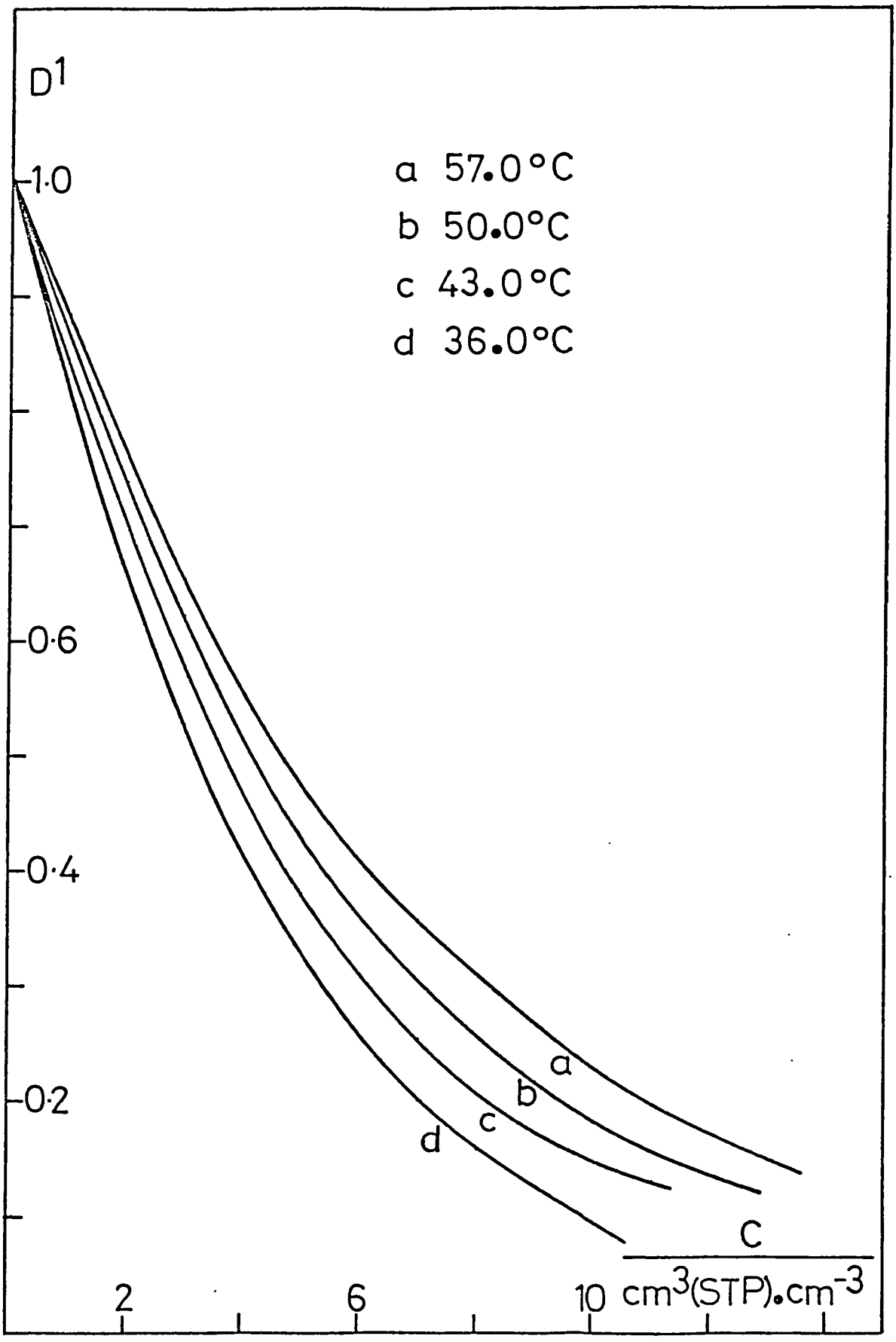


FIGURE 6.27 PDMS–MeOH
CONCENTRATION-DEPENDENCE OF DIFFUSIVITY

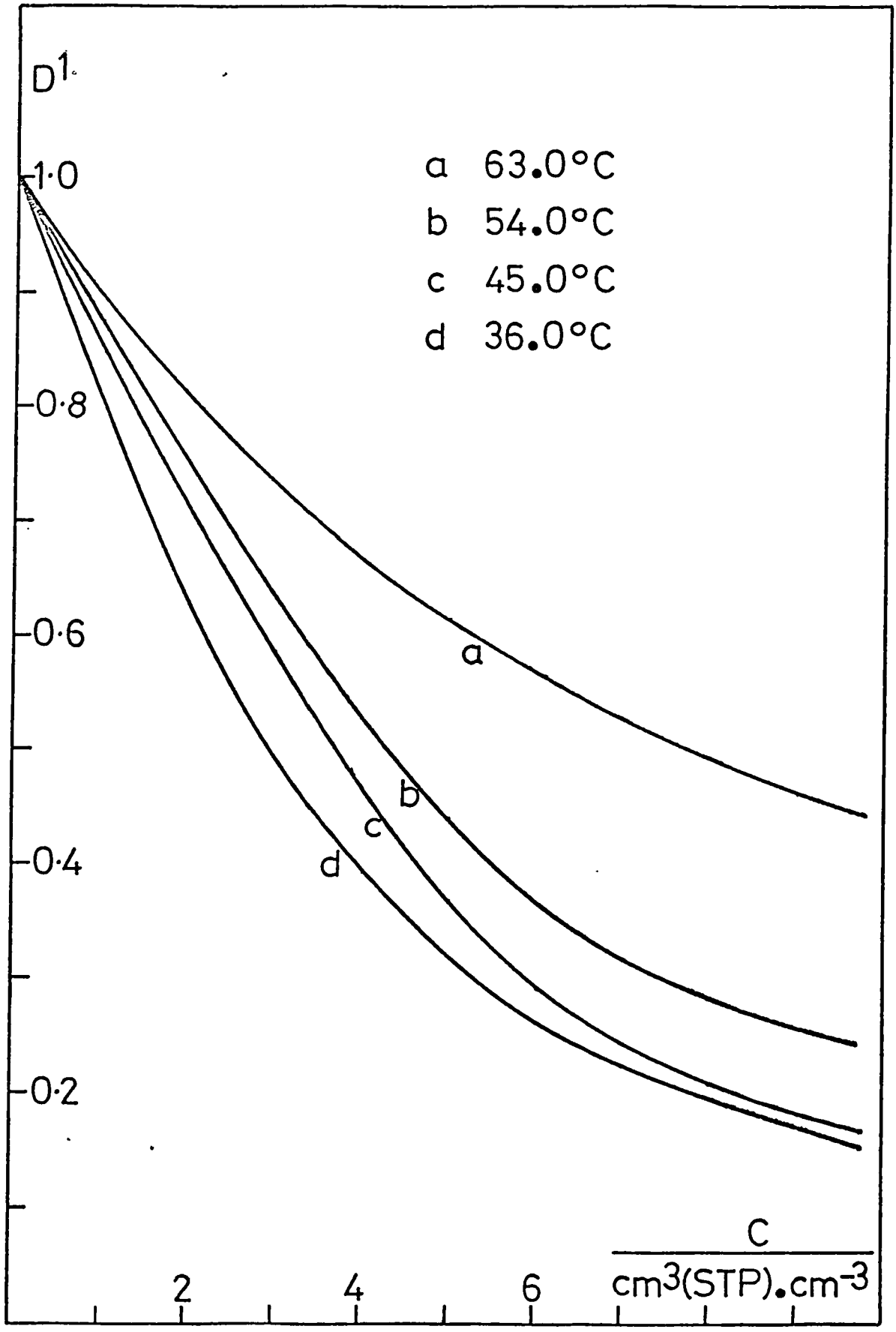


FIGURE 6.28 PDMS–EtOH
CONCENTRATION-DEPENDENCE OF DIFFUSIVITY

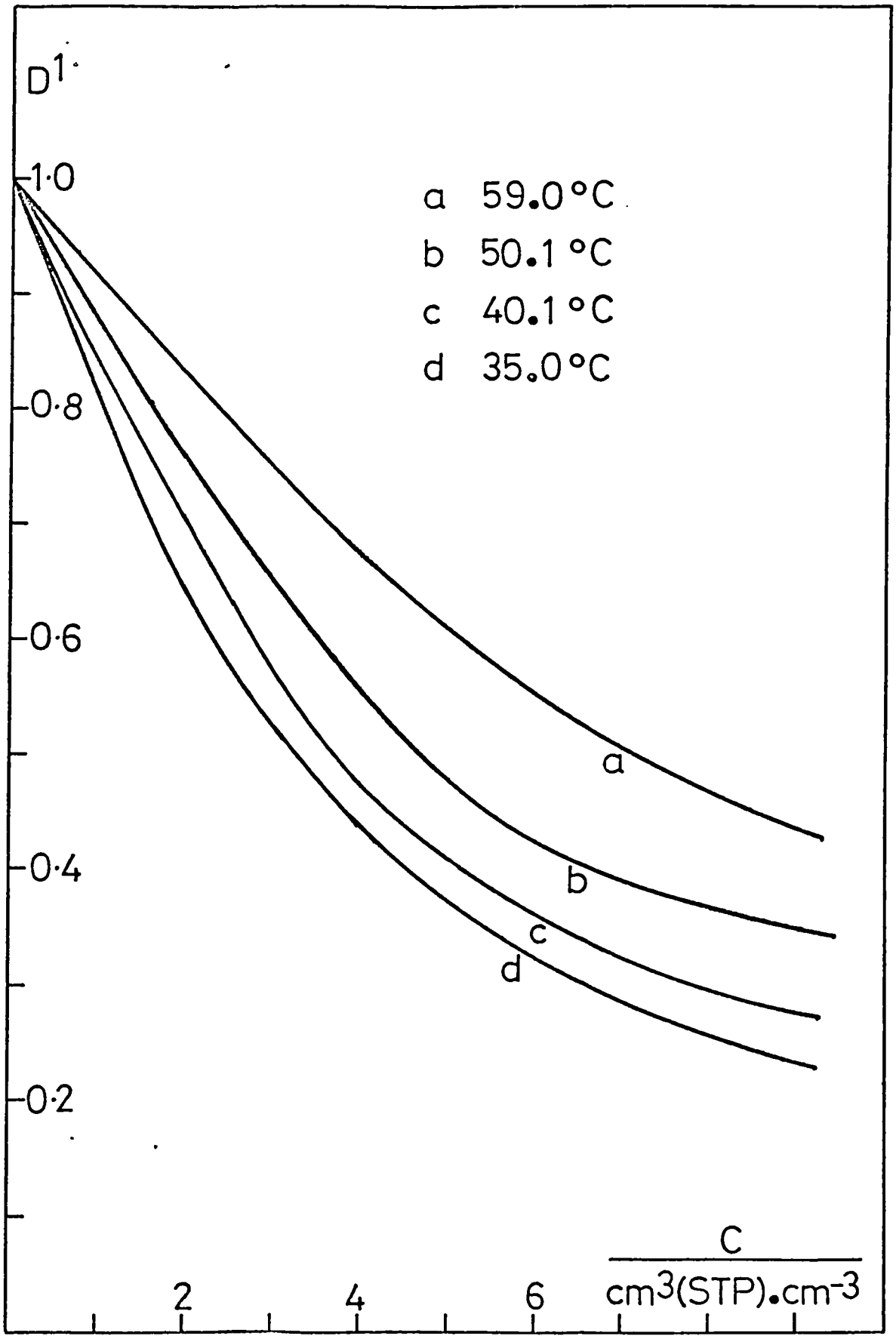


FIGURE 6.29 PDMS–(2–PrOH)
CONCENTRATION-DEPENDENCE OF DIFFUSIVITY

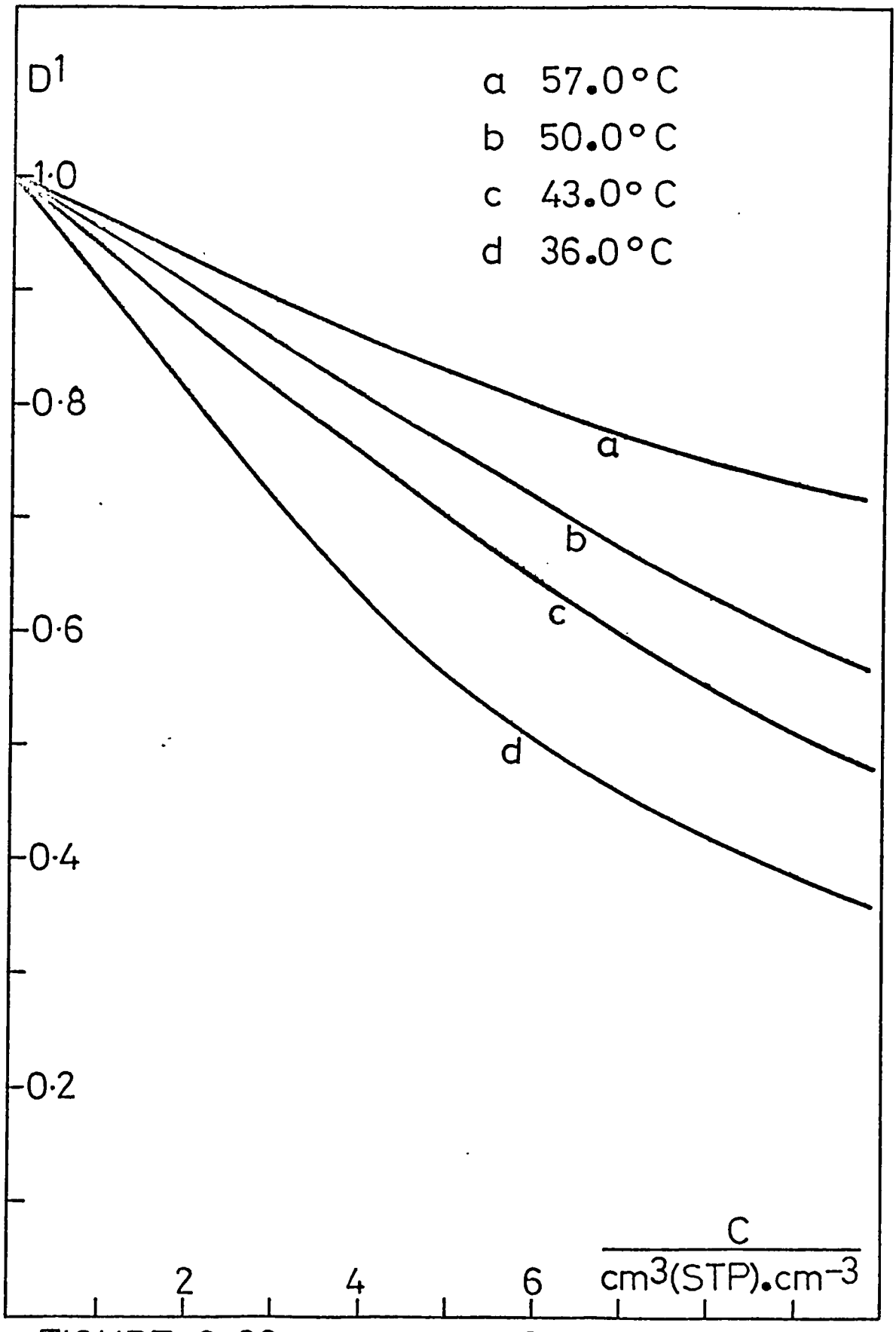


FIGURE 6.30 FMS-(2-PrOH)
CONCENTRATION-DEPENDENCE OF DIFFUSIVITY

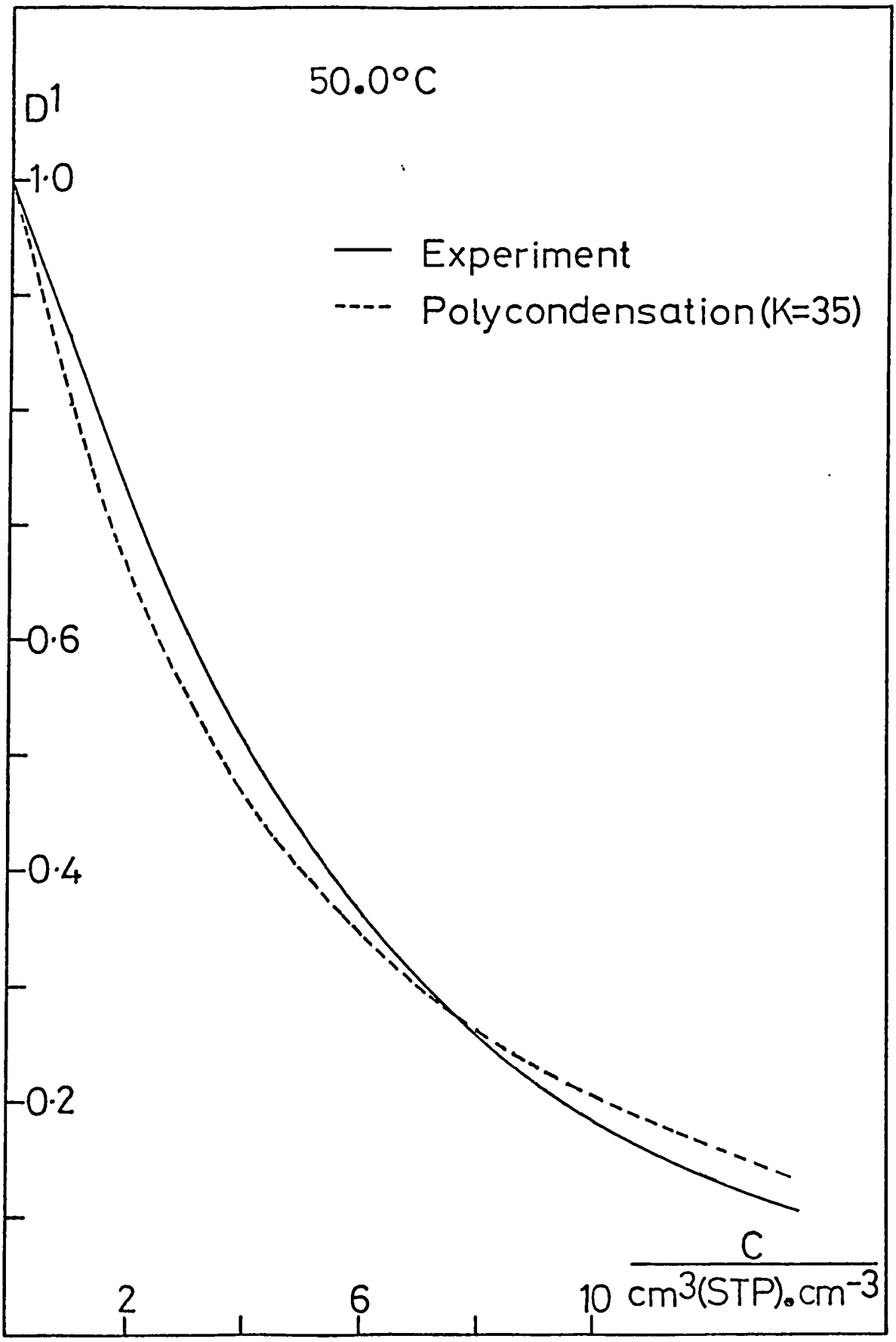


FIGURE 6.31 PDMS-MeOH
EXPERIMENTAL & THEORETICAL D-C CURVES

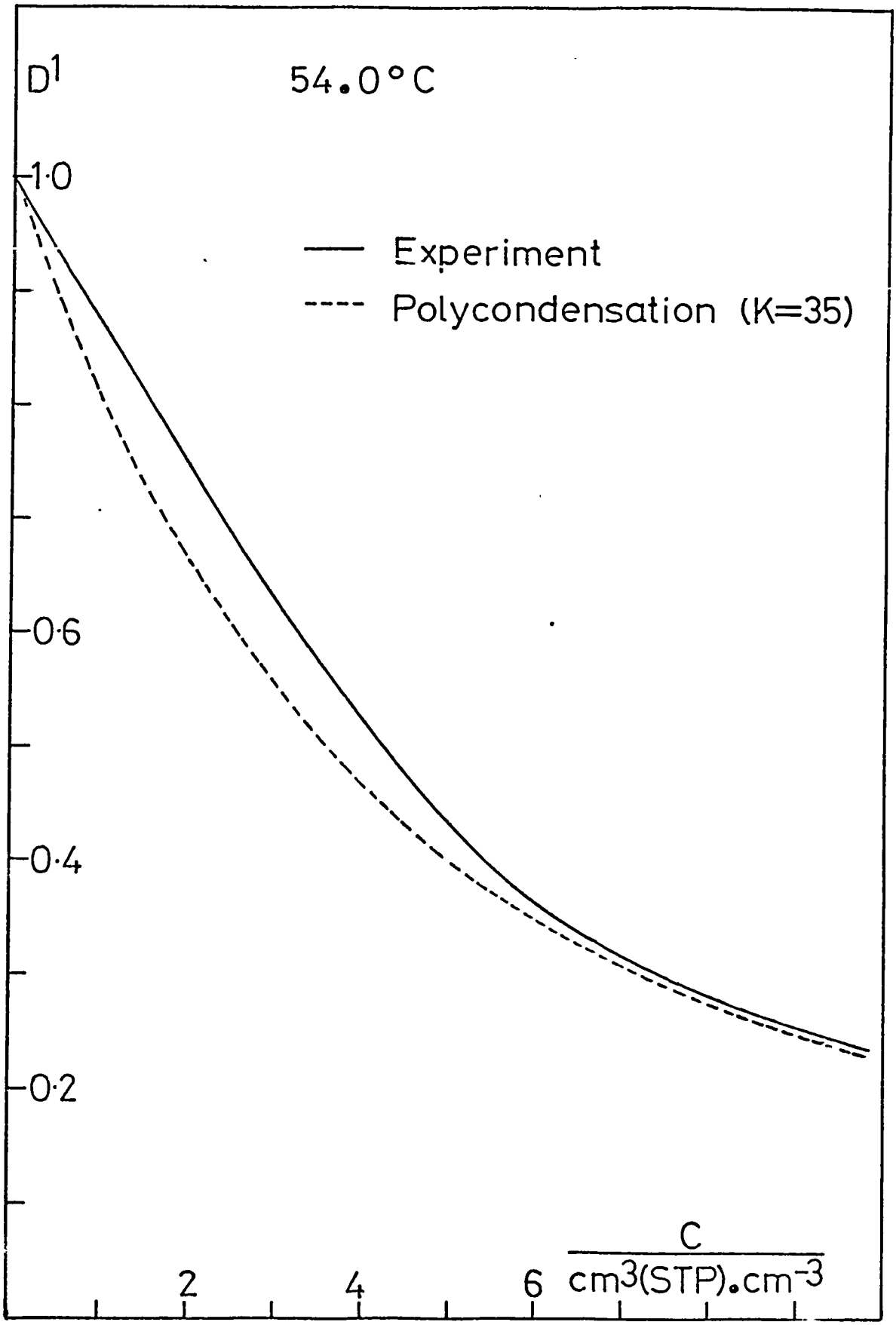


FIGURE 6.32 PDMS-EtOH
EXPERIMENTAL & THEORETICAL D-C CURVES

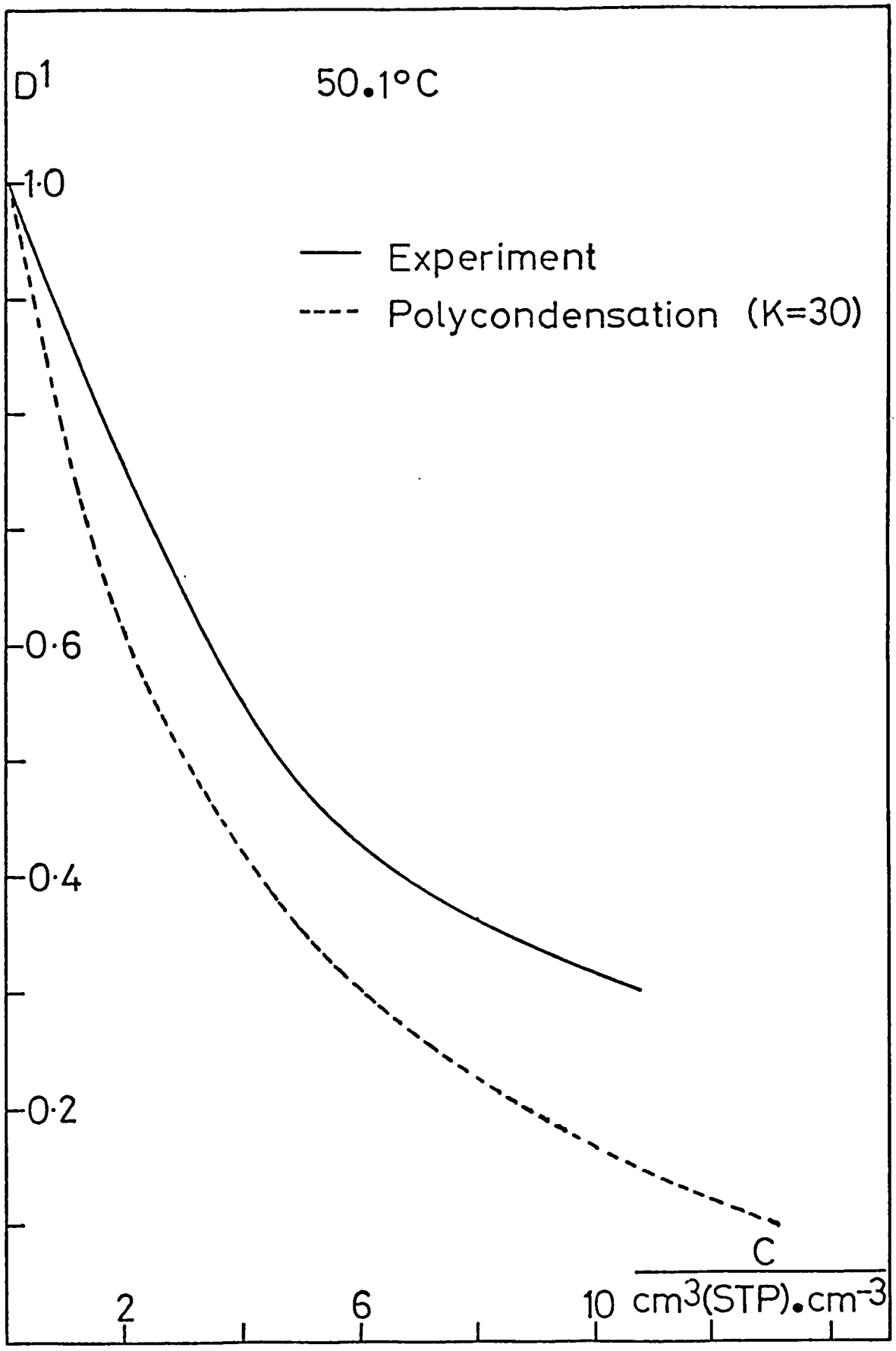


FIGURE 6.33 PDMS–(2-PrOH)
EXPERIMENTAL & THEORETICAL D–C CURVES

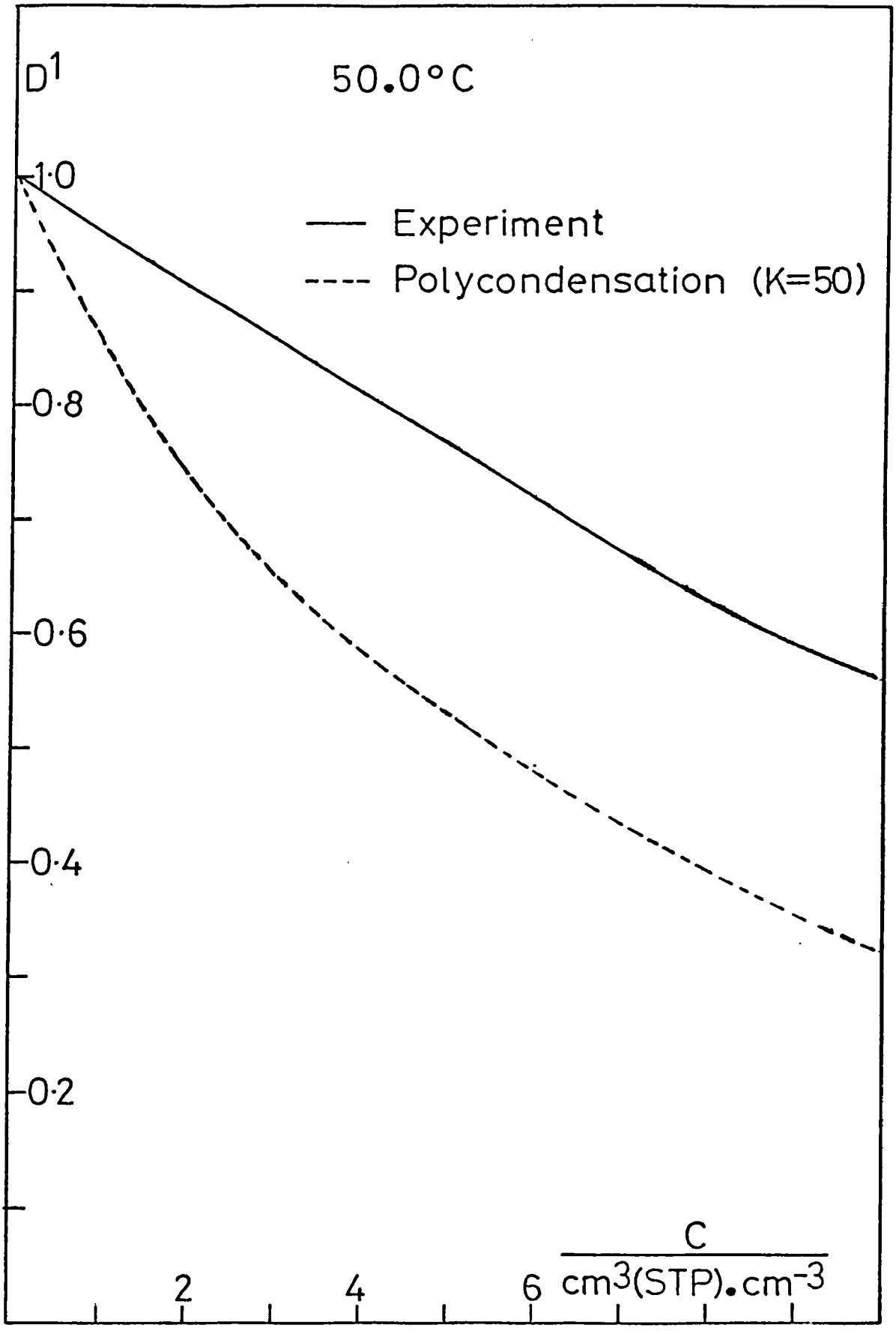


FIGURE 6.34 FMS-(2-PrOH)
EXPERIMENTAL & THEORETICAL D-C CURVES

sorption isotherm analysis, is not very good and gets worse as plasticisation increases.

When considering diffusion in a swelling membrane, an alternative diffusion coefficient, the intrinsic diffusion coefficient $\mathcal{D}_A$, may be considered. Thus in a system in which the membrane is swollen by penetrant, part of the D-C dependence is due to the mass flow of penetrant as the membrane swells. Hence, by taking a frame of reference with respect to the changing volume of polymer, it is possible to separate out this mass flow contribution and leave the contribution due to diffusion by random displacements of the penetrant molecules. The intrinsic diffusion coefficient ($\mathcal{D}_A$) is related to the experimental diffusion coefficient (D_A^B) by :

$$\mathcal{D}_A = D_A^B / \phi_B^3$$

where A and B refer to penetrant and polymer respectively and ϕ is the volume fraction of any component. Comparisons of $\mathcal{D}_A$ and D_A^B values for each system are illustrated in Figures 6.35 - 6.38. This effect is greatest for those systems in which there is considerable swelling and, in each instance, it reduces the decrease of D with concentration.

6.4.3 Temperature Dependence of D

Plots of log D vs. 1/T at various concentrations are shown for each system in Figures 6.39 - 6.42. Values of E_D have been calculated at these concentrations and are given in Table 6.8.

At zero concentration for PDMS, E_D is constant as the penetrant size increases (including the PDMS - H_2O system results of Section 5.4.3) and is a consequence of the relative ease of hole formation within the PDMS matrix for diffusion of relatively small penetrants.

FMS, on the other hand, does exhibit E_D (c=o) increasing with penetrant size if previous data is included (20, 84) : FMS - H_2O, E_D = 16.7 kJ . mol^{-1} and FMS - MeOH, E_D = 25.1 kJ . mol^{-1}. This is a consequence of the bulky trifluoropropyl group reducing segmental motions within the polymer matrix (D a factor of 8 lower than PDMS) and hence penetrant size becomes important.

All systems exhibit E_D increasing with increasing concentration in agreement with that expected qualitatively from the clustering analysis. The presence of clusters provide a more tortuous path length

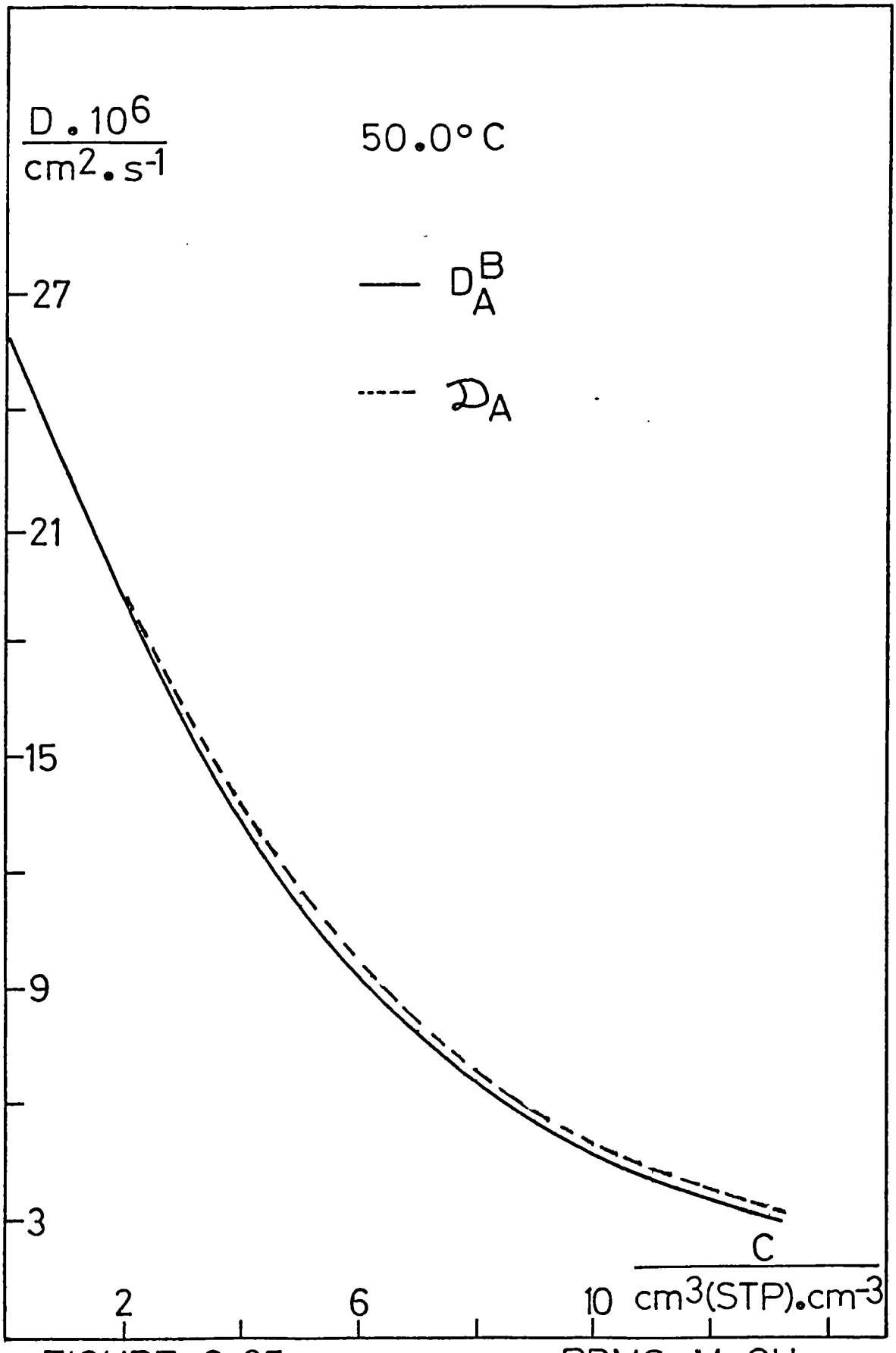


FIGURE 6.35 PDMS–MeOH
INTRINSIC DIFFUSION COEFFICIENTS

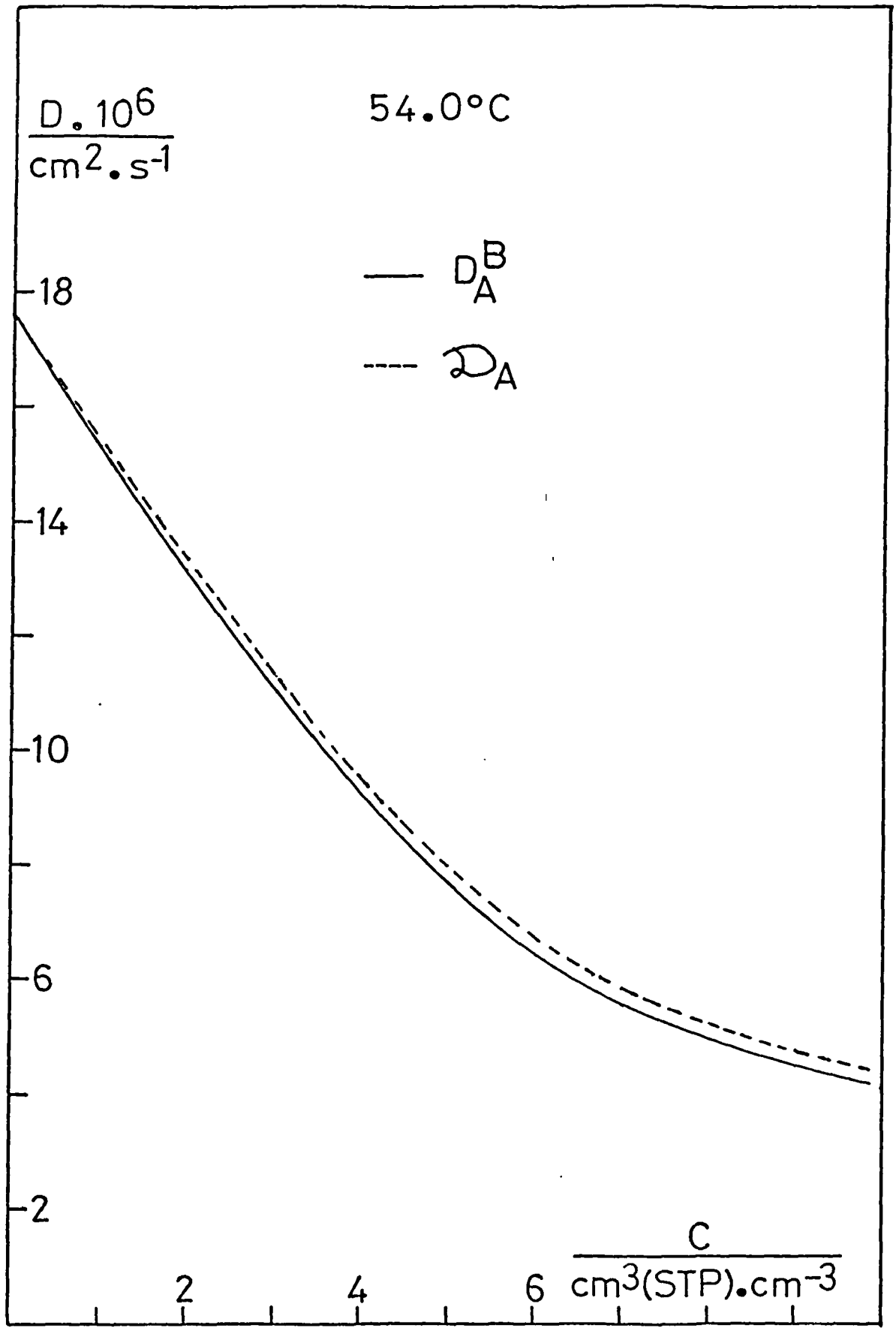


FIGURE 6.36 PDMS-EtOH
INTRINSIC DIFFUSION COEFFICIENTS

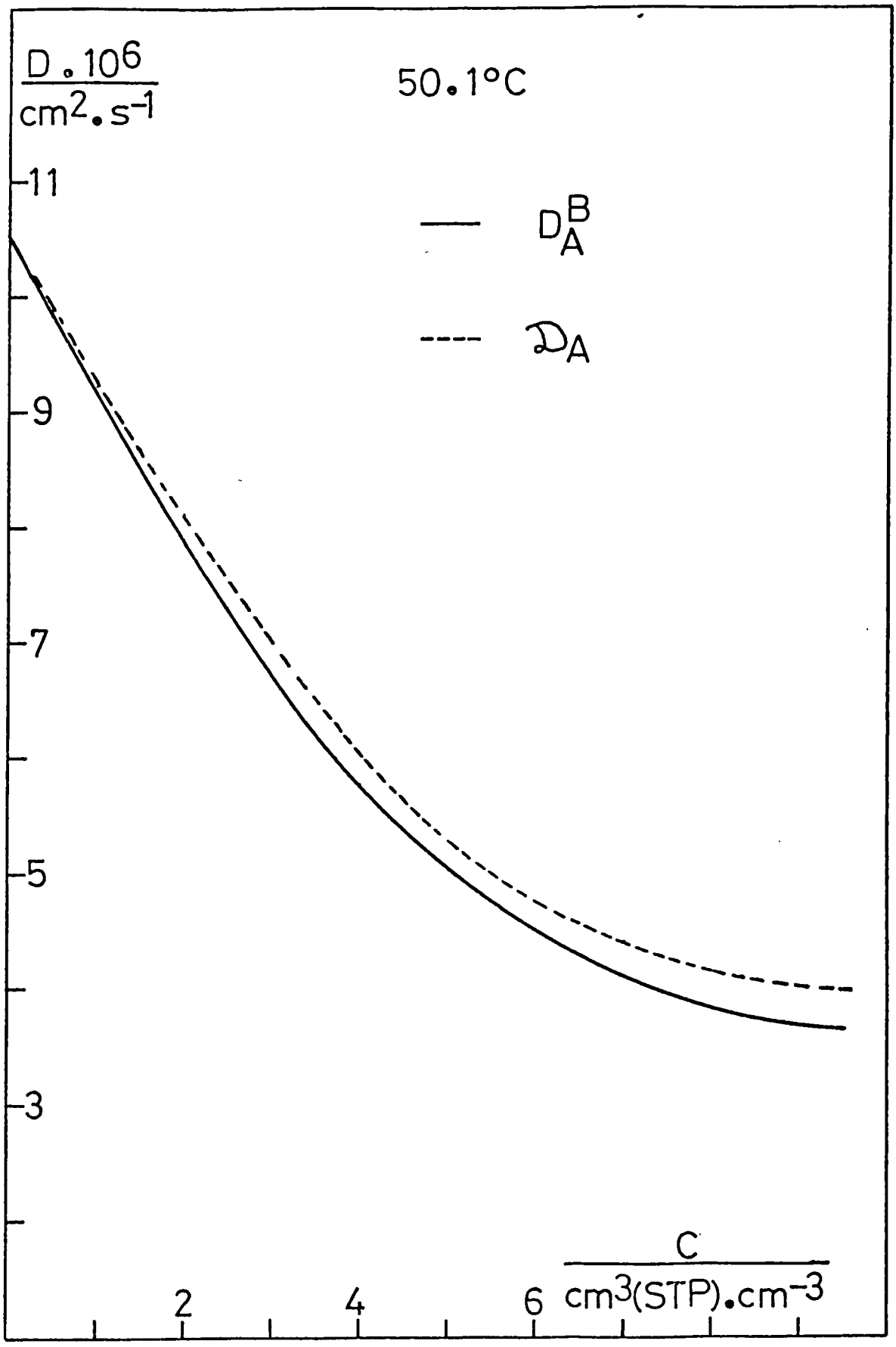


FIGURE 6.37 PDMS–(2-PrOH)
INTRINSIC DIFFUSION COEFFICIENTS

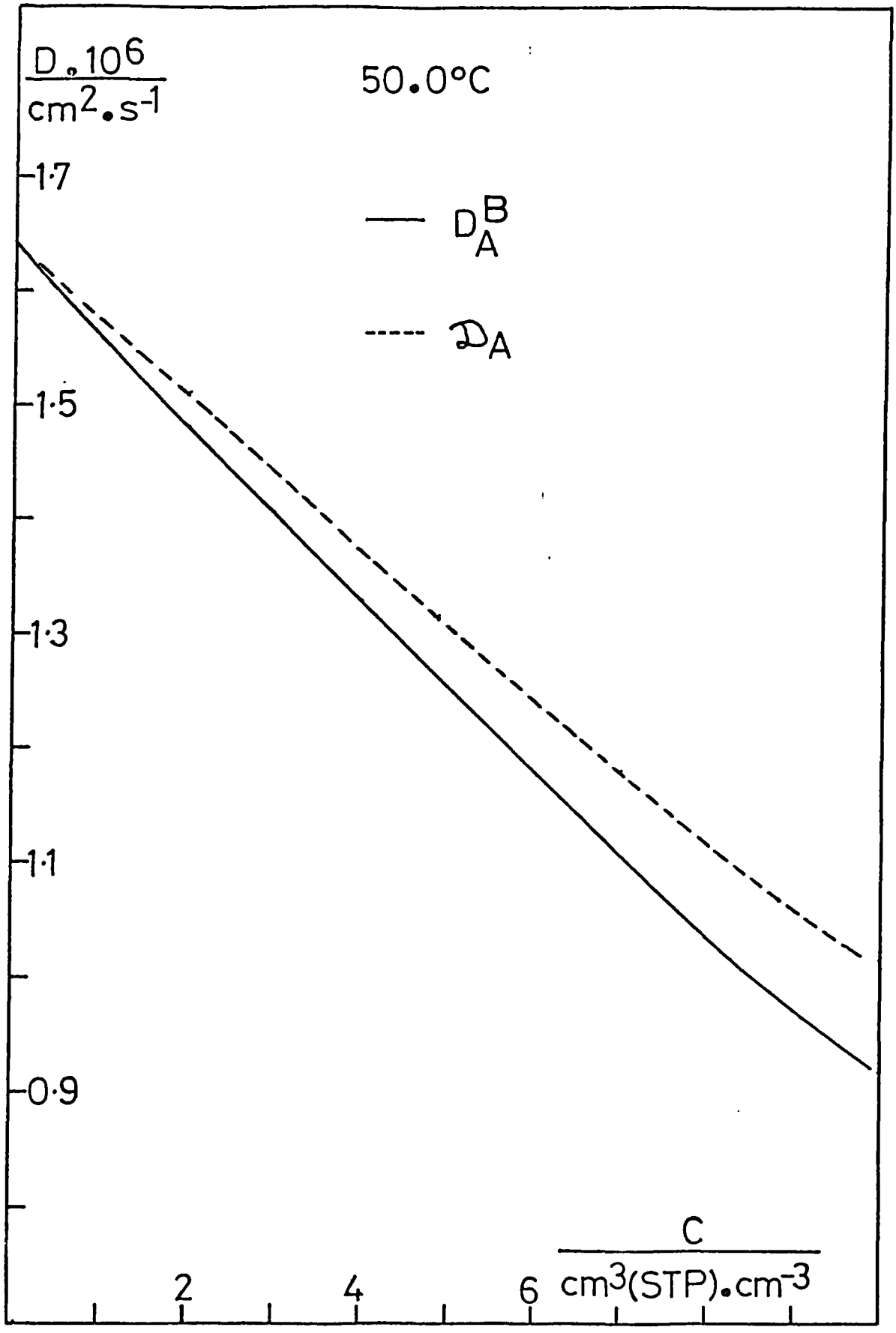


FIGURE 6.38 FMS-(2-PrOH)
INTRINSIC DIFFUSION COEFFICIENTS

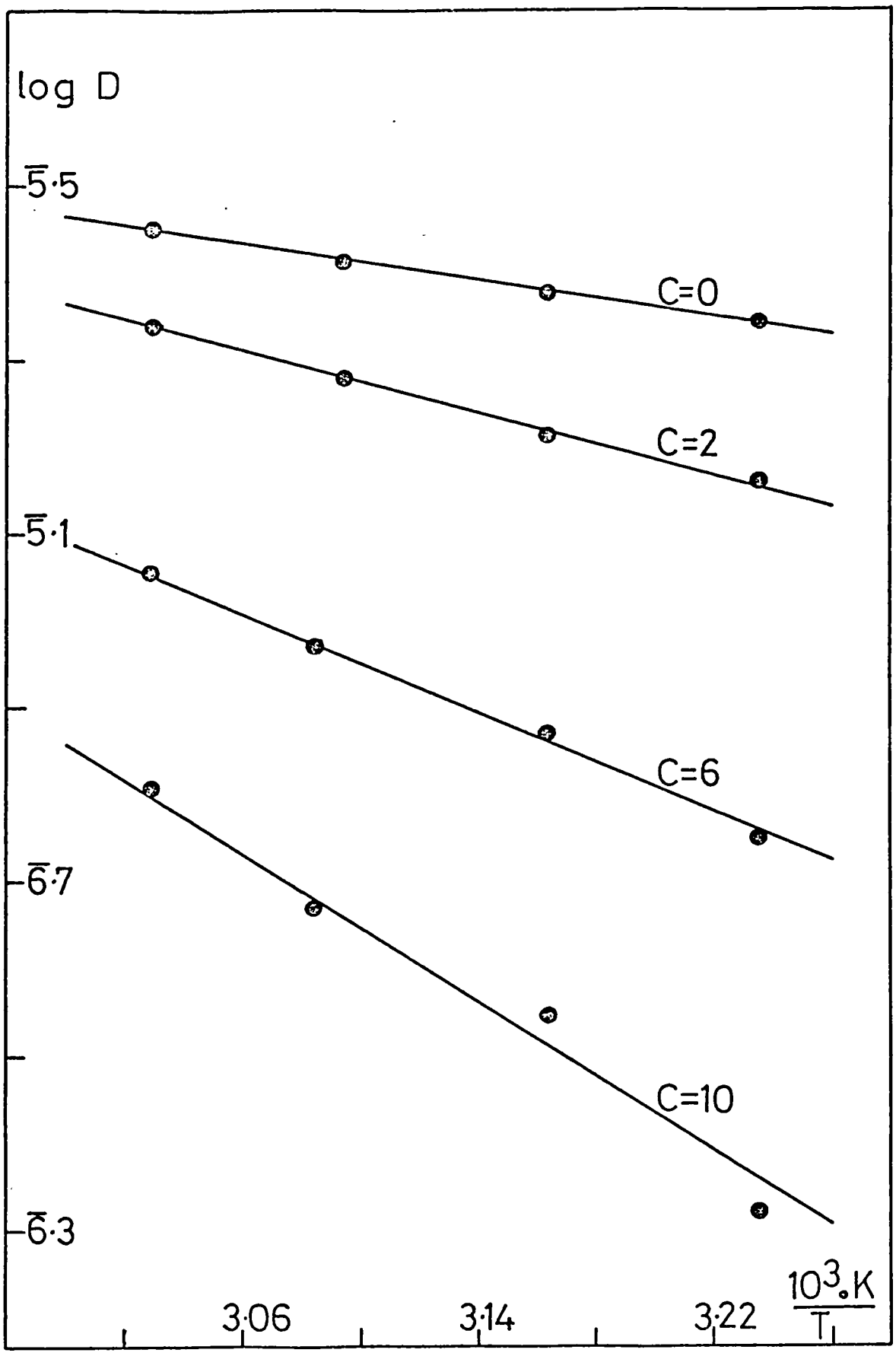


FIGURE 6.39 PDMS–MeOH
TEMPERATURE VARIATION OF DIFFUSIVITY

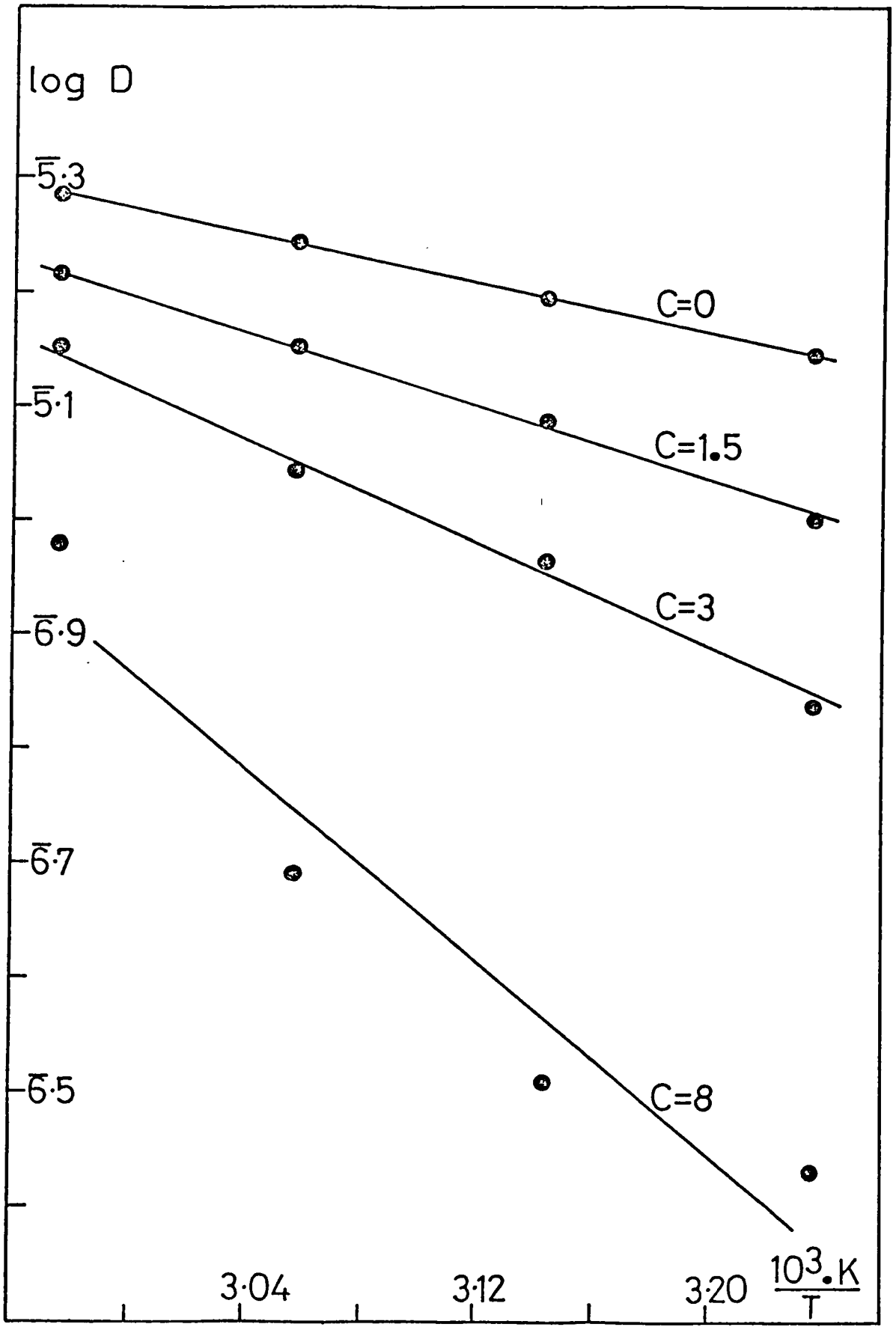


FIGURE 6.40 PDMS-EtOH
TEMPERATURE VARIATION OF DIFFUSIVITY

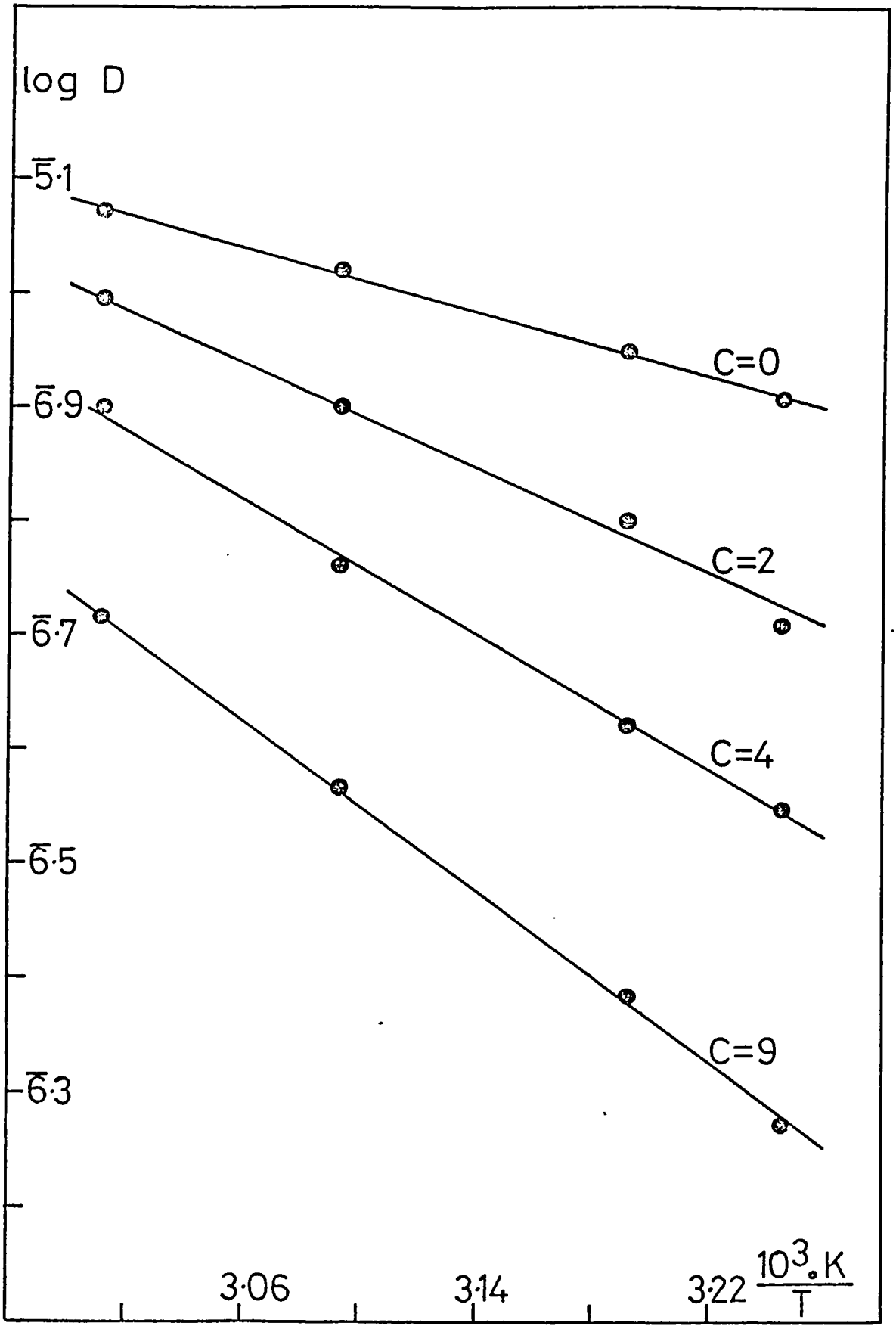


FIGURE 6.41 PDMS–(2-PrOH)
TEMPERATURE VARIATION OF DIFFUSIVITY

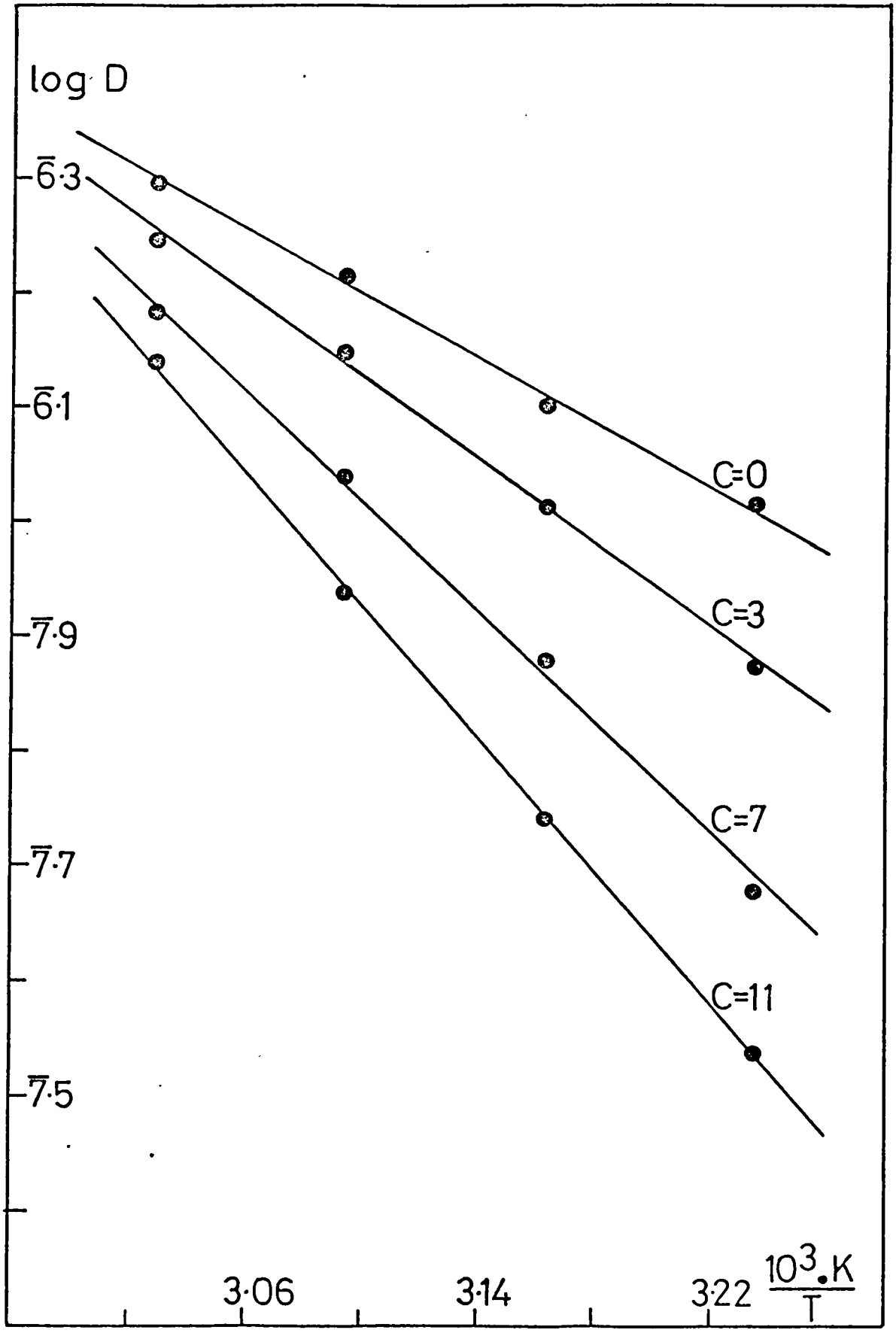


FIGURE 6.42 FMS–(2-PrOH)
TEMPERATURE VARIATION OF DIFFUSIVITY

Table 6.8

Values of E_D (kJ . mol^{-1}) at various Concentrations (C, cm^3 (S.T.P.) . cm^{-3})

System	T°C	C	E_D
PDMS - MeOH	36 - 57	0	10.0
		2	16.9
		6	28.5
		10	44.0
PDMS - EtOH	36 - 63	0	10.4
		1.5	15.9
		3	22.6
		8	40.2
PDMS -(2-PrOH)	35 - 59	0	13.6
		2	21.9
		4	28.6
		9	35.8
FMS -(2-PrOH)	36 - 57	0	26.8
		3	35.3
		7	47.2
		11	60.0

for the penetrant molecule and reduces the mobility of the polymer segments. The relative increase of E_D decreases for increasing penetrant size and for FMS due to the lower clustering tendencies as polymer-penetrant interactions become more prominent.

CHAPTER 7

CONCLUSIONS

7.1 Summary and Reappraisal of Results

A number of interesting features have emerged during the course of this work and the principal points are discussed in this Section.

7.1.1 Heterogeneous Media

Although patents have been granted for the preparation of the P(DMS-g-VAc) system, the method of mutual irradiation for this type of system has been established. It was found to be comparatively straightforward to prepare copolymers containing up to 25% PVAc by volume but, from this point on, it was progressively more difficult to prepare copolymers with higher PVAc contents. Perhaps the most promising method of producing systems containing PVAc as the major component is by the use of blends of the two homopolymers. Provided that some control over the composition can be maintained during the irradiation process, it ought to be possible to graft some PVAc onto PDMS gum. By blending this with homopolymeric PVAc a high content PVAc film can be prepared in which the minor component (PDMS) is not present as large aggregates.

A study of water transport in these systems is particularly relevant to the growing knowledge concerning heterogeneous media (Chapter 4) in that this appears to be an ideal system which is well characterised. Thus both homopolymers are amorphous and above their respective glass transition temperatures in the temperature range studied so that most anomalies associated with the transition should be absent. Characterisation of the copolymers revealed a two-phase system with PDMS as the continuum and with PVAc present within discrete spherical domains of uniform size. There appears to be complete phase separation within these systems as indicated by the fact that both the density and solubility of any copolymer was found to be a linear combination of the contributions of each phase.

A permeability analysis was undertaken in order to compare experimental data with those predicted by some of the available models derived for this type of system. The ones chosen are those which are not entirely empirical by nature and which have had some degree of success when applied to other systems. It was found that those models

derived for a random lattice of domains and which included domain interactions, namely the Higuchi, Böttcher and Bruggeman models, gave the better representations of the experimental data. Of these the Higuchi model appears to be the best fit in the range 0-40% PVAc region which was the main testing ground of the comparison. However the approach of Böttcher offers distinct advantages over the others in that it spans the whole of the composition range in the sense that one set of data could be generated irrespective of which phase was deemed continuous, in contrast to the other models which generated one set of data for each component as the continuum. Hence the permeability behaviour of such systems could be predicted to a high degree of accuracy by the Böttcher model over the whole of the composition range which naturally includes the phase inversion region. The Maxwell, Rayleigh-Runge, Meredith & Tobias, Wagner and Series/Parallel models were reasonable representations but are not as accurate as the above models.

It was found that, for these systems in which there is only a factor of 5 in the permeabilities of the homopolymers, it is relatively difficult to differentiate accurately between the various models in the region of PDMS continuous (high P). On the other hand the low P region with PVAc continuous differentiates to a relatively greater extent between the models as domain-domain and domain-continuum interactions become important. Therefore, in order to ascertain conclusively which model is the best representation of experimental data, further work should be undertaken, with this system or another, in the region where the disperse phase has the higher permeability.

Transient diffusion measurements have been undertaken for these systems in order to assess whether any non-Fickian features are introduced by the presence of two phases. In practice it was found that the domains were of such small size (radius less than 100 nm) that transient and steady-state results were in reasonable agreement. However the possibility of pseudo-Fickian mechanisms of diffusion could not be ruled out for results obtained close to the glass transition temperature of PVAc. For both steady-state and transient techniques, D decreased with increased concentration of penetrant as a consequence of the enhanced immobilisation of penetrant within the PVAc domains as sorption of penetrant increases.

7.1.2 Alcohol Vapour Transport

The main theme that emerged from this analysis was that, despite increasing plasticisation of the polymer as penetrant size (hydrophic content) increases, the dominant feature is still clustering of penetrant through hydrogen-bond formation. Comparisons with theoretical models based on the Polycondensation approach showed reasonable agreement; however the model contains an adjustable parameter which facilitates the sorption isotherm fit. The D-C relationships derived from the Polycondensation model were not in particularly good agreement with experimental results since plasticisation showed its presence more clearly.

Confirmation of the relationships between solubility, diffusivity and penetrant molar volume ensured that it is possible, with a reasonable degree of certainty, to estimate solubility, diffusivity and permeability data for any penetrant within these systems.

Time lag data show interesting trends in that, for the diffusion of ethanol and 2-propanol in PDMS, measured time lags increase with increasing concentration. This is consistent with the D decreasing with increasing concentration as obtained from steady-state measurements, and is one of the few systems for which this has been found. Due to the small variation of the time lags and the difficulty in establishing the time lag at zero concentration, it was not possible to determine the corresponding D-C relationships derived from this data.

7.1.3 Water Vapour Permeation

A major problem was found when pressures were monitored on a Baratron as water sorbed into the ceramic supports of the capacitance electrodes. A calibration was thus necessary to convert these measured permeabilities into those measured by a spring-permeation technique for which no such problem was present. The reduction in measured permeability as measured by the Baratron was reproducible and only depended upon the flux-rate of penetrant through the membrane and was found to be independent of the temperature of the membrane and Baratron and of the outgoing volume. The use of a single-sided Baratron should overcome this difficulty.

CHAPTER 8

APPENDIX

8.1 Scanning Electron Microscopy

Typical electron micrographs are shown here to illustrate the size and distribution of the disperse phase. In each case, the white regions are those of PVAc whilst the dark ones are PDMS and these represent scattering of the electrons, presumably by the silicon atoms. The magnification of the micrographs is given in Table 8.1, there being some magnification due to enlargement of the negatives as well as the inherent magnification of the microscope.

TABLE 8.1

Magnification of the Electron Micrographs

ϕ(PVAc)	Figure	Magnification	Figure	Magnification
0.034	8.2	80,000		
0.093	8.1	80,000		
0.157	8.3	106,000	8.4	53,000
0.214	8.5	160,000	8.6	32,000
0.442	8.7	20,000	8.8	44,000

The average radii and ranges of the domains are given in Table 5.1.

8.2 Basic Experimental Data

The following symbols will be used throughout this section.

V = Volume of polymer (cm^3)

C = Concentration of sorbed penetrant (cm^3(S.T.P.).cm^{-3})

p = Pressure of penetrant vapour (cm Hg)

p_o = Saturated vapour pressure of penetrant at the membrane temperature (cm Hg)

T_m = Membrane temperature (^oC)

T_b = Microbalance head temperature (^oC)

k = Sorption-spring sensitivity ($cm.g^{-1}$)

K = Permeation-spring sensitivity ($cm.g^{-1}$)

A = Cross-section area of membrane available for permeation (cm^2)

ℓ = Membrane thickness (cm)

J = Steady-state permeation flux (cm^3(S.T.P.).$cm^{-2}.s^{-1}$)

V = "Down-stream" volume (cm^3)

L = Time Lag (s)

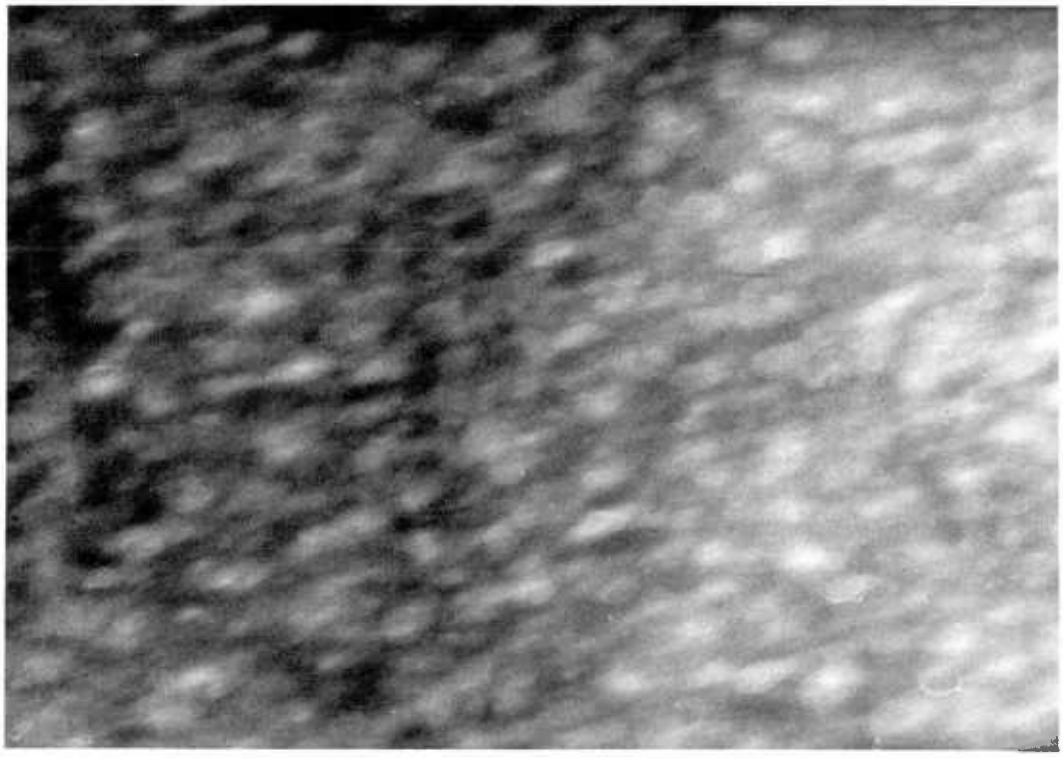


FIGURE 8.1 P(DMS-g-0.093 VAc)

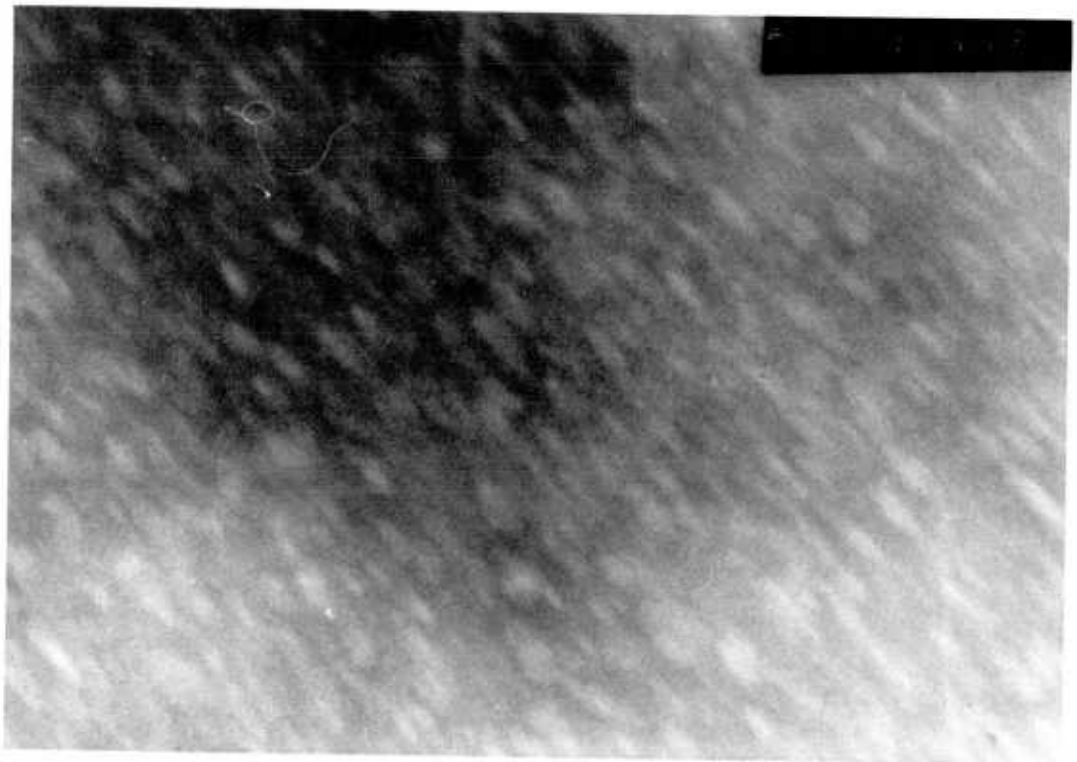


FIGURE 8.2 P(DMS-g-0.034 VAc)

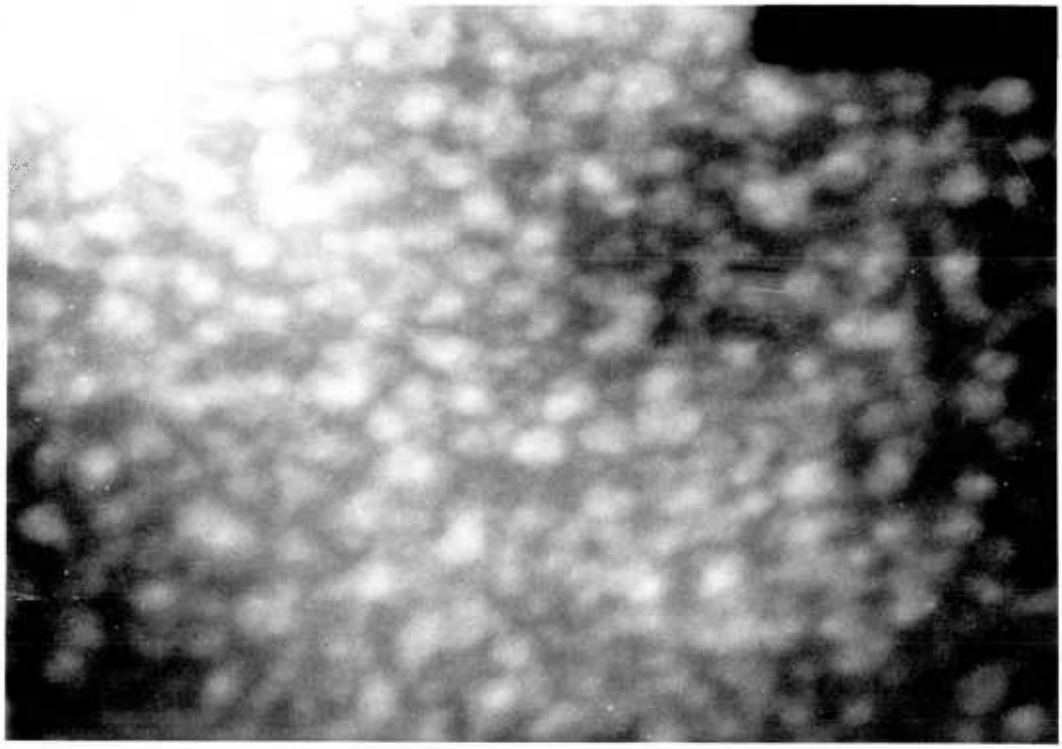


FIGURE 8.3 P(DMS-g-0.157 VAc)

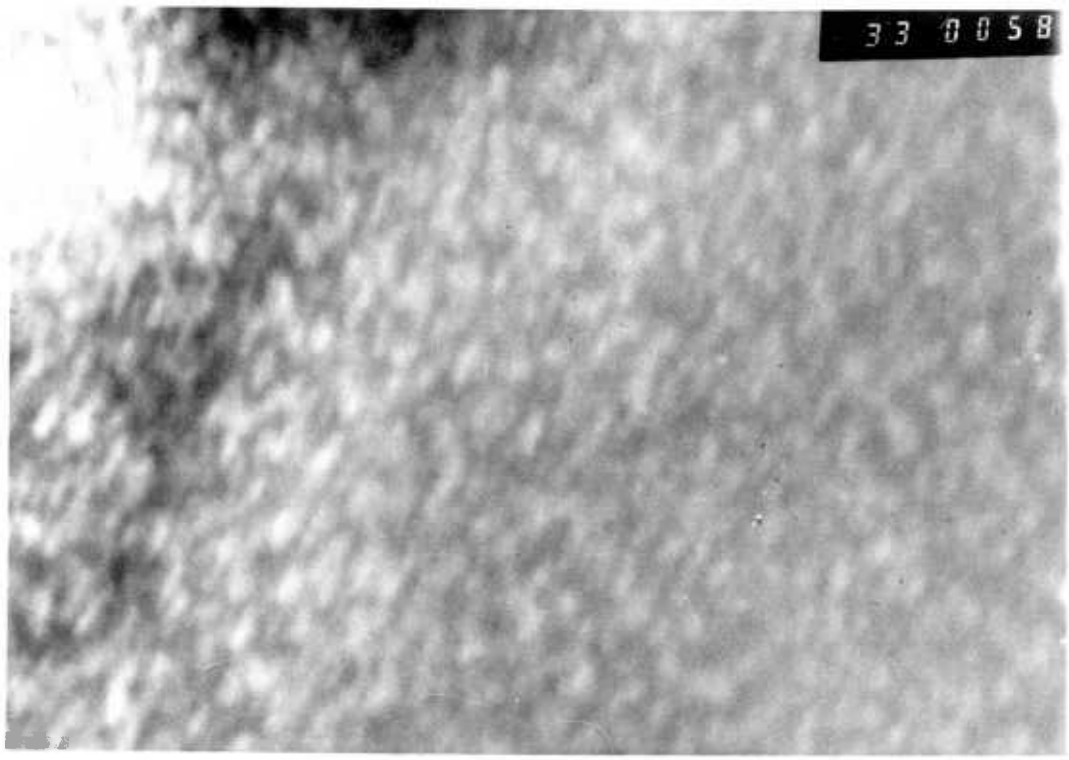


FIGURE 8.4 P(DMS-g-0.157 VAc)

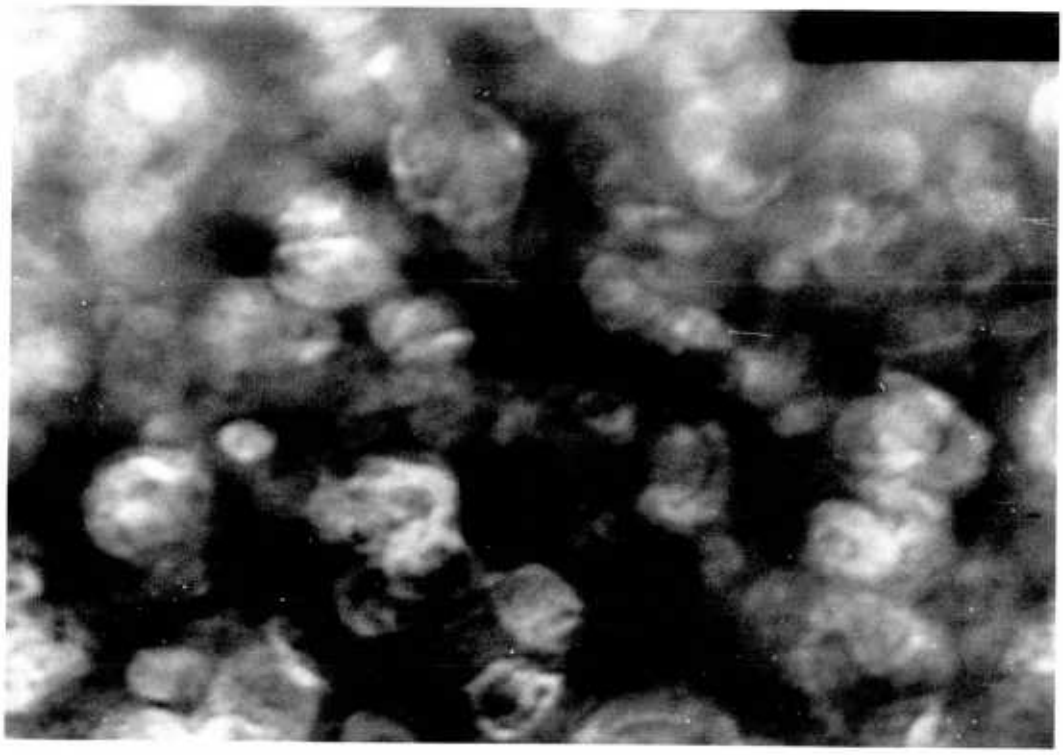


FIGURE 3.5 P(DMS-g-0.214 VAc)

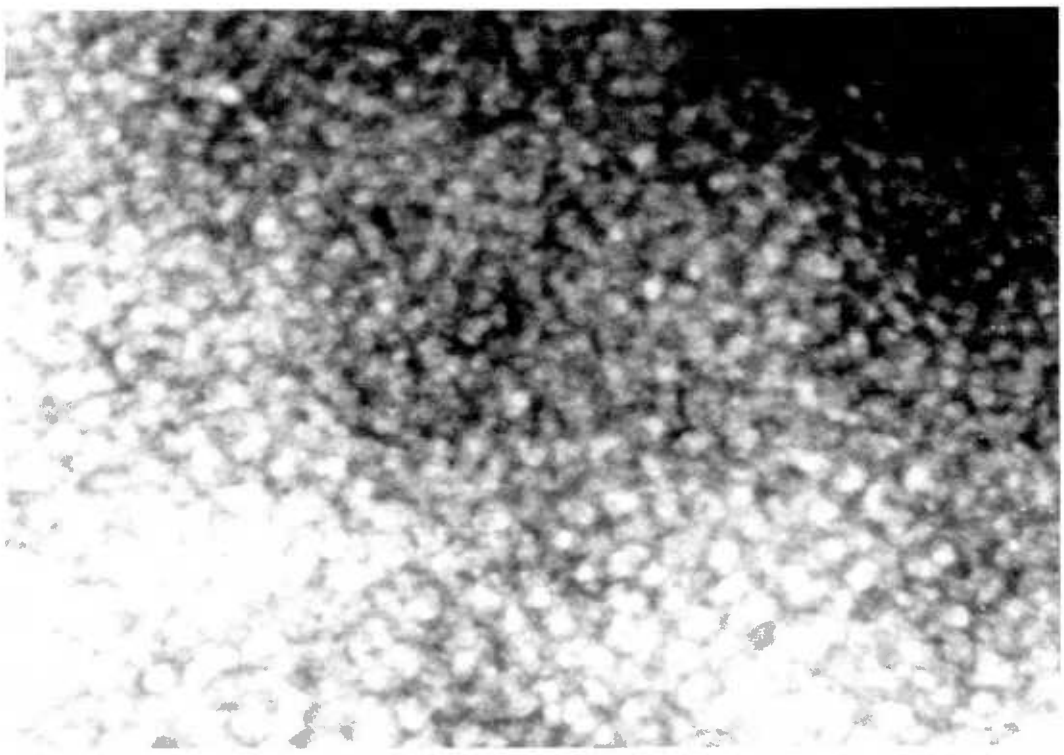


FIGURE 3.6 P(DMS-g-0.214 VAc)

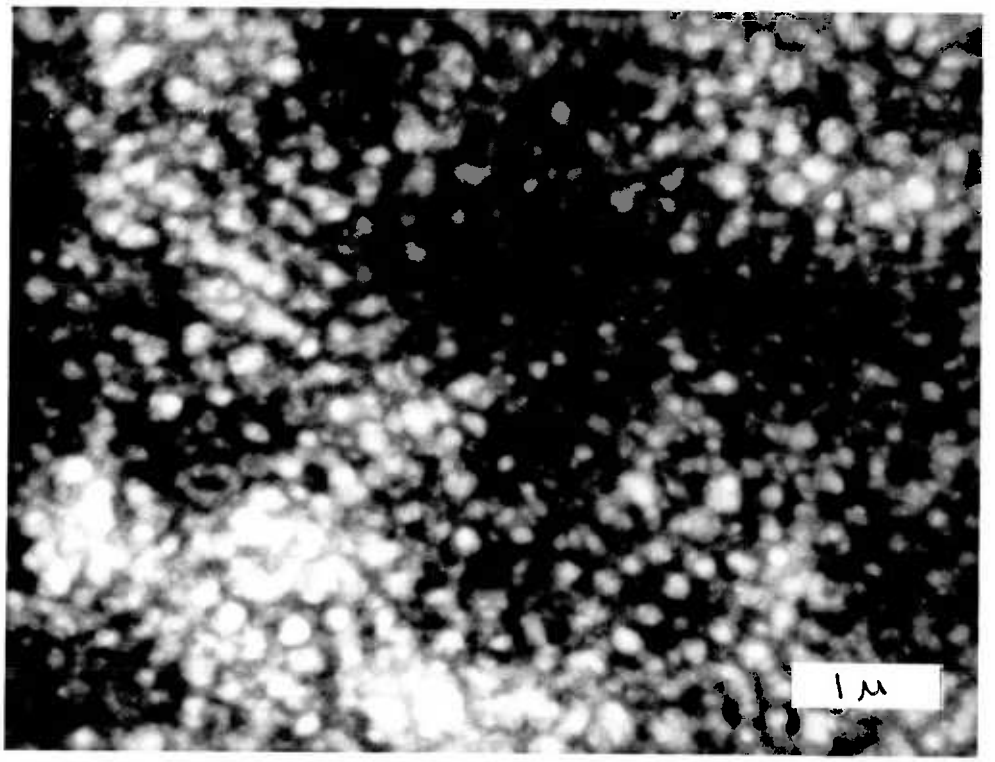


FIGURE 8.7 P(DMS-g-0.442 VAc)

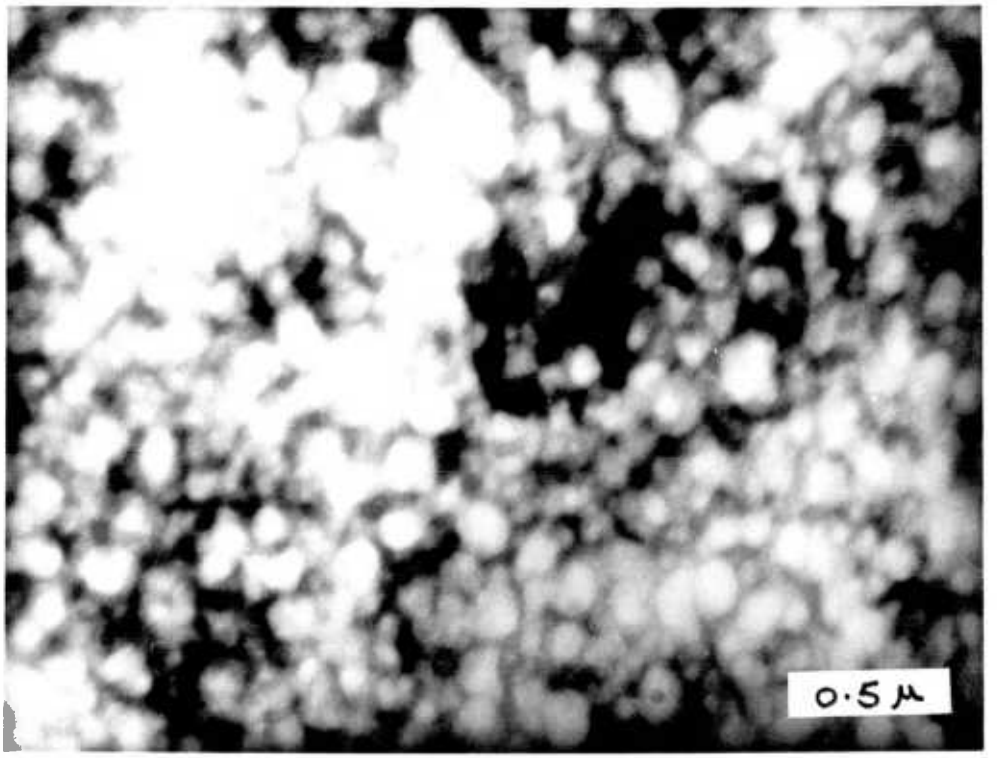


FIGURE 8.3 P(DMS-g-0.442 VAc)

M_t = Weight of penetrant sorbed at time t (μg)

M_∞ = Weight of penetrant sorbed at equilibrium (μg)

X = Pressure-transducer calibration ((cm Hg).mv^{-1})

$\bar{D}_s, \bar{D}_d$ = Average sorption-(desorption-) kinetic diffusion coefficient ($cm^2.s^{-1}$)

$\bar{D}_{av} = 1/2\ (\bar{D}_s + \bar{D}_d)$

8.2.1 Equilibrium Sorption Results

Sorption data for water vapour in P(DMS-g-VAc) copolymers were measured on a microbalance and alcohol vapours in PDMS and FMS on a calibrated spring-balance.

All concentrations include buoyancy and blank isotherm corrections where appropriate. Some constants applicable to the sorption measurements are given below.

microbalance : 1 cm^3 (S.T.P.) ≡ 805 μg

X ≡ 1.130

calibrated spring : k ≡ 32.11

X ≡ 1.795

1 mole vapour ≡ 22414 cm^3 (S.T.P.)

The volume of polymer used in each measurement is given in the respective Tables.

TABLE 8.2

PDMS - H_2O ($V = 0.7540\ cm^3$)

$T_m = 35.0^oC$		$T_m = 42.0^oC$		$T_m = 49.0^oC$		$T_m = 55.0^oC$	
$p_o = 4.214$		$p_o = 6.146$		$p_o = 8.800$		$p_o = 11.80$	
$T_b = 43.0^oC$		$T_b = 49.3^oC$		$T_b = 57.0^oC$		$T_b = 61.4^oC$	
p/p_o	C	p/p_o	C	p/p_o	C	p/p_o	C
0.130	0.061	0.100	0.059	0.093	0.064	0.130	0.108
0.235	0.109	0.250	0.154	0.189	0.134	0.260	0.217
0.310	0.147	0.453	0.271	0.241	0.167	0.351	0.294
0.360	0.166	0.501	0.301	0.281	0.196	0.477	0.403
0.408	0.193	0.600	0.373	0.372	0.263	0.630	0.553
0.483	0.239	0.702	0.455	0.467	0.333	0.695	0.633
0.510	0.244	0.808	0.563	0.548	0.400	0.787	0.738
0.595	0.312	0.845	0.608	0.639	0.485	0.839	0.809
0.621	0.309	0.924	0.750	0.749	0.584	0.860	0.840
0.728	0.390			0.755	0.600	0.913	0.982
0.731	0.409			0.850	0.714	0.915	1.036
0.849	0.512			0.900	0.802		
0.862	0.545			0.914	0.868		
0.897	0.611			0.946	1.013		
0.900	0.616						
0.920	0.654						

TABLE 8.3

P(DMS - g - 0.034 VAc) - H_2O (V = 0.9319 cm^3)

T_m = 35.0°C p_o = 4.214 T_b = 41.6°C		T_m = 42.0°C p_o = 6.146 T_b = 49.0°C		T_m = 49.0°C p_o = 8.800 T_b = 55.6°C		T_m = 55.0°C p_o = 11.80 T_b = 60.3°C	
p/p_o	C	p/p_o	C	p/p_o	C	p/p_o	C
0.055	0.074	0.056	0.094	0.068	0.115	0.076	0.141
0.142	0.206	0.132	0.214	0.119	0.209	0.100	0.192
0.160	0.244	0.176	0.293	0.197	0.363	0.157	0.307
0.171	0.258	0.198	0.332	0.239	0.435	0.201	0.379
0.191	0.277	0.235	0.399	0.306	0.575	0.256	0.505
0.235	0.353	0.260	0.457	0.367	0.698	0.257	0.517
0.241	0.357	0.283	0.495	0.380	0.729	0.346	0.692
0.283	0.448	0.357	0.645	0.454	0.907	0.388	0.803
0.361	0.539	0.381	0.680	0.530	1.078	0.464	0.957
0.386	0.612	0.435	0.777	0.600	1.284	0.551	1.191
0.396	0.624	0.460	0.850	0.657	1.479	0.660	1.560
0.422	0.708	0.528	1.013	0.721	1.696	0.728	1.857
0.492	0.810	0.588	1.165	0.759	1.869	0.793	2.092
0.558	0.996	0.605	1.204	0.807	2.080	0.838	2.404
0.637	1.156	0.679	1.424	0.848	2.305	0.884	2.708
0.678	1.315	0.684	1.475	0.875	2.463	0.919	3.047
0.750	1.504	0.737	1.642	0.902	2.757	0.947	3.109
0.788	1.675	0.769	1.780	0.932	2.933		
0.873	2.105	0.782	1.793				
0.876	2.064	0.825	2.009				
0.924	2.489	0.858	2.206				
0.936	2.462	0.902	2.526				
0.951	2.690	0.920	2.653				

TABLE 8.4

P(DMS - g - 0.093 VAc) - H_2O ($V = 0.8873\ cm^3$)

$T_m = 35.0^oC$		$T_m = 42.0^oC$		$T_m = 49.0^oC$		$T_m = 55.0^oC$	
$p_o = 4.214$		$p_o = 6.146$		$p_o = 8.800$		$p_o = 11.80$	
$T_b = 42.0^oC$		$T_b = 49.8^oC$		$T_b = 57.0^oC$		$T_b = 62.4^oC$	
p/p_o	C	p/p_o	C	p/p_o	C	p/p_o	C
0.122	0.386	0.080	0.283	0.080	0.296	0.116	0.494
0.184	0.570	0.154	0.509	0.194	0.788	0.137	0.592
0.226	0.702	0.171	0.586	0.213	0.832	0.167	0.707
0.323	1.111	0.201	0.712	0.335	1.393	0.224	0.981
0.382	1.268	0.235	0.821	0.395	1.689	0.299	1.305
0.396	1.434	0.301	1.102	0.399	1.699	0.368	1.634
0.433	1.554	0.368	1.360	0.492	2.176	0.425	1.984
0.439	1.572	0.402	1.551	0.561	2.659	0.495	2.347
0.459	1.626	0.419	1.610	0.638	3.190	0.522	2.491
0.527	1.972	0.497	2.022	0.651	3.235	0.590	3.034
0.555	2.137	0.540	2.273	0.687	3.656	0.601	3.059
0.643	2.720	0.687	3.246	0.801	4.716	0.702	3.851
0.659	2.695	0.702	3.326	0.813	4.857	0.729	4.174
0.675	2.972	0.784	4.065	0.853	5.427	0.799	4.973
0.733	3.299	0.822	4.243	0.907	6.303	0.823	5.247
0.832	4.207	0.844	4.660	0.925	6.621	0.824	5.290
0.882	4.774	0.871	4.946			0.895	6.284
0.920	5.520	0.927	5.683			0.923	6.783
		0.952	6.636				

TABLE 8.5

P(DMS - g - 0.157 VAc) - H_2O (V = 0.6939 cm^3)

T_m = 35.0°C p_o = 4.214 T_b = 36.0°C		T_m = 42.0°C p_o = 6.146 T_b = 43.1°C		T_m = 49.0°C p_o = 8.800 T_b = 51.6°C		T_m = 55.0°C p_o = 11.80 T_b = 56.7°C	
p/p_o	C	p/p_o	C	p/p_o	C	p/p_o	C
0.091	0.421	0.057	0.318	0.067	0.353	0.040	0.216
0.115	0.530	0.064	0.332	0.071	0.377	0.103	0.612
0.160	0.761	0.072	0.353	0.088	0.503	0.167	0.981
0.193	0.957	0.081	0.389	0.112	0.612	0.203	1.150
0.244	1.199	0.103	0.504	0.144	0.820	0.240	1.463
0.318	1.638	0.125	0.617	0.162	0.890	0.282	1.693
0.365	1.945	0.159	0.848	0.249	1.423	0.323	2.052
0.442	2.508	0.173	0.835	0.256	1.463	0.378	2.392
0.475	2.737	0.230	1.243	0.277	1.576	0.415	2.704
0.528	3.121	0.254	1.330	0.351	2.135	0.477	3.276
0.582	3.742	0.292	1.578	0.397	2.447	0.519	3.589
0.611	4.011	0.335	1.881	0.460	2.960	0.568	4.161
0.676	4.525	0.396	2.287	0.528	3.537	0.630	4.838
0.708	5.000	0.428	2.527	0.555	3.749	0.688	5.594
0.768	5.927	0.452	2.713	0.613	4.393	0.730	6.328
0.805	6.565	0.517	3.240	0.656	4.875	0.774	7.124
0.848	7.271	0.570	3.774	0.700	5.507	0.817	7.967
0.904	8.770	0.642	4.502	0.741	6.048	0.883	9.582
0.929	9.720	0.701	5.271	0.778	6.639		
		0.741	5.835	0.811	7.371		
		0.789	6.712	0.859	8.424		
		0.851	7.905	0.917	9.940		
		0.901	9.301				

TABLE 8.6

P(DMS - g - 0.214 VAc) - H_2O ($V = 0.7528\ cm^3$)

$T_m = 35.0^oC$		$T_m = 42.0^oC$		$T_m = 49.0^oC$		$T_m = 55.0^oC$	
$p_o = 4.214$		$p_o = 6.146$		$p_o = 8.800$		$p_o = 11.80$	
$T_b = 37.5^oC$		$T_b = 46.5^oC$		$T_b = 51.3^oC$		$T_b = 56.4^oC$	
p/p_o	C	p/p_o	C	p/p_o	C	p/p_o	C
0.121	0.665	0.059	0.368	0.082	0.556	0.103	0.786
0.204	1.218	0.149	0.939	0.185	1.306	0.180	1.359
0.284	1.822	0.195	1.338	0.321	2.465	0.309	2.460
0.405	2.848	0.217	1.460	0.401	3.207	0.453	3.950
0.493	3.743	0.244	1.682	0.508	4.456	0.523	4.830
0.649	5.646	0.287	1.958	0.571	5.203	0.585	5.637
0.697	6.491	0.332	2.380	0.645	6.341	0.698	7.493
0.826	8.980	0.370	2.721	0.701	7.194	0.767	9.103
0.904	11.24	0.405	3.120	0.765	8.591	0.824	10.66
		0.436	3.338	0.847	10.65	0.901	13.40
		0.440	3.375	0.900	12.63		
		0.444	3.380				
		0.495	3.925				
		0.590	5.132				
		0.598	5.167				
		0.699	6.766				
		0.783	8.478				
		0.793	8.700				
		0.853	10.06				
		0.896	11.55				

TABLE 8.7

P(DMS - g ÷ 0.442 VAc) - H_2O (V = 0.4365 cm^3)

T_m = 35.0°C p_o = 4.214 T_b = 36.2°C		T_m = 42.0°C p_o = 6.146 T_b = 43.3°C		T_m = 49.0°C p_o = 8.800 T_b = 50.0°C		T_m = 55.0°C p_o = 11.80 T_b = 56.5°C	
p/p_o	C	p/p_o	C	p/p_o	C	p/p_o	C
0.113	1.310	0.107	1.361	0.102	1.414	0.102	1.528
0.194	2.334	0.188	2.585	0.120	1.724	0.220	3.488
0.335	4.373	0.199	2.612	0.213	3.105	0.317	5.277
0.464	6.682	0.256	3.628	0.317	4.939	0.412	7.258
0.542	8.363	0.322	4.620	0.419	6.968	0.508	9.620
0.660	11.45	0.364	5.456	0.522	9.395	0.601	12.37
0.787	16.34	0.384	5.740	0.618	12.21	0.697	15.90
0.845	19.58	0.465	7.463	0.715	15.81	0.770	19.04
0.888	23.04	0.575	10.14	0.772	18.79	0.834	23.48
		0.647	12.23	0.853	24.19	0.836	22.99
		0.736	15.52	0.900	28.61	0.897	28.85
		0.800	19.16				
		0.820	19.88				
		0.852	22.17				
		0.884	24.58				
		0.888	26.28				

TABLE 8.8

PVAc - H_2O ($V = 0.1585\ cm^3$)

$T_m = 35.0^oC$		$T_m = 42.0^oC$		$T_m = 49.0^oC$		$T_m = 55.0^oC$	
$p_o = 4.214$		$p_o = 6.146$		$p_o = 8.800$		$p_o = 11.80$	
$T_b = 46.5^oC$		$T_b = 52.4^oC$		$T_b = 60.4^oC$		$T_b = 63.6^oC$	
p/p_o	C	p/p_o	C	p/p_o	C	p/p_o	C
0.103	2.919	0.090	2.672	0.082	2.562	0.078	2.617
0.123	3.496	0.117	3.182	0.105	3.347	0.082	2.876
0.189	5.328	0.191	5.409	0.212	6.862	0.163	5.407
0.251	7.353	0.215	6.599	0.291	9.722	0.174	5.913
0.266	7.808	0.252	7.358	0.407	14.45	0.221	7.498
0.363	11.25	0.263	7.680	0.498	18.94	0.277	9.660
0.405	12.87	0.340	10.90	0.612	25.83	0.315	11.15
0.405	13.27	0.347	11.25	0.702	32.63	0.366	13.50
0.498	16.77	0.418	14.36	0.777	39.69	0.417	15.78
0.585	22.00	0.493	18.00	0.846	48.36	0.470	18.55
0.622	23.65	0.555	20.49	0.903	57.63	0.568	24.33
0.653	25.70	0.616	24.79			0.651	30.31
0.746	34.27	0.701	30.56			0.725	36.67
0.756	32.29	0.751	34.76			0.782	42.28
0.791	37.52	0.774	37.64			0.834	49.01
0.873	46.14	0.827	44.28			0.867	54.09
0.900	50.49	0.861	46.92				
		0.892	53.38				

TABLE 8.9

PDMS - MeOH ($V = 0.8299\ cm^3$)

$T_m = 36.0^oC$ $p_o = 21.52$		$T_m = 43.0^oC$ $p_o = 29.85$		$T_m = 50.0^oC$ $p_o = 40.60$		$T_m = 57.0^oC$ $p_o = 55.07$	
p/p_o	C	p/p_o	C	p/p_o	C	p/p_o	C
0.149	0.563	0.135	0.650	0.104	0.573	0.089	0.579
0.205	0.839	0.208	0.990	0.178	0.974	0.094	0.504
0.286	1.227	0.283	1.462	0.263	1.406	0.180	1.080
0.425	1.997	0.298	1.467	0.332	1.989	0.345	2,229
0.495	2.514	0.375	1.913	0.415	2.421	0.477	3.386
0.582	3.244	0.402	2.237	0.477	3.080	0.574	4.442
0.666	4.132	0.465	2.731	0.531	3.484	0.673	5.867
0.757	5.388	0.520	3.170	0.598	4.211	0.755	7.597
0.817	6.638	0.614	3.963	0.622	4.511	0.823	9.764
0.887	8.939	0.660	4.478	0.678	5.350	0.902	13.33
0.909	10.07	0.750	5.900	0.742	6.403		
		0.814	7.365	0.785	7.447		
		0.848	8.585	0.836	8.992		
		0.887	10.33	0.891	11.33		
		0.942	12.95				

TABLE 8.10

PDMS - EtOH ($V = 0.7536\ cm^3$)

$T_m = 36.0^oC$ $p_o = 10.95$		$T_m = 45.0^oC$ $p_o = 17.40$		$T_m = 54.0^oC$ $p_o = 26.80$		$T_m = 63.0^oC$ $p_o = 40.59$	
p/p_o	C	p/p_o	C	p/p_o	C	p/p_o	C
0.051	0.168	0.053	0.253	0.052	0.299	0.039	0.261
0.107	0.458	0.092	0.463	0.080	0.509	0.039	0.281
0.121	0.661	0.154	0.818	0.099	0.616	0.112	0.820
0.177	0.890	0.170	0.882	0.127	0.746	0.115	0.741
0.203	0.854	0.203	1.071	0.157	1.018	0.133	0.951
0.215	1.056	0.234	1.279	0.173	1.083	0.200	1.567
0.247	1.162	0.296	1.755	0.210	1.397	0.277	2.209
0.280	1.408	0.336	2.045	0.219	1.481	0.284	2.212
0.323	1.615	0.400	2.442	0.273	1.820	0.346	2.867
0.351	1.740	0.431	2.911	0.273	1.801	0.434	3.875
0.388	2.006	0.453	3.057	0.327	2.261	0.492	4.668
0.426	2.213	0.485	3.265	0.426	3.159	0.538	5.334
0.479	2.783	0.505	3.591	0.441	3.344	0.595	6.509
0.495	2.926	0.536	3.779	0.475	3.657	0.636	7.454
0.556	3.498	0.553	4.185	0.489	3.964	0.648	7.821
0.597	4.107	0.620	4.963	0.523	4.277	0.687	8.906
0.623	4.452	0.637	5.329	0.568	5.056	0.727	10.39
0.656	4.980	0.668	5.899	0.576	4.917	0.764	12.06
0.718	6.738	0.713	7.416	0.615	5.835	0.798	13.85
0.729	6.639	0.715	7.276	0.651	6.490	0.834	16.62
0.788	8.939	0.768	9.398	0.665	6.978		
0.816	10.17	0.805	10.83	0.714	8.542		
0.856	12.83	0.821	11.48	0.746	9.618		
0.859	12.10	0.854	14.30	0.782	11.02		
0.869	13.49	0.890	16.38	0.824	12.98		
0.892	15.53			0.868	17.68		

TABLE 8.11

PDMS - (2 - PrOH) ($V = 0.7536\ cm^3$)

$T_m = 35.0^oC$		$T_m = 40.1^oC$		$T_m = 50.1^oC$		$T_m = 59.0^oC$	
$p_o = 7.89$		$p_o = 10.67$		$p_o = 17.78$		$p_o = 27.48$	
p/p_o	C	p/p_o	C	p/p_o	C	p/p_o	C
0.052	0.267	0.052	0.271	0.019	0.128	0.016	0.113
0.057	0.253	0.077	0.410	0.056	0.350	0.059	0.496
0.109	0.550	0.128	0.696	0.079	0.539	0.061	0.481
0.137	0.692	0.173	0.948	0.146	0.939	0.081	0.657
0.193	1.036	0.234	1.341	0.152	0.986	0.116	0.991
0.243	1.289	0.242	1.480	0.232	1.620	0.180	1.518
0.264	1.458	0.242	1.475	0.253	1.870	0.187	1.614
0.296	1.678	0.313	1.972	0.296	2.249	0.291	2.631
0.355	2.255	0.323	1.984	0.398	3.349	0.336	3.215
0.403	2.568	0.350	2.295	0.424	3.707	0.423	4.336
0.468	3.391	0.372	2.480	0.484	4.599	0.468	5.120
0.473	3.345	0.384	2.716	0.532	5.549	0.521	6.292
0.537	4.507	0.409	2.873	0.545	5.860	0.567	7.384
0.573	5.203	0.438	3.217	0.582	6.731	0.619	9.142
0.621	6.412	0.458	3.650	0.632	8.667	0.623	9.329
0.648	7.215	0.512	4.428	0.661	9.320	0.656	10.50
0.705	9.071	0.576	6.070	0.691	10.70	0.694	12.57
0.705	9.363	0.577	5.838	0.716	12.35	0.752	16.06
0.735	10.62	0.604	6.537	0.740	13.22	0.762	17.09
0.760	12.13	0.638	7.248	0.750	14.21	0.787	19.38
0.796	14.04	0.678	9.043	0.809	18.95		
0.826	16.52	0.705	9.955	0.850	24.23		
0.842	18.82	0.730	10.99				
		0.776	14.06				
		0.815	16.69				
		0.862	22.41				

TABLE 8.12

FMS - (2 - PrOH) (V = 0.7626 cm^3)

T_m = 36.0°C p_o = 8.372		T_m = 43.0°C p_o = 12.35		T_m = 50.0°C p_o = 17.68		T_m = 57.0°C p_o = 25.03	
p/p_o	C	p/p_o	C	p/p_o	C	p/p_o	C
0.109	0.498	0.100	0.593	0.095	0.613	0.113	0.869
0.210	1.041	0.195	1.124	0.191	1.287	0.161	1.232
0.332	1.708	0.286	1.716	0.271	1.881	0.238	1.908
0.444	2.465	0.379	2.430	0.347	2.477	0.342	2.835
0.536	3.251	0.491	3.375	0.436	3.376	0.443	3.883
0.622	4.051	0.600	4.502	0.512	4.077	0.530	4.958
0.718	5.264	0.708	5.934	0.603	5.237	0.616	6.200
0.834	7.027	0.780	7.251	0.696	6.657	0.733	8.517
0.896	8.465	0.894	9.966	0.785	8.472	0.802	10.52
				0.864	10.65	0.858	12.51

8.2.2 Sorption- and Desorption- Kinetic Results

These results were obtained using the vacuum microbalance only since it was not possible to maintain a constant penetrant pressure within the spring-sorption apparatus.

Most of the measurements have been made with the edge of the sample covered so as to reproduce the theoretical condition of an infinitely thin sheet. The covering was aluminium foil which was stuck to the sample by solvent (1,1,1-trichloroethane). One sample (P(DMS-g-0.214 VAc), (*Aℓ Foil Round Edge)) had the aluminium foil stuck with Silastic gum to ensure that a good bond was formed between the sample and the foil. Some measurements were made with the edge of the sample open so as to see the magnitude of the edge effect.

The measurements include buoyancy corrections but no blank corrections except for equilibrium uptakes. Membrane thicknesses and volumes of the samples are given in the respective Tables.

TABLE 8.13

P(DMS - g - 0.034 VAc) - H_2O (T_m = 42.0°C)

ℓ = 0.197 V = 0.9319 (Free Edge)

C	M_∞	$\overline{D}_s \cdot 10^6$	$\overline{D}_d \cdot 10^6$	$\overline{D}_{av} \cdot 10^6$
0.293	219	15.53	16.15	15.84
0.399	299	16.48	16.29	16.39
0.497	372	16.13	15.58	15.86
0.624	468	18.45	14.46	16.46
0.635	476	16.83	16.67	16.76
0.645	483	14.46	15.85	15.16
0.777	582	16.66	16.37	16.52
0.830	622	16.62	16.69	16.66
0.850	637	16.40	16.76	16.58
1.013	759	15.30	15.61	15.46
1.204	902	14.16	15.28	14.71
1.455	1105	13.45	14.62	14.03
1.547	1172	12.87	14.15	13.51
1.772	1334	11.99	13.63	12.81
1.793	1343	12.13	14.38	13.26
1.989	1505	10.44	13.24	11.84
2.188	1653	11.47	13.13	12.30
2.500	1893	10.61	12.84	11.72
2.641	1988	9.33	13.31	11.32
2.680	2015	9.02	12.01	10.52

TABLE 8.14

P(DMS - g - 0.034 VAc) - H_2O (T_m = 42.0°C)

ℓ = 0.197 V = 0.9343 (Aℓ Foil round Edge)

C	M_∞	$\overline{D}_s \cdot 10^6$	$\overline{D}_d \cdot 10^6$	$\overline{D}_{av} \cdot 10^6$
0.252	189	17.48	16.04	16.77
0.292	219	17.48	16.72	17.10
0.293	220	16.68	16.14	16.40
0.389	293	16.61	16.80	16.70
0.389	293	18.26	16.87	17.56
0.434	326	15.68	15.54	15.62
0.621	467	16.99	16.81	16.89
0.778	585	14.76	16.23	15.50
0.894	671	14.93	16.02	15.48
1.135	853	13.51	16.20	14.86
1.143	859	13.57	14.40	13.99
1.387	1042	12.90	14.47	13.69
1.683	1265	11.43	14.47	12.95
2.056	1545	9.70	13.17	11.44
2.601	1954	8.17	11.37	9.78

TABLE 8.15

P(DMS - g - 0.093 VAc) - H_2O (T_m = 42.0°C)

ℓ = 0.214 V = 0.6826 (Aℓ Foil round Edge)

C	M_∞	$\overline{D}_s \cdot 10^6$	$\overline{D}_d \cdot 10^6$	$\overline{D}_{av} \cdot 10^6$
0.509	279	8.94	8.39	8.67
0.586	322	8.71	8.60	8.66
0.709	389	8.99	8.43	8.71
0.821	451	9.16	8.56	8.86
0.965	530	8.66	7.97	8.32
1.142	627	8.59	8.77	8.68
1.360	746	7.83	8.43	8.13
1.551	852	7.40	7.89	7.65
1.724	946	7.60	8.36	7.98
2.022	1110	6.71	8.01	7.36
2.545	1397	6.44	8.26	7.55
3.326	1826	5.41	6.68	6.05
4.243	2329	4.51	6.38	5.45
4.946	2715	4.00	6.37	5.19
5.683	3119	3.58	6.08	4.83

TABLE 8.16

P(DMS - g - 0.093 VAc) - H_2O (T_m = 55.0°C)

ℓ = 0.213 V = 0.8873 (Free Edge)

C	M_∞	$\overline{D}_s \cdot 10^6$	$\overline{D}_d \cdot 10^6$	$\overline{D}_{av} \cdot 10^6$
0.494	352	10.77	10.79	10.78
0.513	366	11.39	10.15	10.77
0.592	422	10.92	10.61	10.77
1.305	931	10.65	10.86	10.76
1.984	1415	10.12	11.07	10.60
2.491	1777	9.34	10.86	10.10
3.034	2164	8.82	10.16	9.49
3.851	2747	8.04	9.81	8.93
4.973	3547	6.22	9.28	7.75
5.290	3773	6.11	9.15	7.63
6.284	4482	5.36	8.81	7.09

TABLE 8.17

P(DMS - g - 0.157 VAc) - H_2O (T_m = 42.0°C)

ℓ = 0.210 V = 0.6939 (Aℓ Foil round Edge)

C	M_∞	$\overline{D}_s \cdot 10^6$	$\overline{D}_d \cdot 10^6$	$\overline{D}_{av} \cdot 10^6$
0.824	460	5.25	5.08	5.16
0.955	533	4.68	4.69	4.69
1.108	618	4.56	4.56	4.56
1.182	660	4.94	4.86	4.90
1.424	794	5.12	4.90	5.01
1.913	1067	4.37	4.77	4.57
2.186	1219	4.53	4.81	4.67
3.094	1727	4.19	4.70	4.45
3.665	2046	3.96	4.47	4.22
4.652	2596	3.70	4.37	4.04
5.766	3216	3.17	3.96	3.57
6.821	3804	2.85	3.76	3.31
8.444	4710	2.38	-	-
8.795	4905	2.22	-	-

TABLE 8.18

P(DMS - g - 0.214 VAc) - H_2O (T_m = 42.0°C)

ℓ = 0.208 V = 0.9493 (Free Edge)

C	M_∞	$\overline{D}_s \cdot 10^6$	$\overline{D}_d \cdot 10^6$	$\overline{D}_{av} \cdot 10^6$
1.649	1259	3.63	3.81	3.72
1.822	1391	3.65	3.73	3.69
2.276	1738	3.59	3.81	3.70
2.670	2039	3.73	3.51	3.62
3.354	2561	3.42	3.53	3.47
4.616	3524	3.07	3.55	3.31
5.457	4166	2.84	3.43	3.13
6.396	4883	2.67	3.26	2.96
8.315	6347	2.35	3.12	2.74
11.70	8928	1.83	2.74	2.28

TABLE 8.19

P(DMS - g - 0.214 VAc) - H_2O (T_m = 42.0°C)

ℓ = 0.208 V = 0.9493 (Aℓ Foil Round Edge)

C	M_∞	$\overline{D}_s \cdot 10^6$	$\overline{D}_d \cdot 10^6$	$\overline{D}_{av} \cdot 10^6$
1.339	1022	3.46	3.45	3.45
1.461	1115	3.50	3.54	3.52
1.683	1285	3.43	3.55	3.49
1.959	1496	3.46	3.45	3.45
2.382	1818	3.40	3.47	3.44
2.722	2078	3.40	3.48	3.44
3.121	2383	3.30	3.46	3.38
3.340	2550	3.23	-	-
3.927	2998	3.11	3.35	3.23
5.135	3920	2.80	3.22	3.01
6.769	5168	2.43	2.99	2.71
8.482	6475	2.10	2.83	2.47
8.704	6644	2.10	2.73	2.42
10.07	7685	1.89	2.60	2.24
11.55	8817	1.69	2.57	2.13

TABLE 8.20

P(DMS - g - 0.214 VAc) - H_2O (T_m = 42.0°C)

ℓ = 0.208 V = 0.7537 (* Aℓ Foil round Edge)

C	M_∞	$\overline{D}_s \cdot 10^6$	$\overline{D}_d \cdot 10^6$	$\overline{D}_{av} \cdot 10^6$
1.337	811	3.41	3.41	3.41
1.695	1028	3.32	3.35	3.34
1.860	1128	3.26	3.46	3.36
1.898	1151	3.18	3.43	3.31
2.101	1274	3.34	3.37	3.34
2.457	1489	3.22	3.31	3.27
2.852	1729	3.25	3.53	3.39
3.870	2346	2.98	3.30	3.14
4.546	2755	2.81	3.23	3.02
5.461	3310	2.53	2.99	2.76
6.100	3697	2.39	3.03	2.71
8.836	5355	2.03	2.81	2.42
10.66	6459	1.70	2.63	2.16

TABLE 8.21

P(DMS - g - 0.442 VAc) - H_2O (T_m = 42.0°C)

ℓ = 0.110 V = 0.4365 (Aℓ Foil round Edge)

C	M_∞	$\overline{D}_s \cdot 10^6$	$\overline{D}_d \cdot 10^6$	$\overline{D}_{av} \cdot 10^6$
2.398	842	0.969	0.976	0.973
2.585	907	0.991	1.025	1.008
3.225	1132	0.985	0.979	0.982
3.628	1273	0.996	0.996	0.996
4.076	1430	0.970	0.979	0.975
5.456	1915	0.933	0.930	0.932
5.972	2096	0.900	0.941	0.921
6.377	2238	0.908	0.932	0.920
7.983	2801	0.828	0.900	0.864
9.811	3442	0.777	0.871	0.824
14.18	4974	0.661	0.806	0.734
19.16	6725	0.579	0.730	0.655
22.17	7778	0.532	0.701	0.616
26.28	9223	0.447	0.658	0.553

TABLE 8.22

PVAc - H_2O (T_m = 42.0°C)

(a) ℓ = 0.0210 V = 0.0434 (Free Edge)

C	M_∞	$\overline{D}_s \cdot 10^6$	$\overline{D}_d \cdot 10^6$	$\overline{D}_{av} \cdot 10^6$
6.894	240	0.161	0.140	0.151
9.015	314	0.158	0.142	0.150
9.110	317	0.164	0.149	0.157
10.52	367	0.164	0.147	0.156
15.15	528	0.153	0.142	0.148
15.37	542	0.149	0.147	0.148
19.29	672	0.145	0.140	0.143
20.79	725	0.156	0.153	0.155
28.83	1005	0.145	0.135	0.140
37.87	1320	0.129	0.143	0.136
57.36	1999	0.098	0.127	0.113

(b) ℓ = 0.0414 V = 0.1482 (Free Edge)

C	M_∞	$\overline{D}_s \cdot 10^6$	$\overline{D}_d \cdot 10^6$	$\overline{D}_{av} \cdot 10^6$
7.281	868	0.153	0.151	0.152
7.400	882	0.158	0.151	0.155
9.250	1102	0.151	0.150	0.151
18.69	2227	0.149	0.149	0.149
18.74	2233	0.150	0.149	0.150

TABLE 8.22 (cont'd)

(c) ℓ = 0.0230 V = 0.1565 (Free Edge)

C	M_∞	$\bar{D}_s \cdot 10^6$	$\bar{D}_d \cdot 10^6$	$\bar{D}_{av} \cdot 10^6$
6.913	870	0.154	0.144	0.149
7.640	961	0.153	0.143	0.148
10.84	1364	0.151	0.147	0.149
14.25	1793	0.153	0.152	0.153
17.91	2253	0.153	0.148	0.151
22.31	2808	0.144	0.146	0.145
28.73	3614	0.141	0.145	0.143
30.98	3897	0.138	0.142	0.140
36.56	4599	0.125	0.137	0.131
39.28	4941	0.128	0.136	0.132

8.2.3 Steady-State Permeation Results

All permeation measurements were obtained using the Baratron to monitor the "down-stream" pressure.

The following are applicable for all measurements.

X = 1.698, A = 2.861, V = 6362

TABLE 8.23

PDMS - H_2O (ℓ = 0.2025)

$T = 35.0^oC$, p_o^m = 4.214		$T = 42.0^oC$, p_o^m = 6.146		$T = 49.0^oC$, p_o^m = 8.800		$T = 55.0^oC$, p_o^m = 11.80	
p/p_o	$J\ell.10^6$	p/p_o	$J\ell.10^6$	p/p_o	$J\ell.10^6$	p/p_o	$J\ell.10^6$
0.439	8.055	0.398	10.19	0.407	13.89	0.227	9.887
0.645	11.94	0.564	14.37	0.506	17.81	0.335	14.57
0.790	14.75	0.761	19.62	0.625	21.53	0.404	17.96
0.935	17.34	0.904	23.46	0.747	25.61	0.501	22.59
						0.642	28.37
						0.685	30.37

TABLE 8.24

P(DMS - g - 0.034 VAc) - H_2O (ℓ = 0.203)

T_m = 35.0°C p_o = 4.214		T_m = 42.0°C p_o = 6.146		T_m = 49.0°C p_o = 8.800		T_m = 55.0°C p_o = 11.80	
p/p_o	$J\ell.10^6$	p/p_o	$J\ell.10^6$	p/p_o	$J\ell.10^6$	p/p_o	$J\ell.10^6$
0.471	8.266	0.602	15.00	0.509	17.04	0.379	16.17
0.637	11.39	0.746	18.45	0.643	21.70	0.502	21.80
0.762	13.77	0.912	22.88	0.787	26.36	0.623	26.73
0.895	16.16					0.714	31.13
						0.839	35.51

TABLE 8.25

P(DMS - g - 0.093 VAc) - H_2O (ℓ = 0.213)

T_m = 35.0°C p_o = 4.214		T_m = 42.0°C p_o = 6.146		T_m = 49.0°C p_o = 8.800		T_m = 55.0°C p_o = 11.80	
p/p_o	$J\ell.10^6$	p/p_o	$J\ell.10^6$	p/p_o	$J\ell.10^6$	p/p_o	$J\ell.10^6$
0.488	7.877	0.464	10.55	0.405	12.45	0.302	12.00
0.592	9.764	0.593	13.47	0.558	17.14	0.400	15.82
0.657	10.65	0.748	17.07	0.691	21.39	0.441	17.61
0.749	12.31	0.912	21.18	0.859	27.25	0.509	20.24
0.862	14.30					0.604	24.32
						0.643	25.52
						0.758	30.05

TABLE 8.26

P(DMS - g - 0.157 VAc) - H_2O (ℓ = 0.215)

T_m = 35.0°C p_o = 4.214		T_m = 42.0°C p_o = 6.146		T_m = 49.0°C p_o = 8.800		T_m = 55.0°C p_o = 11.80	
p/p_o	$J\ell.10^6$	p/p_o	$J\ell.10^6$	p/p_o	$J\ell.10^6$	p/p_o	$J\ell.10^6$
0.447	6.484	0.356	7.406	0.203	5.577	0.129	4.676
0.596	8.627	0.586	12.00	0.257	7.380	0.333	12.24
0.814	11.88	0.696	14.38	0.392	11.06	0.442	16.33
		0.798	16.47	0.577	16.35	0.593	21.71
				0.832	23.62	0.712	26.03
						0.778	28.45

TABLE 8.27

P(DMS - g - 0.214 VAc) - H_2O (ℓ = 0.218)

T_m = 35.0°C p_o = 4.214		T_m = 42.0°C p_o = 6.146		T_m = 49.0°C p_o = 8.800		T_m = 55.0°C p_o = 11.80	
p/p_o	$J\ell.10^6$	p/p_o	$J\ell.10^6$	p/p_o	$J\ell.10^6$	p/p_o	$J\ell.10^6$
0.641	8.606	0.561	10.70	0.546	14.35	0.606	20.79
0.745	10.01	0.674	12.87	0.639	16.75	0.701	24.09
0.838	11.28	0.793	15.14	0.724	18.99	0.790	27.13
				0.837	21.93		

TABLE 8.28

P(DMS - g - 0.442 VAc) - H_2O (ℓ = 0.111)

T_m = 35.0°C, p_o = 4.214		T_m = 42.0°C, p_o = 6.146		T_m = 49.0°C, p_o = 8.800		T_m = 55.0°C, p_o = 11.80	
p/p_o	$J\ell.10^6$	p/p_o	$J\ell.10^6$	p/p_o	$J\ell.10^6$	p/p_o	$J\ell.10^6$
0.282	2.750	0.249	3.417	0.210	4.016	0.233	6.222
0.443	4.647	0.417	6.097	0.398	8.131	0.357	9.721
0.568	6.047	0.566	8.563	0.506	10.76	0.432	11.90
0.645	6.758	0.671	11.22	0.556	12.17	0.508	14.57
0.878	10.15	0.674	9.950	0.612	13.35	0.588	17.00
		0.760	12.42	0.652	14.20	0.692	21.07
		0.829	13.64	0.722	16.33	0.722	21.74
		0.879	14.49	0.774	17.59	0.809	25.20
				0.845	19.22	0.888	28.31
				0.897	20.66		

TABLE 8.29

PVAc - H_2O (ℓ = 0.0262)

T_m = 35.0°C, p_o = 4.214		T_m = 42.0°C, p_o = 6.146		T_m = 49.0°C, p_o = 8.800		T_m = 55.0°C, p_o = 11.80	
p/p_o	$J\ell.10^6$	p/p_o	$J\ell.10^6$	p/p_o	$J\ell.10^6$	p/p_o	$J\ell.10^6$
0.171	0.428	0.144	0.581	0.120	0.860	0.101	1.139
0.230	0.615	0.193	0.826	0.220	1.743	0.183	2.199
0.330	0.975	0.257	1.131	0.322	2.709	0.268	3.428
0.355	1.047	0.309	1.497	0.338	2.973	0.338	4.569
0.480	1.620	0.370	1.993	0.407	3.764	0.432	6.260
0.645	2.499	0.461	2.534	0.452	4.273	0.517	7.923
0.749	3.322	0.481	2.781	0.573	6.082	0.601	9.963
0.826	4.089	0.586	3.622	0.683	8.209	0.658	11.61
		0.588	3.764	0.737	9.379	0.706	13.27
		0.718	5.156	0.762	10.07	0.786	16.20
		0.809	6.397	0.812	11.51	0.814	17.58

TABLE 8.30

PDMS - MeOH (ℓ = 0.197)

T_m = 36.0°C		T_m = 43.0°C		T_m = 50.0°C		T_m = 57.0°C	
p_o = 21.52		p_o = 29.85		p_o = 40.60		p_o = 55.07	
p/p_o	$J\ell.10^6$	p/p_o	$J\ell.10^6$	p/p_o	$J\ell.10^6$	p/p_o	$J\ell.10^6$
0.317	27.63	0.229	24.50	0.212	28.45	0.192	32.01
0.348	29.57	0.334	36.41	0.343	46.14	0.324	53.50
0.434	37.97	0.435	47.76	0.459	61.67	0.432	69.96
0.510	44.07	0.548	60.27	0.558	75.44	0.517	84.53
0.612	54.66	0.658	73.85	0.655	90.03	0.658	109.3
0.724	65.50	0.777	91.02	0.772	108.7	0.765	133.0
0.784	74.09	0.872	104.4	0.896	134.4	0.880	162.0
0.878	83.96						

TABLE 8.31

PDMS - EtOH (ℓ = 0.2025)

T_m = 36.0°C		T_m = 45.0°C		T_m = 54.0°C		T_m = 63.0°C	
p_o = 10.95		p_o = 17.40		p_o = 26.30		p_o = 40.59	
p/p_o	$J\ell.10^6$	p/p_o	$J\ell.10^6$	p/p_o	$J\ell.10^6$	p/p_o	$J\ell.10^6$
0.216	12.16	0.164	12.86	0.098	10.33	0.065	9.52
0.310	17.57	0.288	22.97	0.303	32.14	0.131	17.58
0.357	21.11	0.354	28.72	0.404	43.22	0.182	24.95
0.451	25.85	0.424	34.82	0.463	50.84	0.240	33.63
0.478	28.74	0.481	39.60	0.524	56.14	0.248	33.97
0.510	30.76	0.518	43.68	0.547	57.63	0.310	42.20
0.515	31.83	0.593	50.71	0.569	60.74	0.318	43.62
0.620	38.84	0.639	54.30	0.588	62.47	0.348	49.33
0.665	44.33	0.683	56.54	0.644	71.73	0.396	56.51
0.698	43.55	0.748	66.26	0.709	81.20	0.484	71.57
0.712	46.64	0.854	78.81	0.764	90.96	0.497	73.78
0.772	52.79			0.836	104.7	0.547	82.75
0.774	50.85					0.599	94.67
0.806	54.62					0.650	105.3
0.823	57.89					0.702	120.0
0.844	60.23						

TABLE 8.32

PDMS - (2 - PrOH) (ℓ = 0.2025)

T_m = 35.0°C		T_m = 40.1°C		T_m = 50.1°C		T_m = 59.0°C	
p_o = 7.89		p_o = 10.67		p_o = 17.78		p_o = 27.48	
p/p_o	$J\ell.10^6$	p/p_o	$J\ell.10^6$	p/p_o	$J\ell.10^6$	p/p_o	$J\ell.10^6$
0.194	7.482	0.203	9.93	0.144	9.56	0.092	8.23
0.215	8.441	0.233	11.51	0.179	12.06	0.116	10.35
0.277	11.02	0.303	15.16	0.217	14.92	0.136	12.49
0.320	12.52	0.356	17.92	0.257	17.64	0.176	16.09
0.353	14.09	0.371	18.65	0.263	18.36	0.212	19.54
0.392	15.86	0.408	20.87	0.323	22.49	0.260	24.14
0.435	17.55	0.429	22.06	0.344	24.46	0.303	28.61
0.479	20.39	0.449	22.99	0.379	26.92	0.351	34.36
0.522	22.09	0.456	23.53	0.417	29.54	0.392	38.76
0.573	24.91	0.499	26.56	0.428	31.01	0.433	43.23
0.612	27.30	0.516	27.86	0.457	33.45	0.480	49.96
0.652	30.23	0.541	28.81	0.477	35.86	0.518	55.16
0.693	33.49	0.568	31.13	0.520	38.84	0.551	60.38
0.738	36.81	0.599	33.84	0.568	43.62	0.581	64.98
0.776	40.57	0.616	35.89	0.600	47.84	0.610	69.93
		0.629	35.64	0.639	53.14	0.645	77.65
		0.642	37.52	0.661	56.73		
		0.692	42.70	0.678	59.53		
		0.694	42.88				
		0.708	43.92				

TABLE 8.33

FMS - (2 - PrOH) (ℓ = 0.0838)

T_m = 36.0°C		T_m = 43.0°C		T_m = 50.0°C		T_m = 57.0°C	
p_o = 8.372		p_o = 12.35		p_o = 17.68		p_o = 25.03	
p/p_o	$J\ell.10^6$	p/p_o	$J\ell.10^6$	p/p_o	$J\ell.10^6$	p/p_o	$J\ell.10^6$
0.201	1.005	0.148	1.096	0.109	1.153	0.095	1.450
0.314	1.564	0.260	1.874	0.202	2.148	0.194	2.952
0.446	2.345	0.377	2.852	0.301	3.260	0.302	4.650
0.560	2.989	0.485	3.729	0.406	4.600	0.410	6.442
0.679	3.775	0.579	4.767	0.502	5.894	0.509	8.678
0.785	4.657	0.687	5.922	0.585	7.241	0.604	10.68
0.929	5.970	0.785	7.253	0.703	9.237	0.685	12.95
		0.892	8.933	0.838	11.95	0.772	15.82

8.2.4 Time Lag Results

These were all obtained from measurements using a Baratron. Although it does not enter the calculations, the outgoing volume throughout these measurements was 6362 cm^3. (This becomes important when water vapour is the penetrant as extraneous sorption effects come into play).

TABLE 8.34

P(DMS - g - 0.157 VAc) - H_2O (ℓ = 0.215)

T_m = 35.0°C		T_m = 42.0°C		T_m = 49.0°C		T_m = 55.0°C	
p_o = 4.214		p_o = 6.146		p_o = 8.800		p_o = 11.80	
p/p_o	L	p/p_o	L	p/p_o	L	p/p_o	L
0.447	5550	0.356	7560	0.203	5682	0.129	6582
0.596	5208	0.586	4206	0.257	5814	0.333	3636
0.814	5028	0.696	4020	0.392	3960	0.442	3372
		0.798	3906	0.577	3630	0.593	3096
				0.832	3252	0.712	3168
						0.778	2970

TABLE 8.35

PDMS - EtOH (ℓ = 0.2025)

T_m = 36.0°C		T_m = 45.0°C		T_m = 54.0°C		T_m = 63.0°C	
p_o = 10.95		p_o = 17.40		p_o = 26.30		p_o = 40.59	
p/p_o	L	p/p_o	L	p/p_o	L	p/p_o	L
0.216	661	0.164	598	0.098	528	0.065	473
0.451	767	0.424	683	0.588	650	0.182	589
0.510	785	0.518	682	0.764	710	0.310	549
0.665	868	0.748	800			0.590	599
0.823	942					0.650	604

TABLE 8.36

PDMS - (2- PrOH) (ℓ = 0.2025)

T_m = 35.0°C		T_m = 40.1°C		T_m = 50.1°C		T_m = 59.0°C	
p_o = 7.89		p_o = 10.67		p_o = 17.78		p_o = 27.48	
p/p_o	L	p/p_o	L	p/p_o	L	p/p_o	L
0.215	1101	0.203	899	0.144	848	0.092	759
0.320	1122	0.233	1013	0.257	904	0.116	763
0.435	1185	0.303	1049	0.323	931	0.303	814
0.573	1210	0.408	1061	0.344	942	0.433	879
0.776	1406	0.449	1067	0.477	982	0.610	920
		0.516	1130	0.569	1031		
		0.694	1243	0.678	1159		

8.2.5 Steady-State Spring-Permeation Results

The apparatus was arranged such that the "down-stream" pressure in a permeation experiment could be monitored by the Baratron or a calibrated quartz spring on which a bucket of molecular sieve was suspended.

The following constants are applicable:

K = 28.70, A = 2.861, V = 6392, 4096, 2458, X = 1.698.

TABLE 8.37

PDMS - (2 - PrOH) (Spring Permeation) (ℓ = 0.202)

T_m = 40.1°C		T_m = 50.1°C	
p_o = 10.67		p_o = 17.78	
p/p_o	$J\ell.10^6$	p/p_o	$J\ell.10^6$
0.175	7.36	0.133	6.85
0.237	11.66	0.141	8.61
0.376	18.87	0.183	11.88
0.379	17.42	0.195	12.46
0.472	24.97	0.243	17.01
0.519	28.33	0.335	22.52
0.592	34.03	0.356	25.30
0.673	42.56	0.433	32.63
		0.470	35.00
		0.470	35.04
		0.493	36.83
		0.524	39.27
		0.548	41.08
		0.552	47.58

TABLE 8.38

Baratron- and Spring - Permeation Comparison

PVAc - H_2O (T_m = 55.0°C) (ℓ = 0.0202)

(a) Baratron - Permeation (Buffer Volumes Prewetted)

cm^3 Outgoing Volume	$cm^3(S.T.P.).cm^{-1}.s^{-1}$ $J\ell.10^6$
6392	7.695
4092	7.637
2458	7.568

TABLE 8.38 (cont'd)

(b) Spring - Permeation (Buffer Volumes Prewetted)

cm^3 Outgoing Volume	$cm^3(S.T.P.).cm^{-1}.s^{-1}$ $J\ell.10^6$
∿ 2000	8.238
∿ 4500	8.247
∿ 8500	8.236

(c) Spring- and Baratron- Permeation (No Prewetting)

The figures are values of $J\ell.10^6$.

Baratron V = 6392	Spring V = ∿ 2000	Spring V = ∿ 8500	Spring V ∿ 8500 + B*
4.199	4.561	4.478	3.661
6.279	6.926	-	6.182
10.74	12.10	11.28	9.980

* The Baratron was open to the Spring- permeation section as a check on residual pressures.

8.3 Sample Calculations

8.3.1 Equilibrium Sorption

The following examples illustrate how to obtain a point on an equilibrium sorption isotherm from primary experimental measurements.

(i) Quartz Spring : FMS - (2 - PrOH)

Temperature (T_m) of sample = 57.0°C
Volume (V) of sample = 0.7626 cm^3
Observed spring extension (Δh^1) = 0.806 cm
Pressure transducer output = 11.97 mv
Spring calibration (k) = 32.11 $cm.g^{-1}$
Transducer calibration (K) = 1.795 (cm Hg).mv^{-1}
Molecular weight of 2 - PrOH = 60.10
Saturated Vapour pressure (p_o) of 2 - PrOH at 57.0°C = 25.03 cm Hg
Volume of quartz spring + platinum support (V^1) = 0.0110 cm^3
Density of 2 - PrOH vapour per unit pressure at 57.0°C = 29.19 x 10^{-6} g . cm^{-3} . (cm Hg)$^{-1}$

Vapour pressure p = 1.795 x 11.97 = 21.49 cm Hg

Relative pressure $p/p_o = \frac{21.49}{25.03} = 0.858$

Buoyancy correction to be added = $29.19 \cdot 10^{-6} \times p \times (V + V^1) \times k$ cm

$= 29.19 \cdot 10^{-6} \times 21.49 \times 0.7736 \times 32.11$ cm

= 0.0154 cm

Hence true extension $\Delta h = 0.806 + 0.0154 = 0.8214$ cm

Amount of Vapour sorbed (Q) $= \frac{\Delta h \times 22414}{k \times 60.10}$

$= \frac{0.8214 \times 22414}{32.11 \times 60.10} = 9.540$ cm^3 (S.T.P.)

Concentration (C) of sorbed 2-PrOH = Q/V

= 9.540/0.7626

= 12.51 cm^3 (S.T.P.). cm^{-3}

Hence the isotherm point (p/p_o, C) is (0.858, 12.51)

(ii) Microbalance : P(DMS - g - 0.442 VAc) - H_2O

Temperature (T_m) of sample = 35.0°C

Temperature (T_b) of balance head = 36.2°C

Volume (V) of sample = 0.4365 cm^3

Observed weight increase (Δw) = 4002 µg

Transducer output = 2.46 mv

Transducer calibration = 1.130 (cm Hg).mv^{-1}

Molecular weight of H_2O = 18.02

S.V.P. (p_o) of H_2O at 35.0°C = 4.214 cm Hg

S.V.P. ($(p_o)_b$) of H_2O at 36.2°C = 4.501 cm Hg

Volume of platinum support for sample (V^1) = 0.0058 cm^3

Volume of metal counterweight (V^{11}) = 0.0573 cm^3

Density of H_2O vapour per unit pressure at 35.0°C = $9.377.10^{-6}$ g. cm^{-3} . (cm Hg)$^{-1}$

Vapour pressure p = 1.130 x 2.46 = 2.780 cm Hg

Relative pressure $p/p_o = \frac{2.780}{4.214} = 0.660$

Relative pressure at balance head $(p/p_o)_b = 2.780/4.501 = 0.618$

From a pre-constructed isotherm (Figure 3.6), the blank correction B^1 to be added = $(p/p_o)_b \times 10.7 = 10.7 \times 0.618 = 6.6$ µg

Buoyancy correction B to be added

$= 9.377.10^{-6} \times p \times (V + V^1 - V^{11}) = 9.377.10^{-6} \times 2.780 \times 0.3850 = 10.0$ µg

Hence total amount Q of H_2O sorbed = $\Delta w + B + B^1$

$= 4002 + 6.6 + 10.0 = 4018.6$ μg

$= \frac{4019 \times 10^{-6} \times 22414}{18.02} = 4.998$ cm^3 (S.T.P.)

Concentration (C) of sorbed H_2O = Q/V = 4.998/0.4365 = 11.45 cm^3 (S.T.P.).cm^{-3}

Hence the isotherm point (p/p_o, C) is (0.660, 11.45)

8.3.2 Sorption- and Desorption - Kinetics : PVAc - H_2O

A point on a reduced curve is calculated for each time t (s) by calculating the amount of water taken up by the polymer as a weight (μg) as shown in Section 8.3.1 (including the buoyancy but excluding the blank correction). The corresponding amounts M_∞ at equilibrium are likewise calculated and include both corrections.

Sample thickness (ℓ) = 0.0414 cm

Slope (I) of the graph of M_t/M_∞ vs. $t^{\frac{1}{2}}$ = 0.0211 $s^{-\frac{1}{2}}$

$$\overline{D} = \frac{\pi I^2 \ell^2}{16} = \frac{\pi \times (0.0211 \times 0.0414)^2}{16} = 0.150 \cdot 10^{-6} \text{ cm}^2.\text{s}^{-1}$$

Equilibrium uptake = 2233 μg

and hence concentration of penetrant (C)

= 18.74 cm^3 (S.T.P.).cm^{-3}

∴ A point on the concentration - diffusion coefficient curve (C, $\overline{D}$) is (18.74, $0.150.10^{-6}$)

8.3.3 Steady-State Permeability

The following example illustrates how a point on a graph of $J\ell$ vs. p/p_o is calculated from primary experimental measurements.

(i) Baratron : PDMS - EtOH

Temperature of sample (T_m) = 57.0°C

Average Room Temperature (T_R) = 17.3°C

Membrane thickness (ℓ) = 0.2025 cm

Area of membrane (A) = 2.861 cm^2

"Down-stream" Volume (V) = 6362 cm^3

Transducer output = 5.22 mv

Transducer calibration = 1.698 (cm Hg) . mv^{-1}

S.V.P. of EtOH at 57.0°C (p_o) = 30.75 cm Hg

Steady-state increase in pressure with time $dp/dt = 4.750. 10^{-6}$ (mm Hg) . s^{-1}

Vapour pressure = 1.698 x 5.22 = 8.864 cm Hg

Relative pressure $p/p_o = \frac{8.864}{30.75} = 0.288$

Permeation rate $J\ell = \frac{dp}{dt} \times \frac{V\ell}{760\ A} \times \frac{273.16}{T_R}$

$$= \frac{4.750.10^{-6} \times 6362 \times 0.2025 \times 273.16}{760 \times 2.861 \times 290.5}$$

$$= 2.646 . 10^{-6}\ cm^3\ (S.T.P.).\ cm^{-1}.\ s^{-1}$$

Hence the $(p/p_o, J\ell)$ point is $(0.288, 2.646.10^{-6})$

(ii) Quartz Spring : PDMS - (2-PrOH)

Temperature of sample (T_m) = 50.1°C

Temperature of 2-PrOH reservoir = 38.6°C

Membrane thickness (ℓ) = 0.204 cm

Area of membrane (A) = 2.861 cm^2

S.V.P. of 2-PrOH at 38.6°C = 9.739 cm Hg

MW of 2-PrOH = 60.11

Spring extension (Δh^1) = 0.3234 cm

Spring calibration (K) = 28.70 $cm.g^{-1}$

Time of run = 124.0 minutes

S.V.P. of 2-PrOH at 50.1°C (p_o) = 17.78 cm Hg

Calibrated change of length of spring with temperature = -0.003 cm. $(^oC)^{-1}$

Initial room temperature = 24.5°C

Final room temperature = 25.6°C

Temperature correction of spring extension

= -0.003 (24.5 - 25.6) = + 0.0033 cm

∴ Total extension (Δh) = Δh^1 + 0.0033 = 0.3267 cm

Total amount of permeated vapour (Q)

$$= \frac{\Delta h \times 22414}{K \times 60.11} = \frac{0.3267 \times 22414}{28.70 \times 60.11}\ cm^3\ (S.T.P.)$$

$$= 4.245\ cm^3\ (S.T.P.)$$

Permeation Rate $J\ell = \frac{Q\ell}{At} = \frac{4.245 \times 0.204}{2.861 \times 60 \times 124}$

$$= 40.68.10^{-6}\ cm^3\ (S.T.P.).cm^{-1}.s^{-1}$$

Ingoing vapour pressure = 9.739 cm Hg

Relative pressure p/p_o = 9.739/17.78 = 0.548

Hence the (p/p_o, $J\ell$) point is (0.548, 40.68 . 10^{-6})

8.3.4 Models of Permeation in Heterogeneous Media

The relevant equations are given in Section 4.2 and the only data required are the permeabilities and solubilities of the two homopolymers (Table 8.39). From these it is possible to generate the curves shown in Chapter 5 for various volume fractions of PVAc.

TABLE 8.39

Solubility (σ, $cm^3(S.T.P.).cm^{-3}.(cm\ Hg)^{-1}$) and Permeability ($P$, $cm^3(S.T.P.).cm^{-1}.(cm\ Hg)^{-1}.s^{-1}$) Data for PDMS and PVAc

	σ		$P \cdot 10^6$	
Temperature	PDMS	PVAc	PDMS	PVAc
35.0	0.112	6.529	4.410	0.555
42.0	0.097	4.647	4.184	0.681
49.0	0.080	3.484	3.923	0.847
55.0	0.071	2.775	3.743	0.977

8.4 Accuracy of Measurements

8.4.1 Baratron - Permeability Measurements

The permeability coefficient (P) is given by

$$P = \frac{dp_2}{dt} \times \frac{V \times \ell \times 273.16}{760 \times A \times T_R \times p}$$

with symbols as in Section 8.3. The accuracy of measurement of the individual quantities in this expression is discussed below:-

dp_2/dt :- The Baratron had a 5 figure pressure read-out accurate to within $\pm$ 0.1% and the final pressure increase with time was obtained from the slope of p_2 vs. t so that greater accuracy may be expected. Pressure magnitude depends upon temperature but room temperature remained reasonably constant during any particular run.

V :- This was obtained by gas expansion using accurate buffer volumes and was accurate to within $\pm$ 0.5%.

ℓ :- Thicknesses (ℓ) were measured in several places with a micrometer-screw gauge. The accuracy of the rubbery poly(siloxanes) was estimated

at ± 1% and of PVAc at ± 3%.

A :- The diameter of the holes of the plate was measured with vernier calipers to within ± 0.5%. The presence of the supporting gauze and filter paper may however reduce the effective area.

p :- The transducer output was measured on a potientiometer to within ± 0.5%. The sensitivity obtained from a calibration graph, was known to within ± 1%.

The maximum error involved in a determination of P was estimated at about ± 3% and about ± 1% for the same membrane. This was found to be a slight overestimation of the errors involved and permeabilities were found to be reproducible to within ± 1%.

8.4.2 Spring - Permeability Measurements

The permeability coefficient (P) is given by

$$P = \frac{\Delta h \times \ell \times 22414}{M \times K \times A \times t \times p}$$

where M is the molecular weight of penetrant. The accuracy of individual quantities is the same as those in Section 8.4.1 except for the ones discussed below.

Δh :- The length of spring was measured by a cathetometer to 0.001 cm so that each extension was measured to within ± 0.002 cm. Thus extensions could be measured to within ± 1%. Changes in room temperature cause a change in length of the spring but as this is taken into consideration the error introduced is expected to be no greater than ± 2%.

K :- A good straight line plot of extension vs. load was obtained. The error in the slope (K) was estimated at about ± 0.5%.

The maximum error in each determination was estimated at about ± 5% and for a given membrane the error involved was about ± 2%.

8.4.3 Microbalance- Sorption Measurements

The solubility coefficient (σ) is given by

$$\sigma = \frac{22414 \times 10^{-2}}{18.02 \times p \times V} (\Delta w + B + B^{1})$$

with symbols as in Section 8.3.1. Individual errors were :-

Δw :- Weights could be measured to within ± 0.5 μg for small uptakes and ± 2μg for large ones. This meant that the error involved was less than ± 2%.

B :- The volumes of sample, platinum wire and copper counterweight were accurately known and so, since B itself was only a small correction,

errors in buoyancy were considered negligible.

B^1 :- Blank corrections were estimated to $\pm$ 0.5 µg and in the majority of measurements these corrections are very small so that errors associated with them are negligible.

V :- There was negligible error in weighing the sample. The density was measured to within $\pm$ 0.5% and this was the error involved in V.

The remaining errors (p) are the same as given in Section 8.4.1. The maximum possible error for a particular isotherm point was estimated at $\pm$ 5% although this will be greater at low pressures where there is less sorption. However since the data points were part of an isotherm the overall accuracy is expected to be somewhat reduced.

8.4.4 Spring- Sorption Measurements

In this case

$$\sigma = \frac{\Delta h \times 22414}{k \times M \times p \times V} + \frac{B}{p + V}$$

with symbols as described previously. The accuracy of individual quantities have been discussed previously except those below.

Δh :- Using a cathetometer, Δh could be measured to $\pm$ 0.002 cm and as the average extension was about 0.3 cm this entails an error of $\pm$ 1%. However this is much larger at low pressures and may be as much as $\pm$ 10%.

Hence there is a considerable difference over the range of the isotherm although the average error was estimated at $\pm$ 2% when the isotherm was drawn through all the data points.

8.4.5 Rates of Sorption Measurements

These were measured on the vacuum microbalance and the errors in individual quantities are given below (symbols as previously described).

t :- Significant early time errors were introduced in those samples having a high diffusion coefficient since the balance response time was comparable with the smaller values of t.

M_t, M_∞ :- Values of M_∞ were, on average, about 800 µg so that errors in M_t at early times are about $\pm$ 1-10%. Rates of water sorption on the balance itself were similar to the rates of uptakes by the samples but could be ignored as they were very much smaller than sorption by the polymers.

p :- Times for vapour pressures to increase to their equilibrium values were about 20s and were comparable to smaller values of t in some samples. Hence this could introduce appreciable errors since boundary conditions were not always constant.

Heats of Sorption :- This is quite high for PVAc and could have introduced some errors in those samples containing high percentages of PVAc.

The absolute errors involved in calculating the slope of the reduced sorption curve were estimated at $\pm$ 5 - 15% but relative errors between runs were found to be much smaller.

REFERENCES

1. A. Aitken, and R.M. Barrer, Trans. Farad. Soc., 51, 116 (1955).
2. P. Aptel, J. Cuny, J. Jozefowicz, G. Morel, and J. Neel, European Poly. J., 9, 877 (1973).
3. P. Aptel, J. Cuny, J. Jozefowicz, G. Morel, and J. Neel, J. Appl. Poly. Sci., 16, 1061 (1972).
4. P. Aptel, J. Cuny, J. Jozefowicz, G. Morel, and J. Neel, J. Appl. Poly. Sci., 18, 351 (1974).
5. P. Aptel, J. Cuny, J. Jozefowicz, G. Morel, and J. Neel, J. Appl. Poly. Sci., 18, 365 (1974).
6. R. Ash, R.W. Baker, and R.M. Barrer, Proc. Roy. Soc. (London), A304, 407 (1968).
7. U. Azizov, Kh.U. Usmanov, and M.U. Sadykov, Poly. Sci. U.S.S.R., 7, 18 (1965).
8. Kh.S. Bagdasar'yan, "Theory of Free-Radical Polymerisation", Israel Program for Scientific Translations, Jerusalem, 1968.
9. D. Ballentine, A. Glines, G. Adler, and D.J. Metz, J. Poly. Sci., 34, 419 (1959).
10. D. Ballentine, D.J. Metz, J. Gard, and G. Adler, J. Appl. Poly. Sci., 1, 371 (1959).
11. R.M. Barrer, "Diffusion In and Through Solids", University Press, Cambridge, 1951.
12. R.M. Barrer, op. cit. Ref. 41, Ch.6.
13. R.M. Barrer, J. Phys. Chem., 61, 178 (1957).
14. R.M. Barrer, Trans. Farad. Soc., 35, 628 (1939).
15. R.M. Barrer, Trans. Farad. Soc., 39, 237 (1943).
16. R. M. Barrer, and D.W. Brook, Trans. Farad. Soc., 49, 1049 (1953).
17. J.A. Barrie, op. cit. Ref. 41, Ch.8.
18. J.A. Barrie, J. Poly. Sci., A1, 4, 3081 (1966).
19. J.A. Barrie, and D. Machin, J. Appl. Poly. Sci., 12, 2633 (1968).

20. J.A. Barrie, and D. Machin, J. Macro. Sci., B3, 645 (1969).

21. J.A. Barrie, and D. Machin, J. Poly. Sci., A2, 5, 1300 (1967).

22. J.A. Barrie, and D. Machin, Trans. Farad. Soc., 67, 244 (1971).

23. J.A. Barrie, and D. Machin, Trans. Farad. Soc., 67, 2970 (1971).

24. J.A. Barrie, and B. Platt, Polymer, 4, 303 (1963).

25. A.J. Barry, and H.N. Beck, Ch.5 in "Inorganic Polymers", Ed. F.G.A. Stone, and W.A.G. Graham, Academic Press, New York, 1962.

26. H.A.J. Battaerd, and G.W. Tregear, "Graft Copolymers", Interscience, New York, 1967.

27. C.J.F. Böttcher, "Theory of Electric Polarisation", Elsevier, Amsterdam, 1952.

28. D.A.G. Bruggeman, Ann. Physik (Leipzig), 24, 636 (1935).

29. W.J. Burlant, and A.S. Hoffman, "Block and Graft Polymers", Reinhold Corporation, New York, 1960.

30. A. Casale, and R.S. Porter, Fort. Hochpoly. - Forsch., 17, 1 (1975).

31. R.J. Ceresa, "Block and Graft Copolymers", Butterworths, London, 1962.

32. R.J. Ceresa, "Block and Graft Copolymerisation", Vol. 1, John Wiley and Sons, London, 1973.

33. A. Chapiro, "Radiation Chemistry of Polymeric Systems", High Poly. Series, Vol. 15, John Wiley & Sons, London, 1962.

34. A. Charlesby, "Atomic Radiation and Polymers", Pergamon Press, London, 1960.

35. J.-C. Chuang, and H. Morawetz, Macro., 6, 43 (1973).

36. J. Crank, "Mathematics of Diffusion", 2nd Edn., Clarendon Press, Oxford, 1975.

37. J. Crank, op. cit. Ref. 36, Ch.4.

38. J. Crank, op. cit. Ref. 36, Ch.10.

39. J. Crank, op. cit. Ref. 36, Ch.12.

40. J. Crank, Trans. Farad. Soc., 51, 1632 (1955).

41. J. Crank, and G.S. Park, "Diffusion in Polymers", Academic Press, London, 1968.

42. J. Crank, and G.S. Park, op. cit. Ref. 41, Ch.1.

43. J. Crank, and G.S. Park, Trans. Farad. Soc., 45, 240 (1949).

44. F.L. Dalton, and R. Roberts, Polymer, 1, 104 (1960).

45. H. Daynes, Proc. Roy. Soc. (London), A97, 286 (1920).

46. J.V. Dawkins, Ch. 8A, 8B in "Block Copolymers", Ed. D.C.Allport, and W.H. Janes, Appl. Sci. Pub. Ltd., London, 1973.

47. D.A. De Vries, Ind. Eng. Chem., 47, 1377 (1955).

48. M. Fels, and R.Y.M. Huang, J. Appl. Poly. Sci., 14, 537 (1970).

49. P.Y. Feng, and E.S. Freeman, Ch.4 in "Physical Methods in Macromolecular Chemistry", Vol. 1, Ed. B. Carroll, Marcel Dekker, New York, 1969.

50. A. Fick, Ann. Physik (Leipzig), 170, 59 (1855).

51. E. Fischer, J. Macro. Sci., A2, 1285 (1968).

52. H.S. Frank, J. Phys. Chem., 33, 970 (1929).

53. H.L. Frisch, J. Phys. Chem., 61, 93 (1957).

54. H. Fujita, op. cit. Ref. 41, Ch.3.

55. H. Fujita, Fort. Hochpoly.-Forsch., 3, 1 (1961).

56. H. Fujita, and A. Kishimoto, Text. Res. J., 22, 94 (1952).

57. T.A. Garrett, and G.S. Park, J. Poly. Sci., C, 10, 601 (1967).

58. H.C. Haas, S.G. Cohen, A.C. Oglesby, and E.R. Karlin, J. Poly. Sci., 15, 427 (1955).

59. R.L. Hamilton, and O.K. Crosser, Ind. Eng. Chem. Fund., 1, 187 (1962).

60. K. Hayakama, K. Kawase, and H. Yamakita, J. Appl. Poly. Sci., 18, 1505 (1974).

61. E. Helfand, Ch.5 in "Recent Advances in Polymer Blends, Grafts and Blocks", Poly. Sci. Tech., Vol. 14, Ed. L.H. Sperling, Plenum Press, New York, 1974.

62. W.I. Higuchi, J. Phys. Chem., 62, 649 (1958).

63. W.I. Higuchi, and T. Higuchi, J. Am. Pharm. Assoc., 49, 598 (1960).

64. A.S. Hoffman, and R. Bacskai, Ch.6 in "Copolymerisation", High Poly. Series, Vol. 18, Ed. G.E. Ham, Interscience, London, 1964.

65. G. Holden, op. cit. Ref. 32, Ch.6.

66. H.B. Hopfenberg, F. Kimura, P.T. Rigney, and V. Stannett, J. Poly. Sci., C, 28, 243 (1969).

67. R.Y.M. Huang, and P.J.F. Kanitz, J. Appl. Poly. Sci., 13, 669 (1969).

68. "International Critical Tables of Numerical Data, Physics, Chemistry and Technology", Vol. 3, p.370, M^{c}Graw-Hill, New York, 1926.

69. C.H.M. Jacques, H.B. Hopfenberg, and V. Stannett, Poly. Eng. Sci., 13, 81 (1973).

70. R. Jenkins, J. Poly. Sci., Al, 4, 771 (1966).

71. W. Jost, "Diffusion in Solids, Liquids and Gases", Rev. Ed., Academic Press, New York, 1960.

72. P.J.F. Kanitz, and R.Y.M. Huang, J. Appl. Poly. Sci., 15, 67 (1971).

73. B. Katchman, and A.D. M^{c}Laren, J. Am. Chem. Soc., 73, 2124 (1951).

74. A. Kishimoto, E. Maekawa, and H. Fujita, Bull. Chem. Soc. Japan, 33, 988 (1960).

75. C.A. Kumins, and T.K. Kwei, op. cit. Ref. 41, Ch.4.

76. J.D. Leeder, A.J. Pratt, and I.C. Watt, J. Appl. Poly. Sci., 11, 1649 (1967).

77. P.F. LePoutre, H.B. Hopfenberg, and V. Stannett, J. Poly. Sci., C, 37, 309 (1972).

78. K. Lichtenecker, Physik Z., 27, 115 (1926).

79. J. Lin Hwang, J. Chem. Phys., 20, 1320 (1952).

80. M.K. Lindemann, Ch.4 in "Kinetics and Mechanisms of Polymerisation", Vol. 1, Part 1, Ed. G.E. Ham, Marcel Dekker, New York, 1967.

81. F.A. Long, and L.J. Thompson, J. Poly. Sci., 15, 413 (1955).

82. J.W. M^{c}Bain, and A.M. Bakr, J. Am. Chem. Soc., 48, 690 (1926).

83. S. Machi, and J. Silverman, J. Poly. Sci., A1, 7, 2737 (1969).

84. D. Machin, Ph.D. Thesis, University of London, 1968.

85. D. Machin, and C.E. Rogers, Die Makro. Chem., 155, 269 (1972).

86. M. Matzner, A. Noshay, L.M. Robeson, C.N. Merriam, R. Barclay, and J.E. M^{c}Grath, Appl. Poly. Symp., 22, 143 (1973).

87. J.C. Maxwell, "Treatise on Electricity and Magnetism", Vol.1, p.365, University Press, Oxford, 1873.

88. P. Meares, Ch.12 in "Polymers : Structure and Bulk Properties", Reinhold Corporation, London, 1965.

89. P. Meares, J. Am. Chem. Soc., 76, 3415 (1954).

90. P. Meares, J. Appl. Poly. Sci., 9, 917 (1965).

91. R.E. Meredith, "Studies on the Conductivities of Dispersions", Lawrence Radiation Laboratory Report UCRL - 8667, 1959.

92. R.E. Meredith, and C.W. Tobias, Ch.2 in "Advances in Electrochemistry and Electrochemical Engineering", Vol.2, Ed. C.W. Tobian, Interscience, New York, 1963.

93. R.E. Meredith, and C.W. Tobias, J. Appl. Phys., 31, 1270 (1960).

94. R.E. Meredith, and C.W. Tobias, J. Electrochem. Soc., 108, 286 (1961).

95. S.P. Mittoff, Ch.4 in "Advances in Materials Research", Vol. 3, Ed. H. Herman, Interscience, New York, 1968.

96. G.E. Molau, and H. Keskkula, J. Poly. Sci., A1, 4, 1595 (1966).

97. A.W. Myers, C.E. Rogers, V. Stannett, and M. Szwarc, J. Appl. Poly. Sci., 11, 159 (1960).

98. G. Odian, "Principles of Polymerisation", M^{c}Graw-Hill, New York, 1970.

99. C.A.R. Pearce, Br. J. Appl. Phys., 6, 113 (1955).

100. C.M. Peterson, J. Appl. Poly. Sci., 12, 2649 (1968).

101. D. Polder, and J.H. Van Santen, Physica, 12, 257 (1946).

102. S. Prager, J. Chem. Phys., 19, 537 (1951).

103. Lord Rayleigh, Phil. Mag., 34, 481 (1892).

104. J.A. Reynolds, and J.M. Hough, Proc. Roy. Soc. (London), B70, 769 (1957).

105. L.M. Robeson, A.Noshay, M. Matzner, and C.N. Merriam, Angew. Makro. Chem., 29, 47 (1973).

106. C.E. Rogers, Ch.6 in "Physics and Chemistry of the Organic Solid State", Vol. 2, Ed. D. Fox, M.M. Labes, and A. Weissberger, Interscience, New York, 1965.

107. C.E. Rogers, J. Poly. Sci., C, 10, 93 (1965).

108. C.E. Rogers, and S. Sternberg, J. Macro. Sci., B5, 189 (1971).

109. W.A. Rogers, R.S. Buritz, and D. Alpert, J. Appl. Phys., 25, 868 (1954).

110. I. Runge, Z. Tech. Phys., 6, 61 (1925).

111. I. Sakurada, Y. Ikada, and F. Horii, Die Makro. Chem., 139, 171 (1970).

112. Y.J. Shur, and B. Ranby, J. Appl. Poly. Sci., 19, 1337 (1975).

113. Y.J. Shur, and B. Ranby, J. Appl. Poly. Sci., 19, 2143 (1975).

114. A. Slawinski, J. Chim. Phys., 23, 710 (1926).

115. G. Smets, and R. Hart, Fort. Hochpoly.-Forsch., 2, 173 (1960).

116. R.L. Stallings, H.B. Hopfenberg, and V. Stannett, J. Poly. Sci., C, 41, 23 (1973).

117. V. Stannett, op. cit. Ref. 41, Ch.2.

118. V. Stannett, J.L. Williams, A.B. Gosnell, and J.A. Gervasi, J. Poly. Sci., B, 6, 185 (1968).

119. H.W. Starkweather, J. Poly. Sci., B, 1, 133 (1963).

120. S.A. Stern, and G.W. Britton, J. Poly. Sci., A2, 10, 295 (1972).

121. S. Sternberg, and C.E. Rogers, J. Appl. Poly. Sci., 12, 1017 (1968).

122. Y. Tabata, Ch.7 in "Kinetics and Mechanisms of Polymerisation", Vol. 1, Part 2, Ed. G.E. Ham, Marcel Dekker, New York, 1969.

123. S.A. Tashmukhamedov, B.U. Sagdullayev, P.P. Larin, M.N. Khasankhanova, G.M. Kozin, F.F. Nurgalieva, R.S. Tillayev, and Kh.U. Usmanov, Poly. Sci. U.S.S.R., 13, 2870 (1971).

124. L.J. Thompson, and F.A. Long, J. Am. Chem. Soc., 76, 5886 (1954).

125. G.T. Tsao, Ind. Eng. Chem., 53, 395 (1961).

126. K. Ueberreiter, and G. Kanig, J. Coll. Sci., 7, 569 (1952).

127. Kh.U. Usmanov, and U. Azizov, J. Poly. Sci., C, 4, 579 (1964).

128. G.J. Van Amerongen, Rubb. Chem. Tech., 37, 1065 (1964).

129. K.W. Wagner, Arch. Elektrotech., 2, 371 (1914).

130. I.C. Watt, and R.L. D'Arcy, J. Macro. Sci., A6, 705 (1972).

131. J.D. Wellons, J.L. Williams, and V. Stannett, J. Poly. Sci., A1, 5, 1341 (1967).

132. O. Wiener, Abhandl. Sächs. Ges. Wiss., 32, 509 (1912).

133. J.L. Williams, and V. Stannett, J. Appl. Poly. Sci., 14, 1949 (1970).

134. J.L. Williams, V. Stannett, and A.A. Armstrong, J. Appl. Poly. Sci., 10, 1229 (1966).

135. H. Yasuda, and V. Stannett, J. Macro. Sci., B3, 589 (1969).

136. K.D. Ziegel, J. Macro. Sci., B5, 11 (1971).

137. B.H. Zimm, J. Chem. Phys., 21, 934 (1953).

138. B.H. Zimm, and J.L. Lundberg, J. Phys. Chem., 60, 425 (1956).